THE UNIVERSITY OF HULL

Investigation into the use of Active Frequency Selective Surfaces to Extend the Absorption Bandwidth of a Conventional Salisbury Screen Absorber

Being a Thesis submitted for the Degree of

Doctor of Philosophy

in the University of Hull

by

Margarita Esther Della-Sera

MEng (Hons)

July 2002

Abstract

It is well accepted that the absorption bandwidth of a metal back-plane absorber, built with either dielectric or magnetic materials, is inherently narrow. It is also well known that in order to increase the absorption bandwidth, the absorber thickness must be increased through decreasing the permittivity or permeability of its spacer. This improved performance, however, comes at a cost. The absorption bandwidth is increased at the expense of not only an increase of absorber thickness, specially at lower frequencies, but also the yielding of a mechanically weaker structure. The most important implication of the former is that there is a trade-off between absorber thickness and absorption bandwidth. These two conflicting absorber properties are, however, of equal importance since the optimum absorber is one which has a small thickness as well as a wideband absorption response. This inherent trade-off is due to the fundamental frequency limitations imposed by the constitutive parameters of materials and is more detrimental at microwave frequencies.

The aim of the research programme described in this thesis was thus to investigate the use of adaptive complex impedance structures, in the form of active frequency selective surfaces (AFSSs), to extend the absorption bandwidth of a small thickness Salisbury screen absorber, thus addressing directly the aforementioned by minimizing the trade-off that exists between absorber thickness and absorption bandwidth.

Declaration

None of the material in this thesis has been submitted in support of an application for another degree or qualification of this or any other university or institution.

Margarita Esther Della-Sera

Acknowledgment

I am in gratitude to my supervisor Dr. Francis C. Smith for his excellent guidance and supervision throughout the course of my research. Without his initial idea this research programme would never had seen the dawn of what has become an excellent outcome. In the etching of the substrates, the help of Steve Coopland was invaluable. My gratitude also extends to the EPSRC and Dr. Peter G. Lederer from DERA for providing the financial backing for this research programme.

I would also like to extend my gratitude to Russell Davies, my office mate, for helping me improve my programming skills and, more importantly, for keeping me company up in the solitary flat. I also want to thank Karen Ow for sparing her precious time to listen to me during my many times of endurance. My eternal gratitude goes also and very dearly to my husband Mark for his support and tolerance during my many tantrums.

And, lastly, Mamá gracias por todo lo que has hecho por mi. Soy la persona que soy por ti. Sin tu guía nunca hubiera logrado lo que he alcanzado hoy en día - te quiero MUCHO.

Margarita

Hull, October 2000

Contents

List of Figures

List of Tables

LIST OF TABLES

Chapter 1

Introduction

This thesis documents research performed by the author at the Faculty of Science and Engineering of the University of Hull between October 1996 and October 2000. The work was co-sponsored by the Engineering and Physical Sciences Research Council (EPSRC) and the Defence and Evaluation Research Agency (DERA) at Malvern. The motivation of the project was to investigate the use of active frequency selective surfaces (AFSSs) loaded with semiconductor devices to extend the absorption bandwidth of conventional Salisbury screen absorbers.

1.1 Radar Absorbing Material: The Beginning

The absorption of energy, being electromagnetic or acoustical, can be thought of being analogous to the concept of "blending with the surrounding". Although the latter has been employed by nature as a survival kit and made perfect by it through millions of years of evolution, it was not until the mid 1930's that mankind started experimenting with absorption technology as a blending mechanism against incoming electromagnetic waves.

Theoretical and experimental work on absorber technology was first carried out

in The Netherlands in the 1930's to improve antenna performance [1]. The first known absorber, a quarter-wave resonant type for the 2-GHz region, was used to cover the back of the antenna to improve its front-to-back ratio. The absorber contained carbon black to achieve dissipation and made use of TiO to obtain a high dielectric constant for reduced thickness.

It was not, however, until the birth of RADAR technology, during World War II, that substantial research and development of absorber materials was carried out by both The United States and Germany [1]. However, while The United States used absorbers to improve radar performance (by reducing interfering reflections from nearby objects), Germany saw absorption technology as a means of radar camouflage. From the German programme, known as Schornsteinfeger (Chimney Sweep), two operational materials were developed and used in the camouflaging of submarine snorkels and periscopes. The first one was a broad-band type absorber known as the Jauman absorber (after J. Jauman) which provided reflection coefficients, at near-normal angles of incidence, of better than -20 dB covering a broad-band between 2-15 GHz. This absorber was a rigid material of about 3-in thickness that comprised alternating layers of rigid plastic and resistive sheets. The other operational material that rose from this programme was a resonant-type[1] absorber known as the Wesch material (after L. Wesch). This material was made of semi-flexible rubber sheet of about 0.3-in thickness loaded with carbonyl iron powder and, to improve bandwidth, its front surface was extended out into a waffle-type geometry.

The American project saw the advancement of two type of materials: the HARP (Halpern-anti-radar-paint) material and the Salisbury screen absorber. The HARP project gave birth to two different types of resonant absorbers for use in two different applications: an airborne type and shipboard version. The airborne one was very thin due to the high permittivity of the artificial dielectric (real part 150)

[1]Energy absorption occurs at about a particular frequency, called the resonant frequency. Below and above this resonant frequency the absorber's absorption properties deteriorates.

used for the base material. These materials were in the form of rubber sheets and not paint, as suggested by the project name. A paint substance was, however, the actual motivation behind the project. The second material, called the Salisbury screen absorber, was created by W. W. Salisbury who realised and consequently showed that absorption could be achieved by placing a 377-Ω/sq-resistive sheet in front of a-quarter-wavelength PEC (Perfect Electrical Conductor) plane. An S-band version of the Salisbury screen was built by placing metal foil on one side of a 0.75-in thick sheet of plywood and the resistive sheet on the other side. All these materials were, however, inherently narrowband [2].

Great Britain was also very active in the absorber field [2]. Although this country was one of the first countries to experiment with magnetic materials to build absorbers, it was not until 1947 that the research programme started. It was then that Plessey's Research Laboratory at Caswell starting experimenting with microwave absorbers [2]. Their first successful product was a resonant material built with carbon-loaded natural rubber. This material, called DX1, was used in the radar bay of the Vulcan Bomber to prevent damage to the radar from bulkhead reflections. Plessey also developed a range of resonant magnetic absorbers operating from 1-18 GHz to counteract EMI. These absorbers were designed to reduce false echoes and clutter produced by reflections of radar energy off masts and yardarms. Due to the success of these absorbers, they are still in use by the British Navy on almost all of their ships.

And, finally, it is interesting to know that many of the absorber design concepts developed then are still in use today.

[2]Their research work into magnetic absorbers was sponsored by the British Radar and Signal Research Establishment at Malvern.

1.2 Motivation of Research

In the area of radar absorbing technology, it is well accepted that a compromise exists between absorption bandwidth and absorber thickness [2]. These two parameters, although conflicting, are of equal importance since the optimum absorber is one which has small thickness together with a wide absorption bandwidth. A design like this is, however, highly idealistic to implement in practice on PEC backplane absorbers since the constitutive parameters of materials employed to build such absorbers are known to impose fundamental limits on their absorption bandwidth [3].

In a recent paper, published by Rozanov [4], the fundamental limit on the absorption bandwidth integral of PEC back-plane absorbers was established to be directly proportional to the static permeability (μ_r'). In other words, for an unlimited broadband-absorption solution the absorber must be built with lossless magnetic materials, wherein $\mu_r'' \approx 0$. However, due to the interdependence imposed by the Kramers-Kronig law on the real and imaginary part of μ_r, materials with such properties are physically unrealistic in practice. [5].

The aforementioned, therefore, leads to the realization that new technological recipes must be searched in the quest for subduing the fundamental limits of conventional materials on absorbers properties. There is, of course, the possibility that new materials with intrinsic broadband properties such as $\mu_r(\omega) = \epsilon_r(\omega)$ [6] will emerge, be re-engineered (artificial materials) or found, for instance, at the bottom of the deepest sea or on the surface of Mars. However, until the latter becomes a reality, it is the task of the absorber investigator to seek alternatives, such as the application of existing technologies, to completely overcome or, at least, substantially minimize the fundamental trade-off of absorbers properties.

The continuous or discrete tuning of reflection nulls is a very appealing attribute in absorber design. This, however, is not the principal aim of the work documented

in this thesis. The main motivation of the investigation was to counteract the fundamental limits imposed by the constitutive parameters of conventional materials upon the absorption bandwidth of thin PEC backplane absorbers, viz. Salisbury screens. The latter has been addressed through the use of bi-state AFSSs with an open/short circuit response.

1.3 Research Objectives

Although the principal motivation behind the programme was to investigate the use of semiconductor-loaded AFSSs to extend the absorption bandwidth of conventional Salisbury screen absorbers, other secondary objectives had to be addressed first. These are as follows:

- Examination of the fundamental aspects of Frequency Selective Surfaces (FSSs).
- Examination of the fundamental operational aspects of P-N junctions so as to understand the effects of semiconductor loading as well as the limitations which these active devices may introduce on broadband absorption.

1.4 Related Research

The most recent published work in the open literature on dynamic radar absorbing materials (DRAM) based on adaptive impedance structures is that documented by researchers at the University of Sheffield (U.K.). The initial motivation behind their investigation was to introduce adaptive properties into the frequency response of passive Salisbury screen absorbers [7]. This was achieved through employing textile substrates loaded with the conducting polymers (CP) polypyrrole (PPy) [8] [9], and polyaniline (Pan). PPy composites are materials whose electrical properties can be controlled by adjusting the concentration of pyrrole monomer in the

manufacturing process. The PPy composites are modelled by a parallel RC circuit whose lumped values are a function of PPy loading. The frequency properties of these materials can be changed through an external stimulus. Their absorber design philosophy is based on a Salisbury screen with the 376.6 Ω/sq resistive sheet replaced by the PPy loaded textile. Their work is now migrating towards smart structure technology [10], [11], [12], [13], [14] with their work targeting a dynamic-absorber design philosophy which has attributes related to incident field sensing, feedback and reconfiguration. The introduction of a sensing network has, however, increased the thickness of the absorber, thus adding more weight and further increasing the trade-off gap between absorption bandwidth and absorber thickness.

In the area of semiconductor loaded AFSSs, these variable impedance structures have been employed in Germany to build an adaptive radar absorber operating from 10-16 GHz [15]. Although details of the build-up and return loss have been omitted, a degree of variation in the absorber's frequency response is shown for different electronic components settings.

Other applications of semiconductor-loaded AFSSs have been reported in the literature. These adaptive impedance planes have been used as artificial dielectrics to change the index of refraction of lenses [16]. In the antenna field, the beam width of an H-plane sectoral horn can be varied through employing AFSSs loaded with PIN diodes [17].

1.5 Outline of Thesis

The thesis is structured as follows:

Chapter 2 - Field Analysis of Frequency Selective Surfaces

This chapter reviews the fundamental theory of frequency selective surfaces (FSSs) together with the principles of the quasi-stationary theory. Knowledge and appli-

cation of the latter is useful for two purposes. First, to exclude grating lobes which are characteristics of periodic structures. And secondly, in order to derive the equivalent complex impedances of arrays composed of capacitive and inductive metallic strips, the underlying of FSSs.

Chapter 3 - Semiconductor Diodes

Dynamic properties can be introduced into the frequency characteristics of passive frequency selective surfaces (FSSs) composed of arbitrarily shaped metallic patches, through loading them with semiconductor devices, viz PIN and varactor diodes. This chapter, thus, serves to outline the fundamental operational aspects of P-N junctions, which are the basis of PIN and varactor devices. The chapter also presents a review of previous investigations into FSSs loaded with semiconductor devices.

Chapter 4 - Dynamic Radar Absorbing Material

In this chapter the design philosophy behind the proposed broadband radar absorbing material is presented. The chapter starts by highlighting the fundamental design theory of metal backplane absorbers, viz Salisbury screen and magnetic absorbers. A discussion of the limiting implications of the Kramers-Kronig law into a broadband absorption solution is also presented.

Chapter 5 - Adaptive Control of Absorption

In the study documented in this thesis a broadband absorption solution is implemented through embedding within a Salisbury screen AFSSs loaded with semiconductor devices. For this purpose, two AFSSs were investigated. The first one was composed of an array of PIN-loaded dipoles while the second one consisted of an array of varactor-loaded dipoles. This chapter presents the AFSSs geometry and physical parameters as well as their dynamic frequency characteristics. A theoretical explanation of the effects of semiconductor loading on the AFSSs' frequency properties is also presented. As well as a general overview of the different uses of passive FSSs, the different techniques available to introduce adaptive impedance

properties into the frequency characteristics of such planar structures are also outlined in this chapter.

Chapter 6 - Dynamic RAM Optimization by Genetic Algorithm

The solution domain in terms of broadband absorption of a thin metal-backplane absorber embedded with a number of semiconductor-loaded AFSSs is not only unknown, but also highly complex. Therefore, in order to find the absorber's global solution space, a simple Genetic Algorithm was employed. It is well accepted that in an optimization procedure the choice of fitness function is of paramount importance in the search of a global solution since it is the only physical link between the problem being optimized and the optimizer. Although the first part of the chapter is devoted to presenting the general aspect of Genetic Algorithms, the chapter's focus is to introduce the fitness function employed to find the global solution of the proposed absorber.

Chapter 7 - Dynamic RAM: Results

Both simulated and measured results of the proposed absorber are presented and discussed in this chapter. These results relate to all theoretical aspects studied in this research programme and presented in this thesis. The data is presented using graphical methods.

Chapter 8 - Conclusions and Further Work

The final chapter is devoted to presenting a set of conclusions as well as future bearings for this research programme.

Bibliography

[1] Emerson, W. H., *Electromagnetic Wave Absorbers and Anechic Chambers through the Years*, IEEE transactions on Antennas and Propagation, Vol. 21, No. 4, July 1973, pp. 484-489.

[2] Johnson, R. N., Radar-Absorbing Material: A Passive Role in an Active Scenario, The International Countermeausre Handbook, 11th Edition.

[3] Brewitt-Taylor, C. R., *Fundamental Limits on the Performance of Radar Absorbing Materials*, Digest of Antennas and Propagation Symposium, Orlando, Florida, Vol. 3, July 1999, pp. 1938-1941.

[4] Rozanov, K. N., *Fundamental Limitations for Thickness to Bandwidth Ratio of Radar Absorbers*, Proceedings of PIERS-98 Conference, Nante, France, July 1998, p. 229.

[5] Wallace, J. L., *Broadband Magnetic Microwave Absorbers: Fundamental Limitations*, IEEE Transactions on Magnetics, Vol. 29, No. 6, November 1993, pp. 4209-4214.

[6] Weston, V. H., *Theory of Absorbers in Scattering*, IEEE Transactions on Antennas and Propagation, September 1963, pp. 578-584.

[7] Chambers, B., *Dynamically Adaptive Radar Absorbing Materials*, Proc 8th European Electromagnetic Structures Conference, Nottingham, UK, 6-7 September 1995, pp. 138-145.

[8] Wright, P. V., Wong, T. C. P., Chambers, B., Anderson, A. P., *Electrical Characteristics of Polypyrrole Composites at Microwave Frequencies*, Advanced Materials for Optics and Electronics, Vol. 4, 1994, pp. 253-263.

[9] Wong, P. T. C., Chambers, B., Anderson, A. P., Wright, P. V., *Large Area Conducting Polymer Composites and their Use in Microwave Absorbing Material*, Electronics letters, Vol. 28, No. 17, 1992, pp. 1651-1653.

[10] Chambers, B., *Internal Monitoring of the Frequency Response of a Dynamically Adaptive Radar Absorbing Material*, Electronics Letters, Vol. 32, No. 18, August 1996, pp. 1711-1712.

[11] Chambers, B., *Dynamically Adaptive Radar Absorbing Material with Improved Self-Monitoring Characteristics*, Electronics Letters, Vol. 33, No. 6, March 1997, pp. 529-530.

[12] Chambers, B., *Surfaces with Adaptive Radar Reflection Coefficients*, Smart Materials and Structures, Vol. 6, October 1997, pp. 521-529.

[13] Chambers, B., *A Smart Radar Absorber*, Smart Materials and Structures, Vol. 8, October 1999, pp. 64-72.

[14] Ford, K. L., Chambers, B., *Smart Microwave Absorber*, Electronics Letters, Vol. 36, No. 1, January 2000, pp. 50-51.

[15] Dittrich, K.W., *Multifunctional Skins*, Six European Electromagnetic Conference Proceedings, 1991, pp. 1-13.

[16] Chekroun, C., Herrick, D., Michel, Y., Pauchard, R., Vidal, P., *Radant: New Method of Electronic Scanning*, Microwave Journal, February 1981, pp. 45-53.

[17] Philips, B., Parker, E.A., Langley, R.J., *Active FSS in an Experimental Horn Antenna Switchable between Two Beamwidths*, Electronics Letters, Vol. 31, No. 1, January 1995, pp. 1-2.

[18] Weile, D. S., Michielssen, E., Goldberg, D. E.,, *Genetic Algorithm Design of Pareto Optimal Broadband Microwave Absorbers*, IEEE Transactions on Electromagnetic Compatibility, Vol 38, No. 3, August 1996, pp. 518-525.

Chapter 2

Field Analysis of Frequency Selective Surfaces

2.1 Introduction

A Frequency Selective Surface (FSS) can be defined as a planar array structure which is composed of either conducting or slot type elements of arbitrarily shapes, which are generally arranged on a 2-D periodic lattice. Due to their periodic symmetry, FSSs are capable of exciting both types of characteristic waves, viz. a propagating field and a series of evanescent fields, when illuminated by a TEM wave. The latter type of fields have the potential of becoming unwanted grating lobes at high enough frequencies.

In this investigation, the theory of uniform transmission lines was used to compute the frequency response of the proposed dynamic radar absorbing material (DRAM). The use of an analytical approach avoids the need to employ time consuming numerical methods. The theory of uniform transmission lines was, however, developed to describe the interaction of a single propagating field travelling from one medium to another having different intrinsic characteristics. As FSSs can gen-

erate secondary main lobes, care must be taken to suppress such fields before the theory of uniform transmission lines can be used. This, nonetheless, is possible by making the periodical placement of the FSSs elements electrically small.

There are two methods which have been employed extensively to analyze the frequency properties of passive FSS. The first one is a full wave analysis called the Modal Wave Analysis [1]. In this method the Helmholtz[1] equation is solved. After all magnetic and electric field components are expanded in terms of Floquet modes, boundary conditions are applied on the conducting elements of the FSS in order to find an integral equation (IE). The IE is then employed to compute the current distribution on the conducting elements which is then used to find the scattered field. The Modal Wave Analysis is a powerful method which not only provides both low and high frequency properties, but also yields cross polarization information due to it being a vector analysis. However, due to its numerical nature, it is a highly time consuming process.

The second method to analyze the frequency properties of FSSs is called the equivalent circuit (EC) analysis. This method solves Laplace's equation[2] and, as such, is a low frequency analysis. It describes the intrinsic properties of an FSS as an equivalent complex impedance, which is in parallel with free space when the FSS is suspended in air. This analytical method facilitates the design of FSSs in that by employing it quick computation of the frequency properties of an FSS can be achieved, thus avoiding the use of time consuming numerical techniques, such as the modal wave analysis.

Hamdy and Parker[2] carried out a comparison of the Modal Wave Analysis and the Equivalent Circuit representation of an E-plane arm of an FSS element type called a Jerusalem cross for both H and E-plane incidence. When comparing the predicted results given by these two approaches with measured data, the Equiva-

[1] $\nabla^2\mathbf{E} + \beta^2\mathbf{E} = 0$

[2] $\nabla^2\mathbf{E} = 0$

lent Circuit method is stated, by the authors, to be satisfactory only for normal incidence. For wider angle of incidences, the measured frequency response shows higher frequency resonant features, which are closely predicted by the Modal Wave Analysis. The Equivalent Circuit approach misses them completely.

In this chapter the theory that describes the behaviour of an FSS normally illuminated by a plane wave is presented. The chapter also shows the modal expansion of all field components due to the periodic symmetry of an FSS. The chapter presents the theory behind the generation of quasi-static evanescent fields for structures with 1-D and 2-D periodicity. By working with quasi-static evanescent fields unwanted grating lobes can be suppressed. This permits the use of transmission line theory to predict the frequency response of the DRAM. The theory of quasi-static field is also used in the impedance formulation of inductive and capacitive gratings which are the underlying of FSSs. The chapter also describes the theory behind the equivalent circuit model as well as the transmission line theory for modal fields.

2.2 The Modal Wave Expansion

The homogeneous scalar Helmholtz equation is given by

$$(\nabla^2 + \beta^2)E(x, y, z) = 0 \tag{2.1}$$

Any rectangular field component, such as $\Xi_t(x, y)$, is known to be a solution of the above equation. In general, a field $E(x, y, z)$ propagating along the z-axis varies with z, such that

$$E(x, y, z) = \Xi_t(x, y)e^{\gamma z} \tag{2.2}$$

By differentiating the above equation twice with respect to z, we get

$$\frac{\partial^2 E(x,y,z)}{\partial z^2} = \gamma^2 \Xi_t(x,y) e^{\gamma z} \tag{2.3}$$

and thus we can re-write equation (2.1) as following

$$\left[\frac{\partial^2}{\partial x^2} + \frac{\partial^2}{\partial y^2} + (\gamma^2 + \beta^2)\right] \Xi_t(x,y) e^{\gamma z} = 0 \tag{2.4}$$

In order to use the separation of variable technique, we must first express $\Xi_t(x,y)$ as a product solution, such that

$$\Xi_t(x,y) = f(x)g(y) \tag{2.5}$$

Differentiating the above equation twice with respect to x and y, and dividing the resulting equation by $f(x)g(y)e^{\gamma z}$, we have

$$\frac{\partial^2 f(x)}{\partial x^2} = -k_x^2 f(x) \tag{2.6}$$

and

$$\frac{\partial^2 g(y)}{\partial y^2} = -k_y^2 g(y) \tag{2.7}$$

where k_x^2 and k_y^2 are separation constants, such that $k_c^2 = k_x^2 + k_y^2$. It then follows that the propagation constant γ is given by

$$\gamma^2 = k_c^2 - \beta^2 \tag{2.8}$$

or

$$\frac{\gamma^2}{k_c^2} + \frac{\beta^2}{k_c^2} = 1 \tag{2.9}$$

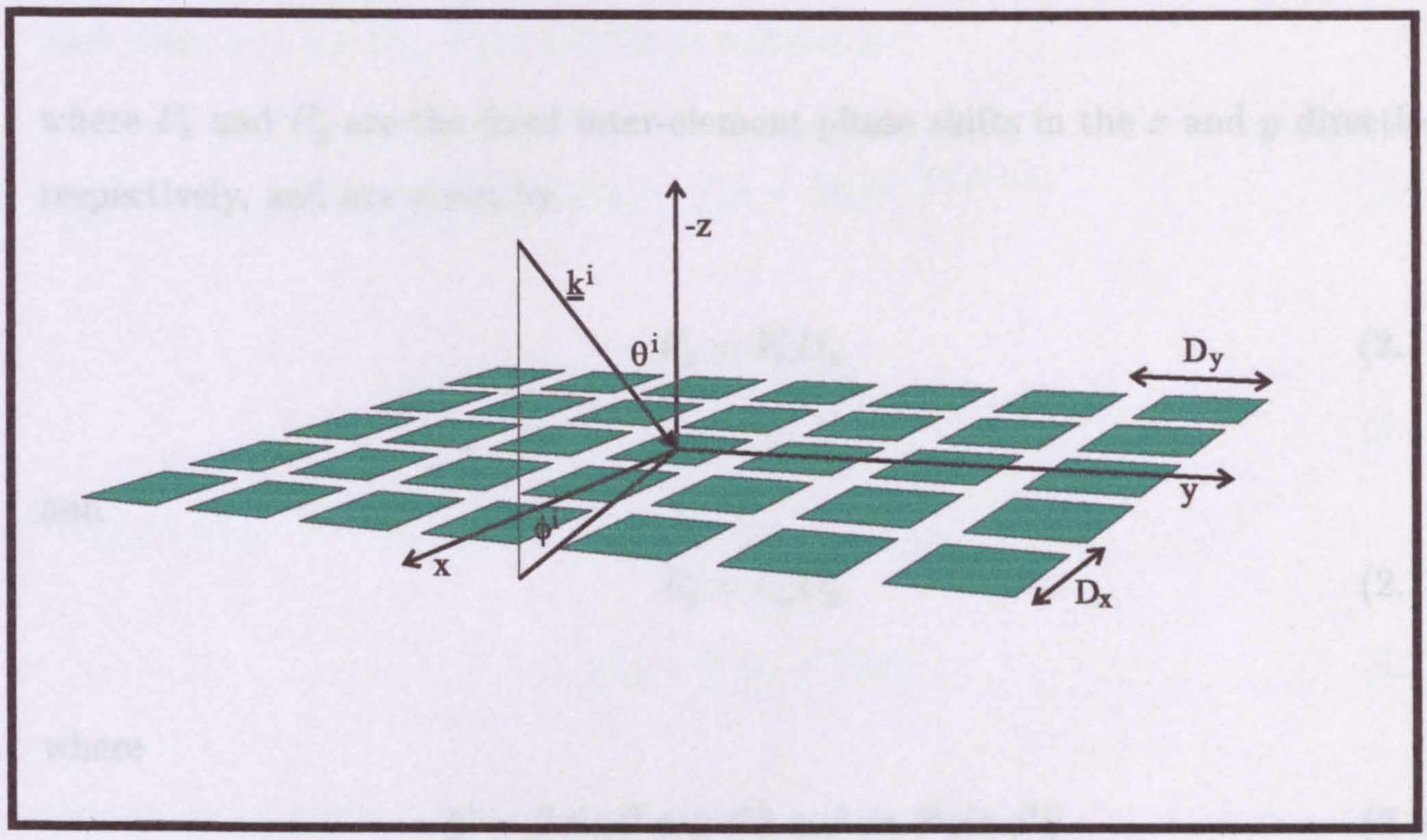

Figure 2.1: Planar array of metallic patches with periodical increments D_x and D_y

k_c^2 is called the *cut-off wavenumber*. The above equation defines a circular region of unit radius. The region outside the radius of the circle is called the propagating space. In this high-frequency region the propagation constant γ, normalised to k_c^2, is imaginary which gives rise to propagating modes or fields. On the other hand, the space confined within the circle is called the evanescent or non-propagating region. Within this low-frequency area γ, normalised to k_c^2, is a real quantity and as a result evanescent or non-propagating fields are present.

2.2.1 Periodic Structures

Consider the FSS shown in figure 2.1. Due to the periodic symmetry of the FSS all the field components must behave as

$$E(x + D_x, y + D_y, z) = E_t(x, y)e^{-j(P_x+P_y)}e^{\gamma z} \tag{2.10}$$

where P_x and P_y are the fixed inter-element phase shifts in the x and y direction, respectively, and are given by

$$P_x = k_x^i D_x \tag{2.11}$$

and

$$P_y = k_y^i D_y \tag{2.12}$$

where

$$\underline{k}^i = \beta \sin\theta^i \cos\phi^i \hat{x} + \beta \sin\theta^i \sin\phi^i \hat{y} \tag{2.13}$$

and

$$\beta = \frac{2\pi}{\lambda} = \omega\sqrt{\mu\epsilon} \tag{2.14}$$

where λ is the free-space wavelength.

Equation (2.10) shows that within each rectangular lattice, bounded by D_x and D_y, the field is the same apart from a phase difference given by $P = P_x + P_y$.

Considering x dependence first. For a periodic increment D_x, the x-component $f(x)$ of the transverse field $\Xi_t(x, y)$ can be expressed as

$$f(x + D_x) = f(x)e^{-jP_x} \tag{2.15}$$

In general, a field $F(x)$ propagating along the x-direction behaves as

$$F(x) = f(x)e^{jk_x^i x} \tag{2.16}$$

where $k_x^i = P_x/D_x$ as given in equation (2.11). Now for a periodic increment D_x, such that $x = x + D_x$, $F(x)$ can be re-written as

$$F(x + D_x) = f(x + D_x)e^{j\frac{P_x}{D_x}(x+D_x)} \tag{2.17}$$

$$F(x + D_x) = f(x)e^{-jP_x}e^{j\frac{P_x}{D_x}x}e^{jP_x} \tag{2.18}$$

$$F(x + D_x) = F(x) \tag{2.19}$$

The above equation is a periodic function with period D_x and, therefore, can be represented as a Fourier series, such as

$$F(x) = \sum_{p=-\infty}^{\infty} a_p e^{j(\frac{2\pi p}{D_x})x} \tag{2.20}$$

Substituting equation (2.20) in (2.16) gives

$$f(x) = \sum_{p=-\infty}^{\infty} a_p e^{j(\frac{2\pi p - P_x}{D_x})x} \tag{2.21}$$

Through differentiating term p of equation (2.21) twice with respect to x, it can be shown that each term of the above Fourier series satisfies equation (2.6), such that

$$\frac{\partial^2 f(x)}{\partial x^2} = -\sum \left(\frac{2\pi p - P_x}{D_x}\right)^2 a_p e^{j(\frac{2\pi p - P_x}{D_x})x} = -k_x^2 f(x) \tag{2.22}$$

It then follows that

$$k_x = \frac{2\pi p - P_x}{D_x} \tag{2.23}$$

or

$$k_x = \frac{2\pi p}{D_x} - \beta \sin\theta^i \cos\phi^i \tag{2.24}$$

Thus equation (2.21) can be written as

$$f(x) = \sum_{p=-\infty}^{\infty} a_p e^{jk_x x} \tag{2.25}$$

Working similarly for y dependence, we have

$$g(y) = \sum_{q=-\infty}^{\infty} a_q e^{j\left(\frac{2\pi q - P_y}{D_y}\right)y} \tag{2.26}$$

and

$$k_y = \frac{2\pi q - P_y}{D_y} \tag{2.27}$$

or

$$k_y = \frac{2\pi q}{D_y} - \beta \sin\theta^i \sin\phi^i \tag{2.28}$$

Thus $g(y)$ in equation (2.26) can be expressed as

$$g(y) = \sum_{q=-\infty}^{\infty} a_q e^{jk_y y} \tag{2.29}$$

Now by substituting equations (2.25) and (2.29) in equation (2.5), the transverse field component $\Xi_t(x, y)$ excited by a periodic array structure can now be written as

$$\Xi_t(x, y) = \sum_{p=-\infty}^{\infty} \sum_{q=-\infty}^{\infty} a_p a_q e^{jk_x x} e^{jk_y y} \tag{2.30}$$

Let $a_{pq} = a_p a_q$ and $\Psi_{pq} = e^{j(k_x x + k_y y)}$. All electric fields can now be expressed as

$$E(x,y,z) = \sum_{p=-\infty}^{\infty} \sum_{q=-\infty}^{\infty} a_{pq} \Psi_{pq} e^{\pm \gamma_{pq} z} \tag{2.31}$$

where, by substituting equation (2.24) and (2.28) into equation (2.8) and assuming normal incidence, γ_{pq} can be expressed as

$$\gamma_{pq} = \left[\left(\frac{2\pi p}{D_x} \right)^2 + \left(\frac{2\pi q}{D_y} \right)^2 - \left(\frac{2\pi \sqrt{\epsilon_r}}{\lambda} \right)^2 \right]^{1/2} \tag{2.32}$$

a_{pq} is the modal amplitude and Ψ_{pq} is the phase shift in the x and y direction. All magnetic fields can be expressed and behave similarly. Equation (2.31) is a periodic solution of (2.1) subject to the boundary condition as expressed in equation (2.10) without the term that contains z. For an oscillatory and non-dying behaviour γ_{pq} must be an imaginary quantity. This will occur when $p = 0$ and $q = 0$. For a dying behaviour γ_{pq} must be a real quantity, which is the case when $p > 0$ and $q > 0$. Equation (2.31) thus demonstrates that a field excited by a structure with periodic properties, such an FSS, is a sum of both types of characteristic waves, a non-evanescent field ($p = 0$ and $q = 0$) together with a number of evanescent waves ($p > 0$ and $q > 0$). Non-evanescent fields can propagate along the $z-$direction without attenuation while evanescent fields are rapidly attenuated along the propagating direction. The field is thus represented by

$$E(x,y,z) = a_{oo} e^{\pm j\beta z} + \sum_{p=1}^{\infty} \sum_{q=1}^{\infty} a_{pq} \Psi_{pq} e^{\pm \gamma_{pq} z} \tag{2.33}$$

Similarly, for structures with 1-D periodicity, such as an array of long metallic strips, equation (2.32) can be written as

$$E(x,z) = a_o e^{\pm j\beta z} + \sum_{p=1}^{\infty} a_p \Psi_p e^{\pm \gamma_p z} \tag{2.34}$$

where $\Psi_p = e^{jk_x x}$. Also the propagation constant γ_p is given by

$$\gamma_p = \left[\left(\frac{2\pi p}{D_x}\right)^2 - \left(\frac{2\pi\sqrt{\epsilon_r}}{\lambda}\right)^2\right]^{1/2} \tag{2.35}$$

2.2.2 Quasi-static Evanescent Fields at Normal Incidence

In the previous section, it was shown how Frequency Selective Surfaces as well as arrays of periodically placed metallic strips are structures that not only excite a propagating field, but also a series of evanescent fields when illuminated by a TEM wave. Due to the frequency dependence of the phases of evanescent fields, this type of field can potentially become secondary main beams or grating lobes at high enough frequencies. How?. This can be explained by examining equation (2.32) for $p > 0$ and $q > 0$. At high frequencies the structure becomes electrically large ($p\lambda < D_x$, $q\lambda < D_y$) which makes λ_{pq} an imaginary quantity and therefore setting off oscillation.

Since the theory of uniform transmission line was developed to deal with a single propagating field, secondary main beams or grating lobes must be avoided when predicting the frequency response of a structure embedded with a number of FSSs or AFSSs. In order to ensure the latter, evanescent fields must become quasi-static.

The following analysis serves to show the conditions for which evanescent fields can become quasi-static.

1-D Periodical Structures

For structures with 1-D periodicity the phase γ_p is given by

$$\gamma_p = \frac{2\pi p}{D_x}\left[1 - \left(\frac{D_x}{p\lambda}\right)^2\right]^{1/2} \tag{2.36}$$

the pth cut-off wavelength occurs when $\gamma_p = 0$, such that $p\lambda_c = D_x$. This implies

that

$$\frac{D_x}{\lambda} = \frac{f}{f_{1c}} \tag{2.37}$$

where f is the working frequency and f_{1c} represents the cut-off frequency of the first evanescent field. It then follows that in order to make γ_p frequency-independent or quasi-static $f_{1c} \gg f$. As shown by (2.37), this condition can be physically fulfilled through making the structure's element periodicity a lot less than the working wavelength, such that $D_x \ll \lambda$. This, thus, will ensure that the structure is operated well below the cut-off frequency of the first evanescent field. In turn, the generation of secondary modes is eliminated thus ensuring the fundamental mode $(p = 0, q = 0)$ is the only propagating field. Following this, γ_p can be written as

$$\gamma_p = \frac{2\pi p}{D_x} \tag{2.38}$$

Under this condition the field can be expressed as

$$E(x,z) = a_o e^{\pm\beta z} + \sum_{p=1}^{\infty} a_p \Psi_p e^{\pm\frac{2\pi p}{D_x} z} \tag{2.39}$$

All magnetic fields behave and can be expressed similarly.

2-D Periodical Structures

For a structure with a 2-D periodicity and standing in free-space the phase γ_{pq} is given by

$$\gamma_{pq} = k_c \left[1 - \left(\frac{\beta}{k_c}\right)^2\right]^{1/2} \tag{2.40}$$

where

$$k_c^2 = k_x^2 + k_y^2 = \left(\frac{2\pi p}{D_x}\right)^2 + \left(\frac{2\pi q}{D_y}\right)^2 \tag{2.41}$$

Now for

$$1 - \left(\frac{\beta}{k_c}\right)^2 \Rightarrow 1 \tag{2.42}$$

so that γ_{pq} becomes frequency independent and thus enforcing evanescent fields to become quasi-static,

$$\left(\frac{\beta}{k_c}\right)^2 \Rightarrow 0 \tag{2.43}$$

For this

$$\lambda \gg \frac{D_x D_y}{\sqrt{(pD_y)^2 + (qD_x)^2}} \tag{2.44}$$

Under the condition stated in equation (2.44) the field can be written as

$$E(x,y,z) = a_{oo} e^{\pm j\beta z} + \sum_{p=1}^{\infty}\sum_{q=1}^{\infty} a_{pq}\Psi_{pq} e^{\pm k_c z} \tag{2.45}$$

All magnetic fields can be expressed and behave similarly.

2.3 The Equivalent Circuit Model

The Equivalent Circuit (EC) model as applied to FSSs was first developed by Anderson[3] who associated the equivalent impedance formulations of free-standing inductive and capacitive strips gratings with, what he called, self-resonant grids, and now known as FSSs. These equivalent impedance formulations, found in Marcuvitz's Waveguide Handbook [4, pp280-285], are an extension to previous work

carried out by G. G. Macfarlane[5]. The aim of Macfarlane's work was to find an analytical formulation for the calculation of shunt admittances generated by the placement of capacitive and inductive diaphragms in planar transmission lines and rectangular waveguides.

The EC model is a low-frequency analysis based upon the condition that the periodicity D of conducting elements on an array or grid must be such that $D \ll \lambda$, where λ is the working wavelength. This condition makes evanescent fields quasi-static (vide section 1.2.2), which, in turn, reduces the scattering problem to an electro- or magneto-static problem. For these types of problems Laplace's equation is solved. The EC approach is a scalar analysis and, as such, no cross polarisation information is permitted. Nevertheless, due to its analytical nature, rapid computation of the frequency properties of a FSS can be achieved.

MacFarlane's approach, although originally intended for analytical formulations of shunt admittances in transmission lines and waveguides, permits, nevertheless, a simple physical understanding of the interaction of TEM waves with capacitive and inductive grids which are, in essence, the basis of FSSs.

2.3.1 Application of Quasi-Stationary Theory to Inductive and Capacitive Gratings

The theory of electromagnetic wave propagation is generally described in terms of modes. A mode can be either little attenuated (non-evanescent or propagating) or it can be rapidly attenuated (evanescent) along the path of propagation. Whether the mode is non-evanescent or evanescent is determined by its cut-off frequency. Each mode is characterised by a wave impedance, which is the ratio of the transverse electric field to the transverse magnetic field. Non-evanescent modes have real wave impedances and can propagate energy while evanescent modes are associated with reactive wave impedances and store either electric or magnetic energy

depending on the electric field polarization of the incoming wave.

At frequencies well below the cut-off frequency there is no wave propagation and the fields or modes decreases exponentially with distance (i.e. they are rapidly attenuated) from their source and are everywhere in phase. The power flow is non-existent and the scattering problem reduces to an electro- or magneto-static field distribution varying harmonically with time. The association of evanescent modes with quasi-static fields allowed MacFarlane[5] to use the quasi-stationary method of the Schwarz-Christoffel[6, pp137-148] transformation for the calculation of shunt admittances, which are originated from the placement of inductive and capacitive diaphragms in transmission lines and waveguides. His motivation was mainly influenced by a need to develop a mathematically-simple and physically direct approach for the calculation of shunt admittances. To tackle the problem, MacFarlane started by considering inductive and capacitive gratings composed of coplanar, equidistant, infinitely long strips of metal. However, for the analytical formulation of shunt admittances he only considered a pair of adjacent metal strips and a single metal strip for the case of capacitive and inductive diaphragms, respectively. His theory, nevertheless, can be readily extended to analytically formulate, respectively, the radiation susceptance and the radiation reactance of infinite capacitive and inductive planar arrays.

2.3.2 Radiation Admittance of a Capacitive Obstacle Placed in a Planar Transmission Line

The derivation of the radiation susceptance of an infinite planar array of free-standing capacitive strips of length 1 metre and spacing D_y is carried out by, firstly, formulating the radiation admittance of a single capacitive obstacle, of similar dimensions, placed within a planar transmission line. The derived formula is then extended so that it can be applicable to the series connected capacitive array shunt across a transmission line which represents propagation in free space.

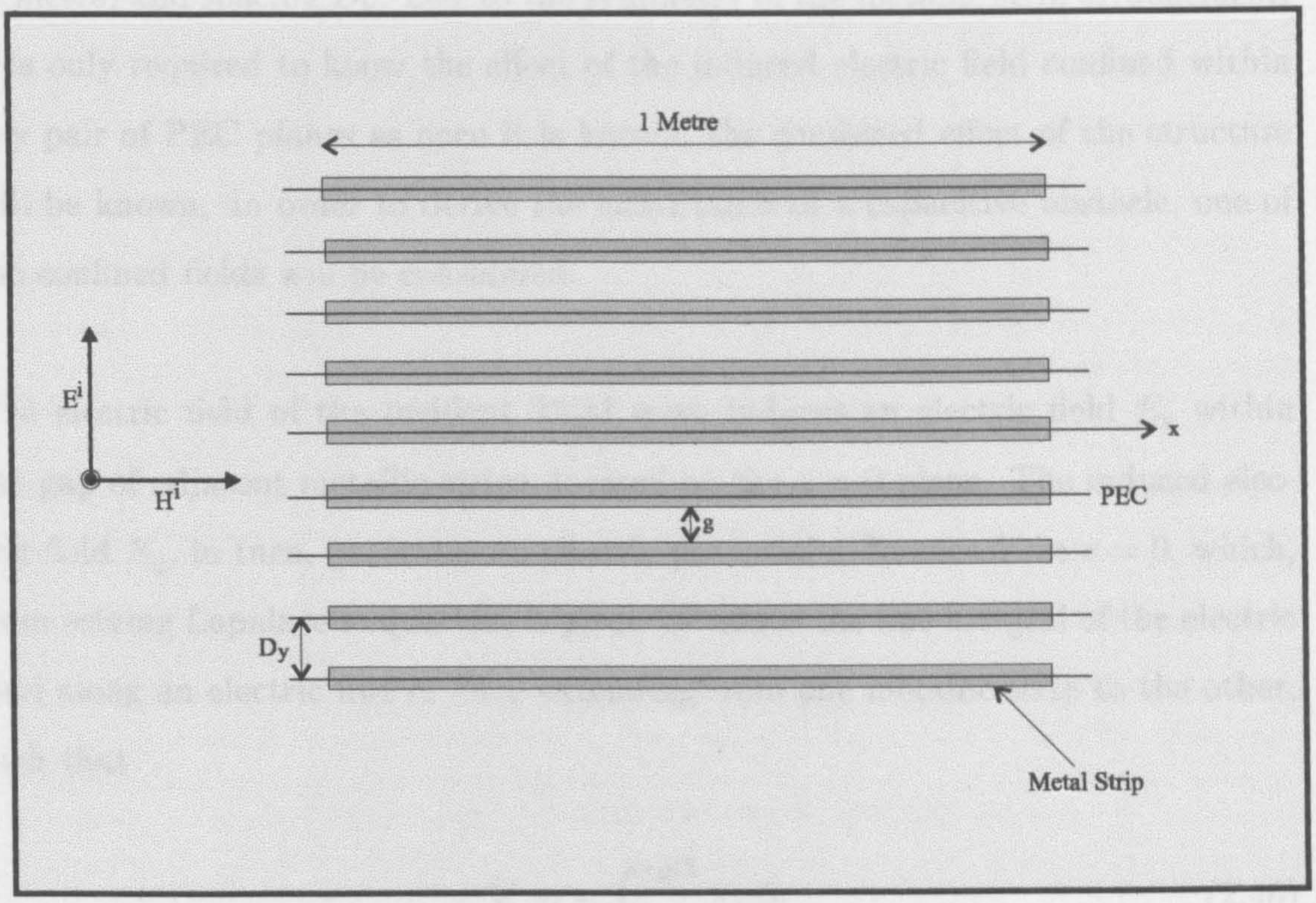

Figure 2.2: Array of free-standing capacitive strips.

Consider a TEM wave normally incident upon an array of coplanar, parallel, equidistant, infinitely long strips of metal, as shown in figure 2.2. The incident field propagates along the z-axis, which looks into the paper, and its electric field E^i is polarised perpendicularly to the edges of the metallic strips. The spacing of the strips is $D_y \ll \lambda$ (λ is the working wavelength) and the width of the gap between the metallic strips is g. We first start the derivation of the array's admittance through dividing the incident field into an infinite number of identical, but independent, fields by means of inserting PEC (Perfect Electrical Conductor) planes through the centre line of the strips, as shown in figure 2.2. This can be done since E^i is normal to the PEC planes and, consequently, it is not disturbed by them. Parallel to the $x = 0$ plane, the electric fields are also identical and therefore the uniform planar transmission lines, formed by pairs of adjacent PEC

planes, can be divided into an infinite number of transmission lines of unit width (1 metre) and spacing D_y. Due to the symmetry of the metallic strip arrangement, it is only required to know the effect of the induced electric field confined within any pair of PEC planes as once it is known, the combined effect of the structure will be known. In order to derive the admittance of a capacitive obstacle, one of the confined fields will be considered.

The electric field of the incident TEM wave induces an electric field E_y within the gap of adjacent metallic strips, located on the $z = 0$ plane. The induced electric field E_y, in turn, generates an electric potential difference V at $z = 0$, which, from solving Lapalace's equation, is given by minus the line integral of the electric field along an electric line of force extending from one metallic strip to the other, such that

$$V = -\int_{-g/2}^{+g/2} E_y dy \tag{2.46}$$

The voltage given in equation (2.46) drives currents along the planar transmission line in opposite direction on opposite sides of the capacitive obstacle, as shown in circuit form in figure 2.3. The induced e.m.f in the gap radiates a field symmetrical about the plane of the capacitive obstacle. The radiation part of the field is the scattered travelling wave whereas the reactive part is the storage field of the obstacle. The obstacle has, therefore, a radiation admittance Y per metre width of strip referred to the voltage and is equal to twice the complex power P supplied by the generator V, per unit voltage, across the gap, such that

$$Y = \frac{2P}{VV^*} \tag{2.47}$$

also,

$$P = \int_s \overline{P} \cdot ds \tag{2.48}$$

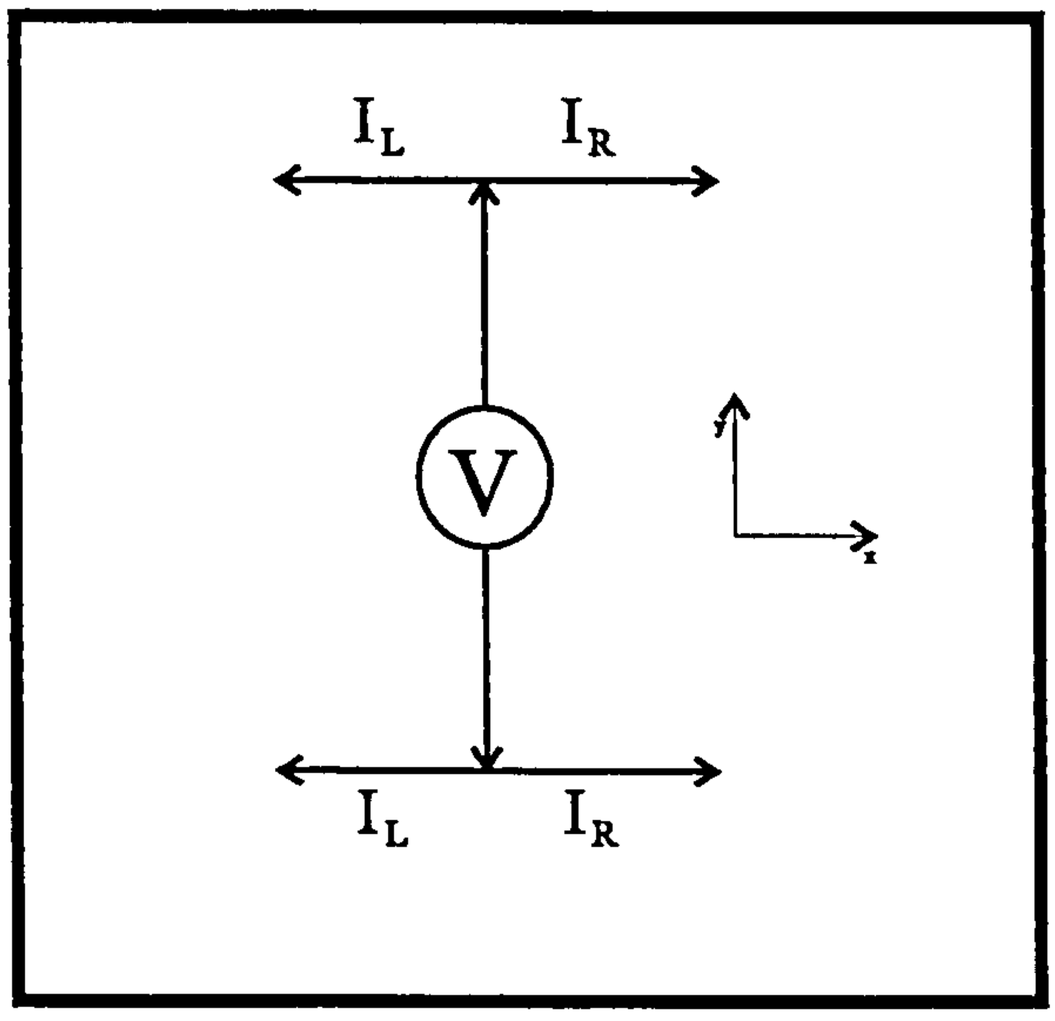

Figure 2.3: Voltage source in the gap.

where $\overline{P}$ is the complex Poynting vector which gives the direction and density of the power density flow, and s represents the surface enclosing the generator V at $z = 0$. $\overline{P}$ is given by

$$\overline{P} = \frac{1}{2}(E \times H^*) \tag{2.49}$$

The complex power P is now expressed as

$$P = -\frac{1}{2}\int_{-g/2,-\partial z}^{g/2,-\partial z} E_y H_x^* dy - \frac{1}{2}\int_{-g/2,+\partial z}^{g/2,+\partial z} E_y H_x^* dy \tag{2.50}$$

$\pm\partial z$ indicates that the path of integration lies slightly to the left (-) and to the right (+) of the capacitive obstacle looking along the positive x-axis, as shown in figure 2.4. The first integral in equation (2.50) represents the complex power radiated to the left while the second one represents that complex power radiated to the right of the diaphragm. The integrals in equation (2.50) can be solved by

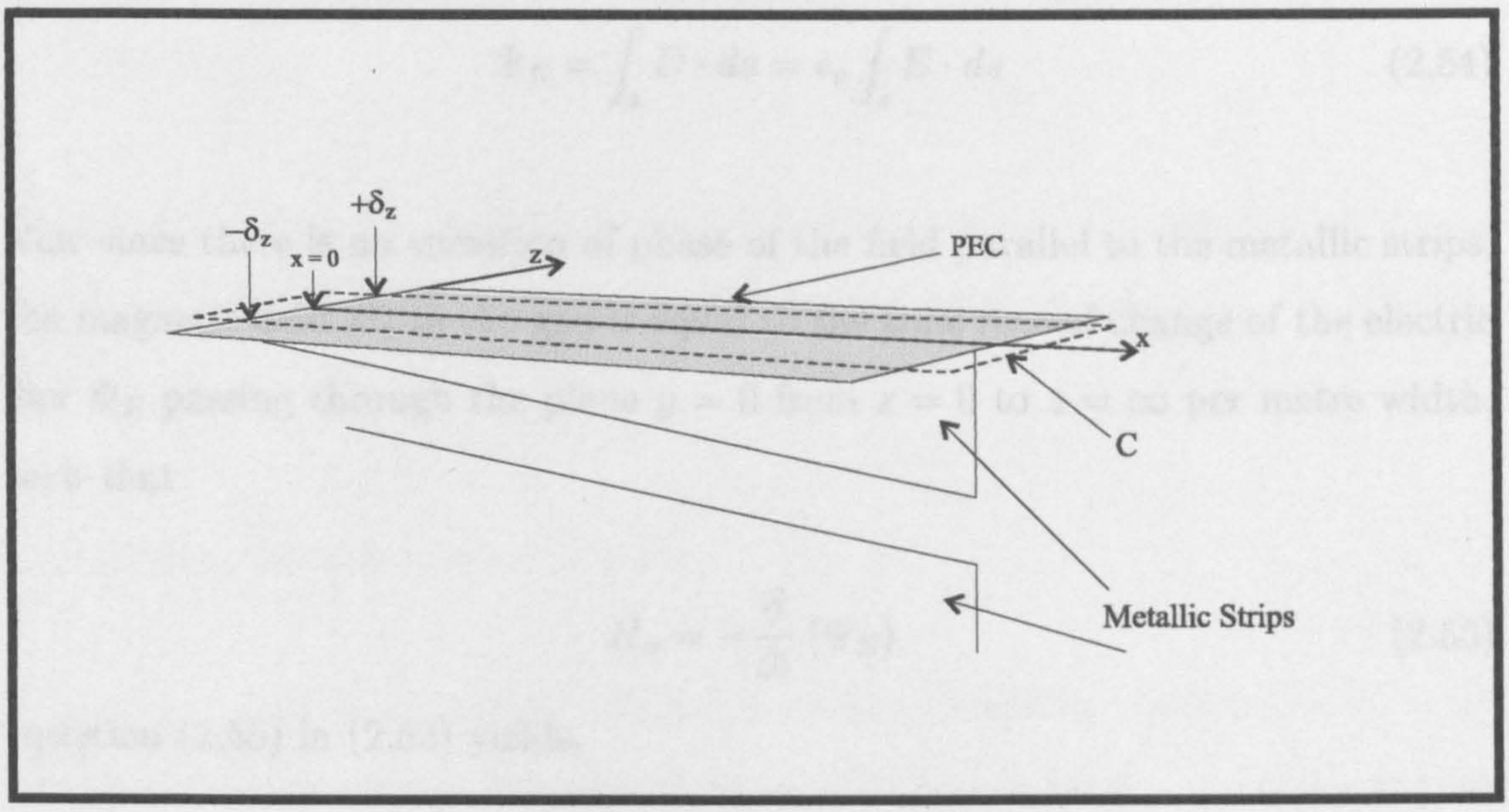

Figure 2.4: Contour C, shown by broken lines, threaded by electric flux Ψ_E.

knowing that the tangential magnetic field H_x is uniform across the gap. The total complex power is then given by

$$P = -2\frac{1}{2}H_x^* \int_{-g/2}^{+g/2} E_y dy \tag{2.51}$$

Substituting equation (2.46) into equation (2.51) gives

$$P = H_x V \tag{2.52}$$

Before we can evaluate the complex power P, so as to derive the admittance due to a capacitive obstacle, H_x must be known. H_x can readily be found by employing the integral form of Ampere's law which is given by

$$\oint_c H \cdot dl = \frac{\partial}{\partial t} \int_s D \cdot ds = \frac{\partial}{\partial t} (\Psi_E) \tag{2.53}$$

where

$$\Psi_E = \int_s D \cdot ds = \epsilon_o \int_s E \cdot ds \tag{2.54}$$

Now since there is no variation of phase of the field parallel to the metallic strips, the magnetic field H_x in the gap is equal to the time rate of change of the electric flux Ψ_E passing through the plane $y = 0$ from $z = 0$ to $z = \infty$ per metre width, such that

$$H_x = -\frac{\partial}{\partial t}(\Psi_E) \tag{2.55}$$

equation (2.55) in (2.52) yields,

$$P = -\frac{\partial}{\partial t}[\Psi_E]_0^\infty V \tag{2.56}$$

Equation (2.56) in (2.47) gives the radiation admittance Y expressed as,

$$Y = -\frac{2}{V}\frac{d}{dt}[\Psi_E]_0^\infty \tag{2.57}$$

$$Y = -\frac{j\omega}{V}[\Psi_E]_{-\infty}^{+\infty} \tag{2.58}$$

$$Y = G + jS \tag{2.59}$$

The principal characteristics of equation (2.58) are

- The radiation admittance is complex since the electric flux Ψ_E includes a reactive field as well as a radiated one.

- The radiation admittance is equal to $j\omega$ times the total complex electric flux, Ψ_E, passing between the conducting strips per metre width from $-\infty$ to $+\infty$ when the potential difference of 1 volt, $e^{j\omega t}$, is maintained between the strips.

To complete the derivation of the radiation admittance Y of a capacitive obstacle within a uniform planar transmission line we first need to derive the electric flux $[\Psi_E]_0^\infty$.

Calculation of Electric Flux Ψ_E

In order to calculate the electric flux Ψ_E, we need to know the electric field $E_y(y,z)$ when the voltage across the gap is V volts. The line integral along the z axis of the product $\epsilon_o E_y$ represents Ψ_E.

The electric field $E_y(y,z)$ across the gap is the sum of both types of characteristic waves, namely *non-evanescent* or propagating wave $E_{y_{ne}}$ and a number of *evanescent waves* E_{y_e}, as shown in section 2.2. In *non-evanescent* waves or modes, the propagation constant β is imaginary and the fields can propagate with no or little attenuation. Their wave impedances are real. On the contrary, *evanescent* waves or modes, for which the propagation constant is a real quantity, are rapidly attenuated along the chosen waveguide. Their amplitudes fall off rapidly with distance from the plane $z = 0$, and equally on both sides of it. Their wave impedances are imaginary. From equation (2.34) the electric field E_y is thus given by

$$E_y(y,z) = E_{y_{ne}} + E_{y_e} \tag{2.60}$$

$$E_y(y,z) = a_o e^{\pm j\beta z} + \sum_{n=1}^{\infty} a_n \Psi_n e^{\pm \gamma_n} \tag{2.61}$$

where Ψ_n and γ_n are given, respectively, by

$$\gamma_n = \left(\frac{2n\pi z}{D_y} \sqrt{1 - \left(\frac{f}{nf_{nc}} \right)^2} \right) \tag{2.62}$$

$$\Psi_n = e^{jk_y y} = \cos\left(\frac{2n\pi y}{D_y} \right) \tag{2.63}$$

where

f is the working frequency and

f_{nc} is the cut-off frequency of the nth mode.

also, $\pm$ depends on the direction of z.

When the the cut-off frequency of the first evanescent wave, $n = 1$, is a lot larger that the working frequency f, such that $f_{1c} \gg f$, the term f/f_{1c} in equation (2.62) can be neglected. This implies that the storage or evanescent field is substantially a rhythmical variation of the electrostatic or quasi-static field. Also, by letting $E_y(y, z)$ be operated at DC, such that $f = 0$, equation (2.61) can thus be re-written as

$$E_{y_e} = a_o + \sum_{n=1}^{\infty} a_n \cos\left(\frac{2n\pi y}{D_y} \right) e^{\mp \frac{2n\pi z}{D_y}} \tag{2.64}$$

Equation (2.64) thus represents an electrostatic field. Since the resulting field is electrostatic, it can therefore be represented by Laplace's equation, such that

$$E_{y_e} = -\frac{\partial V}{\partial y} = -\frac{\partial U}{\partial z} \tag{2.65}$$

where V and U represent equopotentials and line of forces, respectively. V and U

at the point (y, z) are related by[5]

$$\sin(V + jU) = \csc\left(\frac{\pi g}{2D_y}\right) \sin\left[\frac{\pi}{D_y}(y + jz)\right] \tag{2.66}$$

The above equation represents the theory of Schwarz's conformal transformation. This theory relates V (equipotentials) with U (line of forces) at the point (y, z). In the above equation g represents the gap between adjacent metallic strips (see figure 2.2). By employing equation (2.64) the electric field $E_y(y, z)$ can be written as

$$E_y(y, z) = a_o\left(e^{-j\beta z} - 1\right) + E_{y_e} \tag{2.67}$$

In the above equation E_{y_e} represents the sum of the higher evanescent modes. Equation (2.65) in (2.67) gives

$$E_y(y, z) = a_o\left(e^{-j\beta z} - 1\right) - \frac{\partial U}{\partial z} \tag{2.68}$$

The above equation represents the induced electric field $E_y(y, z)$ at a point (y, z) within a pair of metallic strips placed at a distance D_y. Now the electric flux, Ψ_E, along $z = 0$ to $z = l$ is given by the line integral of the product $\epsilon_o E_y$, such that

$$[\Psi_E]_0^l = \epsilon_o \int_0^l E_y dz \tag{2.69}$$

Equation (2.68) in (2.69) thus gives

$$[\Psi_E]_0^l = \epsilon_o \left[a_o \int_0^l e^{-j\beta z} dz - a_o \int_0^l 1 dz - [\partial U]_0^l\right] \tag{2.70}$$

And after integration

$$[\Psi_E]_0^l = \epsilon_o \left[a_o \frac{1}{j\beta} \left(1 - e^{-j\beta l}\right) - a_o l - (U(l) - U(0)) \right] \tag{2.71}$$

Substituting the above equation in equation (2.58) gives,

$$Y = -\frac{2\omega\epsilon_o a_o}{V\beta} \left(1 - e^{-j\beta l}\right) + j\frac{2\omega\epsilon_o}{V} \left(a_o l + U(l) - U(0)\right) \tag{2.72}$$

But the voltage V between the strips is π [5] and $\omega = 2\pi/\lambda\sqrt{\epsilon_o\mu_o}$, therefore, the above equation can be written as

$$Y = -2Y_o a_o \left(1 - e^{-j\beta l}\right) + j\frac{4Y_o}{\lambda} \left(a_o l + U(l) - U(0)\right) \tag{2.73}$$

a_o is the average value of the electric field at the diaphragm and is [5]

$$a_o = -\frac{\pi}{D_y} \tag{2.74}$$

also

$$U(0) = 0 \tag{2.75}$$

As $l \to \infty$, $U(l)$ becomes

$$U(l) \approx \ln \csc\left(\frac{\pi g}{2D_y}\right) + \frac{\pi l}{D_y} \tag{2.76}$$

Now by substituting equations (2.74), (2.75) and (2.76) in equation (2.73) and

then letting $l \to \infty$, the radiation admittance Y per metre width is given by

$$Y = \frac{2Y_o}{D_y} + j\frac{4Y_o}{\lambda} \ln \csc\left(\frac{\pi g}{2D_y}\right) \tag{2.77}$$

Equation (2.77) clearly demonstrates that a capacitive obstacle placed within a uniform planar transmission line of unit metre width and spacing D_y generates a complex radiation admittance. The real part of the radiation admittance is the radiation conductance G which is responsible for the radiated field. The radiation conductance G on each side of the capacitive obstacle is given by

$$\frac{G}{2} = \frac{Y_o}{D_y} \tag{2.78}$$

The imaginary part is the radiation susceptance, S, which is responsible for the storage field. For each side of the capacitive obstacle the radiation susceptance is given by

$$\frac{S}{2} = j\frac{2Y_o}{\lambda} \ln \csc\left(\frac{\pi g}{2D_y}\right) \tag{2.79}$$

Thus,

$$Y = G + jS \tag{2.80}$$

2.3.3 Radiation Susceptance of an Infinite Capacitive Planar Array

The formulation of susceptance given in equation (2.79) only applies to a single capacitive obstacle placed within a planar transmission line of unit width and spacing D_y. This formula can, however, be readily extended so as to be applicable to a free-standing planar capacitive array of infinite transverse dimensions

and which is illuminated by a TEM wave with its electric field perpendicularly polarised to the edges of the metallic strips (vide figure 2.2). When we started the derivation of equation (2.79), we began by considering an array of coplanar, equidistant, infinitely long strips of metal, where the spacing or periodicity of the strips is $D_y \ll \lambda$. We then proceeded by dividing the normally incident TEM wave into a number of identical fields through means of periodically inserting one-metre width PEC planes through the centre line and perpendicular to the edges of the metallic strips. We, then, considered one of these fields to derive the admittance from a single capacitive obstacle within a uniform planar transmission line. Since the incident electric field and resulting electric fields, between any pair of metallic strips, are identical, it then follows that the admittances from such obstacles are also identical. The radiation susceptance S_A of a free-standing planar and transversely infinite capacitive array is, therefore, the series sum of the individual susceptances from any pair of adjacent metallic strips.

In order to derive the susceptance of a planar and transversely infinite capacitive array, as the one shown in figure 2.2, we consider an infinite array of capacitive strips of length one metre and spacing D_y upon which a TEM wave is incident. The total capacitance C_T of the array is given by the sum of the series connection of the individual capacitances C_1, such that

$$C_T = \frac{C_1}{n-1} \tag{2.81}$$

where n is the number of metallic strips of length one metre.

Now as $n \to \infty$, equation (2.81) becomes

$$C_T = \frac{C_1}{n} \tag{2.82}$$

The number of metallic strips is inversely proportional to the spacing D_y, such that

$$n = \frac{k}{D_y} \tag{2.83}$$

where k is the constant of proportionality and is equal to unity since the minimum number of metallic strip can only be increased by one as the array goes to infinity.

Substituting equation (2.83) in (2.82) and assuming $k = 1$, we get

$$C_T = D_y C_1 \tag{2.84}$$

In general, capacitance is related to susceptance through $S = j\omega C$. By substituting equation (2.79) in this formula, C_1 can be written as

$$C_1 = \frac{2\epsilon_o}{\pi} \ln \csc \left(\frac{\pi g}{2D_y} \right) Fm \tag{2.85}$$

Equation (2.85) in (2.84) yields

$$C_T = \frac{2D_y \epsilon_o}{\pi} \ln \csc \left(\frac{\pi g}{2D_y} \right) F \tag{2.86}$$

The susceptance S_A of an infinite array of capacitive strips is thus given by

$$S_A = j\frac{4D_y}{\lambda} Y_o \cos\theta \left[\ln \csc \left(\frac{\pi g}{2D_y} \right) \right] + jC.F. \tag{2.87}$$

The above equation shows that the susceptance S_A of a planar and transversely infinite capacitive grating is given by the susceptance S of a single capacitive obstacle or diaphragm, placed within a uniform planar transmission line, multiplied by the periodicity of the metallic strips, D_y. The $\cos\theta$ term has been added to account for angular dependence. C.F. is a correction factor that takes into account high frequency behaviour while $\cos\theta$ accounts for angular dependence. Both of these terms had been added by Marcuvitz [4]. For a discussion of C.F., please

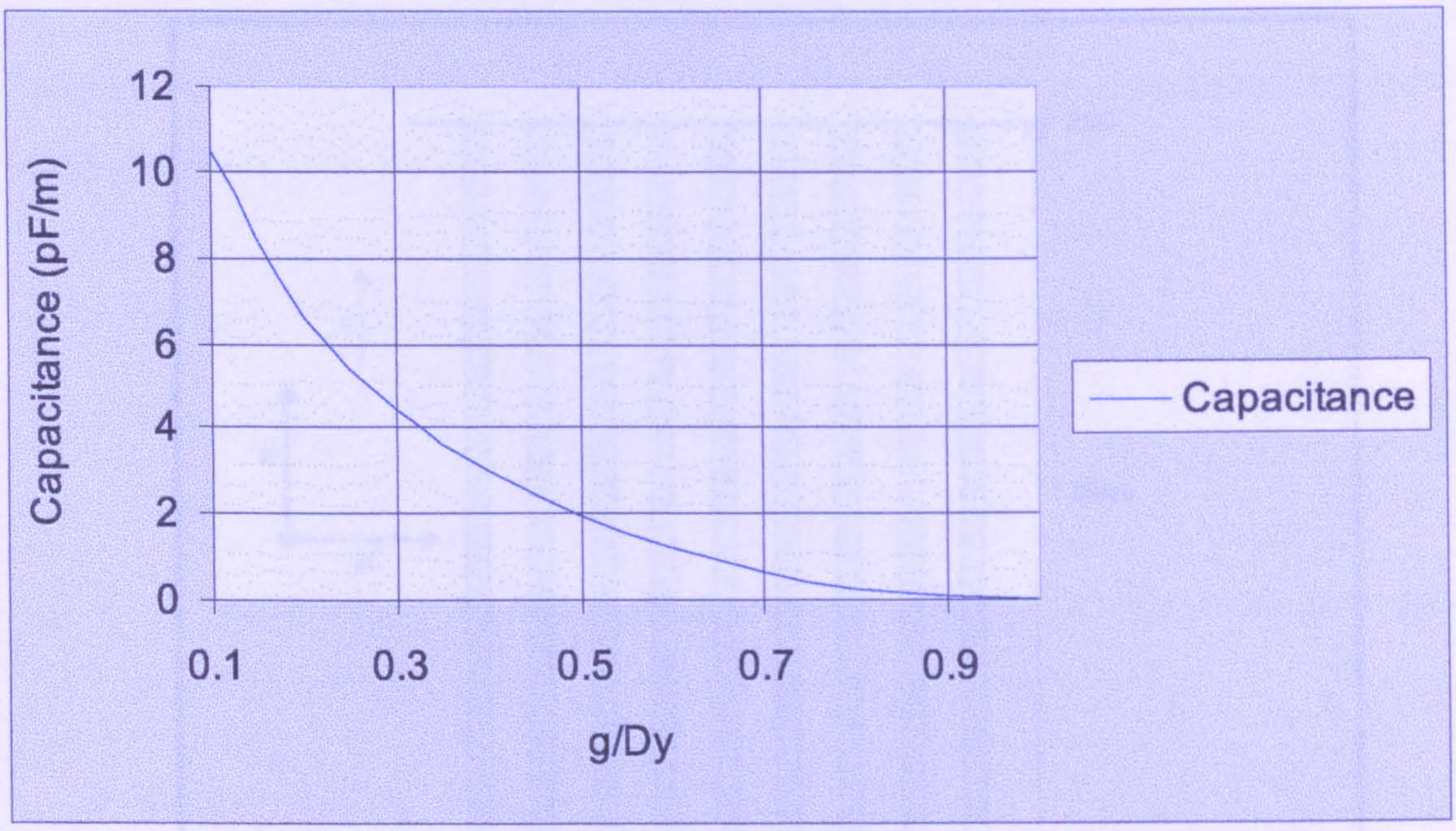

Figure 2.5: Capacitive response as a Function of the gap width g to array periodicity D_y ratio.

refer to Marcuvitz [4].

The array capacitance as a function of the gap width to periodicity is plotted in figure 2.5. The figure shows that as this ratio increases the array capacitance decreases, as expected by analogy with a metal plate capacitor.

2.3.4 Radiation Impedance of an Inductive Obstacle Placed in a Planar Transmission Line

The derivation of the radiation reactance of an infinite planar array composed of coplanar infinitely long inductive strips will be carried out by analytically formulating the radiation impedance from a single inductive obstacle located within a uniform planar transmission line of infinite transverse dimensions and which is capable of supporting a travelling TEM wave. The formula so derived will be extended so that it can be applicable to a transversely infinite planar array of

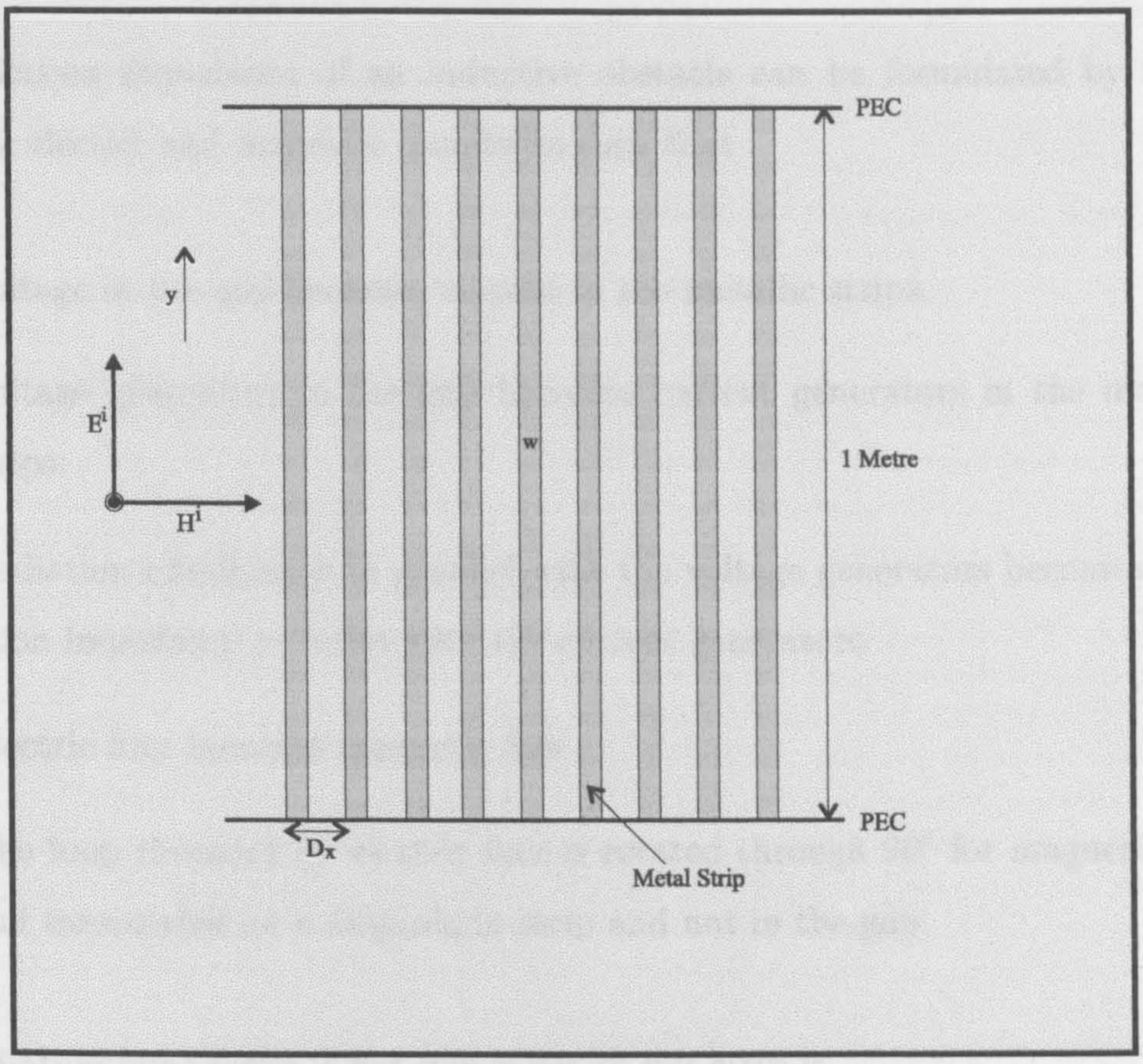

Figure 2.6: Array of free-standing inductive strips.

inductive strips.

Consider a TEM wave normally illumunating an array of coplanar, parallel, equidistant, infinitely long metallic strips as depicted in figure 2.6. The incident TEM wave propagates along the z axis and its electric field component E^i vibrates parallel to the edges of the metallic strips, which are placed on the $z = 0$ plane. The spacing of the strips is D_x, where $D_x \ll \lambda$, and the width of the metallic strips is w. The insertion of PEC planes, one metre apart, parallel to the $y = 0$ plane will not alter the electric field, since the electric field is perpendicular to the this plane. Also, the electric fields along the x axis are the same so we can divide these fields into an infinite number of fields by placing PEC planes at $x = (n - 1/2)D_x$, where $n = 0, \pm 1, \pm 2, ...$, without disturbing the field. By doing the latter we have created a scenario where a one-metre long inductive obstacle is placed within a uniform planar transmission line of width D_x and unit spacing.

2.3. THE EQUIVALENT CIRCUIT MODEL

The radiation impedance of an inductive obstacle can be formulated by interchanging electric and magnetic quantities such that

- Voltage in the gap becomes current in the metallic strips.
- Voltage generators in the gap becomes current generators in the metallic strips.
- Radiation admittance in parallel with the voltage generators becomes radiation impedance in series with the current generators.
- Electric flux becomes magnetic flux
- The loop threaded by electric flux is rotated through 90° for magnetic flux and terminated on a diaphragm strip and not in the gap.

The radiation impedance Z per metre length per strip is

$$Z = \frac{2P}{II^*} \tag{2.88}$$

where I is the current generated by the incident TEM wave on the one-metre long metallic strip, and is given by Ampere's circuital law, such that

$$I = \oint_C H_x dl \tag{2.89}$$

The incident electric field E_y, which induces an e.m.f., can be related to the time-varying magnetic flux Ψ_M through Faraday's induction law. Such

$$e.m.f. = \oint_c E_y dl = -\frac{\partial}{\partial t}\int_s B \cdot ds = -\frac{\partial \Psi_M}{\partial t} \tag{2.90}$$

The incident electric field is everywhere in parallel to the edges of the strips and zero at an infinite distance from the grating. In addition, no magnetic flux passes through the metallic strips. These, therefore, imply that the tangential electric field E_y, across the surface of each strip and which is necessary to maintain a uniform current I along each strip, is uniform. Thus

$$E_y = -\left[\frac{d\Psi_M}{dt}\right]_0^{\infty} = j\omega\left[\Psi_M\right]_0^{\infty} = -j\omega\left[\Psi_M\right]_0^{-\infty} \tag{2.91}$$

The complex power radiated per metre length is given by

$$P = -\frac{1}{2}E_y \oint_C H_t ds \tag{2.92}$$

Substituting equations (2.89) and (2.91) in the above equation gives

$$P = -j\frac{\omega}{2}\left[\Psi_M\right]_0^{\infty}\overline{I} \tag{2.93}$$

The complex radiation impedance per metre length per strip is thus equal to

$$Z = -j\frac{\omega}{I}\left[\Psi_M\right]_0^{\infty} \tag{2.94}$$

$$Z = R + jX \tag{2.95}$$

where

R: represents the radiation resistance and

X: represents the radiation reactance

In order to find the radiation impedance of a one-metre long inductive obstacle placed within a uniform transmission line of width D_x and spacing one metre

the derivation of the magnetic flux $[\Psi_M]_0^\infty$ when a current I flows in each strip must followed.

Calculation of the Magnetic Flux Ψ_M

The magnetic field $H_x(x,z)$ at a point (x,z) can be expressed as (section 2.2)

$$H_x(x,z) = a_o e^{\pm j\beta z} + \sum_{n=1}^{\infty} a_n \Psi_p e^{\pm \gamma_p} \tag{2.96}$$

γ_p and Ψ_p are given respectively by

$$\gamma_p = \pm \frac{2n\pi z}{D_x} \sqrt{1 - \left(\frac{f}{nf_{nc}}\right)^2} \tag{2.97}$$

$$\Psi_p = e^{jk_x x} = a_n \cos \frac{2n\pi x}{D_x} \tag{2.98}$$

also

f is the working frequency

f_{nc} is the cut-off frequency of mode n

and $\mp$ depends on the direction of z.

For quasi-static behaviour of the evanescent fields (i.e. $f_{1c} >> f$), the above equation can be written as

$$H_x = a_o e^{\mp j\beta z} + \sum_{n=1}^{\infty} a_n \cos\left(\frac{2n\pi x}{D_x}\right) e^{\mp \frac{2n\pi z}{D_x}} \tag{2.99}$$

By letting $f = 0$ the above field becomes magnetostatic, such that

$$H_{x_e} = a_o + \sum_{n=1}^{\infty} a_n \cos\left(\frac{2n\pi x}{d}\right) e^{\mp \frac{2n\pi z}{D_x}} \tag{2.100}$$

Since the resulting field is magnetostatic field it can be represented by Laplace's equation, such that

$$H_{x_e} = \frac{\partial V}{\partial x} = -\frac{\partial U}{\partial z} \tag{2.101}$$

where $V = constant$ are lines of flow of currents as well as surfaces of equal magnetic potentials, and $U = constant$ are magnetic lines of forced between the conducting strips. A relationship between V and U are possible through Schwarz's conformal transformation [5]. This is given by

$$\sin(V + jU) = \csc\left(\frac{\pi w}{2D_x}\right) \sin\left[\frac{\pi}{D_x}(x + jz)\right] \tag{2.102}$$

The magnetic flux Ψ_M is thus given by the line integral of the product $\mu_o H_x$ along a path of integration between $z = 0$ to $z = l$, such that

$$[\Psi_M]_0^l = \mu_o \int_0^l H_x dz \tag{2.103}$$

where

$$H_x(x, z) = a_o\left(e^{-j\beta z} - 1\right) - \frac{\partial U}{\partial z} \tag{2.104}$$

The radiation impedance Z per metre length of the inductive obstacle is thus given by

$$Z = -\frac{Z_o a_o}{I}\left(1 - e^{-j\beta l}\right) + j\frac{2\pi Z_o}{\lambda I}\left[a_o l + (U(l) - U(0))\right] \tag{2.105}$$

a_o represents the average value of the magnetic field and is given by [5]

$$a_o = -\frac{\pi}{D_x} \tag{2.106}$$

also

$$U(0) = 0 \tag{2.107}$$

and as $l \to \infty$, $U(l)$ becomes

$$U(l) \approx \ln \csc\left(\frac{\pi w}{2D_x}\right) + \frac{\pi l}{D_x} \tag{2.108}$$

Equations (2.106), (2.107), (2.108) in equation (2.105) and assuming $l \to \infty$ as well as $I = \pi$ [5] gives

$$Z = \frac{Z_o}{2D_x} + j\frac{Z_o}{\lambda} \ln \csc\left(\frac{\pi w}{2D_x}\right) \tag{2.109}$$

The above equation represents the complex radiation impedance of an inductive obstacle placed within a uniform transmission line of width D_x and spacing one metre. The real part is the radiation resistance R which is responsible for the radiated field. The radiation impedance on each side of the inductive obstacle is given by

$$R = \frac{Z_o}{2D_x} \tag{2.110}$$

The imaginary part is the radiation reactance X, which is responsible for the storage or evanescent field. The radiation reactance on each side of the diaphragm

is given by

$$X = j\frac{Z_o}{\lambda}\ln\csc\left(\frac{\pi w}{2D_x}\right) \tag{2.111}$$

Thus

$$Z = R + jX \tag{2.112}$$

2.3.5 Radiation Reactance of an Infinite Inductive Planar Array

The formulation of the radiation reactance given in equation (2.111) applies to a one-metre long inductive obstacle placed within a uniform planar transmission line of width D_x and unit spacing. To derive that equation we started by dividing the total incident field into an infinite number of elementary fields by means of periodically placing PEC planes one metre apart and parallel to the $y = 0$ plane. The radiation reactance of such inductive obstacle was then derived through considering one of these fields. However, the scattering field due to an transversely infinite array of inductive strips is the contribution from the induced currents on all the strips. It then follows that, in order to calculate the radiation reactance of an array of metallic strips it is necessary to consider the impedances generated by the current flow on each metallic strip.

Consider an array of free-standing inductive strips of length one metre and spacing D_x, as shown in figure 2.6, upon which a TEM wave is normally incident with its electric field polarised parallel to the edges of the strips. The array's inductance L is then given by the parallel connection of the inductance L_1 from each metallic strip. Such that,

$$L_T = \frac{1}{n}L_1 \tag{2.113}$$

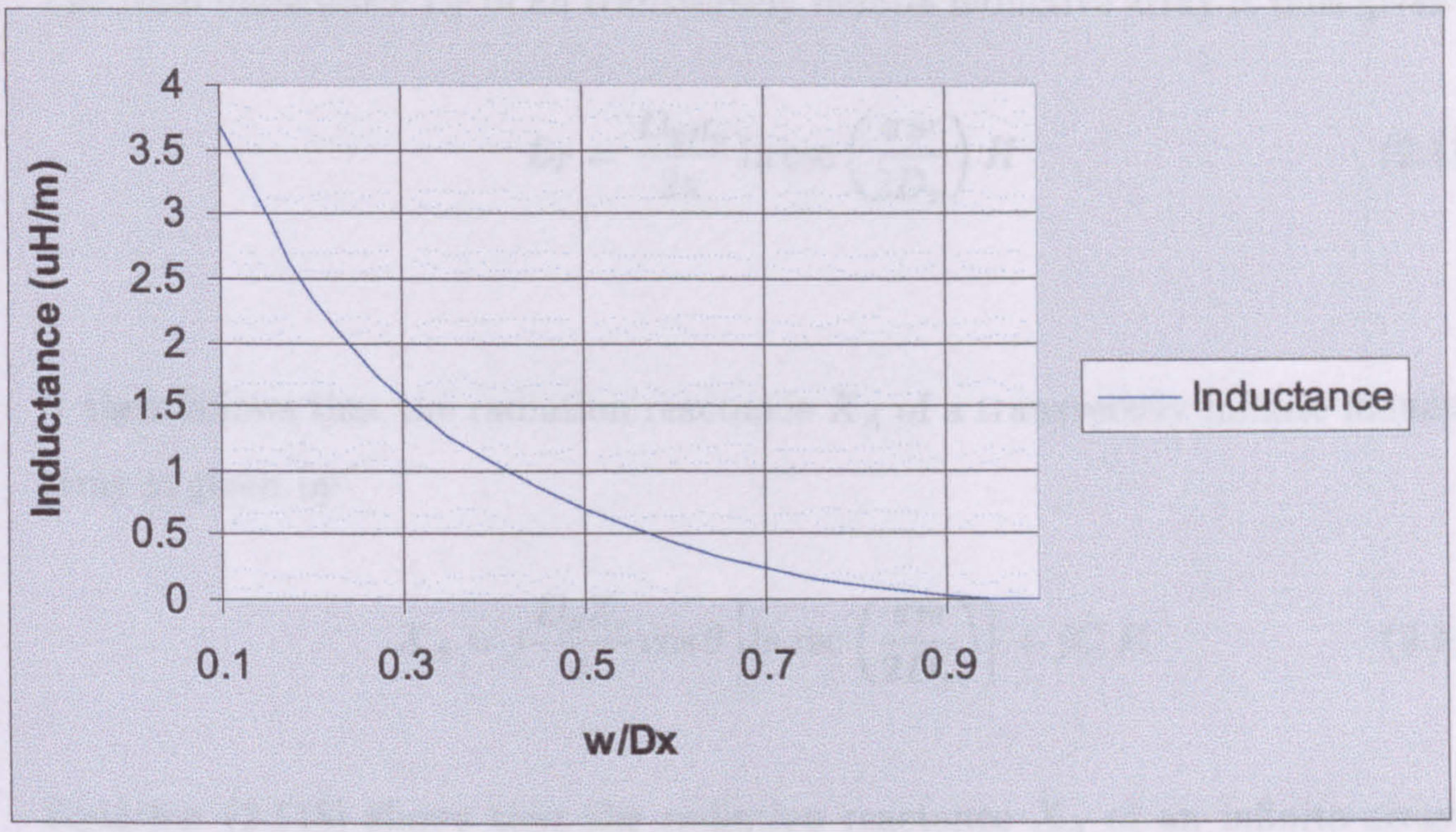

Figure 2.7: Inductive response as a function of the element width w to array periodicity D_x ratio.

where n represents the number of inductive strips in the array and is given by

$$n = \frac{1}{D_x} \tag{2.114}$$

The total inductance L_T of an transversely infinite inductive array is thus given by

$$L_T = D_x L_1 \tag{2.115}$$

In general, inductance is related to radiation reactance through $X = j\omega L$. The inductance L_1 from a single inductive obstacle is given by substituting equation (2.111) in this relationship, such that

$$L_1 = \frac{\mu_o}{2\pi} \ln \csc\left(\frac{\pi w}{2D_x}\right) Hm \tag{2.116}$$

The total inductance L_T of an transversely infinite inductive array is thus given by

$$L_T = \frac{D_x \mu_o}{2\pi} \ln \csc\left(\frac{\pi w}{2D_x}\right) H \tag{2.117}$$

It then follows that the radiation reactance X_A of a transversely infinite inductive array is given by

$$X_A = j\frac{D_x Z_o}{\lambda} \cos\theta \left[\ln \csc\left(\frac{\pi w}{2D_x}\right)\right] + jC.F. \tag{2.118}$$

Equation (2.118) shows that the radiation reactance X_A of an infinite array of inductive strips is equal to the radiation reactance X of a single inductive obstacle multiplied by the periodical placement of the metallic strips D_x, in the array. C.F. is a correction factor that accounts for high frequency performance whereas $\cos\theta$. accounts for angular dependance. Both of these terms were included by Marcuvitz [4]. For a discussion of C.F., please refer to Marcuvitz [4].

The array inductance as a function of the ratio of the element width to periodicity is plotted in figure 2.7. The figure clearly shows that as this ratio increases the array's inductance decreases.

2.3.6 Implementation of the Equivalent Circuit Analysis

With reference to figure 2.8, which shows a schematic diagram of a FSS, the EC is implemented as follows. The magnetic field about the grid, due to current flow along vertical inductive strips, is approximately the same as that about a corresponding uniform inductive grid of period D_y and element width w (as shown figure 2.6). On the other hand, the electric flux concentration between the gaps of periodically-placed capacitive segments of length l_x is l_x/D_x times that of a corresponding uniform capacitive grid of period D_y and gap width g (as shown in

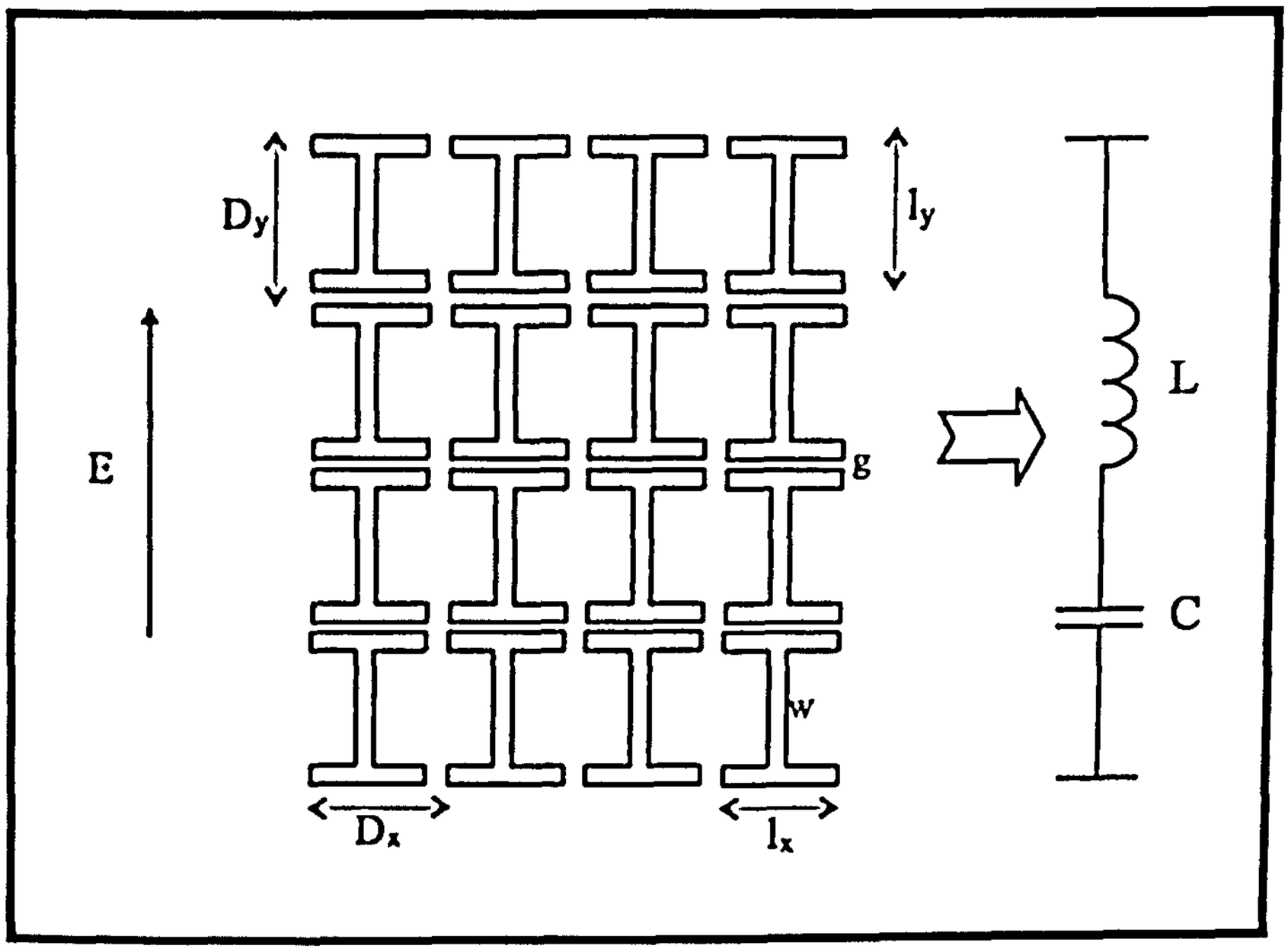

Figure 2.8: Schematic diagram of a passive FSS and its equivalent circuit.

figure 2.2). The overall grid impedance X_T is then the series connection of the inductive and capacitive effects, such that

$$X_T = j\left(X_A - \frac{1}{S_A}\right) \tag{2.119}$$

where X_A and S_A are given by equations (2.118) and (2.87), respectively[3]. The EC analysis is valid providing that $D_x \ll \lambda$, $D_y \ll \lambda$ and $l_x \gg g$ [3].

[3]Without the j

Bibliography

[1] Amitay, N., Galindo, V., Chen, P. W., *Theory and Analysis of Phased Array Antennas*, Wiley-Interscience, 1972.

[2] Hamdy, S. M. A., Parker, E. A., *Comparison of Modal Analysis and Equivalent Circuit Representation of E-Plane Arm of the Jerusalem Cross*, Electronics Letters, Vol. 18, No. 2, 1982, pp. 94-95.

[3] Anderson, I., *On the Theory of Self-Resonant Grids*, The Bell System Technical Journal, Vol. 54, No. 10, 1975, pp. 1725-1731.

[4] Marcuvitz, N., *Waveguide Handbook*, McGraw-Hill Book Company Inc., First Edition, 1951.

[5] MacFarlane, G.G., *Quasi-Stationary Field Theory and its Application to Diaphragms and Junctions in Transmission Lines and Wave Guides*, Journal of the IEE, Pt. 3A, 93, 1946, pp. 703-285.

[6] Collin, R.E., *Field Theory of Guided Waves*, McGraw-Hill Book Company, 1960.

[7] Ott, R. H., Kouyoumjian, R. G., Peters, L., *Scattering by a Two-Dimensional Period Array of Narrow Plates*, Radio Science, Vol. 2, No. 11, 1967, pp. 1347-1359.

[8] Chen, Chao-Chun, *Scattering by Two-Dimensional Periodic Array of Conducting Plates*, IEEE Transactions on Antennas and Propagation, Vol. AP-18, No. 5, 1970, pp. 660-665.

[9] Craig Scott, *The Spectral Domain Method in Electromagnetics*, Artech House, 1989.

[10] Vardaxoglou, J. C., *Frequency Selective Surfaces -Analysis and Design-*, Research Studies Press, 1997.

[11] Kraus, J. D., *Electromagnetics*, Ed. 4th, McGraw-Hill, 1992.

[12] Marshall, S. V., Skitek, G. G., *Electromagnetic Concepts and Applications*, Ed. 3rd, prentice-Hall International Editions, 1990.

Chapter 3

Semiconductor Diodes

3.1 Introduction

The loading of a frequency selective surface with semiconductor devices offers not only a viable, but also a straightforward means to introduce adaptive properties into its intrinsic characteristics. Through semiconductor loading abrupt as well as continuous changes of an FSS's complex impedance can be achieved in quasi-real time. This can be exploited to introduce adaptive frequency properties into the frequency characteristics of a thin Salisbury screen absorber so as to increase its operational bandwidth.

Applications of FSSs populated with semiconductor devices have been reported. These structures have been used to change the index of refraction of lenses [1]; to vary the return loss of an absorber [2] as well as change the beam width of a horn antenna [3].

Although there are a number of semiconductor devices with different properties available to date, the loading properties of two were studied in this research programme. These were PIN and varactor diodes. The former can be used to in-

troduce abrupt and, to a certain extent, continuous changes into the complex impedance of an passive FSS. The latter, on the other hand, facilitate continuous changes of an FSS's complex impedance.

It is important, however, to thoroughly understand the properties of PIN and varactor diodes. It is only then that one can start to understand the limitations which these devices may impose on the adaptive frequency properties of an absorber embedded with FSS populated with diodes. For this a thorough understanding of a PN junction must precede. The aim of this chapter is, therefore, to describe the fundamental operation of PN junctions. The chapter also presents a review of the work done throughout the years on frequency selective surfaces loaded with semiconductor devices.

3.2 PN Junctions

PN diodes are electronic devices made from single crystal semiconductors which are doped in such a way as to contain both p and n type materials. In general, semiconductor materials are characterised by having an electrical conductivity which lies between that of a good conductor ($10^6/\Omega$cm) and that of a good insulator ($10^{-5}/\Omega$cm) and hence the name. Although a PN junction is made from a single crystal, it can be thought of as a structure formed by bringing together two pieces of n-type and p-type materials into close contact. This "assumption" leads to the derivation of a mathematically simple model to describe the physical properties and operation of a PN junction.

3.2.1 PN Junctions in Equilibrium

Let us consider a PN junction whose schematic diagram is depicted in figure 3.1. In general, there are more holes in the p side than in the n side, and hence holes will

diffuse from the p region into the n region. Similarly, due to the high concentration of electrons in the n-type side, diffusion of electrons into the p-type region occurs. As a result, holes diffusing out of the p region leave behind ionized acceptors and, thus, a built-up of negative charge takes place. In like manner, a positive-charge layer, composed of donors, is developed from the diffusion of electrons into the p region. It then follows that a charge layer, called the *transition* or *depletion* layer, is formed to the right and left of the junction. Within this double-space-charge layer an electric field is set up whose direction inhibits further diffusion of the majority carriers. The electric field builds up until the currents, due to diffusing electrons and holes, are equal, thus indicating that an equilibrium state has been reached within the crystal as a whole. The induced electric field establishes a contact potential ψ_o across the transition region which is given by [4]

$$\psi_o = \frac{kT}{q} \ln \left(\frac{N_a N_d}{n_i^2} \right) \tag{3.1}$$

where

N_a is the acceptor density

N_d is the donor density

n_i is the intrinsic carrier density

k is the Boltzmann's constant (1.38×10^{-23} J/K)

q is the electronic charge (1.602177×10^{-19} C)

and T is the temperature in Kelvins.

Under equilibrium the transition region is very resistive to current flow when compared to the other regions (bulk region) of the device since it has almost been depleted of its majority carriers.

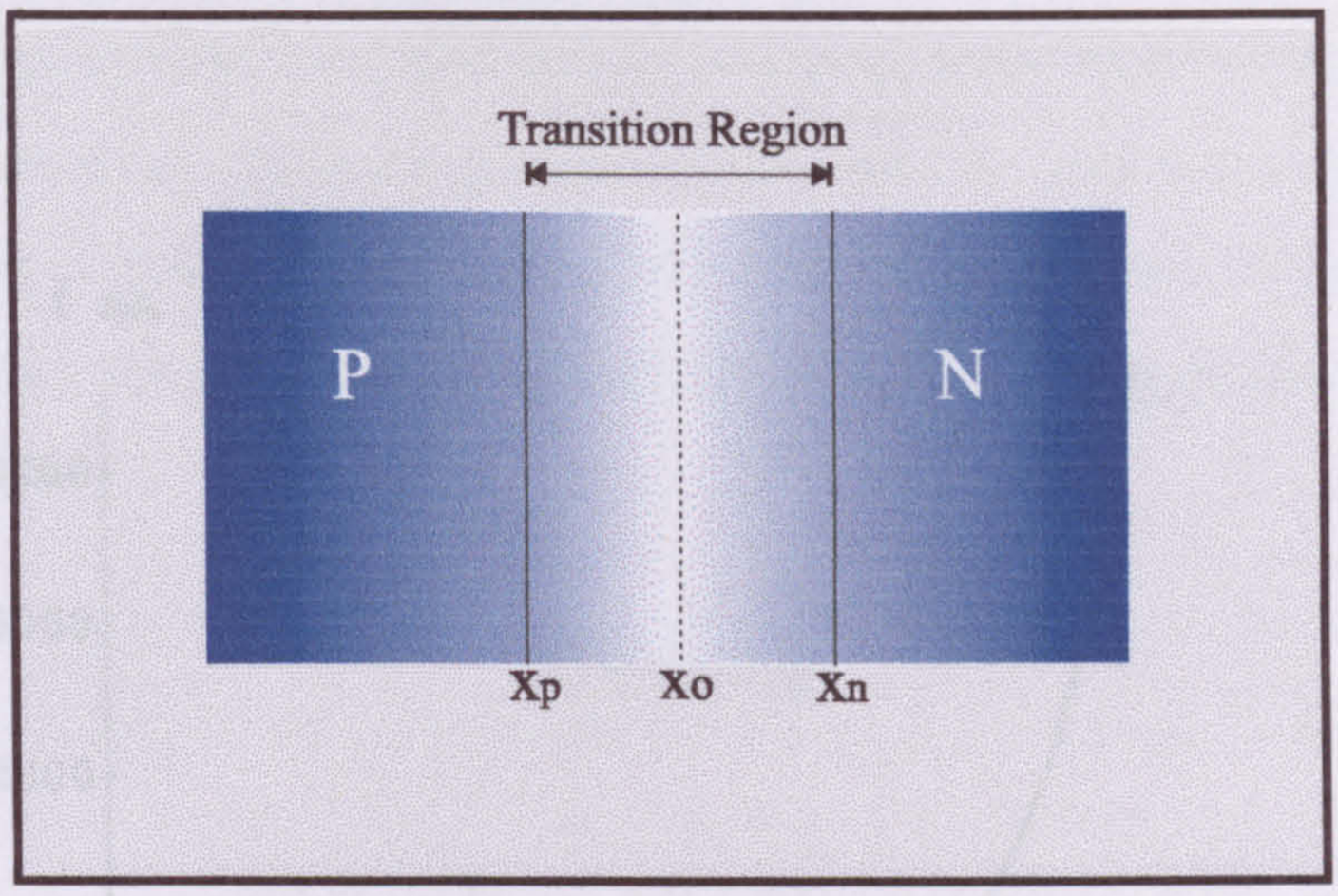

Figure 3.1: Schematic diagram of a bulk PN junction.

The Effects of Forward and Reverse Bias Voltages

When an external voltage V_d is applied across the highly resistive transition layer the equilibrium situation no longer holds. A forward-bias voltage will have the effect of lowering the height of the built-in potential barrier to $(\psi_o - V_D)$ and, consequently, majority carriers are able to surmount the potential barrier easier than in the equilibrium. This results in a net current flow from the p to the n region in the conventional forward sense. On the other hand, an externally applied reverse voltage V_R increases the height of the potential barrier to $(\psi_o + V_R)$ which results in carrier extraction, no current can flow from the p to the n region and the device is said to be open circuit.

The relationship between the externally applied voltage V_D and current I is given by [4]

$$I = I_s \left[exp\left(\frac{qV_D}{kT}\right) - 1 \right] \tag{3.2}$$

I_s is called the saturation or reverse leakage current and is the result of minority carriers diffusing to the transition layer edges to be swept across or recombine.

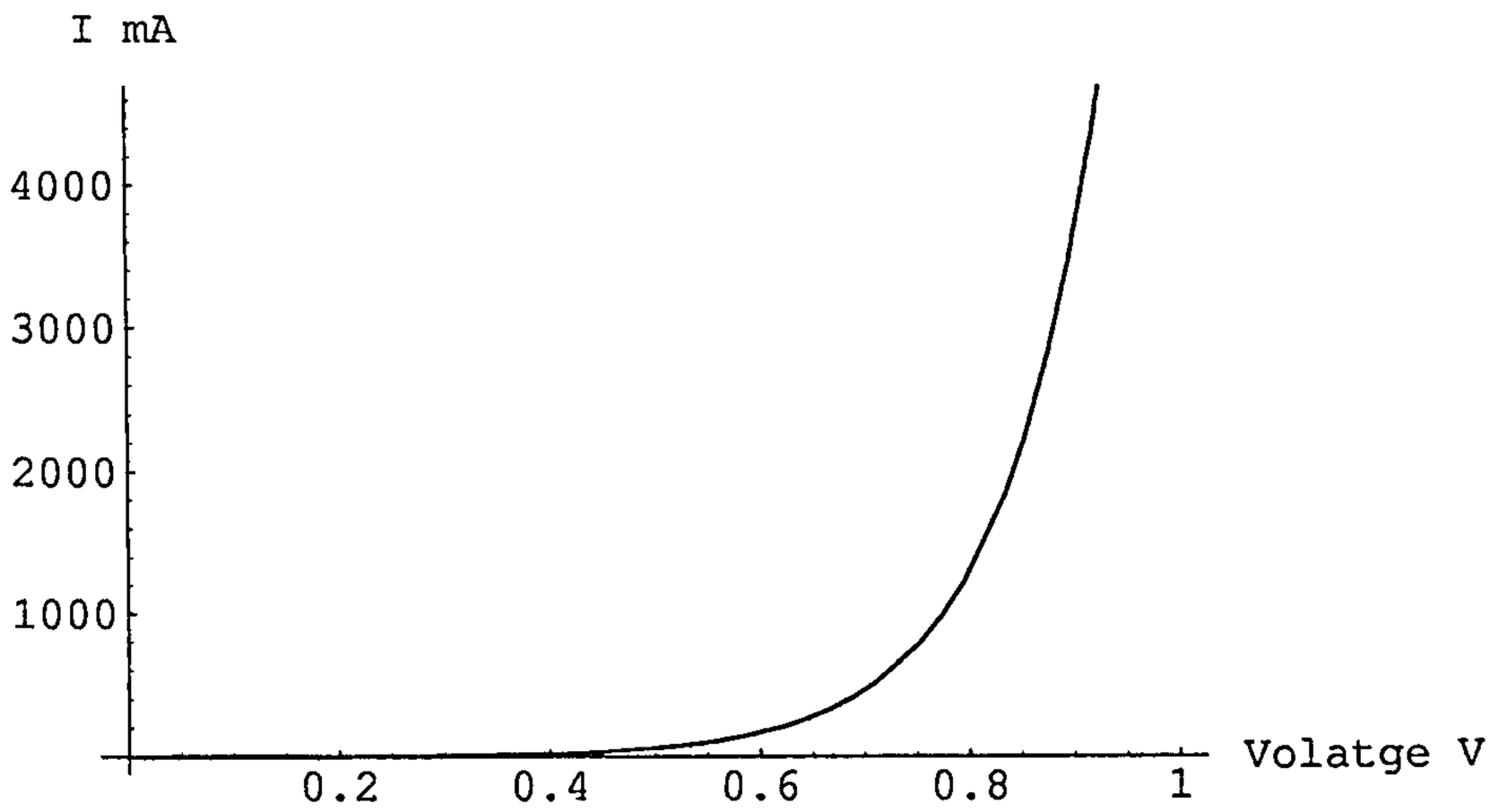

Figure 3.2: PN junction: voltage-current characteristic.

The current-voltage characteristic of an ideal PN junction is shown in figure 3.2. The figure shows that under forward bias the current increases exponentially with increasing voltage.

3.2.2 Transition Region Width and Capacitance

The width of the transition layer, an important property of PN junction devices for microwave applications, varies according to the applied reverse voltage. Under an increasing reverse-bias voltage, the largely depleted region becomes wider, while a decreasing reverse-bias voltage narrows it. This phenomenon gives rise to an effective transition layer capacitance C_t. C_t together with the diffusion capacitance C_d are the principal factors responsible for the high frequency limitations of PN junction devices. C_d is due to the charge storage of the excess minority carriers stored at the edges of the transition region and is present under forward bias.

In the transition region, the charge density is either the donor density N_d in the

n-type part or the acceptor density N_a in the p-type part. A relationship exists between the electric field and the charge density ρ, wand this is given by Poisson's equation. This states that *the gradient of the electric field is proportional to the charge density* ρ. The constant of proportionality is $1/\epsilon$, where ϵ is the permittivity of the material. In the n-region and in the p-region, this law can be expressed, respectively, as

$$\frac{\partial E_x}{\partial x} = \frac{q}{\epsilon} N_d \tag{3.3}$$

$$\frac{\partial E_x}{\partial x} = -\frac{q}{\epsilon} N_a \tag{3.4}$$

where $\rho = qN_d = -qN_a$.

Integrating equations (3.3) and (3.4) and knowing that at the metallurgical junction the electric field is E_j and that, at the edges of the transition region $x = x_n$, $x = x_p$ (see figure 3.1) the electric field is zero. We get

$$-E_j = \frac{q}{\epsilon} N_d x_n = -\frac{q}{\epsilon} N_a x_p \tag{3.5}$$

But

$$E_j = -\frac{\partial V}{\partial x} \tag{3.6}$$

and therefore

$$V_j - V_n = -q \frac{N_d x_n^2}{2\epsilon} \tag{3.7}$$

$$V_p - V_j = -q \frac{N_a x_p^2}{2\epsilon} \tag{3.8}$$

x_n and x_p are the distances that the transition region extends into the n- and

p-side, respectively. The total voltage drop V across the transition region is calculated by adding together equations (3.7) and (3.8). V can also be written in terms of the applied voltage V_D plus the built-in contact potential ψ_o, such that

$$V = V_p - V_n = V_D + \psi_o = -\frac{q}{2\epsilon}\left(N_d x_n^2 + N_a x_p^2\right) \tag{3.9}$$

The transition region width w_t is the distances that x_n and x_p extend into the $n-$ and $p-$ regions, respectively, such that $w_t = x_n + x_p$. The magnitude of the charge in each side of the transition region is the same (vide equation 3.5), therefore, after some re-arranging, w_t can be written as

$$w_t \approx x_n + x_p = \sqrt{\frac{2\epsilon}{q}(-V_D - \psi_o)(\frac{1}{N_a} + \frac{1}{N_d})} \tag{3.10}$$

Equation (3.10) shows that the transition region width w_t of an abrupt PN junction is, essentially, proportional to the applied reverse voltage to the power 1/2. The equation also shows that w_t can be either increased or decreased by light or heavy doping, respectively. Figure 3.3 depicts the variation of w_t with applied reverse voltage. The figure clearly demonstrates that w_t increases with increasing reverse bias voltage and vice-versa. Above 0V, the transition region width is decreased further.

The capacitance of an abrupt junction can now be calculated. In general, the magnitude of the capacitance is the rate of change of charge in either part of the transition region with change of voltage across the junction. The capacitance is derived by using the n-type side of the transition region.

$$C_t = AqN_d\frac{\partial x_n}{\partial V_D} \tag{3.11}$$

But

$$x_n = K(-V_D - \psi_o)^{1/2} \tag{3.12}$$

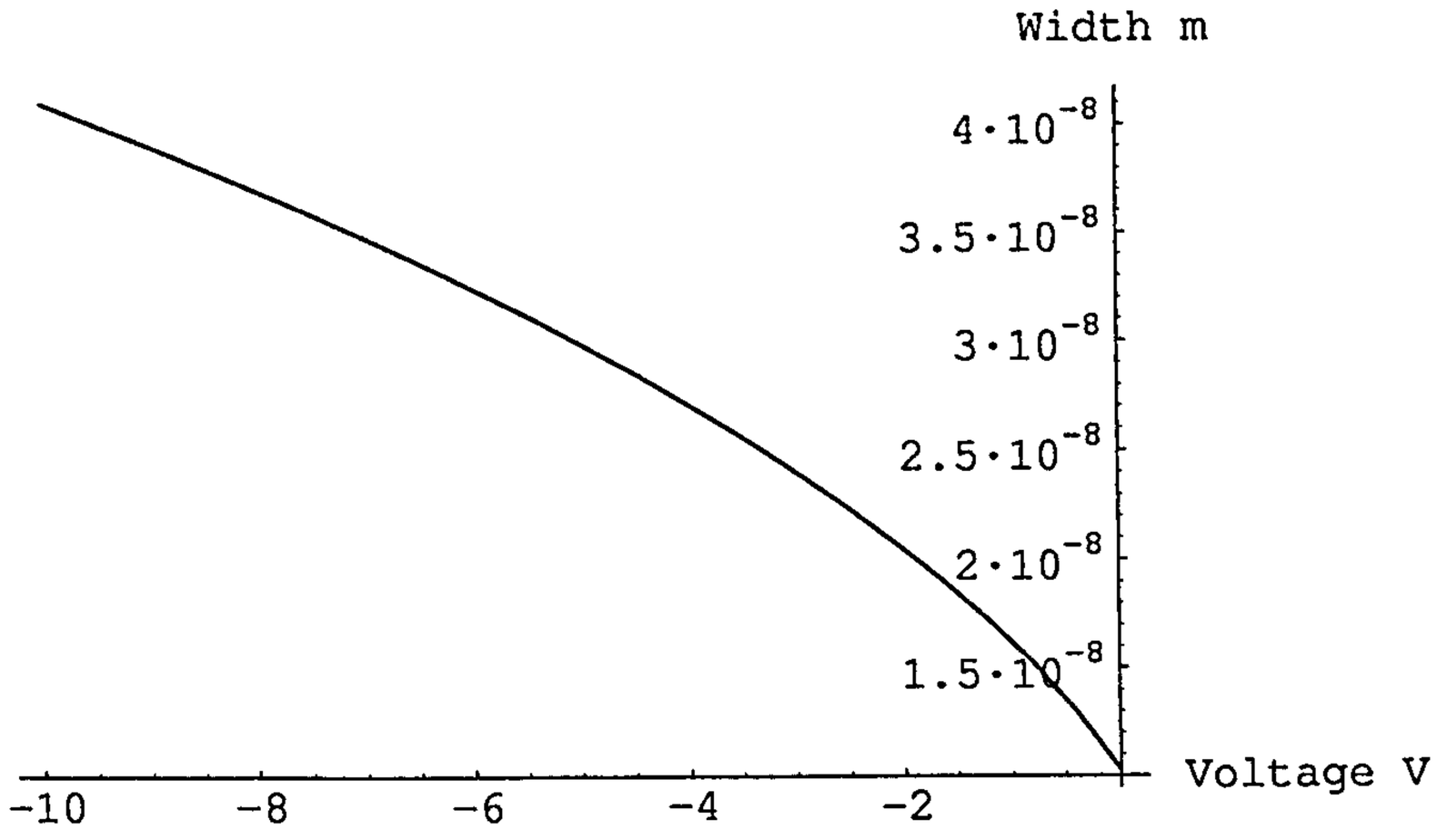

Figure 3.3: PN junction: variation of transition region width as a function of reverse-bias voltage.

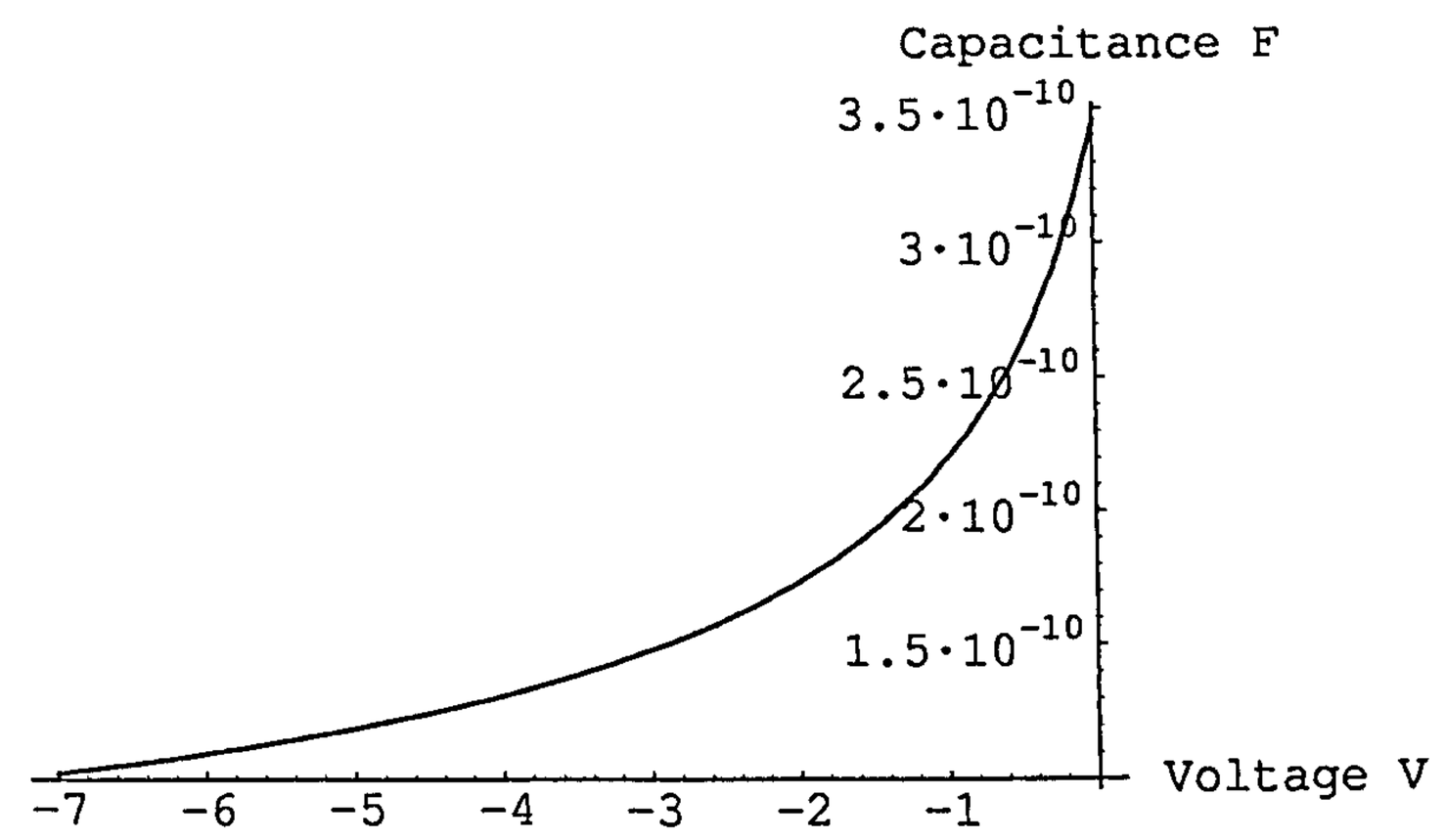

Figure 3.4: PN junction: variation of capacitance as a function of reverse bias voltage.

where $K = \frac{1}{N_d}\sqrt{\frac{2\epsilon}{q(1/N_d+1/N_a)}}$

Differentiating equation (3.12) w.r.t V_D gives

$$\frac{\partial x_n}{\partial V_D} = \frac{K}{2}(-V_D - \psi_o)^{-1/2} \tag{3.13}$$

And therefore C_t can be written as

$$C_t = A\sqrt{\frac{q\epsilon}{2(1/N_a + 1/N_d)(-V_D - \psi_o)}} \tag{3.14}$$

The above equation shows that the capacitance in the transition region is inversely proportional to externally applied reverse voltage V_D to the power 1/2. This effect is clearly shown in figure 3.4. Increasing the reverse-bias voltage across a PN junction will result in an increase of the transition region width which, in turn, will cause C_t to decrease. On the other hand, a decreasing reverse-bias voltage will narrow the transition layer width which will, consequently, effect an increase of C_t. The equation also shows that by light-doping the transition width, a drop in capacitance can be achieved which, in turn, increases the device impedance. In practice, this is done to introduce a hard OFF-state into the characteristics of PIN diodes.

3.3 PIN and Varactor Diodes

A PIN (p-i-n) diode is fundamentally a PN junction device with an added intrinsic region, (i-region), located within the p- and the n-type layers. By adding an intrinsic region, generally composed of weakly n- or p-type material, the transition region width can be increased thus reducing the device's junction capacitance, vide equation (3.14). This, together with a 0 bias voltage, creates a device with a large

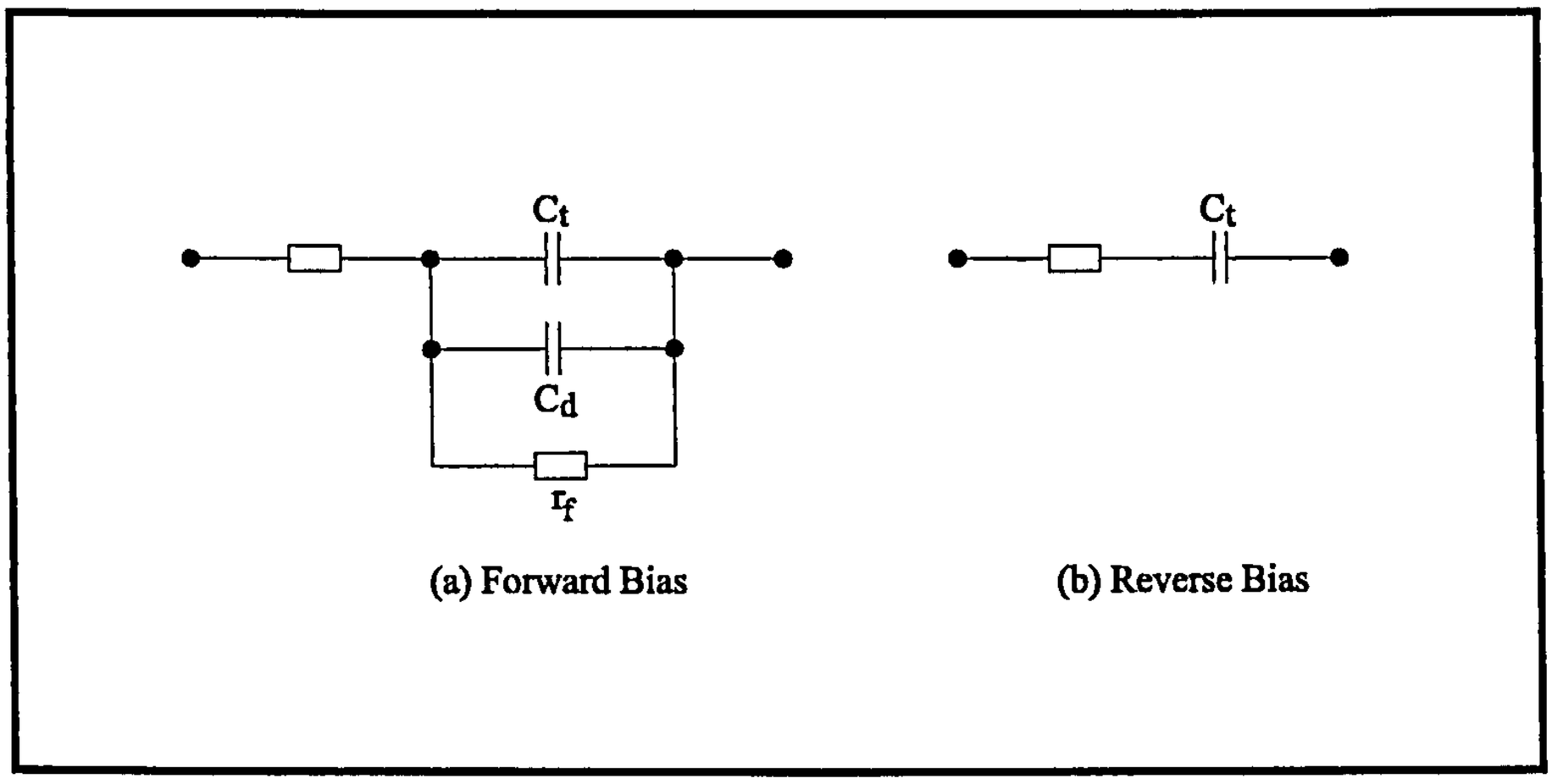

Figure 3.5: Equivalent circuit diagram of a PN Junction. C_t is not the same in (a) and (b) because of different bias voltage.

impedance and thus impeding the flow of electrons. On the other hand, its low forward resistance acts as a bridge which permits the flow of current. Varactor diodes, on the other hand, are PN junctions operated under a reverse bias voltage. Under a forward-bias voltage, varactor diodes behave as a conventional diode.

Figure 3.5 shows the equivalent circuit diagram of a PN junction device under forward and reverse bias [5]. Under a forward-bias voltage the junction can be represented by an equivalent circuit of a parallel connection of the forward-bias transition capacitance C_t, the diffusion capacitance C_d and a a low forward resistance r_f. The schematic of the equivalent circuit shows that, under a forward-bias voltage, the junction's impedance response is dominated by r_f. Under a reverse bias voltage, a PN junction is a series connection of the reverse-bias transition capacitance C_t and a large resistance r_r

Figure 3.6 shows the equivalent circuit diagram of a PIN diode [6]. As the transition region width is decreased with an increasing bias voltage, the junction ca-

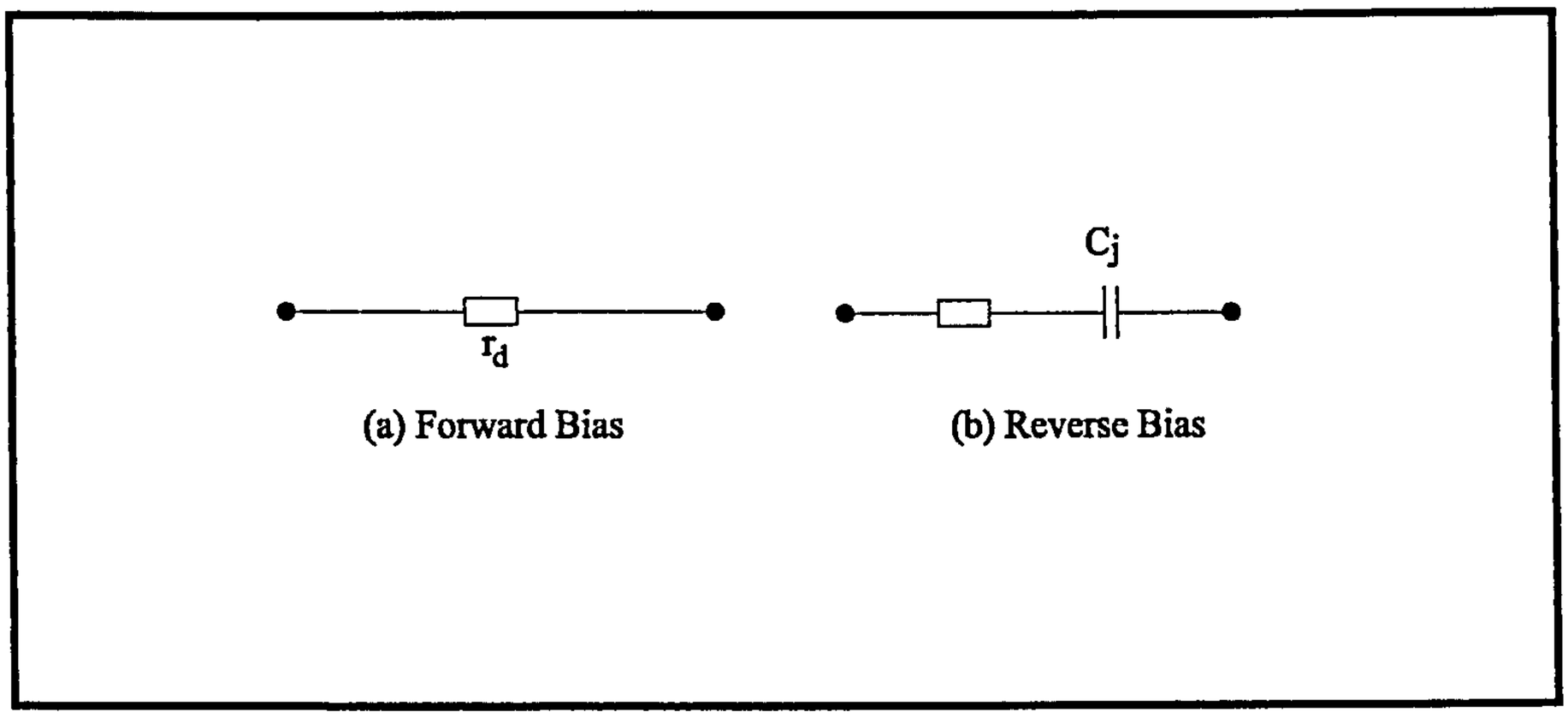

Figure 3.6: Equivalent circuit diagram of a PIN diode.

pacitance is increased. This, in turn, causes the reactive impedance due to the junction capacitance to move towards a short circuit. Thus, allowing the flow of current.

3.4 Semiconductor Devices in FSSs

Over the years a series of investigations into the effects of loading single dipoles and FSSs with semiconductor devices has been carried out. Applications of semiconductor loaded FSSs have also been reported. Semiconductor loaded FSSs have been used to change the index of refraction of lenses built from artificial dielectrics [1]; to vary the return loss of an absorber [2]; and also to change the beam width of a H-plane sectoral horn [3].

Chekroun[1] et al employed inductive wire grids periodically loaded with PIN diodes to realize externally controllable artificial dielectrics. By parallel-cascading a number of these artificial dielectrics a frequency-dependent phase-controlling lens can be created. The OFF-ON characteristics of the diodes is used to change the

index of refraction of the lens which, in turn, changes the direction of the incident beam. Rapid changes of the beam direction is accomplished by the high speed switching times of the semiconductor devices.

Dittrich [2] built and measured an adaptive radar absorber based on two vertically spaced gratings with integrated electronic components. Although details of the buildup and return loss have been omitted a degree of variation of the frequency response for different electronic components settings is shown, predominantly, over a frequency bandwidth that extends from 10 to 16 GHz (less than one octave).

Philips et al [3] placed two switchable FSSs within an H-plane sectoral horn to change, as and when desired, the size of its radiating aperture so as to vary the width of beam. The type of active FSS employed by the authors was one composed of an array of dipoles connected together by microwave diodes. In the OFF state, the FSS behaves as an ordinary dipole array, reflecting the incident field at its resonance frequency. The active FSSs thus simulate metallic walls, reducing the horn's radiating aperture and thereby broadening the beam. When the diodes are forward biased, the strip dipoles are joined together to form arrays of inductive strips with a high transmission coefficient. In the ON-state the FSS walls appear transparent to the incident field and the antenna radiates as the full horn. The use of walls made of active FSSs permits a beamwidth-switching between 32° to 45° which represents a beamwidth change of 40 percent.

Janaswamy [7] looked into the radar cross section (RCS) variation of a narrow strip dipole loaded with a PIN diode. His investigation revealed that two different states in RCS are possible through forward and reverse biasing the PIN diode. When the diode is forward biased the RCS of the loaded dipole almost coincides with the short-circuited case. The diode has a real impedance of a low value when it is forward biased (ON), and has an additional capacitive reactance when it is reverse biased (OFF). The location of the diode on the dipole was varied and the RCS computed showed that centre-loading exhibits the two distinct RCS states

over the widest bandwidth. The method of moments was used to analyse the RCS characteristic of a loaded dipole under the influence of two different bias voltage.

Shuley [8] looked into the scattering phenomenon of a free-standing 2D array composed of strip dipoles centre-loaded with PIN diodes. Both theoretical and measured data is presented over bandwidths that extend from 8 to 18 GHz and 6 to 25 GHz, respectively. Under reverse bias (OFF state), the diodes impede current flow and, consequently, the single dipole element is divided into two identical but smaller elements. However, due to the finite impedance of the PIN diodes, the resonant frequency of the loaded dipoles is different to that yielded by the two separate or unloaded elements. The resonant frequency of the latter occurs at a higher frequency. Under forward bias (ON state), the reflection coefficient, when compared with the unloaded case, never quite equals 1.0 due to the small forward resistance of the PIN diodes. The possibility of resonance frequency tuning was investigated and a degree of tuning was demonstrated by means of varying the bias voltage on the diode so as to alter its capacitance. The method of analysis employed by the author involves formulating the scattering problem in the spectral domain and applying a conjugate gradient FFT algorithm to solve the resultant operator equation. He used rooftop basis function to represent the current since it permits flexible loading schemes.

Chang et al [9] carried out studies on the scattering of an array of segmented half-squares loaded with PIN diodes. Both theoretical and practical data is presented. The paper clearly demonstrates that by applying a bias voltage, either forward or reverse, on the diodes an externally controlled shift of the frequency response of the structure is possible. The frequency response of the structure can thus be readily changed from a reflecting structure to one which is virtually transparent except for a small insertion loss. The authors opted for a PIN-loaded square geometry, rather than strip dipoles or Jerusalem crosses, to illustrate the effect of the diodes capacitance on the overall equivalent capacitance of the structure. Under this arrangement, the elements and the diodes capacitances are connected in series

and thus the smaller capacitance of the diodes dominates the resonance. When the diodes are forward biased (ON-state), the segmented elements are linked together, via the diodes low resistive path, to form square loops. The structure is thus composed of an infinite array of square loops and resonates at f_r, accordingly. A reverse bias voltage (OFF-state) on the diodes effect an extra capacitive load between the half squares and the diodes, the structure then resonates at a higher frequency and, as a result, the surface becomes transmitting at f_r. The authors made use of the Equivalent Circuit approach to analyse the transmission characteristics of the PIN-loaded square array over a frequency range that extends from 7.5 to 16 GHz. The equivalent circuit of the square loops is a series LC circuit where L is due to the vertical sides of the square parallel to the electric field and C is the capacitance between the horizontal sides. In the OFF-state the diode's equivalent circuit is a resistance R_d (typical values 10-100 Ω) in series with a capacitance C_d (typical values 0.01-0.05 pF). In the ON-state the capacitance C_d is short-circuited and the diode's equivalent circuit becomes a series resistance R_d. The computed results closely agree with the measured ones. In the ON-state the active segmented square has a measured resonance of -20 dB depth at 12.5 GHz. The theoretical prediction of the passive array closely matches the measured one, however, its transmission response shows a deeper null of -40 dB. Reverse biasing the diodes moved the resonance to a higher frequency (36 GHz).

In their paper Chang et al [10] investigated the frequency characteristics of PIN-loaded FSSs which comprise arrays of dipole/inductive strips combination and square loop elements. The studies were largely experimental and looked into the transmission response of fully as well as sparsely loaded FSSs. The transmission response of a fully loaded square loop array, modelled by means of an Equivalent Circuit approach, is similar to the one depicted in [9]. The authors reduced the number of active devices by a factor of two. The resonant frequency f_r, due to an ON-state, occurs at the same frequency as that of a fully loaded square loop array, resonating at 12.4 GHz. However, when the diodes are switched off, the active surface becomes nearly transparent at f_r and its transmission response exhibits a

downward shift of f_r, which occurs at 10.3 GHz, rather than the upward displacement which is the case of the transmission response of the fully loaded square loop FSS in [9]. In another attempt to reduce the number of active devices employed the square loops were connected together by short circuiting them. In the OFF state, the FSS resonates at 13.7 GHz. In the ON-state the loops are connected together forming an effectively inductive string of elements and behaving accordingly. The transmission loss was relatively high at about 2.5 dB, which the authors reckon could be reduced to < 0.5 dB if the inductance were to be increased by creating arrays with a larger periodicity. The transmission response of inductive/dipoles arrays were also studied by the authors. An array of strip dipoles were connected together with PIN diodes so as to create an array of inductive strips. Whether the FSS is composed of an array of dipoles or inductive strips depends on the bias voltage applied to the diodes. When the diodes are unbiased the structure behaves as an array of dipoles and resonates at 14.7 GHz. When the dipoles are shorted together, by applying a forward bias voltage, the structure becomes an array of transmitting inductive strips. The transmission response shows that at the resonance frequency there is a loss of 2 dB. This loss can, nevertheless, be reduced by increasing the inductance of the strips through narrowing the elements width. The number of active devices was reduced by interspersing the array with continuous inductive strips. In this configuration the dipoles still provide a strong resonance.

Bibliography

[1] Chekroun, C., Herrick, D., Michel, Y., Pauchard, R., Vidal, P., *Radant: New method of Electronic Scanning*, Microwave Journal, 1981, pp. 45-53.

[2] Dittrich, K.W., *Multifunctional Skins*, Six European Electromagnetic Conference Proceedings, 1991, pp. 1-13.

[3] Philips, B., Parker, E.A., Langley, R.J., *Active FSS in an Experimental Horn Antenna Switchable between Two Beamwidths*, Electronic Letters, Vol. 31, No. 1, 1995, pp. 1-2.

[4] Sparkes J.J., *Semiconductor Devices: How They Work*, Van Nostrand Reinhold (International), 1987.

[5] Carroll, John E., *Physical Models for Semiconductor Devices*, Edward Arnold, 1974.

[6] Sigfrid Yngvesson, *Microwave Semiconductor Devices*, Kluwer Academic Publishers, 1991.

[7] Janaswamy, R., Shung-Wu, L., *Scattering from Dipoles Loaded with Diodes*, IEEE Transactions on Antennas and Propagation, Vol 36, No. 11, 1988, pp. 1649-1651.

[8] Shuley, N.V., *Diode Loaded Frequency Selective Surfaces*, Proceedings of JINA 92 International Conference on Antennas, Nice, France, 1992, pp. 313-316.

[9] Chang, T.K., Langley, R.J., Parker, E.A., *An Active Square Loop Frequency Selective Surface*, IEEE Microwave and Guided Wave Letters, Vol. 3, No. 10, 1993, pp. 387-388.

[10] Chang, T.K., Langley, R.J., Parker, E.A., *Active Frequency Selective Surfaces* IEE Proceedings on Microwave and Antenna Propagation, Vol. 143, No. 1, 1996, pp. 62-66.

Chapter 4

Dynamic Radar Absorbing Material

4.1 Introduction

The continuous or discrete tuning of a reflection null in real time over a broad frequency band is a very attractive design philosophy to create dynamic radar absorbing materials (DRAM). However, the most fundamental reason to implement broadband adaptive frequency properties into the frequency characteristics of passive absorbers is to circumvent the fundamental limitations of the constitutive parameters of materials. These are known to impose limitations on the absorption bandwidth of metal backplane absorbers of fixed thickness [1], viz Salisbury screens and magnetic absorbers.

In the area of absorber design it is well known that a trade-off exists between absorption bandwidth and absorber thickness [2]. For example, a highly desirable narrow-thickness absorber has, in general, a highly undesirable narrow band absorption response. On the other hand, a relative large absorption bandwidth response goes hand in hand with a highly undesirable thick absorber. This

absorption-bandwidth/absorber-thickness trade-off is mainly due to the limitations imposed by the constitutive parameters of conventional materials.

The focus of this chapter is, thus, to present a novel absorber design philosophy, which yields a broadband absorption solution without the need to rely on material properties.

The chapter will start with highlighting the fundamental design theory of PEC backplane absorbers, viz salisbury screens and magnetic absorbers. A discussion of the implications of the Kramers-Kronig law into a broadband absorption solution is also presented.

4.2 Broadband Absorption: Desirable Constitutive Parameters

The absorption concept based on the matched-wave impedance principle fundamentally requires that the input impedance $Z_{in}(\omega)$ at the front surface of an absorber standing in free space be equal to the characteristic impedance of air, Z_o. This, which allows complete transmission of the incident EM energy through the front interface, makes the magnitude of the reflection coefficient $\Gamma(\omega)$ zero. Such that

$$\Gamma(\omega) = \frac{1 - Z_{in}(\omega)/Z_o}{1 + Z_{in}(\omega)/Z_o} = 0 \tag{4.1}$$

In terms of material properties, $Z_{in}(\omega)$ and Z_o are given, respectively, by

$$Z_{in}(\omega) = \sqrt{\frac{\mu_r(\omega)\mu_o}{\epsilon_r(\omega)\epsilon_o}} \tag{4.2}$$

$$Z_o = \sqrt{\frac{\mu_o}{\epsilon_o}} \tag{4.3}$$

where $\mu_r(\omega)$ and $\epsilon_r(\omega)$ are the complex relative permeability and permittivity, respectively, of the employed material; and μ_o and ϵ_o are the permeability and permittivity of free space. It then follows that, in terms of material properties, a broadband impedance match, which extends from DC to daylight, can be achieved providing that $\mu_r(\omega)$ and $\epsilon_r(\omega)$ be equal for all design frequencies. Such that

$$\mu_r(\omega) = \epsilon_r(\omega) \tag{4.4}$$

4.3 RAM on a Conducting Backplane: Fundamental Limits of Absorption Bandwidth

Radar absorbing materials based on conducting backplanes are, generally, built with either dielectric or magnetic/dielectric materials. The absorption properties of these absorbers are, in general, of a resonant nature and, as such, they degrade below and above a resonant frequency. This resonant effect, which introduces restriction on wide band absorption, is fundamentally imposed by the frequency dependence of the constitutive parameters (ϵ_r, μ_r) of the materials employed to build the absorber. The frequency characteristics of dielectric and magnetic materials are fundamentally different to those expected in order to generate a wideband absorption solution on the frequency characteristics PEC backplane absorbers.

Dielectric Based Absorbers (Salisbury Screen)

A Salisbury screen is a narrowband absorber built with dielectric materials. As displayed in figure 4.1, it consists of a 377 Ω/sq resistive layer placed at $\lambda/4$ from

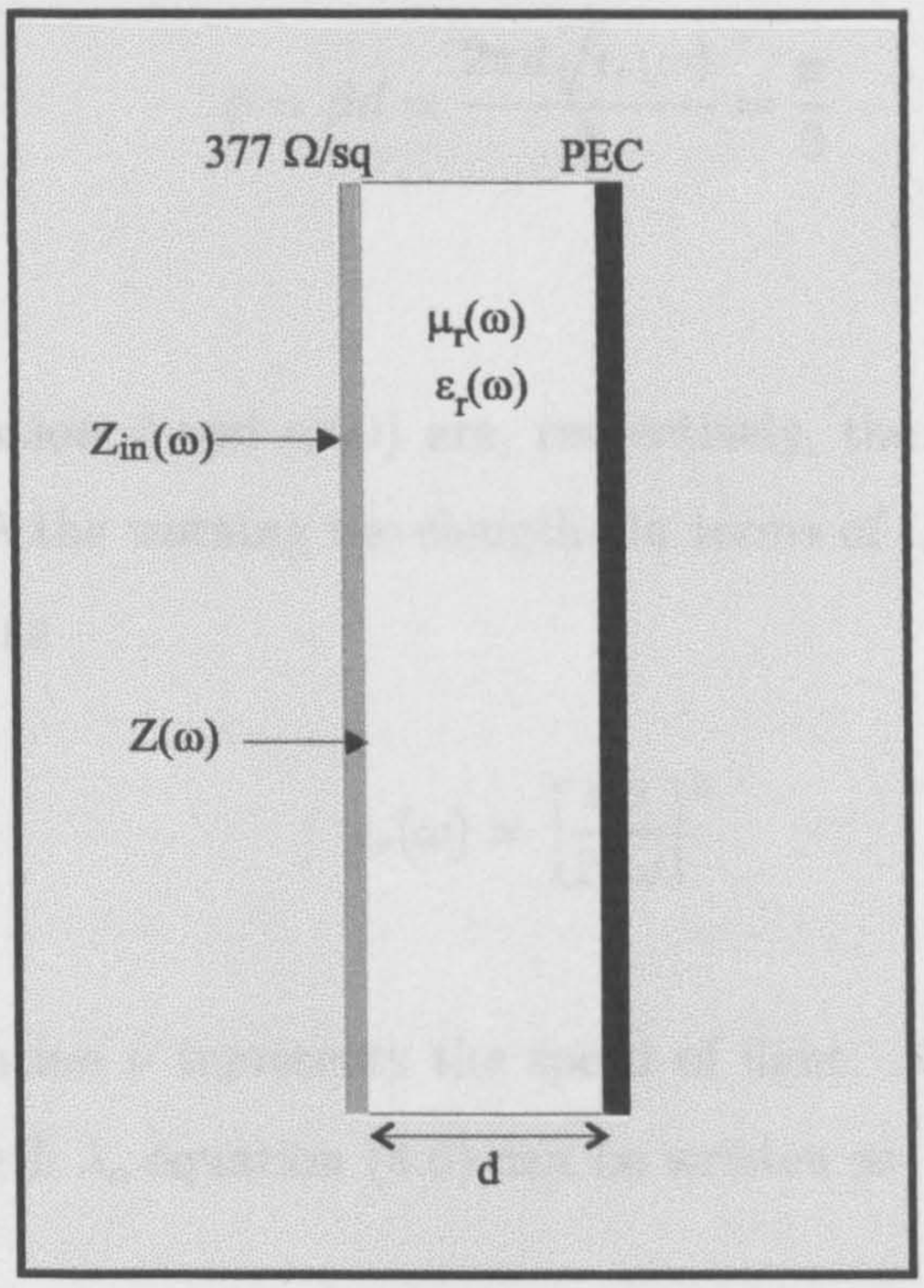

Figure 4.1: Schematic diagram of a Salisbury screen absorber.

a PEC back-plane. In order to achieve transmission of the incoming radiation, the electric field must, in theory, be a maximum at the dielectric-resistive sheet interface. Under this condition the impedance $Z(\omega)$ at the dielectric-resistive sheet interface becomes a maximum. $Z(\omega)$ is given by

$$Z(\omega) = jZ_m(\omega)\tan[\beta d] \tag{4.5}$$

where $Z_m(\omega) = \sqrt{\mu_r(\omega)/\epsilon_r(\omega)}$ and $\beta = \frac{2\pi}{\lambda}\sqrt{\mu_r(\omega)\epsilon_r(\omega)}$.

From equation (4.5) it can be seen that there are two ways to make $Z(\omega)$ a maximum. First, it can be achieved through employing materials with substantially large permeabilities since ϵ_r is usually greater than unity. A second method to maximise $Z(\omega)$ is through making the phase of the electric field ϕ equal to $\pi/2$, in conjunction with using materials with $\mu_r(\omega) = 1$. Such that

$$\phi = \beta d = \frac{2\pi d\sqrt{\epsilon_r(\omega)}}{\lambda} = \frac{\pi}{2} \tag{4.6}$$

In the above equation d and $\epsilon_r(\omega)$ are, respectively, the absorber thickness and permittivity and λ the working wavelength. In terms of $\epsilon_r(\omega)$ the above equation can be re-written as

$$\epsilon_r(\omega) = \left[\frac{\pi\nu}{2d\omega}\right]^2 \tag{4.7}$$

In the above equation ν represents the speed of light. Now as a function of the resonant wavelength λ_o equation (4.6) can be written as

$$\lambda_o = 4d\sqrt{\epsilon_r(\omega)} \tag{4.8}$$

Equation (4.7) shows the dependence of ϵ_r on both frequency and absorber thickness, being $1/\omega^2$ and $1/d^2$, respectively. Now providing that the thickness of the absorber is constant, it then follows that the concept of a wideband absorption solution in terms of the constitutive parameters of material can be achieved through computing at each frequency the value of $\epsilon_r(\omega)$.

The aforementioned, immediately, suggests that the proposed ideal broadband-absorption design, based on purely dielectric materials, fundamentally requires that the dielectric medium be of a dispersive nature. For a dispersive medium, the real and imaginary parts of $\epsilon_r(\omega)$ are defined by the Kramers-Kronig relations as [3] (Portis, 1978)

$$\epsilon'(\omega) = \epsilon_0 + \frac{2}{\pi}\int_0^\infty \frac{\epsilon''(\omega')}{\omega'^2 - \omega^2}\omega' d\omega' \tag{4.9}$$

$$\epsilon''(\omega) = -\frac{2\omega}{\pi}\int_0^\infty \frac{\epsilon'(\omega')}{\omega'^2 - \omega^2}d\omega' \tag{4.10}$$

where

$$\epsilon(\omega) = \epsilon'(\omega) - j\epsilon''(\omega) \tag{4.11}$$

As shown by the above equations, the Kramers-Kronig relationship restricts the interdependence between the real and imaginary part of $\epsilon_r(\omega)$. This raises an important issue concerning the use of dielectric materials in the design of a constant and small thickness Salisbury screen with a wideband absorption response. A broadband absorption solution requires that the medium be dispersive. For this the real and imaginary parts of $\epsilon_r(\omega)$ must co-exist, i.e. the dielectric material must have loss associated with it. When the medium is lossy, the amplitude of the electric field will be attenuated along thr medium. Attenuation is frequency dependent so the shape of the electric field is distorted.

Magnetic/Dielectric Based Absorbers

It is also possible to achieve radar cross section (RCS) reduction by placing lossy magnetic materials on a conducting back-plane. This type of absorber, known as a magnetic absorber, is shown schematically in figure 4.2. In order to achieve zero reflection the absorber design requires that the magnetic field be a maximum on the metallic surface. This is achieved by making the structure's input impedance, $Z_{in}(\omega)$, equal to Z_o. Such that

$$Z_{in}(\omega) = Z_m(\omega)\tanh\gamma d = Z_o \tag{4.12}$$

where

$$Z_m(\omega) = \sqrt{\frac{\mu_o(\mu_r'(\omega) - j\mu_r''(\omega))}{\epsilon_o(\epsilon_r'(\omega) - j\epsilon_r''(\omega))}} \tag{4.13}$$

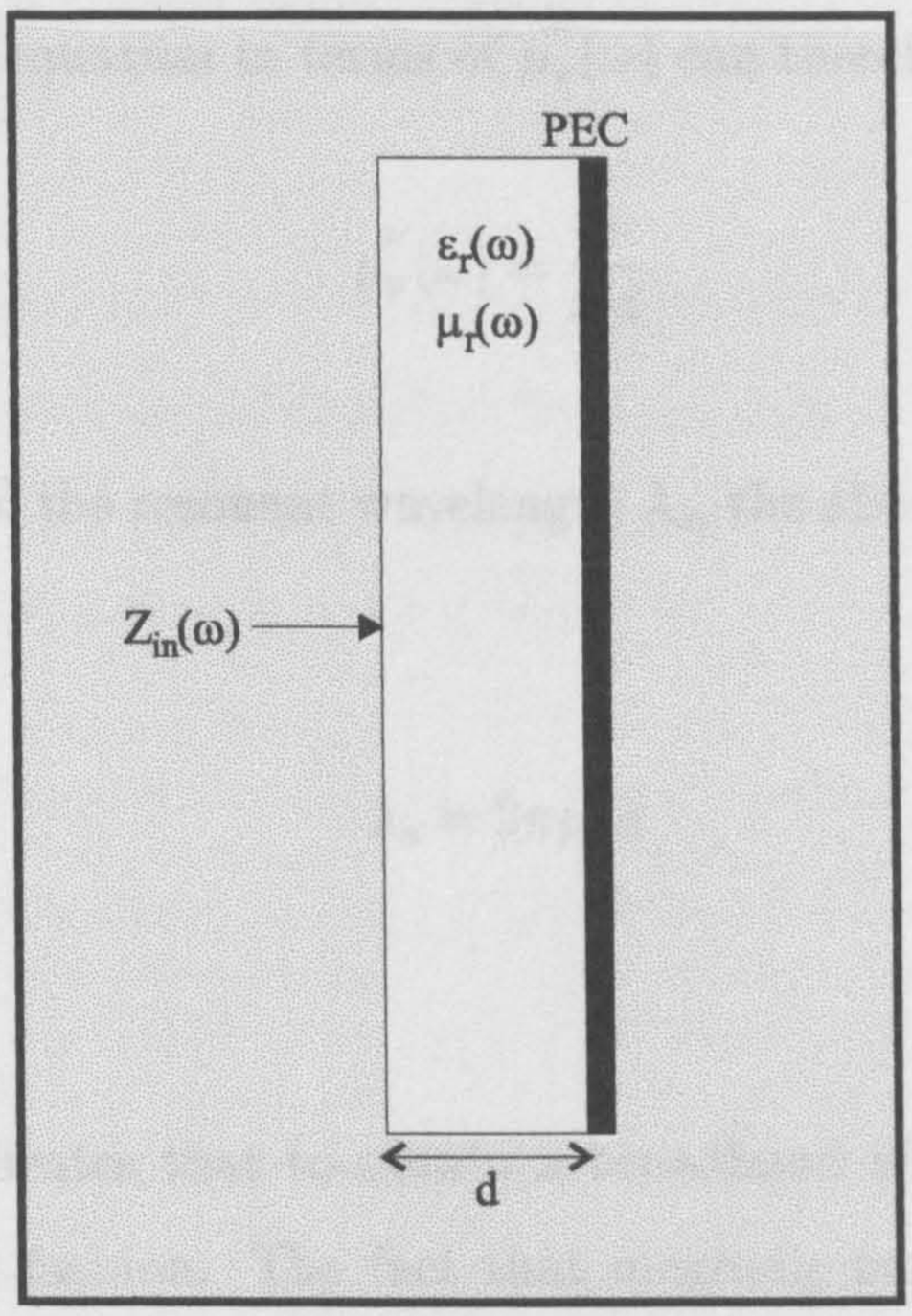

Figure 4.2: Schematic diagram of a magnetic absorber.

$$\gamma = j\omega\sqrt{\mu_o\epsilon_o(\mu_r'(\omega) - j\mu_r''(\omega))(\epsilon_r'(\omega) - j\epsilon_r''(\omega))} \tag{4.14}$$

where $\mu_r'(\omega)$ and $\mu_r''(\omega)$ are the material's real and imaginary parts of the complex relative permeability μ_r, respectively; $\epsilon_r'(\omega)$ and $\epsilon_r''(\omega)$ are the materials' real and imaginary parts of the complex permittivity $\epsilon_r(\omega)$, respectively. Now, providing that the dielectric loss of the medium is small, such that $\epsilon_r'(\omega) \gg \epsilon_r''(\omega)$, and that the medium's magnetic loss is large, such that $\mu_r''(\omega) \gg \mu_r'(\omega)$, equation (4.12) can be re-written in terms of the absorber's thickness d as

$$d = \frac{2\pi}{\lambda\sqrt{j\mu_r''(\omega)\epsilon_r'(\omega)}} tanh^{-1}\left[\sqrt{\frac{j\epsilon_r'(\omega)}{\mu_r''(\omega)}}\right] \tag{4.15}$$

In general the argument of the above equation is small[1] for most practical magnetic RAM [4]. The equation in terms of $\mu_r''(\omega)$ can therefore be re-written as

$$\mu_r''(\omega) = \frac{\nu}{\omega d} \tag{4.16}$$

Now, as a function of the resonant wavelength λ_o, the above equation can be written as

$$\lambda_o = 2\pi\mu_r'' d \tag{4.17}$$

Equation (4.16) indicates that to obtain a broadband absorption solution $\mu_r''(\omega)$ must vary in a $1/\omega$ fashion. The fact that magnetic materials are dispersive in nature [4] immediately suggests that there exists a possibility that broadband absorption can be achieved by means of employing such materials. However, ferromagnetic permeability is fundamentally a resonant phenomenon and, as such, both $\mu_r'(\omega)$ and $\mu_r''(\omega)$ must vary widely and rapidly as functions of frequency [5]. This leads to the realization that the frequency variation of magnetic materials is not of a $1/\omega$ nature, which is the fundamental requirement imposed by equation (4.16) to achieve a broadband absorption solution. Also the condition $\mu_r''(\omega) \gg \mu_r'(\omega)$ is fundamentally impossible since magnetic materials are believed by Wallace [5] to obey the Kramers-Kronig conditions. Work carried out by Walser [6] predicted the real and imaginary parts of the susceptability and an almost perfect Kramers-Kronig transform is achieved. As a consequence, a wideband absorption solution based on lossy magnetic materials of fixed thicknesses cannot be realized in practice.

In a recent paper published by Rozanov [7] the fundamental limit on the absorption-bandwidth integral is established. This is given by

[1] the approximation $\tanh x \cong x$ is therefore applicable

$$\left|\int_0^\infty \ln R(\lambda)\right| \leq 2\pi^2 \mu h \tag{4.18}$$

In the above equation $R(\lambda)$ is the reflection coefficient, μ is the permeability of the material employed to build the absorber, and h is the absorber thickness. An absorber to give at least R_{dB} absorption at all wavelengths shorter that a limiting wavelength must have a thickness of at least [1]

$$h = \frac{172\mu\lambda_o}{R_{dB}} \tag{4.19}$$

In the above equation λ_o is the wavelength at the band centre. The above equation indicates that the thickness of an absorber with a broadband absorption bandwidth exhibits a $1/R_{db}$ reflection coefficient dependence. Now, providing that $\mu = 1$ to achieve smallest absorber thickness, equation (4.19) shows that a large absorption corresponds to small thickness absorbers. The relationship shown in equation (4.19) assumes magnetic materials with constant permeability. Ferromagnetic permeability is, however, a resonance phenomenon and hence μ must vary widely and rapidly as a function of frequency. This indicates that $\mu = 1$ is an unlikely event as the frequency is increased. μ will vary with frequency and therefore to maintain the same level of absorption the absorber thickness will have to be varied accordingly.

The above discussion indicates that a broadband absorption solution is impossible in practice solely through exploiting material properties. As shown by equation (4.8) a broadband absorption solution can, nonetheless, be fundamentally achieved through varying an absorber thickness d. Equation (4.8) indicates that the resonant wavelength λ_o can be translated in frequency through varying d while keeping ϵ_r constant. By adopting this approach, there is no need to rely upon material properties to achieve a broadband absorption solution.

4.4 Dynamic Radar Absorbing Material (DRAM)

In the previous section it has been shown how the constitutive parameters of materials impose fundamental limitations upon the absorption bandwidth of fixed-thickness radar absorbing materials based on a conducting backplane. One way to circumvent such wideband absorption limitations is to introduce adaptive properties into a metal backplane absorber. Built-in adaptive properties can be used to vary the absorber thickness. This, as shown by equations (4.8) and (4.17) enforces the matched impedance concept at adjacent frequencies over a wideband. Such a solution is, thus, independent of material properties.

Adaptive properties may be built into an absorber in various ways. One method is to build into an absorber a mechanical actuator, as depicted in figure 4.3, which can be used to vary the absorber thickness. The disadvantage in employing such method is mechanical fragility coupled with a slow switching response. Another method that can be used to overcome materials' parameters restrictions on wideband absorption is to embed adaptive complex impedance structures into a salisbury screen of fixed and small thickness.

The tuning of a single reflection null over a multi-octave frequency band is an alternative design philosophy to achieve a broadband absorption solution. Figure 4.4 shows the frequency profile of an absorber based on a broadband tunable reflection null. Such design philosophy has been demonstrated by researchers at the University of Sheffield [8]. At Sheffield the tuning of a reflection null was implemented through the use of a single adaptive impedance structure. This is based on a textile substrate loaded with either conducting polymers such as polypyrrole or polyaniline. The absorber configuration was a Salisbury screen wherein the 377 Ω/sq resistive sheet is replaced with the adaptive impedance structure. By applying an external control signal the structure's impedance properties are changed, thus resulting in the ability to tune a reflection null.

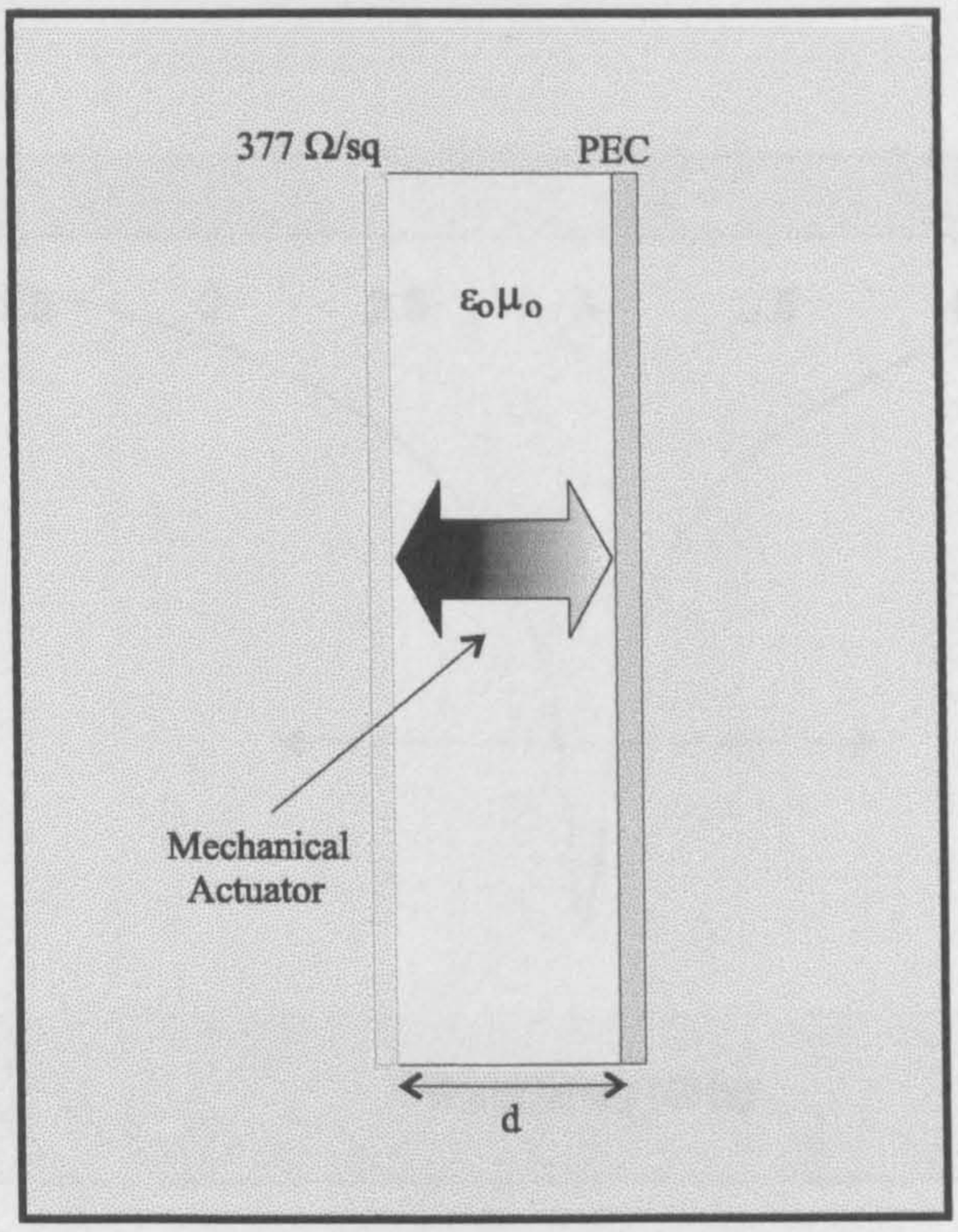

Figure 4.3: Adaptive salisbury screen absorber.

4.4.1 DRAM based on Multiple Adaptive Impedance Structures

As explained earlier a broadband absorption solution is fundamentally impossible to achieve in practice with conventional materials. A broadband absorption solution can, however, be implemented through embedding a number of bi-state planar adaptive impedance structures with an open-short circuit frequency response within a metal backplane absorber of fixed-thickness. The use of such structures facilitates the partitioning of an absorber thickness, thus enforcing the wave match impedance concept at adjacent frequencies over a wideband. Through this method a number of reflection nulls can be generated over a wide frequency band. This design philosophy is fundamentally possible to implement in practice.

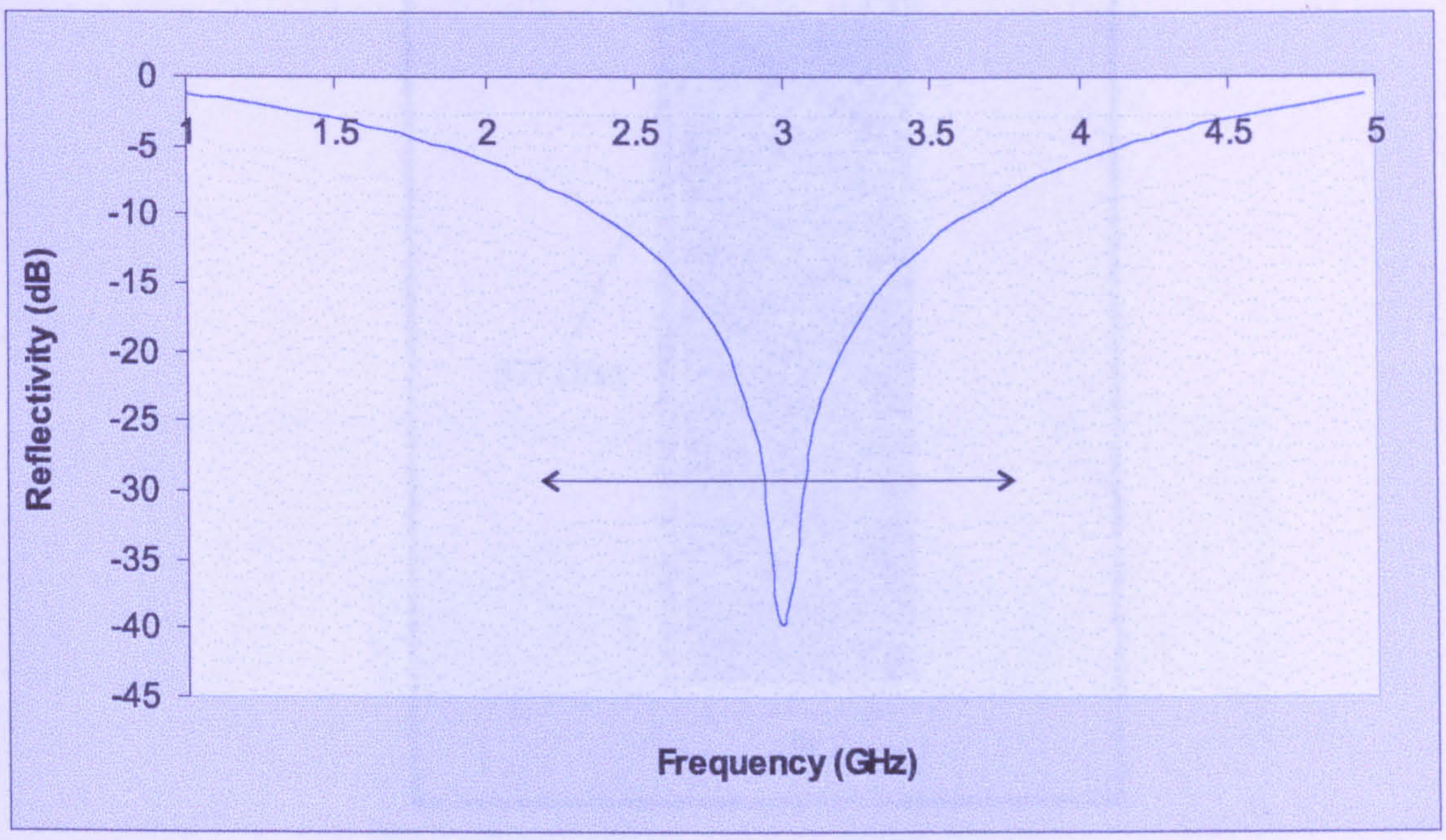

Figure 4.4: Frequency profile of an adaptive broadband absorber with a single reflectivity null.

DRAM Design Philosophy

Figures 4.5 and 4.6 show schematic diagrams of dynamic absorbers incorporating, respectively, a single (A1) and a multiple number (A1 through An) of bi-state adaptive complex impedance structures (ACISs) with an short/open circuit response. Both of these absorbers are based on a Salisbury screen device.

The use of a single ACIS reduces the complexity of the problem, however, by making use of more than one ACIS in the DRAM design more degrees of freedom are achieved, at the expense of a far more complex design. This results in a DRAM with a far more sophisticated solution S in terms of more discrete reflection nulls spread over a broadband.

Theoretically, the DRAM design solution S is composed of a set of sub-solutions or states s_N whose number of elements N is dictated by the number n of AFSSs used. The design solution is expressed as

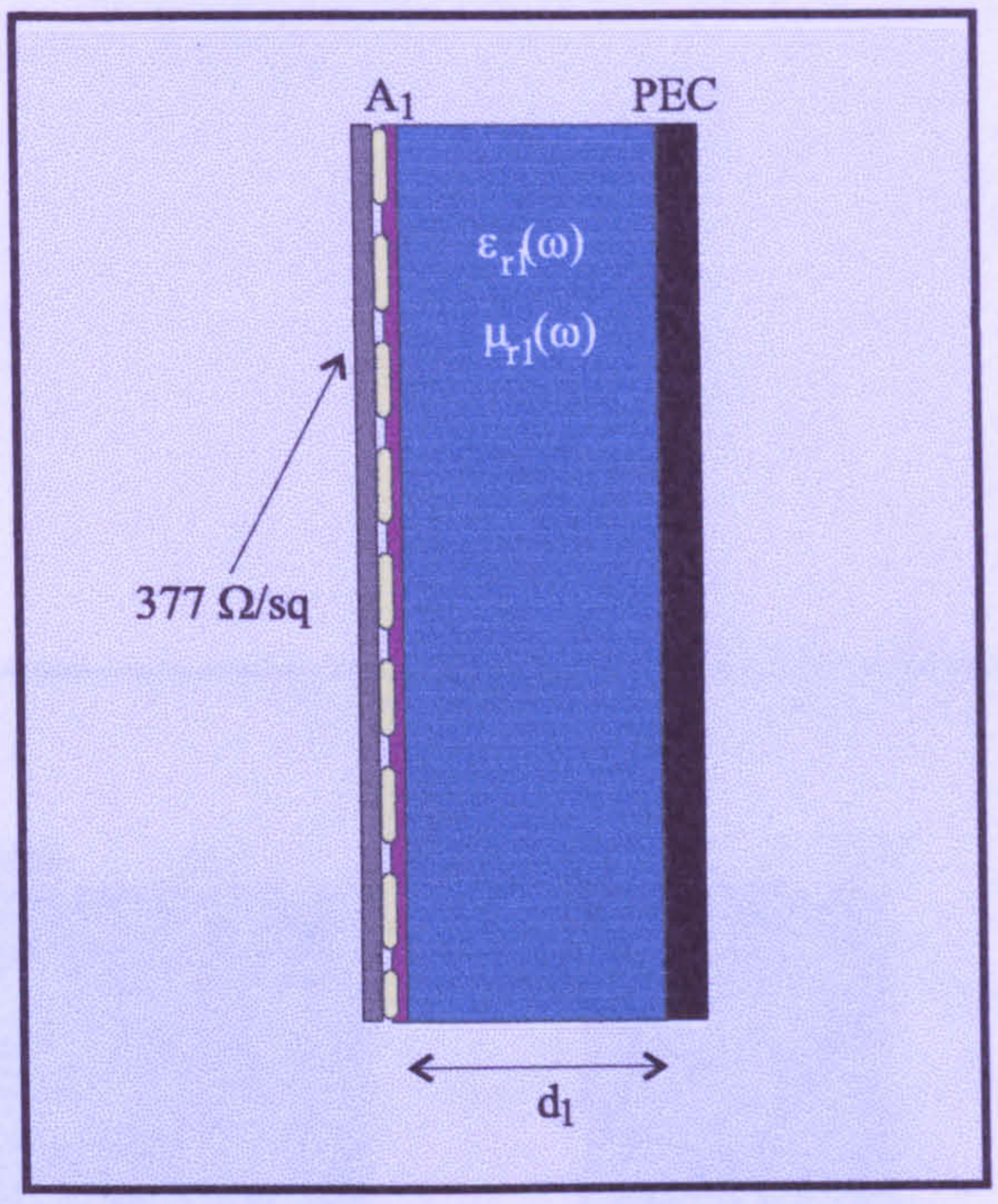

Figure 4.5: Schematic diagram of a typical adaptive absorber incorporating a single bi-state adaptive complex impedance structure.

$$S \in \{s_1, s_2, ..., s_N\} \tag{4.20}$$

Now, due to the bi-state characteristic of the ACISs, the maximum number of sub-solutions or states N obeys the binary rule

$$N = 2^n \tag{4.21}$$

where n is the number of ACISs. This implies that for $n = 1$, a solution composed of 2 sub-solutions or states can be achieved. Whereas for $n = 2$, the overall solution is composed of 4 sub-solutions. This indicates, in theory, that the more ACISs embedded within the absorber the more sub-solutions or states can be generated. This therefore suggests the possibility to realize an absorber with a great number of reflection nulls. The latter, however, is not the case since employing more than two ACISs will result in the generation of redundancy in the absorber

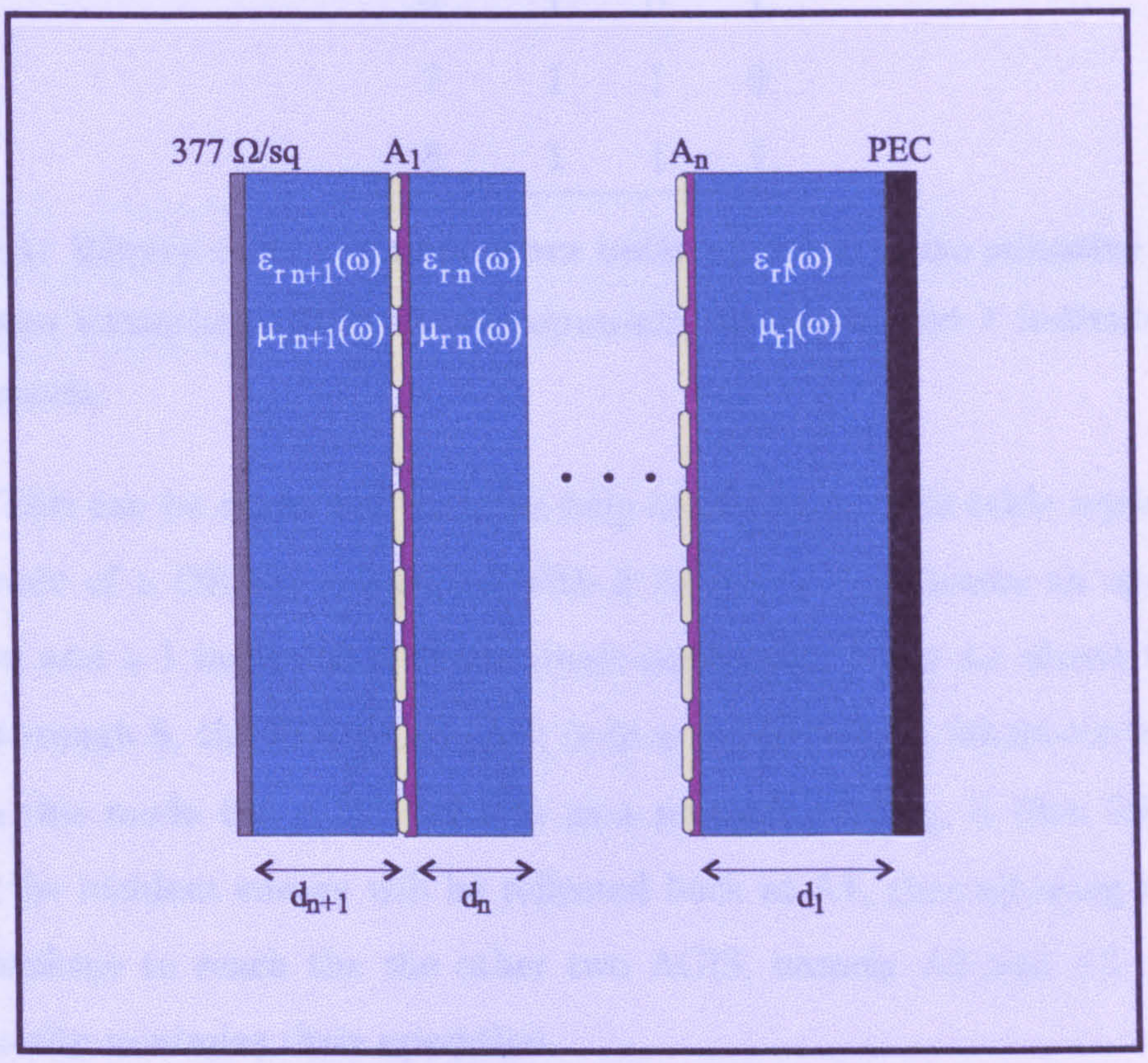

Figure 4.6: Schematic diagram of a typical dynamic absorber incorporating a multiple number of bi-state adaptive complex impedance structures (n represents the number of adaptive complex impedance structures employed in the design.

State	A1	A2	A3
1	0	0	0
2	0	0	1
3	0	1	0
4	0	1	1
5	1	0	0
6	1	0	1
7	1	1	0
8	1	1	1

Table 4.1: Binary code of an absorber built with 3 bi-state adaptive complex impedance structures. 0 indicates open-circuit mode and 1 indicates short-circuit mode.

design. This can be explained with the help of table 4.1. This table represents the binary code of a DRAM embedded with 3 ACISs: a 0 indicates an open-circuit condition and a 1 indicates a short-circuit condition. Table 4.1 shows that from state 5 through 8, the first ACIS (A1) is in a constant high (short-circuit mode). Since in this mode the ACIS behaves as a metallic surface, it then follows that most of the incident energy will be reflected back at A1, thus allowing very small energy leakage to reach the the other two ACIS, namely A2 and A3. This will substantially minimize their operation.

Tables 4.2 and 4.3 display the binary code of DRAMs embedded with a single and two ACISs, respectively.

Discrete Frequency Response

Figure 4.7 shows the theoretical frequency solution S of a Salisbury screen absorber which has been embedded with a multiple number n of bi-state ACISs each with open/short circuit characteristic. Each trace represents a different state or sub-solution s_N. As shown in the figure, the reflection nulls are spread over a

State	A1
1	0
2	1

Table 4.2: Binary code of an absorber built with a single bi-state adaptive complex impedance structures. 0 indicates open-circuit mode and 1 indicates short-circuit mode..

State	A1	A2
1	0	0
2	0	1
3	1	0
4	1	1

Table 4.3: Binary code of an absorber built with 2 bi-state adaptive complex impedance structures. 0 indicates open-circuit mode and 1 indicates short-circuit mode.

broad frequency band.

It is important to know that although all traces for the different sub-solutions are shown simultaneously on the plot, in reality, each trace or sub-solution is present depending on the ACIS present state, as shown in either table 4.2 and 4.3.

The operation of the proposed broadband RAM is as follows. With reference to figure 4.7 and table 4.3, f_1 is generated, for example, by means of setting the ACISs to arbitrarily conditions, such as short circuit and/or open circuit. Now, to switch to f_2 the ACISs are changed to a different set of conditions as shown in table 4.3. In this way f_1 is switched OFF, resulting in f_3 being turned ON. And so on and so forth.

Tuning Frequency Response

The aforementioned generates an absorber whose frequency response depicts a number of switchable reflection nulls discretely spread over a wide frequency band. For such absorber to show absorption properties over the entire frequency band (i.e. between every two adjacent frequency spot), narrowband tunability of its discretely placed reflection nulls must, however, be shown in its frequency properties. For this, the ACISs employed not only must depict in their frequency profile an open and short circuit characteristic, but also a linear and continuous response between their short and open circuit modes.

The following is a discussion on how narrowband tunability of adjacent and coarsely tuned reflection nulls can be achieved through employing ACI structures, whose complex impedance can be linearly and continuously varied.

Consider the diagram in figure 4.8. The diagram schematically depicts a salisbury screen absorber of thickness d_T (where $d_T = d_1 + d_2$), where $\epsilon_{r1} = \epsilon_{r2}$. An ACI structure is embedded within the dielectric as shown in the figure. The input

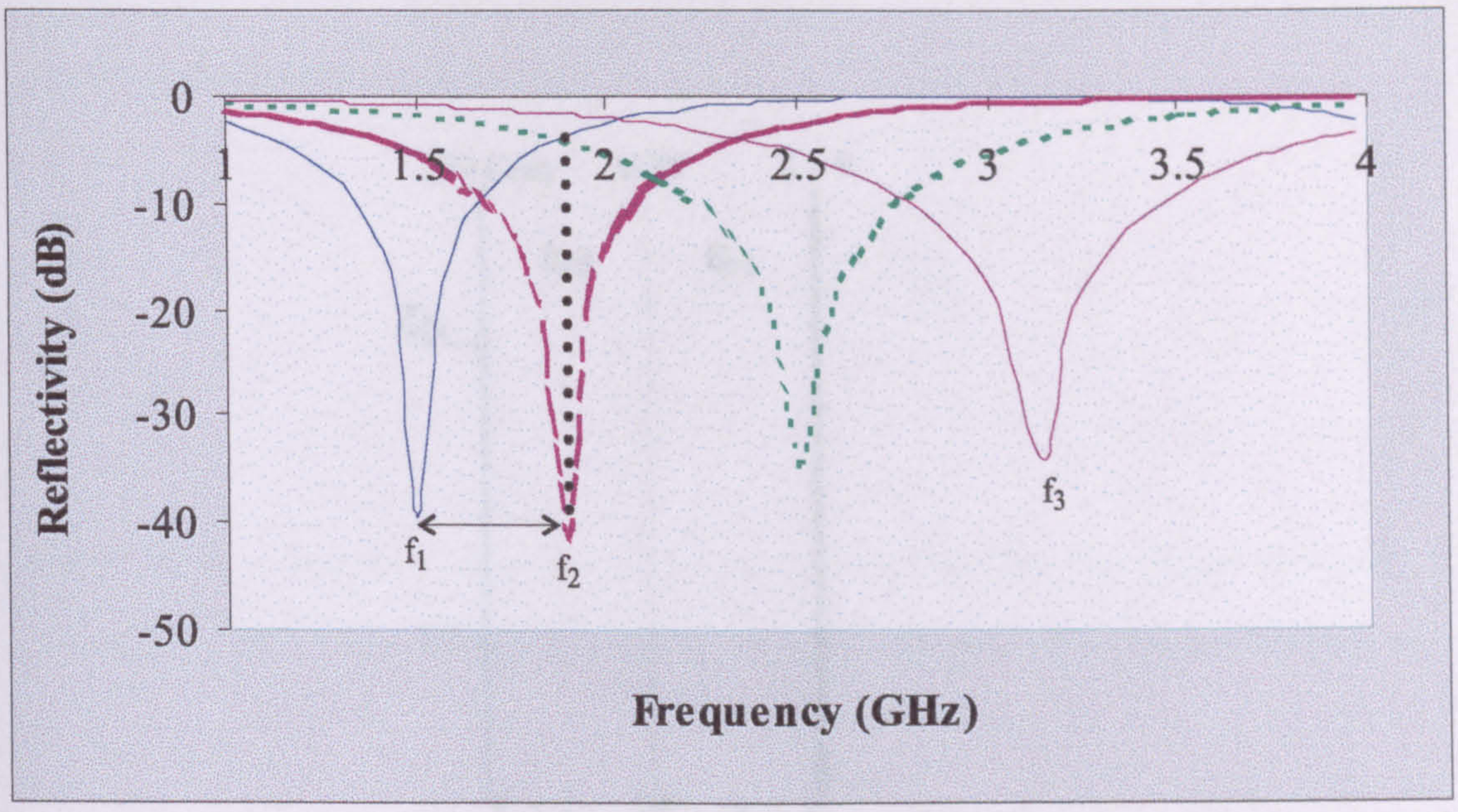

Figure 4.7: Frequency profile of a broadband multi-resonant absorber.

impedance Z_{in} at the interface just before the 376.6 Ω resistive film is given by

$$Z_{in} = jZ_o^2 \frac{\frac{X\tan[\beta d_1]}{Z_o\tan[\beta d_1]+X} + \tan[\beta d_2]}{Z_o - \frac{Z_o X\tan[\beta d_1]}{Z_o\tan[\beta d_1]+X}\tan[\beta d_2]} \tag{4.22}$$

In order to implement the matched-wave concept $Z_{in} \to \infty$. For this, the denominator of equation(4.22) must be equal to zero. Such that

$$Z_o - \frac{Z_o X\tan[\beta d_1]}{Z_o\tan[\beta d_1]+X}\tan[\beta d_2] = 0 \tag{4.23}$$

or

$$Z_o\tan[\beta d_1] + X - X\tan[\beta d_1]\tan[\beta d_2] = 0 \tag{4.24}$$

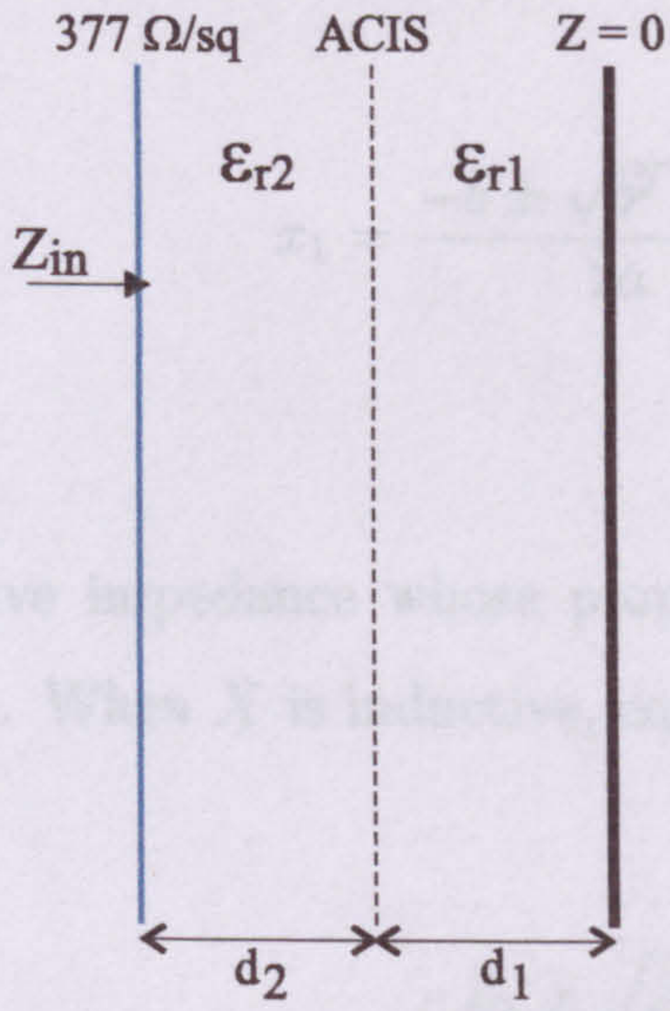

Figure 4.8: Tunable ACI structure embedded within a dielectric material placed on a PEC plane.

Now let $\tan[\beta d_1] = x_1$ and $\tan[\beta d_2] = x_2$. Equation (4.24) can be rewritten as

$$Z_o x_1 + X - X x_1 x_2 = 0 \tag{4.25}$$

Now to show a reflection null tuning response as a function of reactive impedance, let $d_1 = d_2$ (i.e. the ACI structure is placed in the middle of the Salisbury screen absorber). For this $x_1 = x_2$. Equation (4.25) can be rewritten as

$$-X x_1^2 + Z_o x_1 + X = 0 \tag{4.26}$$

$$\lambda_{o_{cap}} = \frac{2\pi\sqrt{\epsilon_r}d_1}{\arctan\left[\frac{-Z_o \pm \sqrt{Z_o^2+4X^2}}{2X}\right]} \tag{4.31}$$

where $\lambda_{o_{cap}}$ is the resonant wavelength. In order to ensure that $\lambda_{o_{ind}}$ and $\lambda_{o_{cap}}$ are positive quantities, the negative and positive solutions of equations (4.29) and (4.31), respectively, must be employed. Such that

$$\lambda_{o_{ind}} = \frac{2\pi\sqrt{\epsilon_r}d_1}{\arctan m} \tag{4.32}$$

where m is given by

$$m = Z_{o_{eff}}\left[\left(1+\left(\frac{1}{Z_{o_{eff}}}\right)^2\right)^{1/2}+1\right] \tag{4.33}$$

And

$$\lambda_{o_{cap}} = \frac{2\pi\sqrt{\epsilon_r}d_1}{\arctan n} \tag{4.34}$$

where n is given by

$$n = Z_{o_{eff}}\left[\left(1+\left(\frac{1}{Z_{o_{eff}}}\right)^2\right)^{1/2}-1\right] \tag{4.35}$$

where $Z_{o_{eff}}$ is given by

$$Z_{o_{eff}} = \frac{376.6}{\sqrt{\epsilon_{r_{eff}}}} \tag{4.36}$$

Equation (4.26) is a quadratic equation whose solutions can be found through employing the following equation

$$x_1 = \frac{-b \pm \sqrt{b^2 - 4ac}}{2a} \tag{4.27}$$

Now X is a reactive impedance whose properties can be either inductive (X) or capacitive ($-X$). When X is inductive, equation (4.27) can be written as

$$x_{1_{ind}} = \frac{-Z_o \pm \sqrt{Z_o^2 + 4X^2}}{-2X} \tag{4.28}$$

Since $x_1 = \tan[\beta d_1]$, the above equation can be expressed as

$$\lambda_{o_{ind}} = \frac{2\pi\sqrt{\epsilon_r} d_1}{\arctan\left[\frac{-Z_o \pm \sqrt{Z_o^2+4X^2}}{-2X}\right]} \tag{4.29}$$

where $\lambda_{o_{ind}}$ is the resonant wavelength. For a capacitive X, x_1 is given by

$$x_{1_{cap}} = \frac{-Z_o \pm \sqrt{Z_o^2 + 4X^2}}{2X} \tag{4.30}$$

And $\lambda_{o_{cap}}$ is thus given by

and $\epsilon_{r_{eff}}$

$$\epsilon_{r_{eff}} = 4X^2\epsilon_r \tag{4.37}$$

Equations (4.32) and (4.34) clearly show that the absorption properties of a Salisbury screen absorber can, indeed, be tuned in frequency through employing adaptive complex impedance structures of purely capacitive or inductive properties. The tuning of a reflection null over frequency is possible through effectively varying the dielectric properties of the absorber by a factor of $4X^2$, as shown by equation (4.37).

Now when $X = 0$, i.e. the embedded structure is a short circuit, equation (4.33) becomes

$$m = \infty \tag{4.38}$$

but $\arctan\infty = \pi/2$, and thus equation (4.32) becomes

$$\lambda_o = 4\sqrt{\epsilon_r}d_1 \tag{4.39}$$

or

$$\lambda_o = 4\sqrt{\epsilon_r}d_2 \tag{4.40}$$

or

$$\lambda_o = 2\sqrt{\epsilon_r}d_T \tag{4.41}$$

since $d_1 = d_2$ in the first instance and $2d_1 = d_T$ in the second instance. Also, when

$X \to \infty$, i.e. the embedded structure is an open circuit, equation (4.35) becomes

$$n = 1 \tag{4.42}$$

but $\arctan 1 = \pi/4$, and thus equation (4.34) becomes

$$\lambda_o = 8\sqrt{\epsilon_r} d_1 \tag{4.43}$$

or

$$\lambda_o = 4\sqrt{\epsilon_r} d_T \tag{4.44}$$

since $2d_1 = d_T$.

The above analysis clearly demonstrates that by switching between an open and a short circuit, the reflection-null properties of a Salisbury screen embedded with a purely reactive structure can be abruptly tuned between two frequencies.

Figure 4.9 and 4.10 depict the absorption wavelength (λ_o) characteristics as a function of reactance of a Salisbury screen absorber embedded with a purely reactive structure. Figure 4.9 shows the overall response, while figure 4.10 is a closed-up of figure 4.9. The absorber thickness is $d_T = 7.5$ mm, while its ϵ_r is 25. The reactive structure is placed in the middle of the absorber. From these figures, the following can be said

- As $X \to \pm\infty$, $\lambda_o \to 4\sqrt{\epsilon_r} d_T$.

- For a purely variable inductive screen. As $X \to 0$, $\lambda_o \to 4\sqrt{\epsilon_r} d_T/2$. The presence of a purely inductive reactance structure within the absorber, thus, effectively decreases the absorber thickness.

- For a purely variable capacitive screen. As $-X \to 0$, $\lambda_o \to (\gg 1)$ m - very

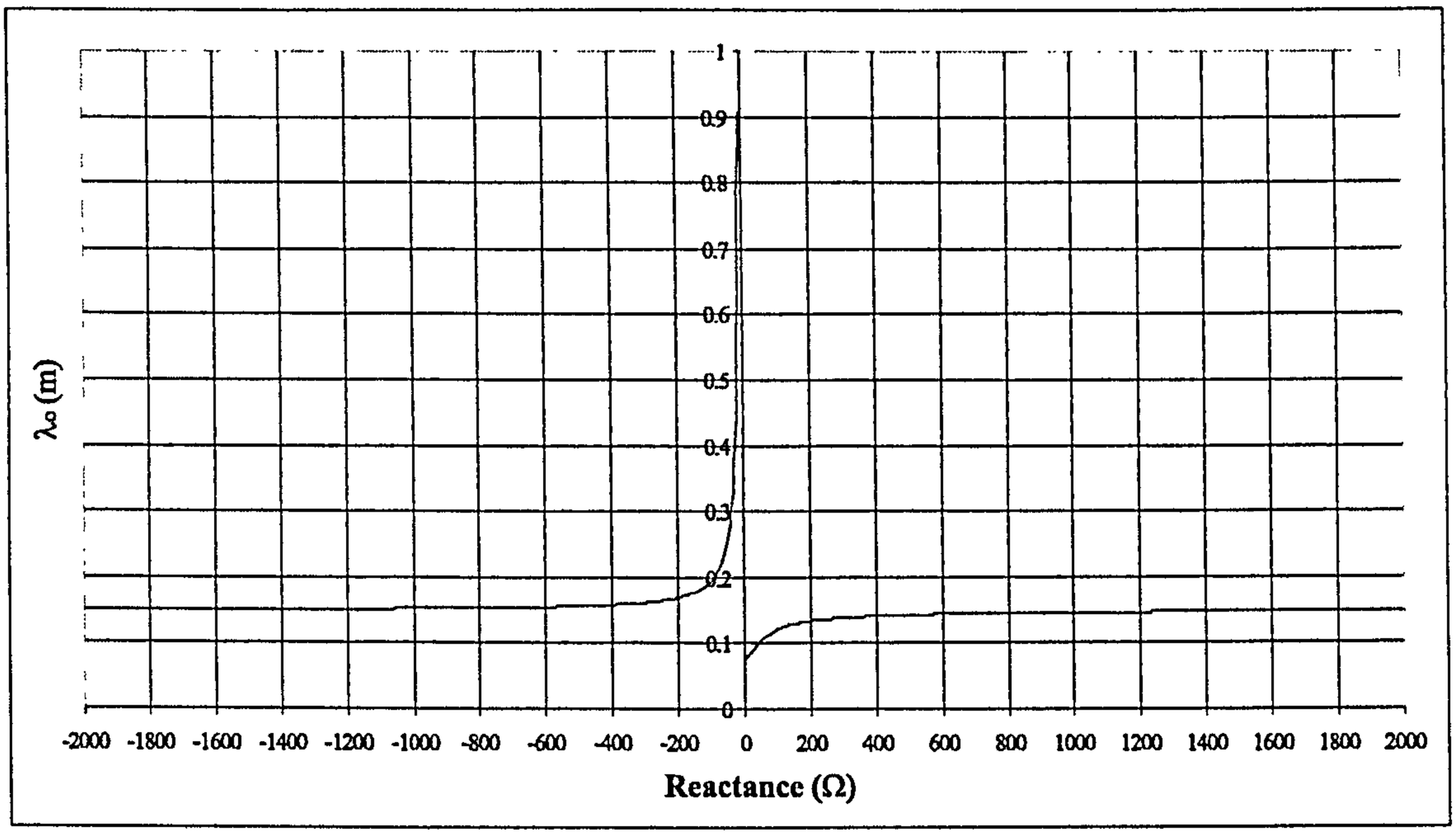

Figure 4.9: Absorption wavelength profile as a function of reactance of a Salisbury screen absorber embedded with a purely reactive structure. $d_T =$ 7.5 mm, $\epsilon_r = 25$, $d_1 = d_2$. λ_o is the resonant wavelength.

interesting result![2]. The presence of a purely capacitive reactance structure within the absorber, thus, effectively increases the absorber thickness.

For the case when $d_1 \neq d_2$, equation (4.25) will need to be solved. The author, however, envisages the following characteristics (please refer to figure 4.8)

- For the case where $d_2 < d_1$. The absorption bandwidth of the inductive absorber (i.e. an absorber embedded with a purely inductive screen) will be increased to $2\sqrt{\epsilon_r}d_2$, while the absorption bandwidth of the capacitive screen will be reduced.

- For the case where $d_2 > d_1$. The absorption bandwidth of the inductive absorber will decrease to $2\sqrt{\epsilon_r}(d_2 + \delta_x)$, ($\delta_x$ represents the increase of d_2 at

[2]for clarity, the absorption wavelength response was truncated close to 0. The wavelength does go to some infinity value near and including 0.

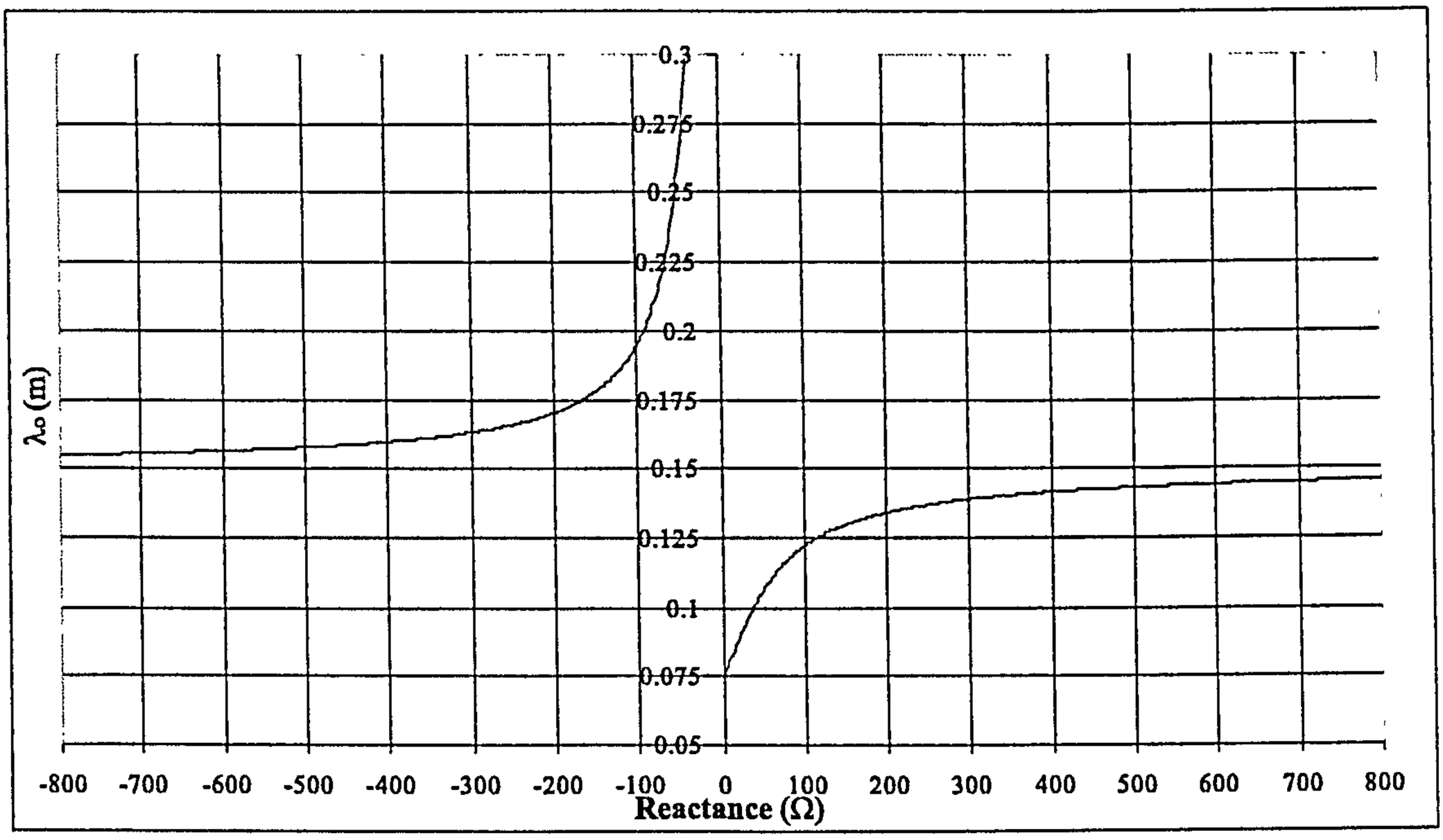

Figure 4.10: Absorption wavelength profile as a function of reactance of a Salisbury screen absorber embedded with a purely reactive structure (Close up of figure 4.9). $d_T = 7.5$ **mm,** $\epsilon_r = 25$, $d_1 = d_2$. λ_o **is the resonant wavelength.**

the expense of the decrease of d_1), while that of the capacitive absorber will increase.

- The absorption bandwidth of the capacitive absorber will change very little with the positioning of the capacitive reactive screen within the absorber.

The above points, however, will need to be mathematically proven.

In general, the frequency properties of a Salisbury screen absorber embedded with a purely reactive structure, having not only open and short electrical characteristics, but also variable reactive properties, and which is placed in the middle of the absorber is given by the following equation (Margarita's equation)

$$\lambda_o = \frac{\pi\sqrt{\epsilon_r}d_T}{\arctan M_{\pm}} \tag{4.45}$$

where

$$M_{\pm} = Z_{o_{eff}} \left[\left(1 + \left(\frac{1}{Z_{o_{eff}}} \right)^2 \right)^{1/2} \pm 1 \right] \tag{4.46}$$

where λ_o is the resonant wavelength, M_+ indicates that the absorber is embedded with a purely inductive screen, while M_- indicates that the absorber is embedded with a purely capacitive screen; $Z_{o_{eff}}$ is as given by equations (4.36) and (4.37); d_T is the absorber total thickness and ϵ_r the absorber's spacer permittivity.

4.5 Summary

A broadband absorption solution requires that the materials employed to build a PEC-backplane type absorber be of a dispersive nature with explicit variations of ϵ_r and μ_r as a function of frequency. As shown in this chapter, dispersive media are, however, governed by the Kramers-Kronig relation, which put very severe restrictions on the extent to which μ' and μ'' as well as ϵ' and ϵ'' can vary independently of each other. As a consequence of this, a broadband absorption solution is difficult to implement in practice on PEC-backplane radar absorbing materials.

In order to circumvent the fundamental limitations of conventional materials, a novel absorber design philosophy has been presented in this chapter. It consists of embedding a multiple number of bi-state adaptive complex impedance structures within a Salisbury screen. The structure must exhibit in its frequency properties not only a short and open circuit response, but also a continuous and linear response of purely reactive properties between the short and open circuit mode. The open and short circuit characteristics permit the abrupt partitioning of an absorber thickness. This, in turn, results in the generation of a number of switchable

reflection nulls spread over a broad frequency band. The continuous and linear reactive response, on the other hand, permits the tuning of a reflection null over a narrow frequency band, as shown by Margarita's equation. This design methodology allows a broadband absorption solution without the need to rely upon material properties. The latter is possible through effectively changing the dielectric properties of the absorber by a factor $4X^2$ - where X is the reactance. This, in turn, effectively increases or decreases the absorber thickness. An effective increase of the absorber thickness is achievable through using purely inductive screens, while and effective decrease of the absorber thickness can be realised through employing purely capacitive screens.

Bibliography

[1] Brewitt-Taylor, C. R., *Fundamental Limit on the Performance of Radar Absorbing Materials*, Digest of IEEE Antennas and Propagation Symposium, Orlando, Florida, Vol 3, July 1999, pp. 1938-1941.

[2] Weile, D. S., Michielssen, E., Goldberg, D. E.,, *Genetic Algorithm Design of Pareto Optimal Broadband Microwave Absorbers*, IEEE Transactions on Electromagnetic Compatibility, Vol 38, No. 3, August 1996, pp. 518-525.

[3] Portis, A. L., *Electromagnetic Fields: Sources and Media*, John Wiley and Sons, 1978.

[4] Vinoy, K. J., Jha, R. M., *Radar Absorbing Materials - From Theory to Design and Characterization*, Kluwer Academic Publishers, 1996.

[5] Wallace, J. L., *Broadband Magnetic Microwave Absorbers: Fundamental Limitations*, Transaction on Magnetics, Vol. 29, No. 6, 1993, pp. 4209-4214.

[6] Walser, R. M., *A Study of Thin Film Magnetodielectric*, Ph.D. Thesis, The University of Michigan.

[7] Rozanov, K. N., *Fundamental Limitation for Thickness to Bandwidth Ratio of radars Absorber*, Proceedings of PIERS-98, Nantes, France, 13-17 July 1998, p. 229.

[8] Chambers, B., *Surfaces with Adaptive Radar Reflection Coefficients*, Smart Materials and Structures, Vol. 6, 1997, pp. 521-529.

Chapter 5

Adaptive Control of Absorption

5.1 Introduction

Radar absorbing materials based on conducting backplanes are passive absorbers whose absorption bandwidths are highly limited by the constitutive parameters of materials [1], namely $\mu_r(\omega)$ and $\epsilon_r(\omega)$. Examples of these conventional absorbers are the Salisbury screen and magnetic absorbers. In chapter 4 a novel absorber design philosophy was presented. This method is used to increase the absorption bandwidth of a Salisbury screen without the need to rely upon material properties. The method makes use of bi-state adaptive complex impedance structures with open/short circuit characteristics. This facilitates input impedance matching at adjacent frequencies over a wideband through the partitioning of an absorber thickness. As shown in chapter 4, the latter is fundamental in the design of broadband absorbers based on conducting backplanes. Adaptive complex impedance properties, which are instigated by means of applying external stimuli, have been found, for instance, in conducting polymer composite materials [2] as well as in a number of AFSSs.

Before the absorber design philosophy presented in chapter 4 can be practically

implemented, bi-state adaptive complex impedance structures need to be realized. For this purpose two active frequency selective surfaces (AFSSs) were investigated. The first one was composed of an array of PIN-loaded dipoles while the second one was composed of an array of varactor-loaded dipoles.

Although an insight into the different applications of passive FSSs as well as the different techniques available to introduce complex impedance adaptability into FSSs are presented in this chapter, the aim of the chapter is to describe the design philosophy and methodology of the two AFSSs investigated in the research programme. The chapter also outlines the theoretical effects of semiconductor loading.

5.2 Applications of Passive Frequency Selective Surfaces

Frequency Selective Surfaces (FSSs) are passive array structures composed of either periodically arranged metallic patch elements, normally printed on a dielectric substrate for support, or aperture elements (Babinet's complement of the former) on a conducting surface. The elements are periodically placed in a given lattice which can be square, rectangular or even skewed. FSS behaviour is, essentially, that of a narrowband passive electromagnetic filter exhibiting at resonance either reflection (patch element) or transmission (aperture element) properties. The most common elements are shown in figure 5.1. These are dipoles, tripoles, crossed dipoles, Jerusalem crosses, square loops and circular loops. These elements have a single resonant frequency, f_r, which is a function of the physical dimension, their periodical placement in the array, and for metallic patch elements, the dielectric substrate upon which they are printed. The angle of incidence and the incoming electric field polarisation also have an effect on the location of f_r.

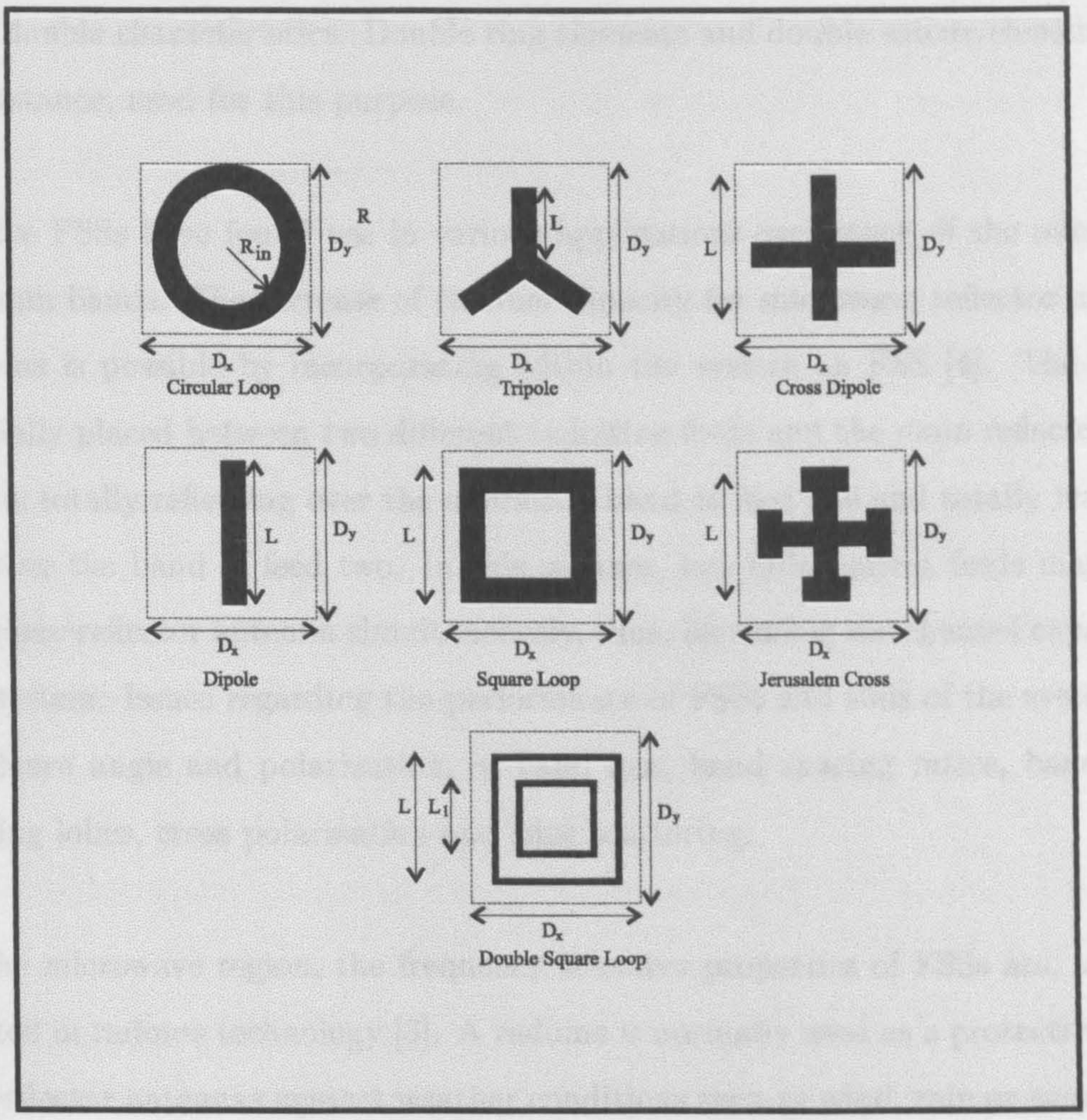

Figure 5.1: Some typical element geometries of FSSs.

5.2. APPLICATIONS OF PASSIVE FREQUENCY SELECTIVE SURFACES

The wavelength of resonance λ_r of a dipole array is, approximately, $2l$, that of a tripole and a square loop array is $4l$, where l is the element's length [3]. For the circular loop or ring $\lambda_r = 2\pi(R_{in} + 0.5w)$, where R_{in} is the inner radius and w is the element width [3]. Multi-static resonance can be achieved by introducing a second element on the array with different dimensions so as to create elements with double characteristics. Double ring elements and double square elements are, for instance, used for this purpose.

Passive FSSs have found use in various applications over much of the microwave and mm bands. The increase of channel capacity for microwave reflector antenna systems is possible by incorporating within the system an FSS [4]. The FSS is normally placed between two different radiating feeds and the main reflector. The FSS is totally reflecting over the operating band of feed one and totally transparent over the band of feed two. In this manner, two independent feeds may share the same reflector antenna simultaneously, thus, increasing the channel capacity of the system. Issues regarding the performance of FSSs and thus of the system are: incidence angle and polarization, in band loss, band spacing ratios, bandwidth, grating lobes, cross polarization and edge scattering.

In the microwave region, the frequency selective properties of FSSs are, also, exploited in radome technology [3]. A radome is normally used as a protective shield for reflector antennas against weather conditions such as wind, rain or snow which may cause detrimental effects on the antenna performance. For this application a band pass transmission characteristic at the operating frequency of the antenna is designed into the FSS's frequency response allowing the antenna to operate normally. At the out-of-band frequencies, the FSS is completely reflective.

The dichroic properties of FSSs have found application as a RF/IR beam combiner [5] for simultaneous transmission and reflection of RF and IR, respectively. The beam combiner (the FSS), whose frequency characteristics must be such that both transmission and reflection are present, may be used to provide dual stimulation

to missile seekers. In the transmission mode the combiner should provide minimum attenuation across a very wide RF band (1-100 GHz). On the other hand, the combiner's rejection response must exhibit maximum reflection of infrared signals between 3 and 12μm. The advantages of employing FSSs upon conventional methods (e.g. dielectric or metallic coatings) is that attenuation is no longer a function of the metal thickness. This optimises RF throughputs while increasing reflectivity in the infrared region. The elements employed for this application are closely-spaced square patches made of gold.

Beamspliting of energy in the millimetre and submillimetre wavebands is possible by utilizing frequency selective surfaces [6]. For this, FSSs are being employed as quasioptical components for front end channel demultiplexing and single side band filtering in radiometers.

Frequency selective surfaces have also been used to suppress harmonic radiation in microwave power transmission systems [7].

5.3 Active Frequency Selective Surfaces AFSSs

The frequency properties of passive FSSs are set at the design stage and the only way to change them is to redesign and build the structure again. However,through the application of a number of adaptive techniques the physical parameters of FSSs, for instance element dimension and periodicity, can be varied in situ. This greatly enhances the frequency properties of passive FSSs. Adaptive techniques not only introduce dynamic properties into the frequency characteristics of FSSs, but also allow quasi-real time control of such properties. FSSs with adaptive frequency properties are called active frequency selective surfaces (AFSSs).

Active frequency selective surfaces find use in a number of applications. They have been used to change the direction of an incident beam [8], in adaptive radar

absorber [9], and to change the beam width of an H-plane sectoral horn [10]. There is also interest in using AFSSs to control the behaviour of waveguiding devices and the radiation beams of leaky wave antennas, particularly, in the millimetre wave region [11].

5.3.1 Techniques used to date to introduce adaptive intrinsic properties into passive FSSs

To date four techniques have been employed to introduce adaptability into the frequency response of passive FSSs. The first one is based on the use of semiconductor substrates. In this technique, which has been the work of Vardaxoglou [12], slot type elements are printed on a single silicon substrate. Adaptability of the frequency properties of such AFSSs is achieved by varying the plasma concentration of the semiconductor substrate through forcing electron-hole pair generation. This is achieved by photo-illuminating the substrate. At low plasma concentration (low illumination intensity) the complex dielectric values remain unchanged. However, as the illumination intensity increases there is a substantial increase in conductivity due to the high plasma concentration. At this point the substrate behaves as a metallic film. Through varying the substrate thickness a shift of the pass-band can be achieved, which, however, is not possible by varying the plasma concentration alone.

In the second technique the elements of an FSS are printed on an exchangeable liquid substrate. In this technique, which has been researched by Lima et al [11], the sensitivity of the pass-band location to the properties of the supporting dielectric is exploited. By varying the permittivity of the liquid substrate from 1 to ϵ_r the bandpass location can be shifted in frequency. The technique, however, requires FSSs with narrow passband characteristics. A degree of both predicted and measured bandpass tuning is demonstrated which, the authors reckon, can be increased by utilizing liquids with larger ϵ_r. Liquids with a low tangent loss are,

however, required to maintain the passband.

The third technique is based on ferrite substrates and have been studied by Chang et al [13]. In this work changes in the frequency characteristics of a FSS composed of square loops are introduced by printing its elements on a ferrite substrate and gradually applying a DC magnetic biasing field to the substrate. This changes the relative permeability μ_r of the substrate thus effecting a continuous shift of the resonance frequency. The fundamental resonant frequency of the FSS can be steadily increased with an increasing bias field, from 11.6 GHz at 0 bias to 14 GHz at 3000Gauss bias.

The last, but not least, technique is based on populating FSSs with semiconductor devices. The previous techniques rely on printing the elements of FSSs on substrates sensitive to property changes. This stems from the fact that the bandpass location of an FSS is affected by the intrinsic properties of the supporting substrate,namely ϵ_r, μ_r, and substrate thickness. Semiconductor loading in conjunction with a bias voltage, on the other hand, effects direct changes in the physical parameters of an FSS, namely element geometry, dimension and periodicity. This effects changes into the frequency response of an FSS since its frequency properties are also a function of these parameters. Because of the fact that a bias voltage can be applied in real time, the frequency properties of semiconductor-loaded FSSs can be change in quasi-real time. The speed of the response being limited by the switching speed of semiconductor devices employed. A number of authors have investigated this phenomenon [14] [15] [16].

5.4 Diode Loaded Active Frequency Selective Surfaces

The adaptive complex impedance properties of semiconductor-loaded AFSSs are investigated in this research programme as a means to overcome the fundamental limitations imposed on a Salisbury screen's absorption bandwidth by the constitutive parameters of conventional materials.

Active frequency selective surfaces loaded with semiconductor devices were investigated in this research programme since their frequency properties are not only easy to manipulate but also to change in quasi-real time. The ease of manipulation arises from the fact that FSSs are structures whose frequency properties and, thus, their operating frequency band are governed by their element geometry, dimension and periodicity. Therefore, by carefully choosing these parameters, the appropriate adaptive response can be designed into the frequency property of an FSS, so that it operates over a desired frequency range. For example, if the operating frequency band is in the low end of the microwave region the element dimension can be carefully chosen for the FSS to operate across this region. On the other hand, for operation at a higher frequency range the element dimension can be made smaller.

Although, as shown in section 5.3.1, there are a number of techniques available to introduce dynamic frequency properties into passive FSSs, semiconductor loading was adopted in this research programme. Why?. Firstly, it is easy to apply an external control signal to semiconductor devices on an AFSS. This is achieved by means of applying a bias voltage through a number of bias lines. The number of bias lines depends mainly of the element geometry while the voltage level on the type and number of devices used. Secondly, semiconductor technology offers fast response. The fast switching speeds, in the order of nanoseconds [17], of semiconductor devices allows quasi-real time switching of an AFSS's frequency properties.

And thirdly, semiconductor devices permit both coarse and gradual tuning of an AFSS's complex impedance response. Compared with ferrite control devices, semiconductor devices are small, fast and inexpensive [18]. Ferrite devices, on the other hand, are large, heavy, slow, and expensive.

Once the complex impedance properties of a structure can be easily manipulated and controlled over a required frequency band in quasi-real time, then so can the frequency response of planar devices embedded with such structures. AFSSs loaded with semiconductor devices offer these versatile characteristics. AFSSs are, therefore, the preferred surface to be investigated as a means to circumvent material properties limitations on wideband absorption bandwidth of a Salisbury screen absorber.

The dynamic frequency responses of two different AFSSs were investigated. The first one was an AFSS comprising an array of PIN-loaded dipoles. The second AFSS was composed of an array of dipoles loaded with varactor diodes.

Before the AFSS design philosophy employed in this research programme is explained, it is important to understand the effects of diode populating an array of dipoles. This follows in the next section.

Diode Loading Effect

A planar array composed of periodically placed dipoles is a resonant structure. The frequency characteristic of such a configuration is composed of two fundamental responses: a radiation susceptance response as well as a radiation reactance response, separated by the point of resonance. This occurs at the resonant frequency f_r. In equivalent circuit concept, a free-standing dipole array can be thought of a series connection of an inductor and a capacitor, as depicted in figure 5.2. The overall reactive impedance of such structure can therefore be written as

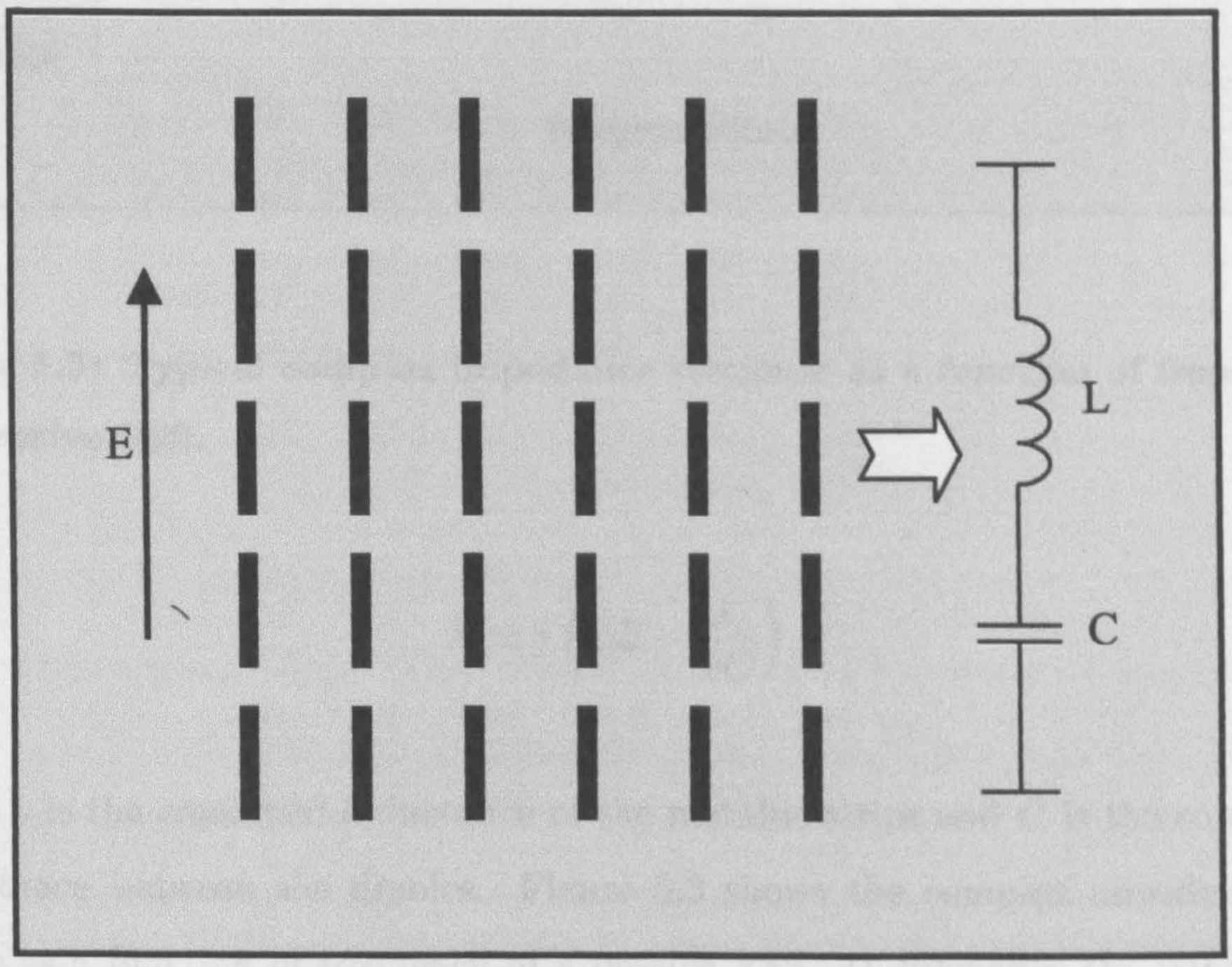

Figure 5.2: Free-standing array of unloaded dipoles and its equivalent circuit.

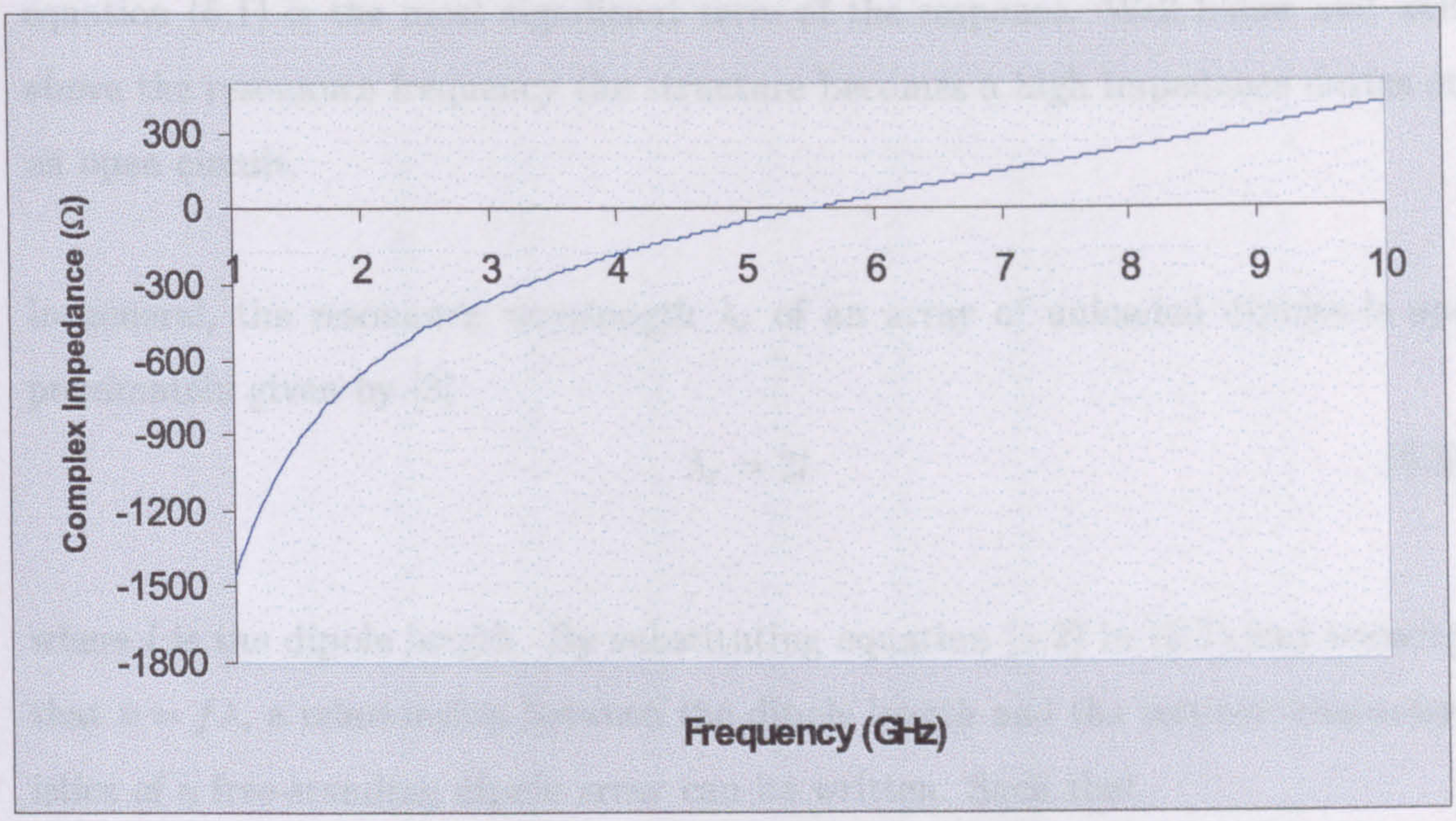

Figure 5.3: Typical complex impedance response as a function of frequency of a passive FSS.

$$X = j\left(\omega L - \frac{1}{\omega C}\right) \tag{5.1}$$

where L is the combined inductance of the metallic strips and C is the combined capacitance between the dipoles. Figure 5.3 shows the complex impedance response as a function of frequency of a passive FSS. At resonance the impedance of the structure is equal to zero (i.e. a short circuit), such that $Z = 0$. For this $\omega L = 1/\omega C$, and, therefore, the resonance frequency f_r is given by

$$f_r = \frac{1}{2\pi\sqrt{LC}} \tag{5.2}$$

The figure also shows that at frequencies below the resonance frequency the FSS behaves as a capacitive structure and, thus, the term $1/j\omega C$ of equation (5.1) dominates the response. On the other hand, at frequencies above the resonance frequency the FSS operates as an inductive structure, whereupon the $j\omega L$ term of

equation (5.1) is the most significant term of the response. Well below and well above the resonance frequency the structure becomes a high impedance device or an open circuit.

In general, the resonance wavelength λ_r of an array of unloaded dipoles is approximately given by [3]

$$\lambda_r = 2l \tag{5.3}$$

where l is the dipole length. By substituting equation (5.2) in (5.3) and knowing that $\nu = f\lambda$, a relationship between the dipole length and the intrinsic characteristics of a free-standing dipole array can be written. Such that

$$l = \pi\sqrt{LC} \tag{5.4}$$

The above equation clearly shows that the length of dipoles placed on an array can, virtually, be varied by changing the capacitance and/or the inductance. An increase of l leads to a downward shift of the resonant frequency. A decrease of l, on the other hand, places the resonant frequency at a higher frequency. When a FSS composed of an array of dipole is loaded with either PIN or varactor diodes[1], the higher capacitance of the diodes dominates. This results in a virtual increase of the dipole length, which, in turn, causes a downward shift of the resonance frequency.

5.4.1 PIN-loaded AFSSs

Design methodology

In order to implement the absorber design methodology introduced in chapter 4 to achieve a broadband absorption solution without the need to rely upon material

[1]Under 0 or reverse bias

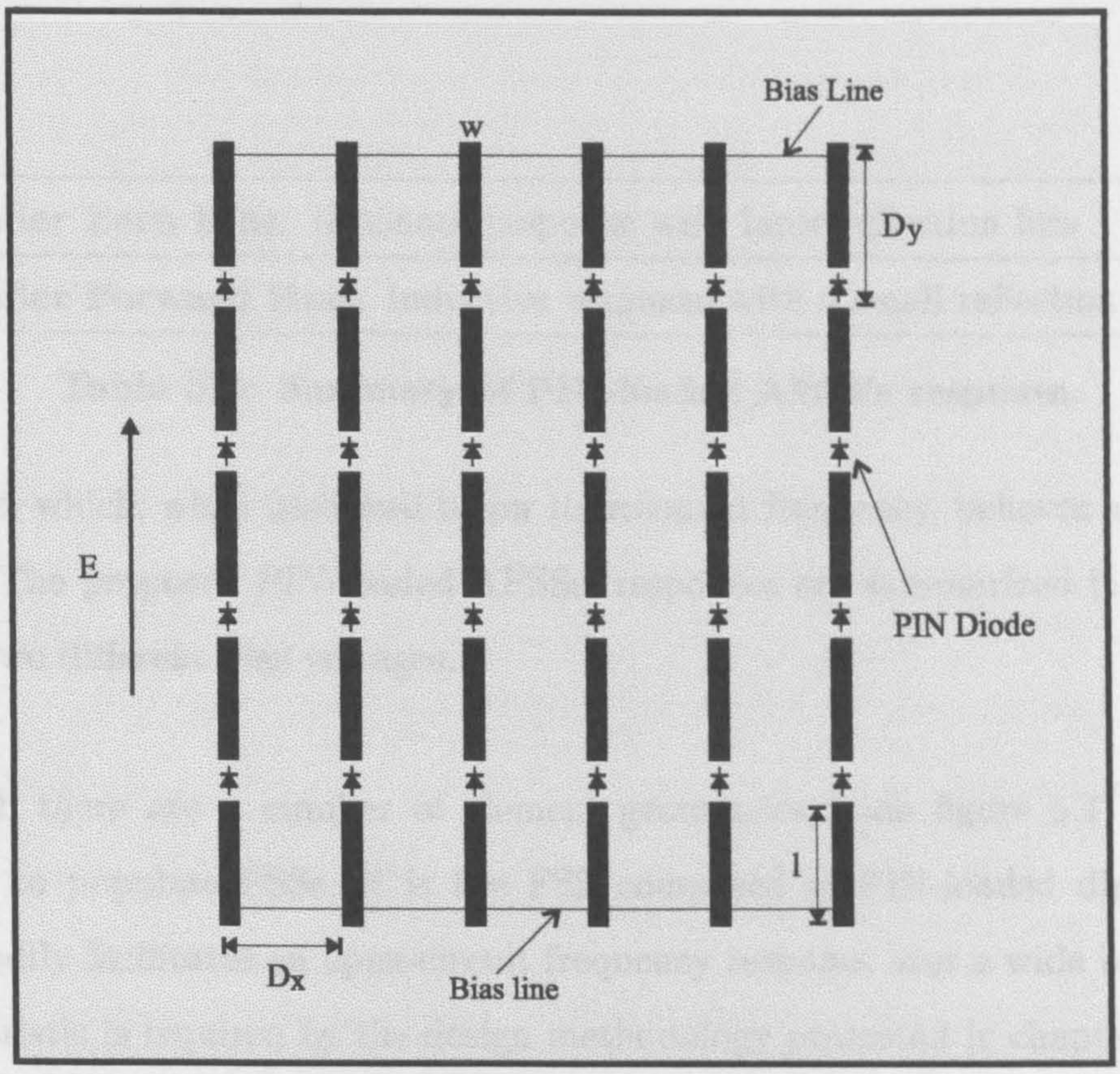

Figure 5.4: Schematic diagram of a free-standing PIN-loaded AFSS.

properties, bi-state adaptive complex impedance structures with an open/short circuit response are required.

An open-short circuit behaviour can be implemented into an AFSS's complex impedance response by composing the structure with periodically placed PIN-loaded dipoles. A schematic diagram of this arrangement is shown in figure 5.4. Through means of applying corresponding ON/OFF bias voltages to the PIN diodes the AFSS becomes a hybrid complex impedance structure, having two distinctive electrical properties. When the diodes are ON the AFSS behaves as an inductive screen and, as such, its frequency response is linear. The short circuit response can, thus, be implemented through reducing the AFSS's inductance. This, as shown by figure 2.8 of chapter 2, can be readily achieved through making the ratio of dipole width w to dipole periodicity D_x as close as possible to unity, such that $w/D_x \Rightarrow 1$. When the diodes are OFF the AFSS becomes a resonant

Under Zero Bias: Resonant response with large reflection loss
Under Forward Bias: Inductive response with a small reflection loss

Table 5.1: Summary of PIN-loaded AFSS's response.

structure, which, when used well below its resonant frequency, behaves as an open circuit. The proposed PIN-loaded AFSSs' responses are summarized in table 5.1 for the two different bias voltages.

Although there are a number of element geometries (vide figure 5.1) that can be used to populate FSSs, it is the FSS composed of PIN-loaded dipoles that most readily facilitates an open-circuit frequency response over a wide band. This characteristic is required by the design methodology presented in chapter 4 to implement an absorber with a broadband absorption solution. The proposed broadband absorber methodology requires complex impedance structures that behave as a quasi-metallic surface as well as a transparent structure over the widest possible frequency band. In comparison with the PIN-loaded square loop AFSS investigated by Chang and the PIN-loaded dipole array as investigated by Shuley (vide chapter three), the PIN-loaded dipole AFSS studied in this research programme permits a quasi-metallic response over a wider frequency band. The AFSSs studied by the aforementioned authors are always resonant structures regardless of the state of the diodes. This means that the structure can only behave as a metallic surface at a single frequency and not over a wide frequency band.

Board	D_x mm	D_y mm	w mm	l mm	g mm	w/D_x	f_{r_c}(GHz)	f_{r_m}(GHz)
DI-1	10	15	1	13	2	0.1	11.5	5.0
DI-2	10	9	1	7	2	0.1	21.4	7.0

Table 5.2: Physical Parameters of Two AFSSs.

Practical Implementation

Two different AFSSs composed of arrays of PIN-loaded dipoles were designed and built, namely DI-1 and DI-2.Their physical parameters are shown in table 5.2. The AFSS were designed so as to operate over a frequency range that extends from 1 GHz up to approximately 5 GHz.

Figure 5.5 shows the calculated and dynamic measured reflectivity responses as a function of frequency of DI-1 AFSS. The AFSS was etched for structural support on a 200x200 mm^2 substrate of thickness 0.611 mm and of ϵ_r 2.20 with 0.5 OZ Cu. The measured short-circuit response was generated by applying a linear forward voltage of 11.0 V across the AFSS. The calculated C data, on the other hand, was predicted using the Macfarlane/Marcuvitz equivalent impedance formulation of an array of inductive strips[2] in conjunction with the theory of uniform transmission lines. Figure 5.7 shows that the measured reflectivity response follows the same pattern as that of the calculated response. However, as shown in the figure, there is a small reflection loss associated with the measured response. Apart from this small insertion loss, the measured response follows the same pattern as the predicted data. This indicates that the Macfarlane/Marcuvitz analytical approach can be used as benchmark to design the inductive response of an AFSS composed of PIN-loaded inductive strips.

A second AFSS comprising an array of PIN-loaded inductive strips was designed

[2]vide equation (2.137) chapter 2

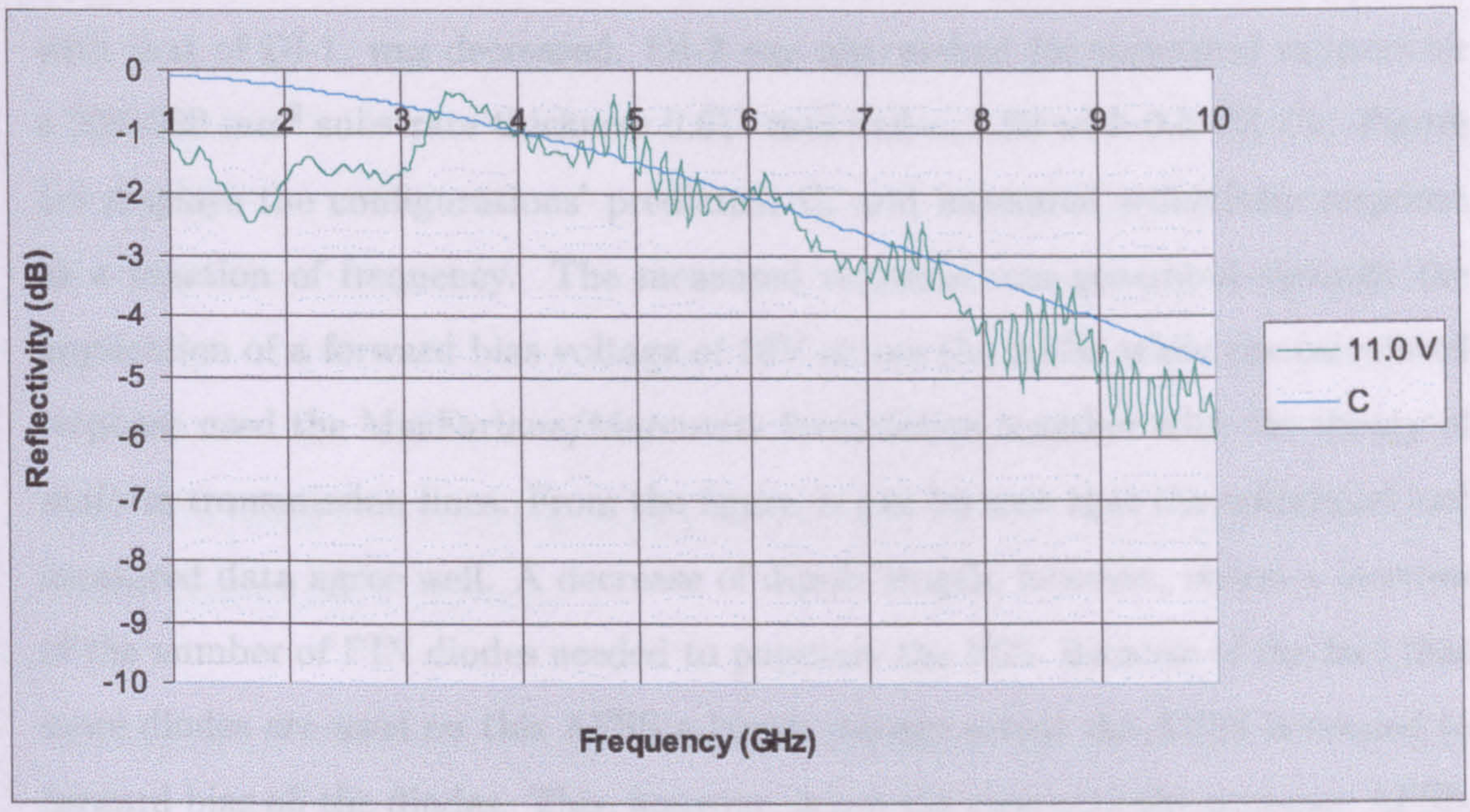

Figure 5.5: Measured and calculated reflectivity responses of DI-1 AFSS under the influence of a full bias voltage: 11.0V.

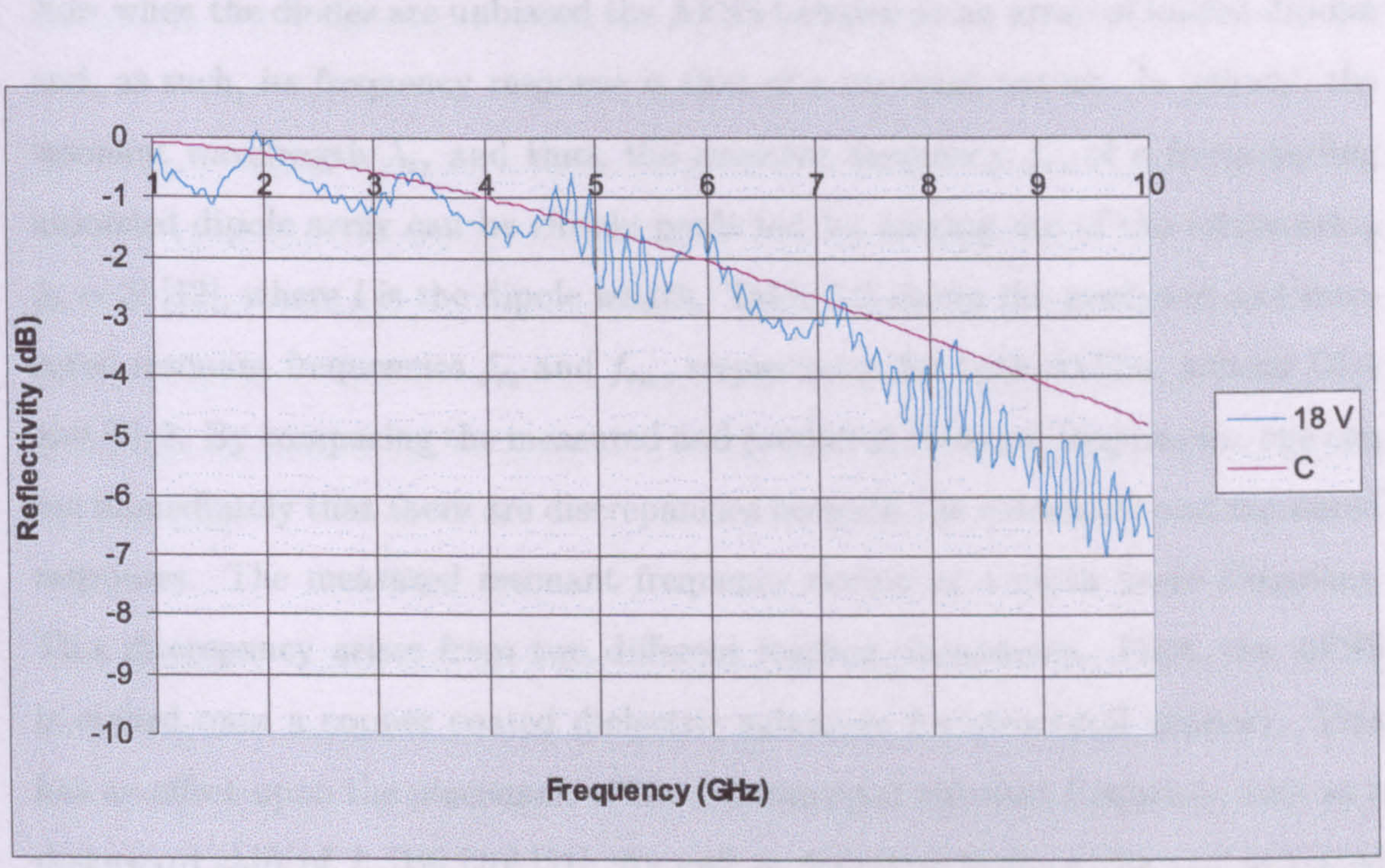

Figure 5.6: Measured and calculated reflectivity responses of DI-2 AFSS under the influence of a full bias voltage: 18V.

and built, namely DI-2. As shown by table 5.2, the dipole length, in comparison with that of DI-1, was decreased. DI-2 was also etched for structural support on a 200x200 mm^2 substrate thickness 0.611 mm and ϵ_r 2.20 with 0.5 OZ Cu. Figure 5.6 displays the configurations' predicted, C, and measured reflectivity response as a function of frequency. The measured response was generated through the application of a forward bias voltage of 18V across the AFSS while the calculated response used the MacFarlane/Marcuvitz formulation together with the theory of uniform transmission lines. From the figure, it can be seen that the calculated and measured data agree well. A decrease of dipole length, however, incurs a increase of the number of PIN diodes needed to populate the FSS. Because of the fact that more diodes are used on this AFSS a larger voltage across the AFSS is needed to forward bias all the diodes. This, however, is not the case with the previous AFSS, which has less diodes on it and, therefore, required a smaller forward bias voltage of 11V.

Now when the diodes are unbiased the AFSS behaves as an array of loaded dipoles and, as such, its frequency response is that of a resonant nature. In general, the resonant wavelength λ_r, and thus, the resonant frequency f_r, of a free-standing unloaded dipole array can be closely predicted by making use of the relationship $\lambda_r = 2l$ [12], where l is the dipole length. Table 5.2 shows the predicted and measured resonant frequencies f_{r_c} and f_{r_m}, respectively, for both AFSSs, namely DI-1 and DI-2. By comparing the measured and predicted resonant frequencies, one can see immediately that there are discrepancies between the calculated and measured responses. The measured resonant frequency occurs at a much lower frequency. This discrepancy arises from two different loading phenomena. First, the AFSS is etched onto a copper coated dielectric substrate for structural support. This has an effect upon the placement of the fundamental resonant frequency, seen as a downward shift of f_r [19] [20] [21]. As well as dielectric loading, the grid is loaded with PIN diodes. This results in an increases of the overall capacitance of the array, which, in turn, causes the resonant frequency to occur at a lower frequency. This phenomenon is mathematically shown by equations (5.2) and (5.4).

It is important to mention that the frequency characteristics of all the AFSSs presented in this chapter were acquired by free-field measurement (appendix A). The complex impedance response as a function of frequency pertaining to each AFSS was then extracted from its measured reflectivity characteristic by applying impedance de-embedding (see appendix B).

High Frequency limitation imposed by FSSs on the proposed broadband radar absorbing material

In chapter 2 it was shown how FSSs are capable of the generation of not only a propagating field, but also a series of evanescent fields when illuminated by a TEM wave. The latter type of fields can potentially become secondary grating lobes. However, providing that the structure is electrically small, through making the periodical placement of its elements a lot less that the working wavelength, the generation of secondary main lobes can be avoided.

If, however, the working wavelength is smaller compared with the periodical placement of the FSSs' elements, in other words, the structure is electrically large, the generation of secondary grating lobes will take place. This, as shown by equation (2.33) of chapter two, will result in a distorted reflected travelling wave composed of the summation of the fundamental frequency and a number of high frequency components.

The proposed broadband absorber is based on the quarter wave concept, which generates a maximum E-field at quarter wave from a metal backplane. A distorted travelling reflected field will not be a maximum at a quarter wave from the metal backplane, and thus wave cancellation with the incoming TEM wave will not take place. This will result in the malfunctioning of the proposed absorber. This, therefore, indicates that for successful operation the AFSSs employed in the absorber must be electrically small.

PIN-loaded AFSS: Open/Short Circuit and Tuning Responses

Because of the fact that a PIN diode has an ON-OFF state as well as a transition region, whose width is a function of the applied bias voltage, it follows that an AFSS comprising an array of PIN-loaded dipoles has in its frequency characteristics an open/short circuit response as well as a tuning response between the short and open circuit responses. The former is determined by the PIN diodes ON-OFF properties while the latter by the width of the diodes transition region for a given applied voltage.

Open/Short Circuit Response

Figure 5.7 shows the measured dynamic reflectivity profile as a function of frequency of one of the AFSSs built, namely DI-1. From the figure, it can be seen that at low frequencies the AFSS's dynamic-range response as a function of reflection levels, closely mimics an open and short circuit. Under a No Bias Voltage (0V) the structure behaves as a open circuit, whereas under the influence of a Full Bias voltage (11V) the structure closely follows the short circuit line. The open-circuit behaviour decreases with increasing frequency. On the other hand, the short-circuit response decreases in a slow fashion with increasing frequency. All in all, the AFSS's reflectivity characteristics as a function of frequency has a dynamic range which decreases with increasing frequency. Figure 5.8 shows the AFSS's measured de-embedded complex impedance response for the two main bias condition (ON and OFF states). The figure clearly shows that at the two extreme bias conditions, the AFSS's complex impedance is mainly reactive, with very little loss.

In order to compare the improvement achieved on dynamic-range as a function of frequency achieved through dipole length decrease, as mentioned earlier, the measured dynamic reflectivity characteristics as a function of frequency of the two PIN-loaded AFSSs, namely DI-1 and DI-2, are depicted in figure 5.9. This figure

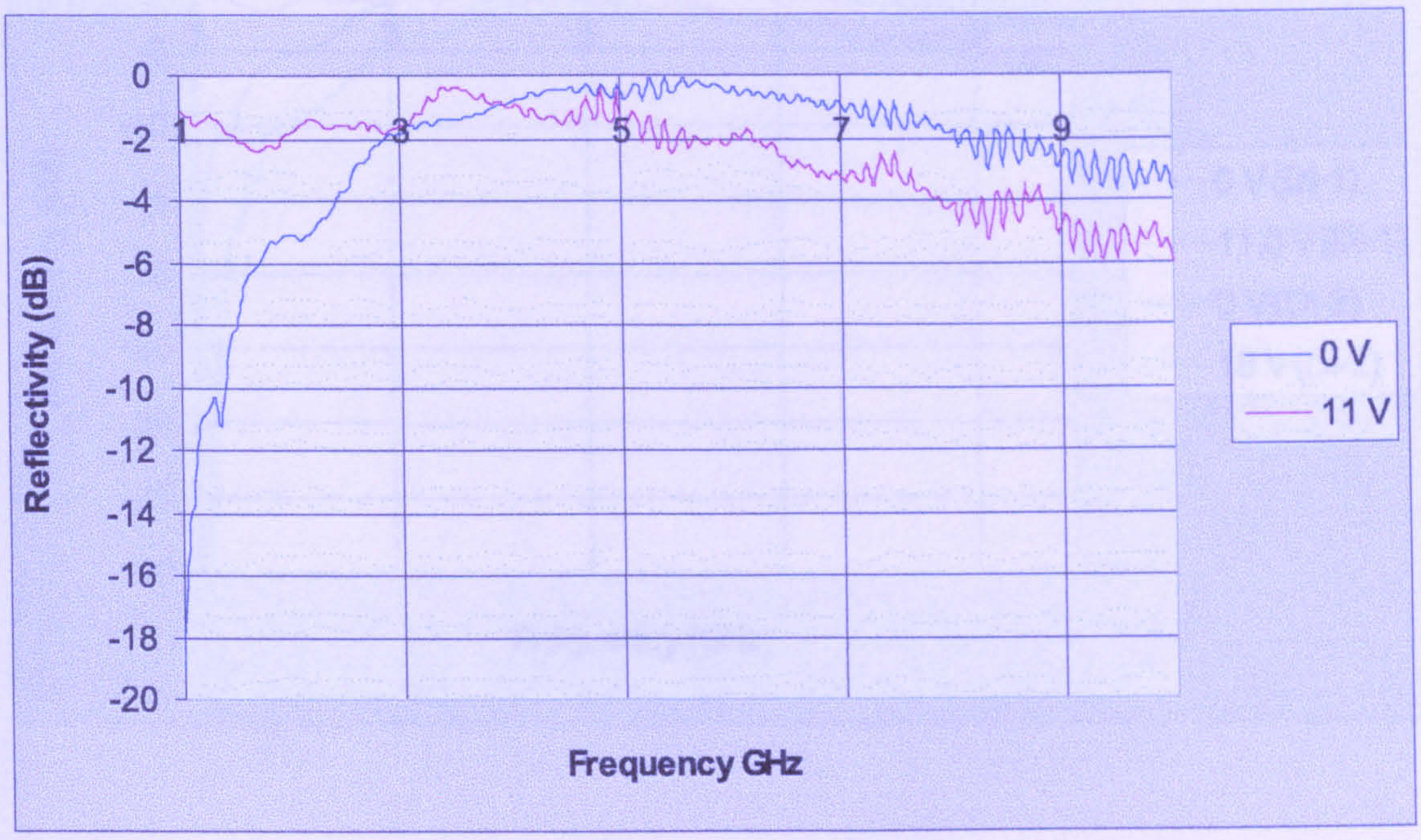

Figure 5.7: Measured dynamic reflectivity response of DI-1 AFSS.

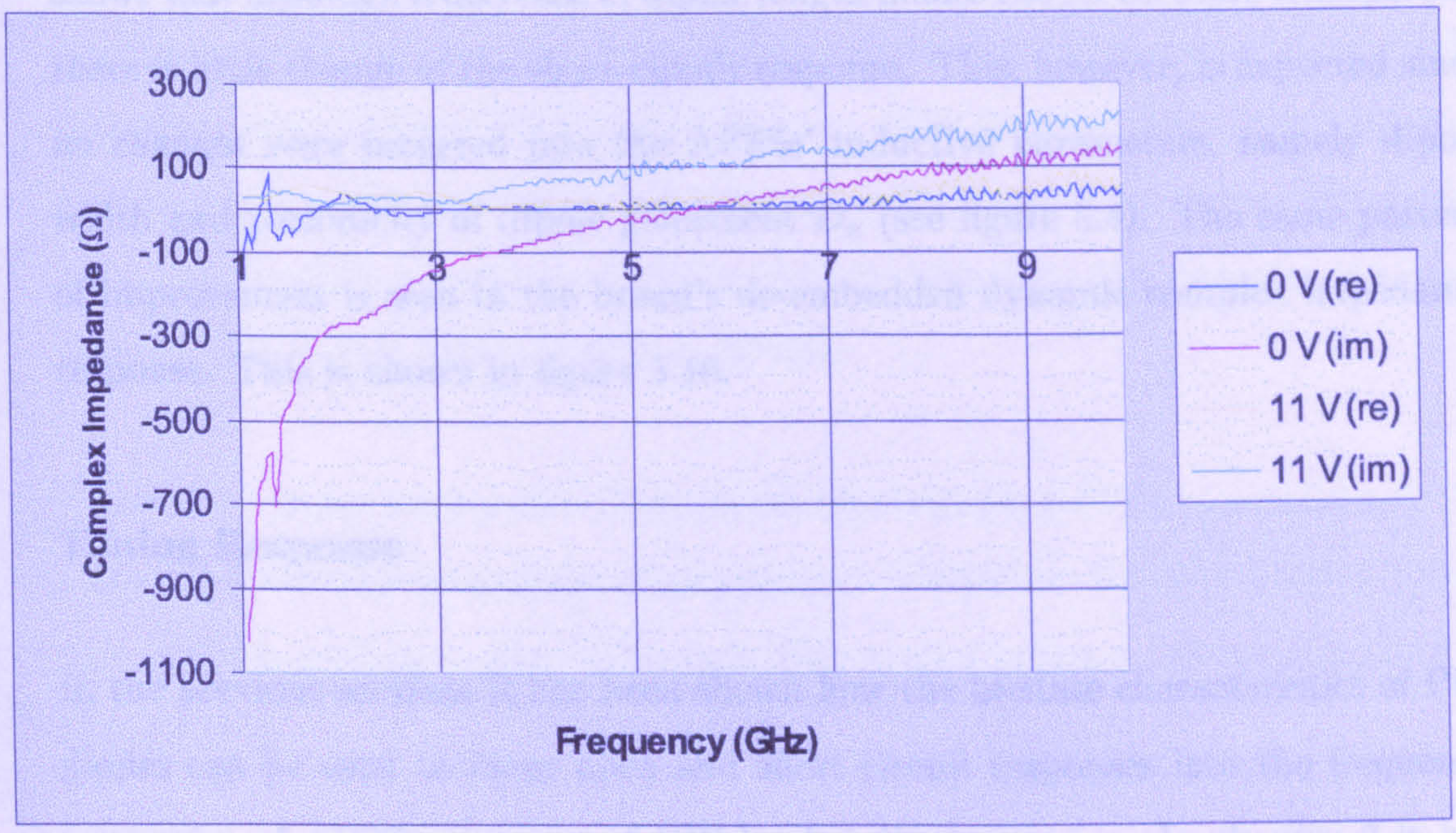

Figure 5.8: Measure de-embedded adaptive complex impedance response of DI-1 AFSS.

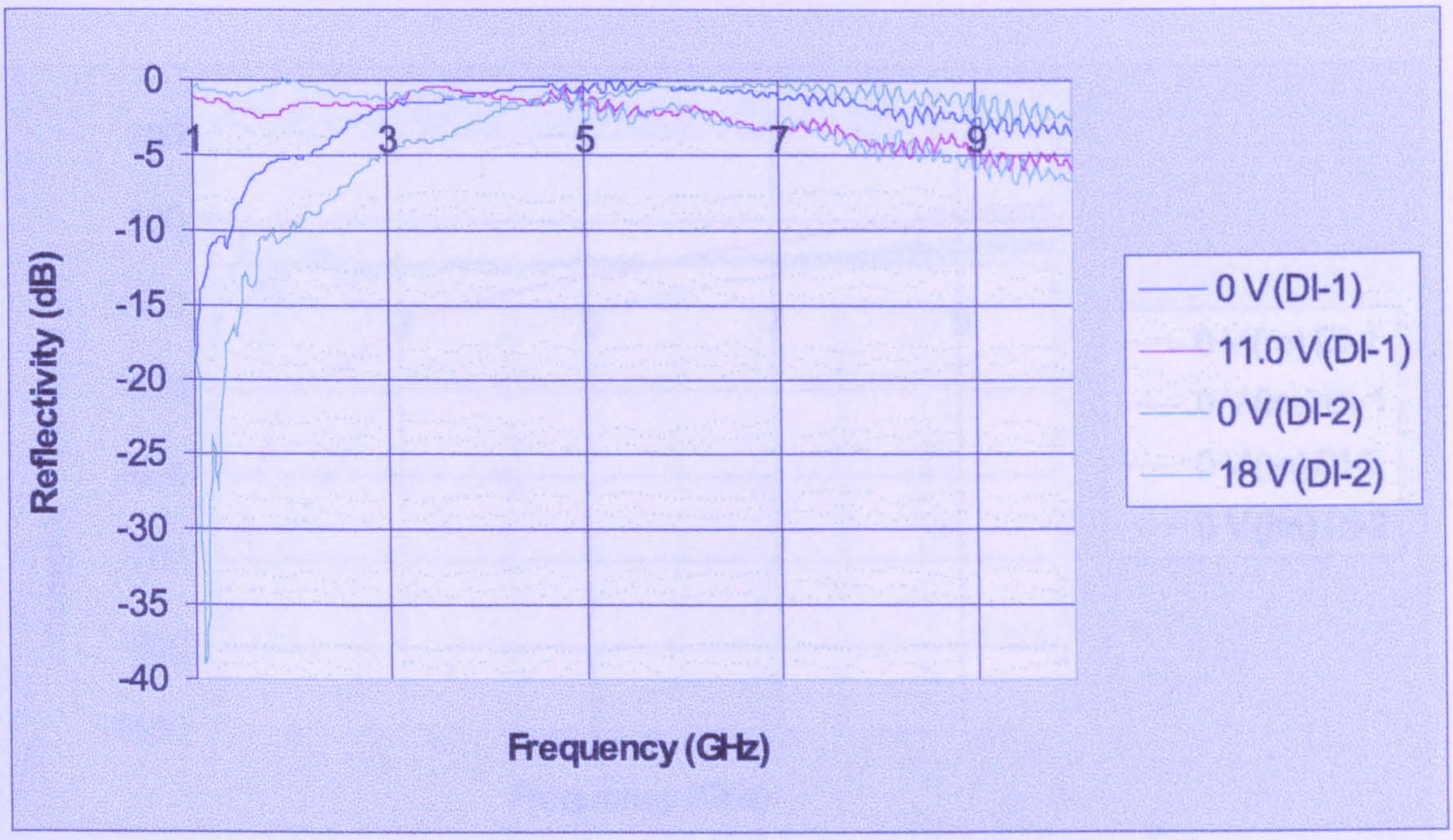

Figure 5.9: Measured dynamic reflectivity responses of the two AFSSs.

clearly shows that the second AFSS (DI-2) exhibits in its frequency profile a larger dynamic range, which is spread over a wider frequency bandwidth. Figure 5.9 also shows that although a decrease of dipole length makes the AFSS more transparent, there is little change of the short-circuit response. This, however, is expected since no changes were incurred into the AFSSs' inductive parameters, namely dipole width and periodicity of dipole placement D_x (see figure 5.4). The same pattern of improvement is seen in the board's de-embedded dynamic complex impedance response. This is shown in figure 5.10.

Tuning Response

In the previous sections it has been shown how the bi-state characteristics of PIN diodes can be used to incur open and short circuit responses into the frequency properties of AFSSs compose of PIN-loaded dipoles arrays. In chapter 3 it has been explained how the transition region width of a PN junction can be varied through the application of a bias voltage. Changes of transition region width in-

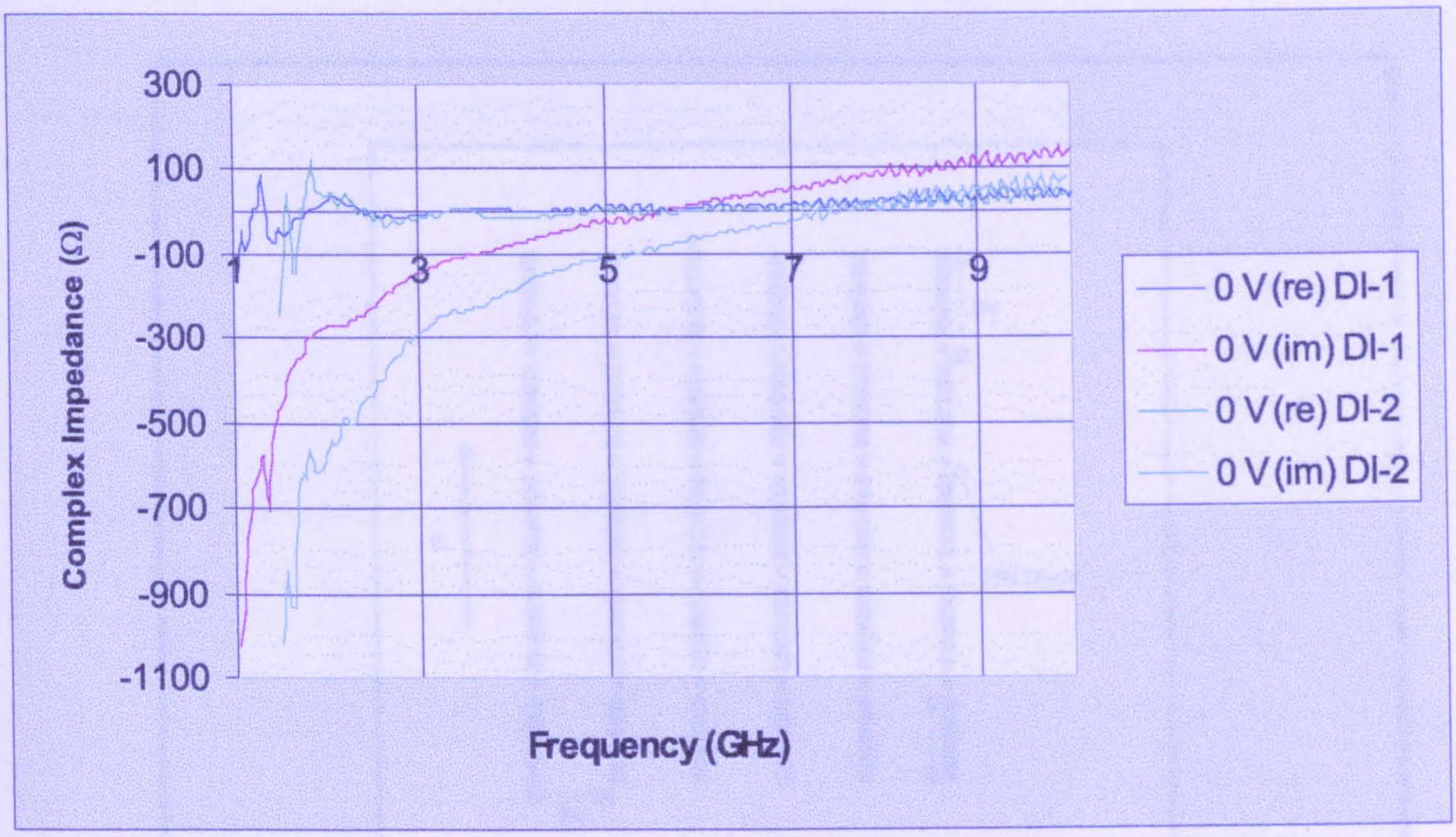

Figure 5.10: Measured de-embedded adaptive complex impedance responses of the two AFSSs.

cur changes of a PN junction capacitance. This led to the realization that changes of capacitance with a small bias voltage could be exploited to incur a linear and continuous shift between the open and the short circuit responses of an AFSS composed of an array of PIN-loaded dipoles. This section, thus, serves to show the effects of applying a linear and continuous biasing voltage to the PIN diodes upon the dynamic reflectivity response and, consequently, the dynamic or tuning complex impedance response of such AFSSs.

Figure 5.11 shows a schematic diagram of a free-standing AFSS composed of PIN-loaded inductive strips together its equivalent circuits for No-Bias/Biasing (when no voltage is applied to the diodes) and Bias modes (when a voltage is applied to the diodes).

Consider the AFSS under the influence of a biasing voltage. Under this condition the PIN diodes are operated within their transition region. The total impedance Z_T of the structure is given by the series connection of the structure inductive

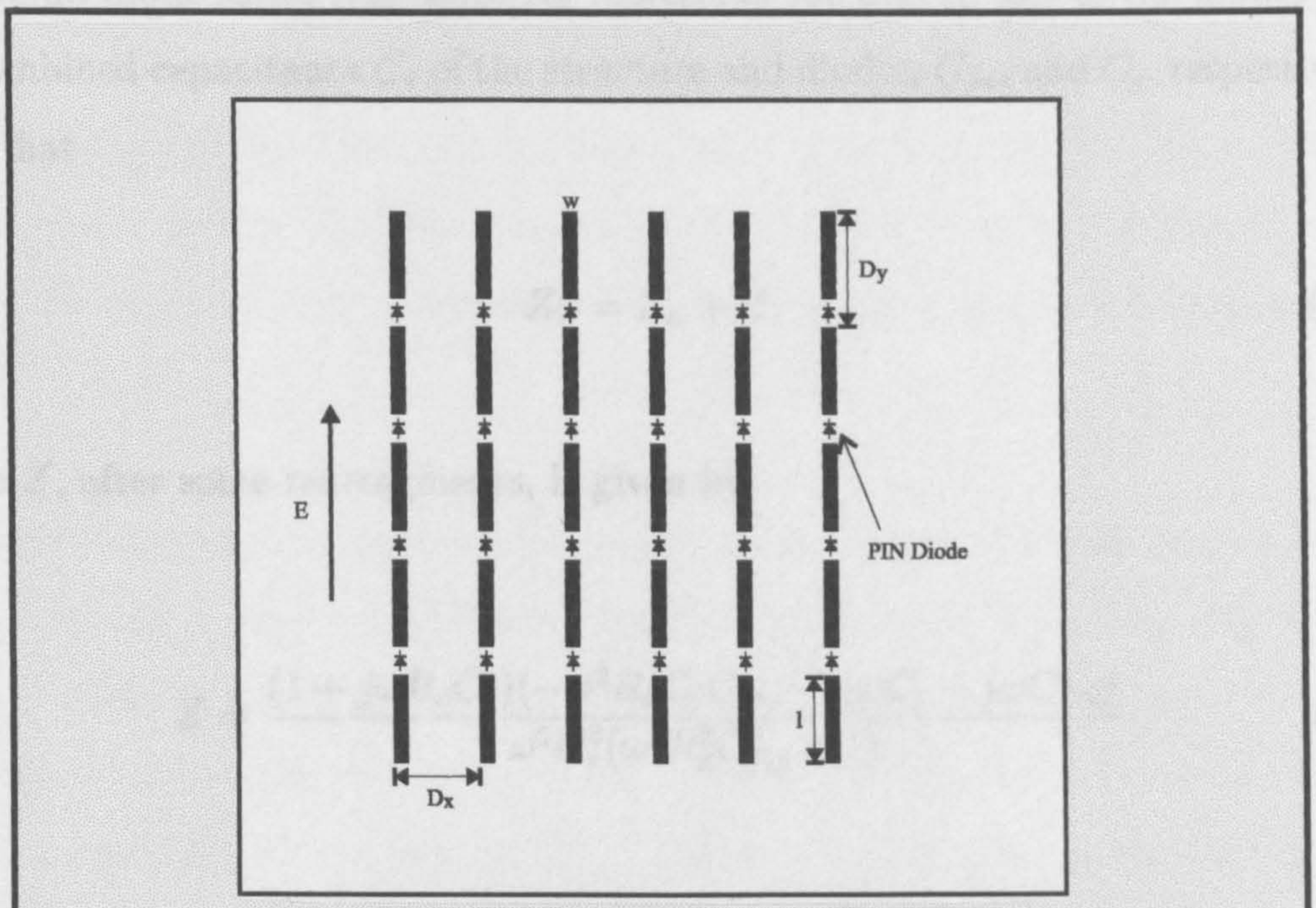

a

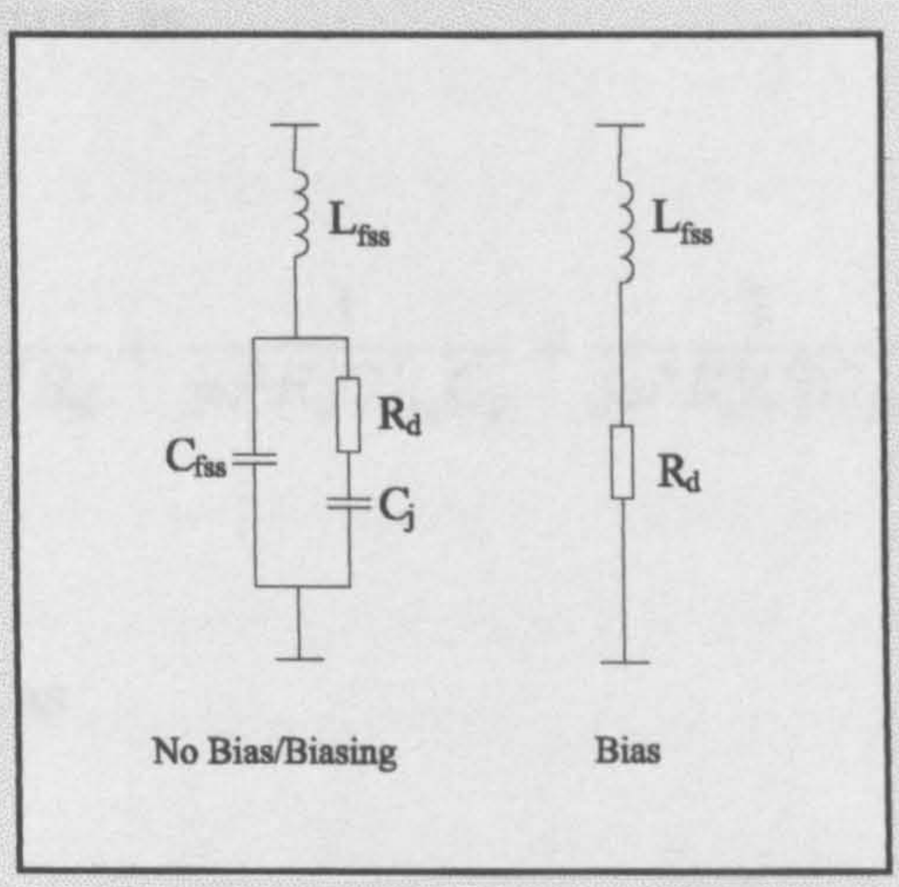

b

Figure 5.11: Schematic diagram of a PIN-loaded AFSS (a) and its equivalent circuits (b) under the two different bias modes: No Bias/Biasing and Bias.

reactive impedance Z_L and the impedance Z formed by the parallel connection of the overall diode series resistance R_d represents the overall loss of the diodes and the combined capacitance C_s of the structure and diodes, C_{fss} and C_j, respectively. Such that

$$Z_T = Z_L + Z \tag{5.5}$$

where Z, after some rearragments, is given by

$$Z = \frac{(1 + j\omega R_d C_j)(-\omega^2 R_d C_j C_{fss} - j\omega C_j - j\omega C_{fss})}{\omega^2 C_j^2 (\omega^2 R_d^2 C_{fss}^2 + 1)} \tag{5.6}$$

now since R_d is very large it follows that $\omega^2 R_d^2 C_{fss}^2 \gg 1$, the above equation can, therefore, be re-written as

$$Z = \frac{1}{(\omega C_{fss})^2 R_d} + \frac{1}{j\omega^3 R_d^2 C_{fss}^2 C_j} + \frac{1}{j\omega^3 R_d^2 C_j^2 C_{fss}} + \frac{1}{j\omega C_{fss}} \tag{5.7}$$

Z_T can thus be written as

$$Z_T = \frac{1}{(\omega C_{fss})^2 R_d} + j\left[\omega L_{fss} - \frac{1}{\omega C_{fss}} - \frac{1}{\omega^3 R_d^2 C_{fss}^2 C_j^2}[C_{fss} + C_j]\right] \tag{5.8}$$

where L_{fss} is the AFSS's inductance. Now, at resonance the reactive part of equation (5.8) is zero and, therefore, this equation becomes

$$Z_r = \frac{1}{(\omega_r C_{fss})^2 R_d} \tag{5.9}$$

where $\omega_r = 2\pi f_r$ and f_r is the resonance frequency. The above equation implies that the resonance impedance Z_r of an AFSS composed of an array of PIN-loaded dipoles under the influence of a biasing voltage is finite and not equal to a short circuit, which is the case of an unloaded FSS. The direct implication of this finding is that the application of a continuous and linear biasing voltage introduces losses into the system.

The above analysis, in particular equation (5.8), clearly demonstrates that the impedance response of an AFSS composed of an array of PIN-loaded dipoles under a biasing condition is of a complex nature, having both loss and a reactive impedance associated with it. The loss is inversely dependent on three components, namely f^2, R_d, as well as C_{fss}^2. Under a 0 bias voltage, the PIN diode's series resistance is very large and therefore the lossy part of the AFSS's impedance is negligible. However, as the biasing voltage increases R_d drops, which results in an increase of the real part of the AFSS's impedance. This is clearly demonstrated in figure 5.12, which shows the measured de-embedded complex impedance response of the PIN-loaded AFSS, named DI-1 [3], under the influence of a linearly increasing bias voltage between 0V through 7.0V dropped across the AFSS. From the figure, one can clearly see that as the voltage is increased the real part of the AFSS's impedance increases. This, however, occurs at low frequencies. At higher frequencies the loss becomes negligible due to it being inversely proportional to frequency. At higher frequencies, the AFSS, thus, becomes a reactive structure. In terms of the AFSS's reflection response, the lossy part is responsible for an insertion loss at resonance, which increases with increasing bias voltage. This is clearly depicted in figure 5.13.

The analysis also indicates that the reactive part of the PIN-loaded AFSS's impedance, under a biasing voltage, is of a resonant nature. The reactive impedance change as a function of voltage is mainly governed by the diodes junction capacitance

[3] with physical parameters shown in table 5.2 next to the heading DI-1

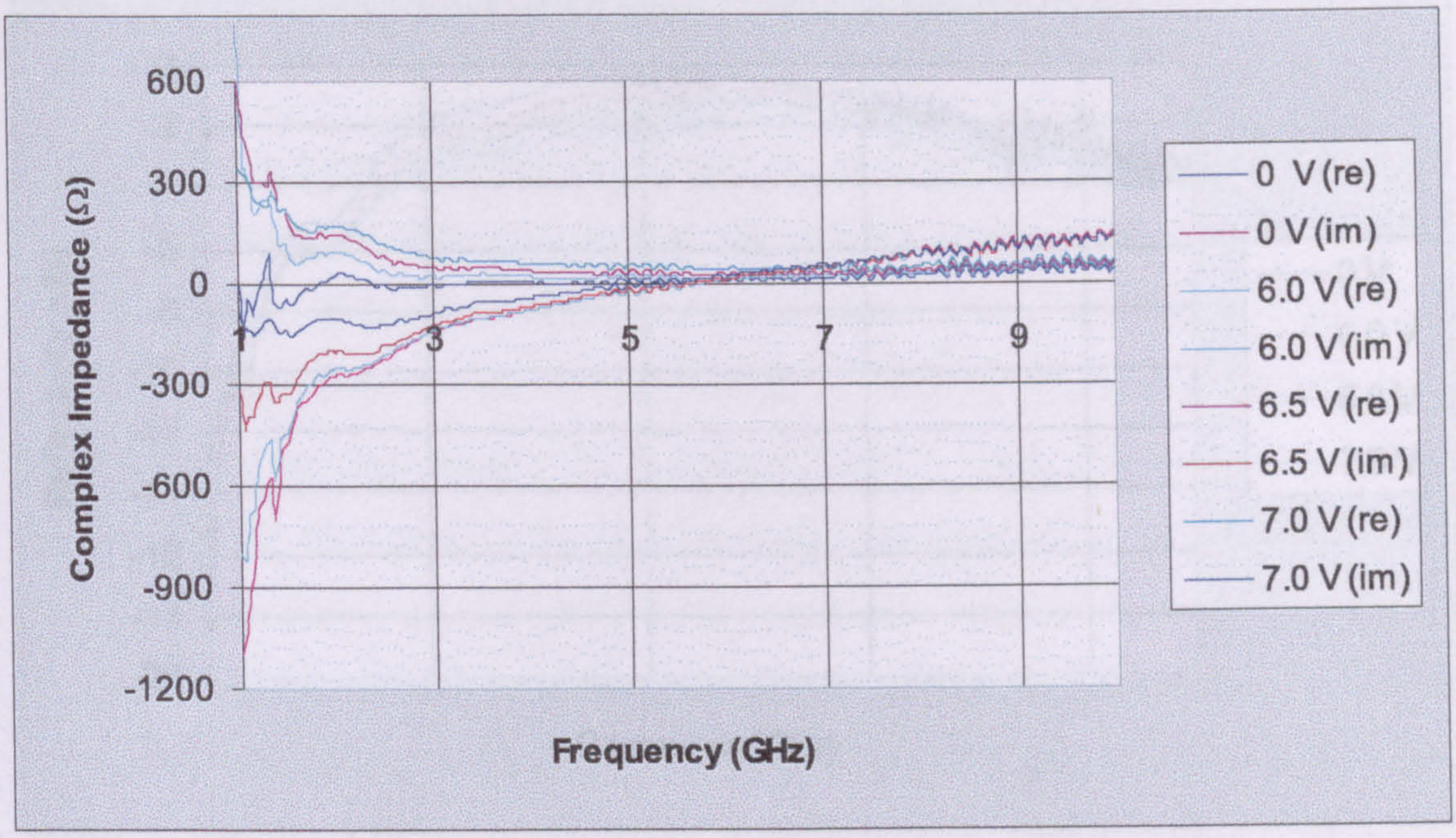

Figure 5.12: Measured adaptive complex impedance response of DI-1 AFSS under Biasing Conditions.

C_j. This increases with increasing bias voltage. In turn the susceptance part of equation (5.8) decreases. This can be seen in figure 5.14. The figure shows that as the bias voltage across the AFSS is increased from 0V to 7.0 V, the reactive part of the complex impedance decreases.

The response discussed above comes to a halt as soon as the PIN-loaded AFSS becomes an inductive screen. Re-writing equation (5.6)

$$Z = \frac{(1 + j\omega R_d C_j)(-\omega^2 R_d C_j C_{fss} - j\omega C_j - j\omega C_{fss})}{\omega^2 C_j^2 (\omega^2 R_d^2 C_{fss}^2 + 1)} \tag{5.10}$$

In this case $\omega^2 R_d^2 C_{fss}^2 \ll 1$ since R_d is small. Equation (5.15) after some re-arrangement can, therefore, be re-written as

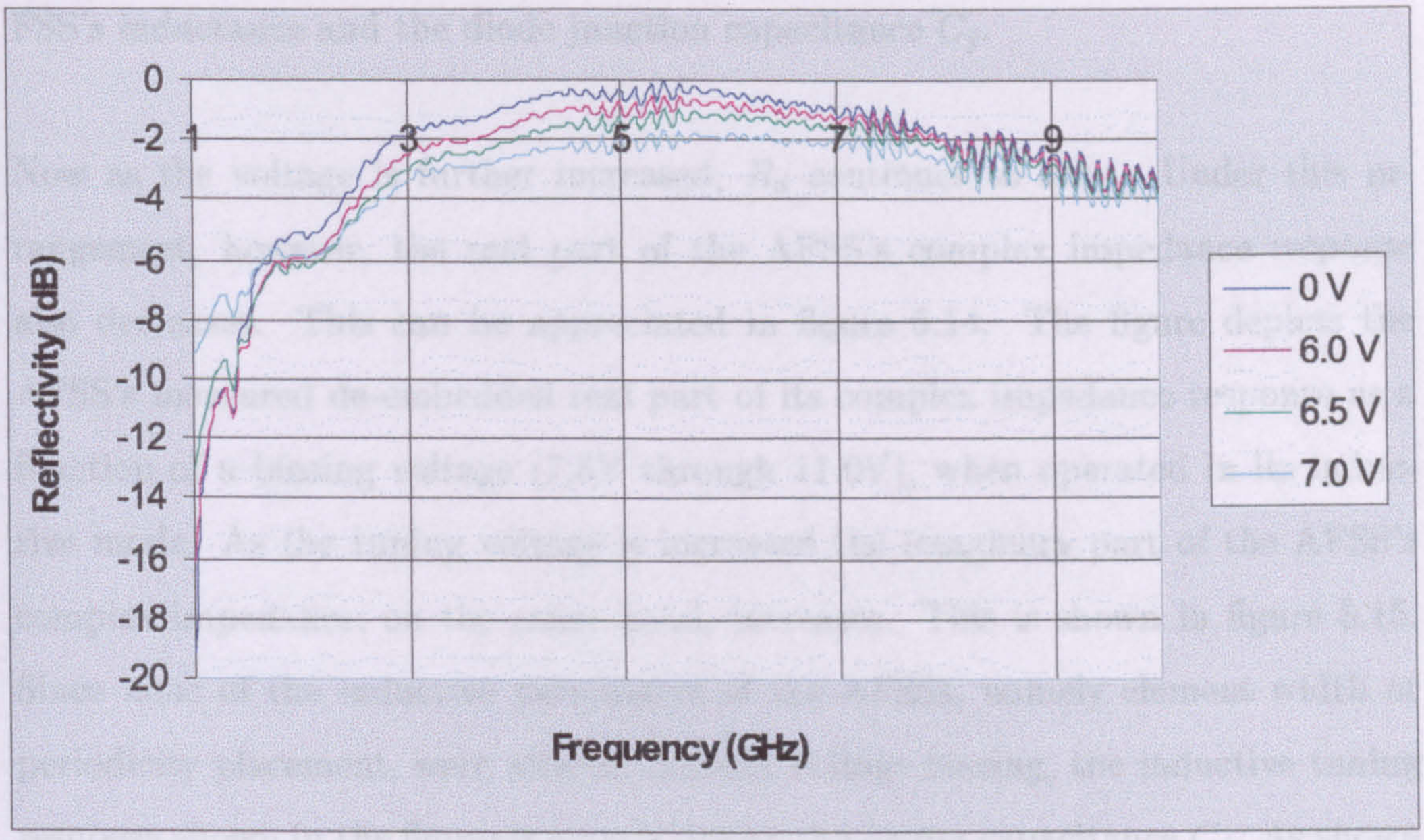

Figure 5.13: Measured dynamic reflection response of DI-1 AFSS under Biasing conditions.

$$Z = R_d + \frac{1}{j\omega C_j} + \frac{C_{fss}}{j\omega C_j}^2 + \frac{\omega R_d^2 C_{fss}}{j} \tag{5.11}$$

The third and fourth term of equation (5.11) are negligible. The total impedance Z_T of a PIN-loaded AFSS when it behaves as an inductive screen is, thus, given by

$$Z_T = R_d + j\left[\omega L - \frac{1}{j\omega C_j}\right] \tag{5.12}$$

The above equation shows that the equivalent impedance of a PIN-loaded AFSS when behaving as an inductive screen is of a complex nature. It has in its impedance response a real and an imaginary part. The real part is a function of the diodes series resistance R_d while its imaginary part is a function of the

FSS's inductance and the diode junction capacitance C_j.

Now as the voltage is further increased, R_d continues to drop. Under this arrangement, however, the real part of the AFSS's complex impedance response also decreases. This can be appreciated in figure 5.14. The figure depicts the AFSS's measured de-embedded real part of its complex impedance response as a function of a biasing voltage (7.5V through 11.0V), when operated in its inductive mode. As the tuning voltage is increased the imaginary part of the AFSS's complex impedance, on the other hand, increases. This is shown in figure 5.15. Since none of the inductive parameters of the AFSSs, namely element width or periodicity placement, were altered through voltage biasing, the inductive tuning response shown in the figure is mainly due to the diodes capacitance C_j. As shown by equation (5.12), this increases with increasing bias voltage and, therefore, its effects become less.

Figure 5.16 shows DI-1's dynamic reflectivity response as a function of a biasing voltage between 8.0 and 11.0 V. The figure also shows the AFSS's calculated reflectivity response. The figure shows that as the voltage is increased the reflection loss decreases.

Figures 5.17 through 5.21 show the dynamic frequency characteristics as a function of biasing voltage of a second AFSS composed of an array of PIN-loaded dipoles, namely DI-2[4], under the influence of a forward biasing voltage. Figure 5.17 displays the measured dynamic de-embedded complex impedance profile under a biasing condition. The figure depicts the same dynamic characteristics as DI-1's under a biasing voltage. However, the new board exhibits a more opaque response. This, nevertheless, is expected since the board was designed to be more transparent through ways on decreasing the dipole length. This shifts the resonant frequency up in frequency and, thus, at lower frequencies the AFSS becomes more transparent.

[4]The AFSS's physical parameters are shown in table 5.2 next to the heading DI-2.

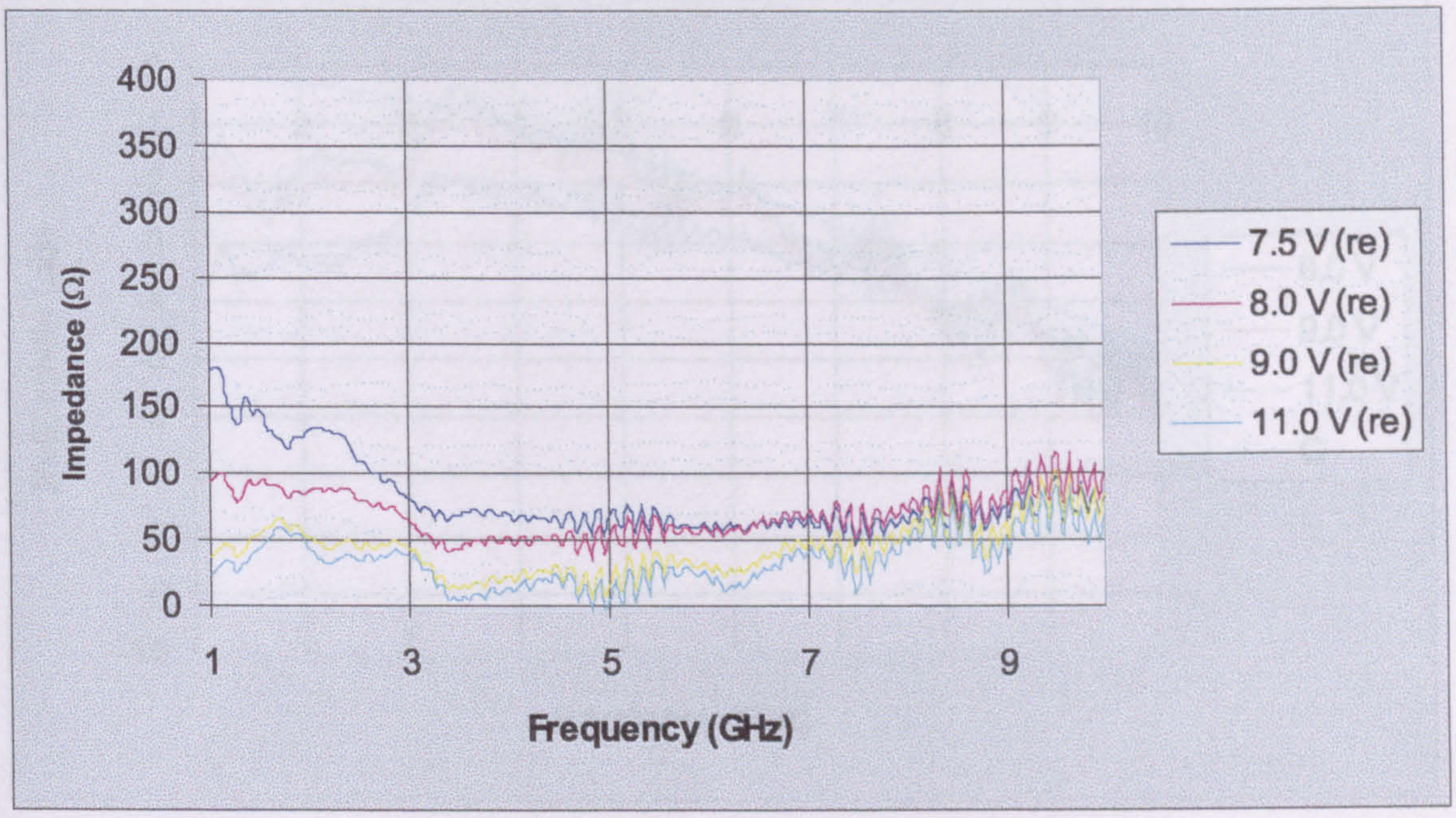

Figure 5.14: Measured dynamic real part of the impedance response as a function of biasing voltage (7.5V through 11.0V) of DI-1 AFSS.

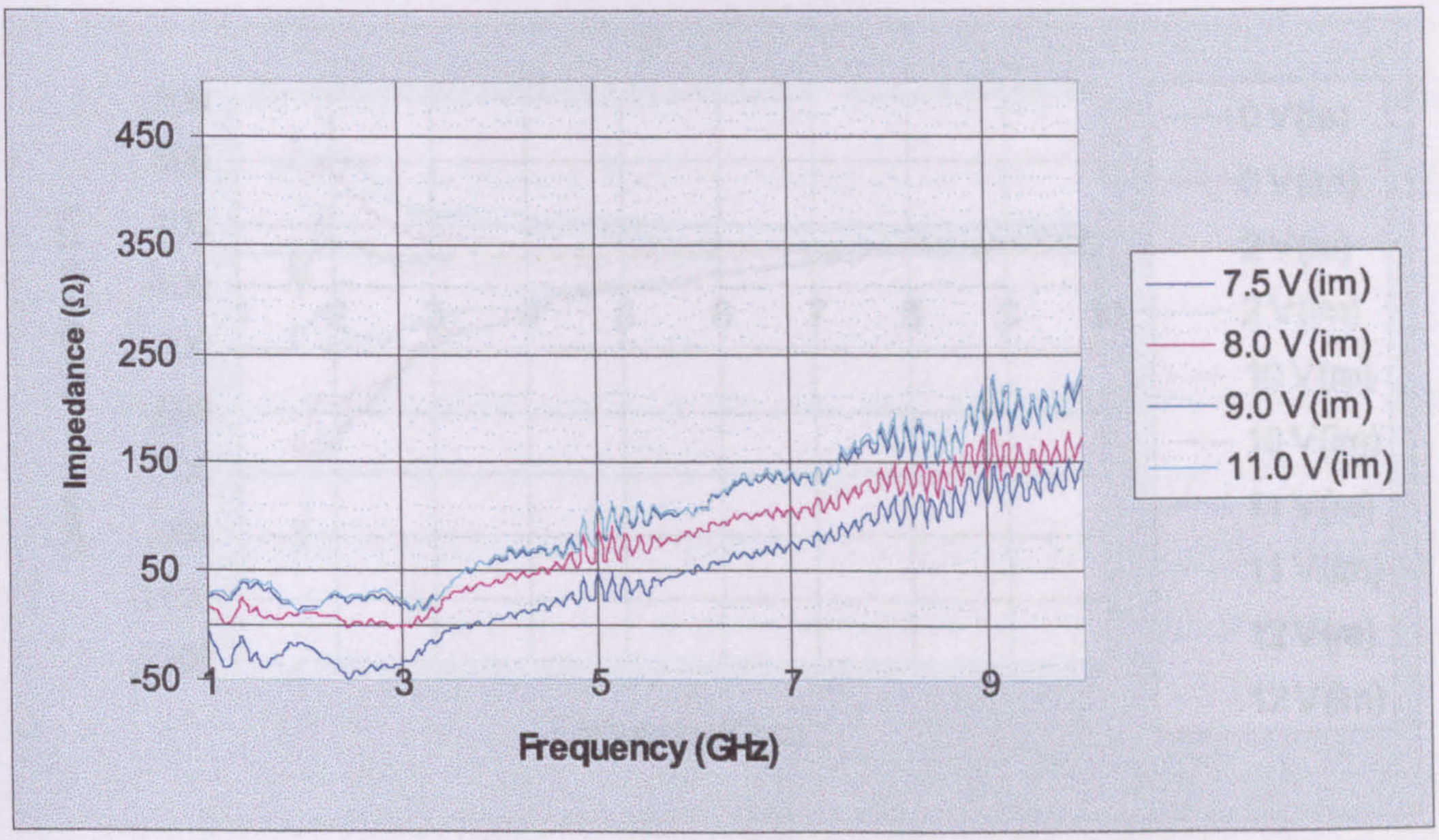

Figure 5.15: Measured dynamic imaginary part of the impedance response as a function of biasing voltage (7.5V through 11.0V) of DI-1 AFSS.

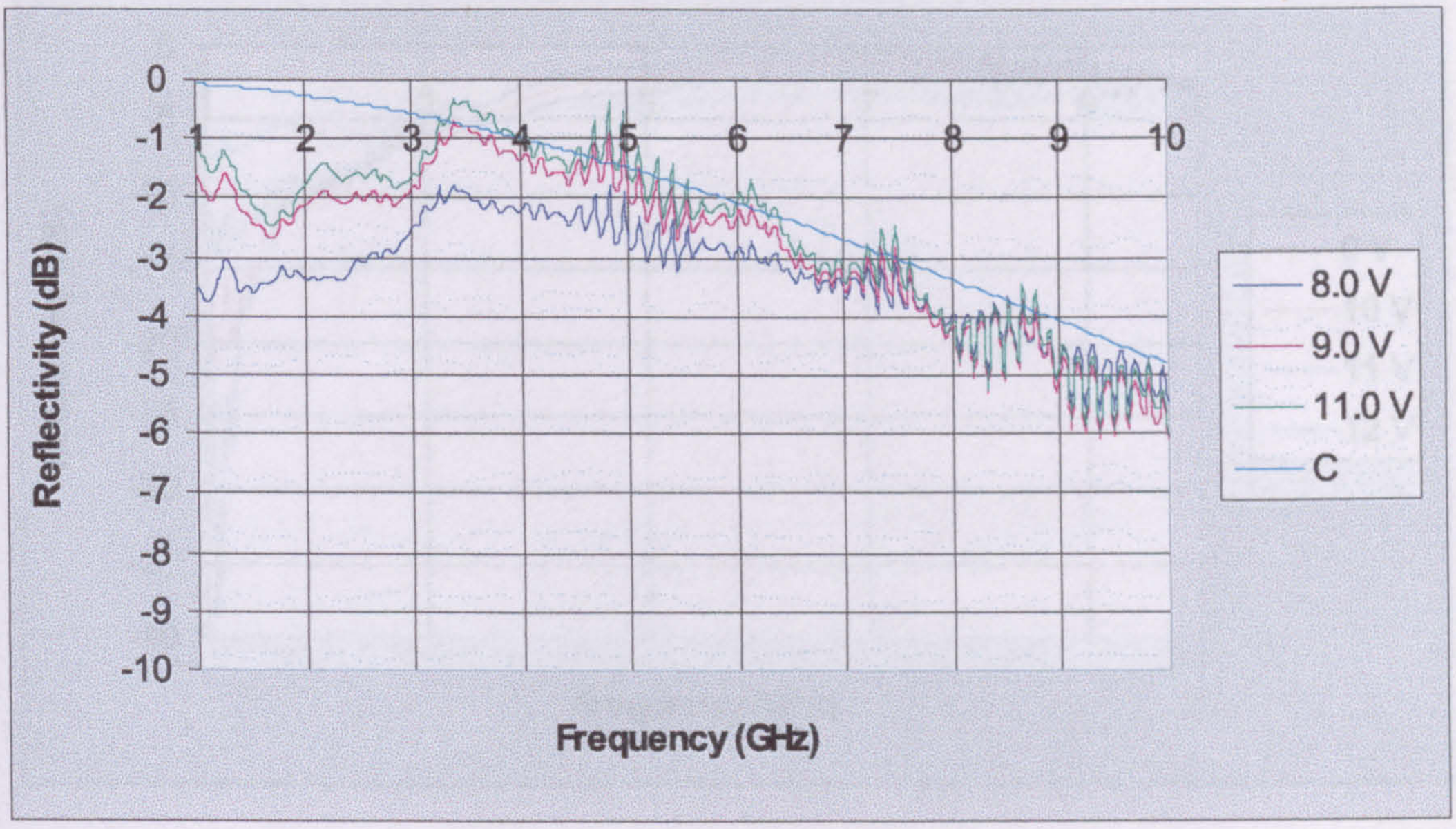

Figure 5.16: Measured dynamic reflectivity response of DI-1 AFSS under the influence of a biasing voltage: 8.0V to 11.0V.

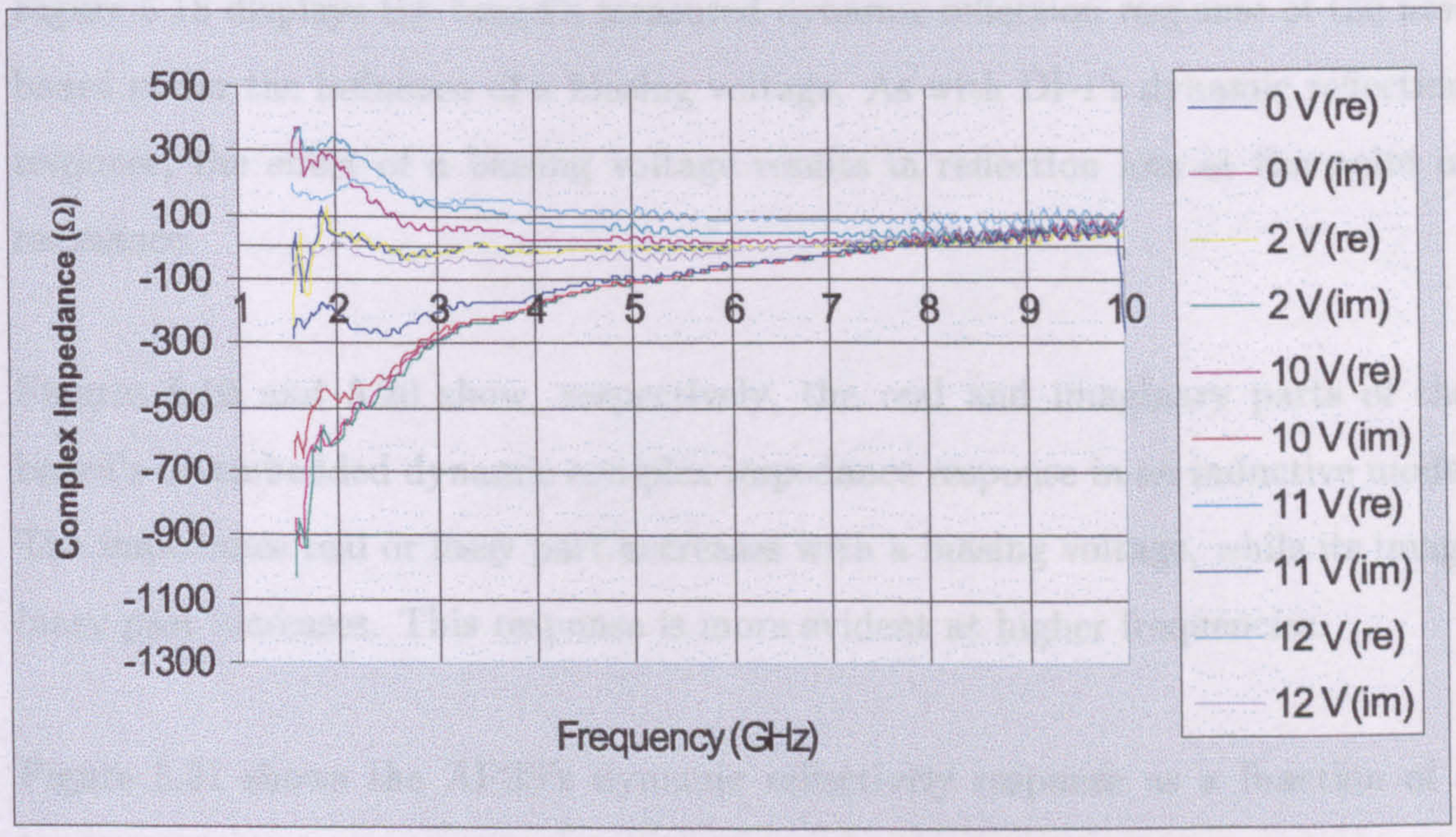

Figure 5.17: Measured dynamic complex impedance response of DI-2 as a function of a biasing voltage between 0V and 12V.

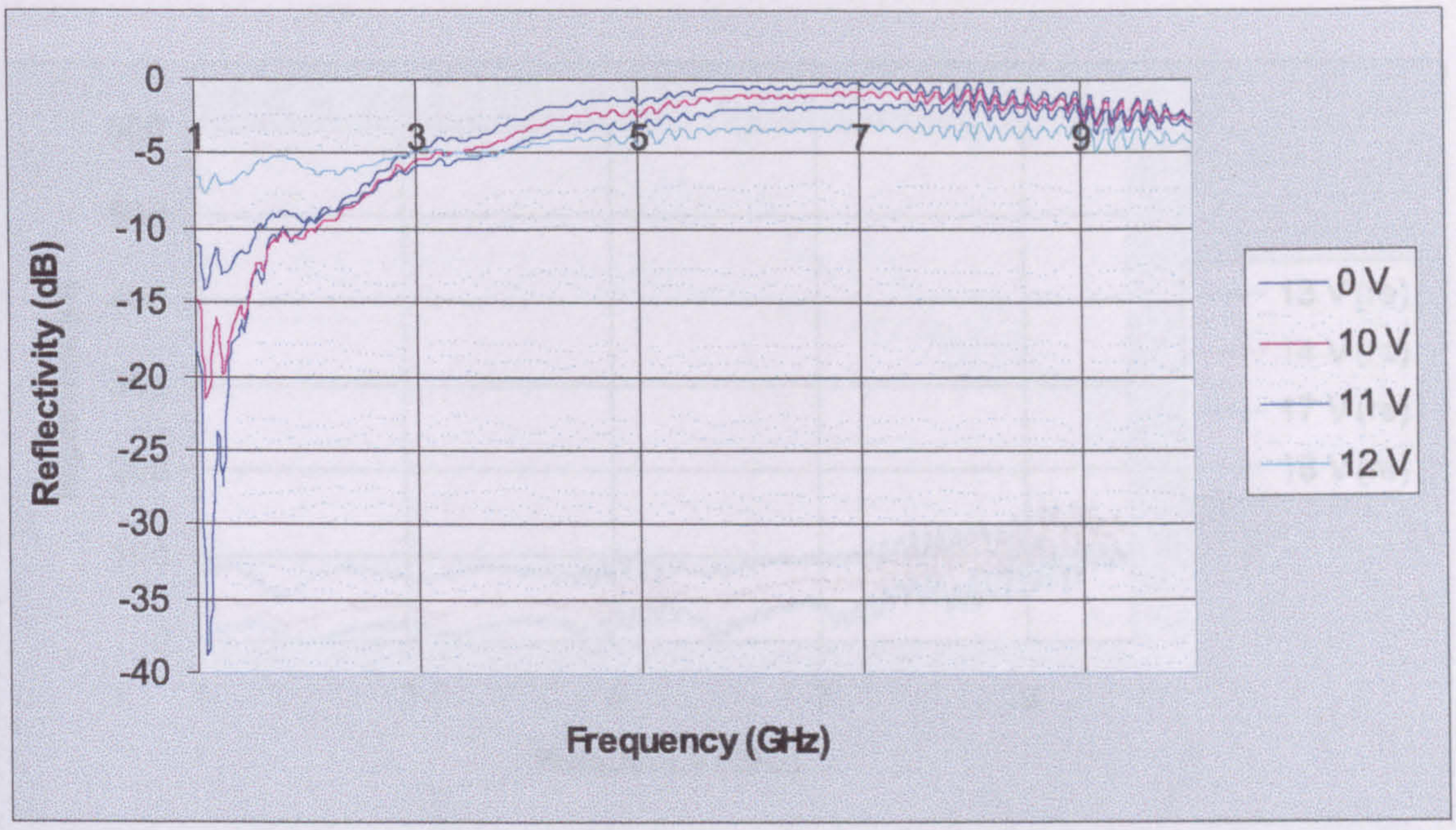

Figure 5.18: Measured dynamic reflectivity response of DI-2 AFSS as a function of a biasing voltage between 0V and 12V.

Figure 5.18 displays the board's measured dynamic reflection response of the new board under the influence of a biasing voltage. As with DI-1's dynamic reflection response, the effect of a biasing voltage results in reflection loss at the point of resonance.

Figures 5.19 and 5.20 show, respectively, the real and imaginary parts of the board's de-embedded dynamic complex impedance response in an inductive mode. The impedance real or lossy part decreases with a biasing voltage, while its imaginary part increases. This response is more evident at higher frequencies.

Figure 5.21 shows the AFSS's dynamic reflectivity response as a function of a biasing voltage between 13V and 18V. From the figure, it can be seen that as the tuning voltage is increased towards 18V the reflection loss decreases.

This section has shown how the bi-state characteristics of PIN diodes can be used

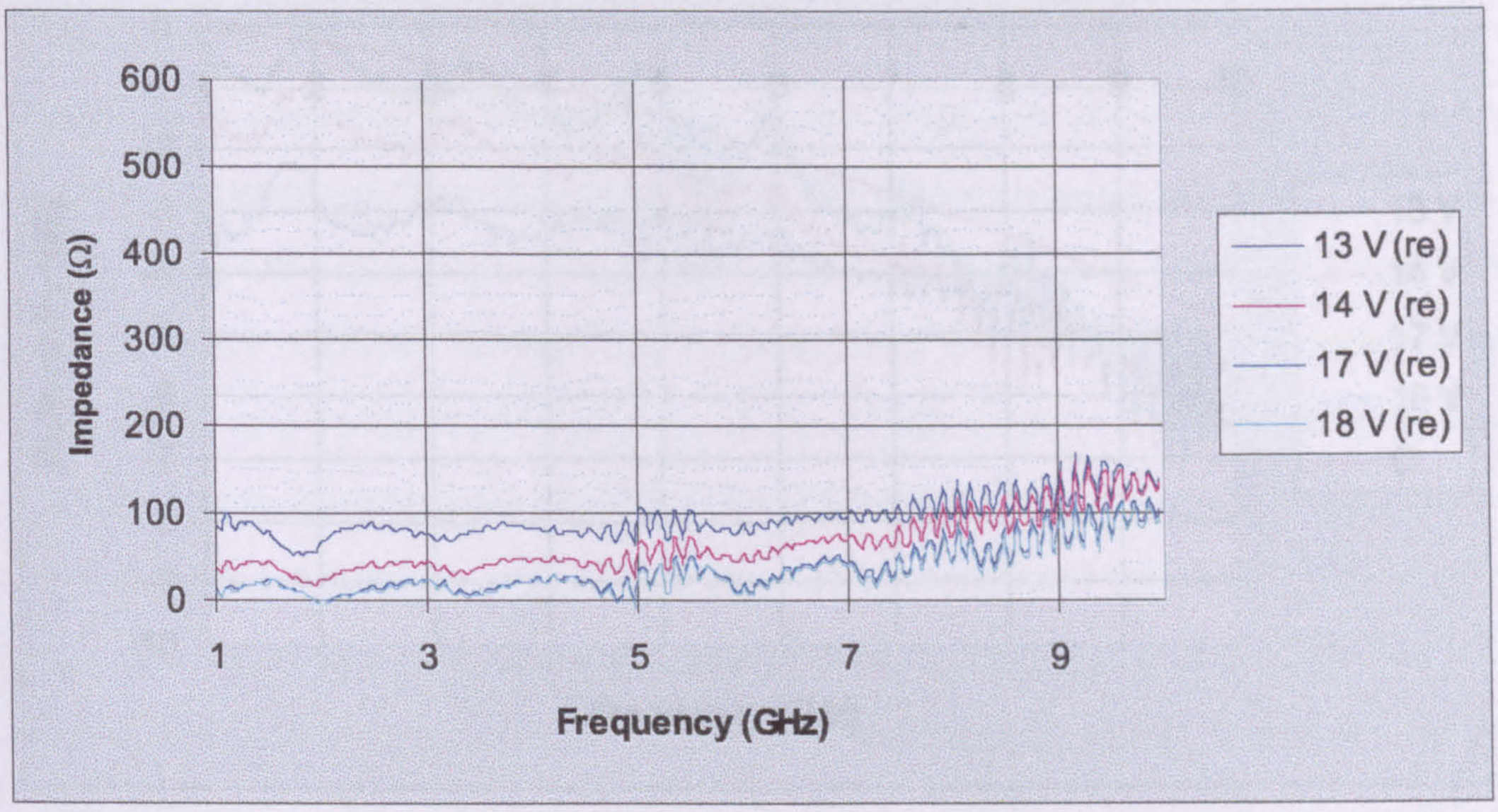

Figure 5.19: Measured dynamic real part of the impedance response of DI-2 AFSS as a function of a biasing voltage between 13V to 18V.

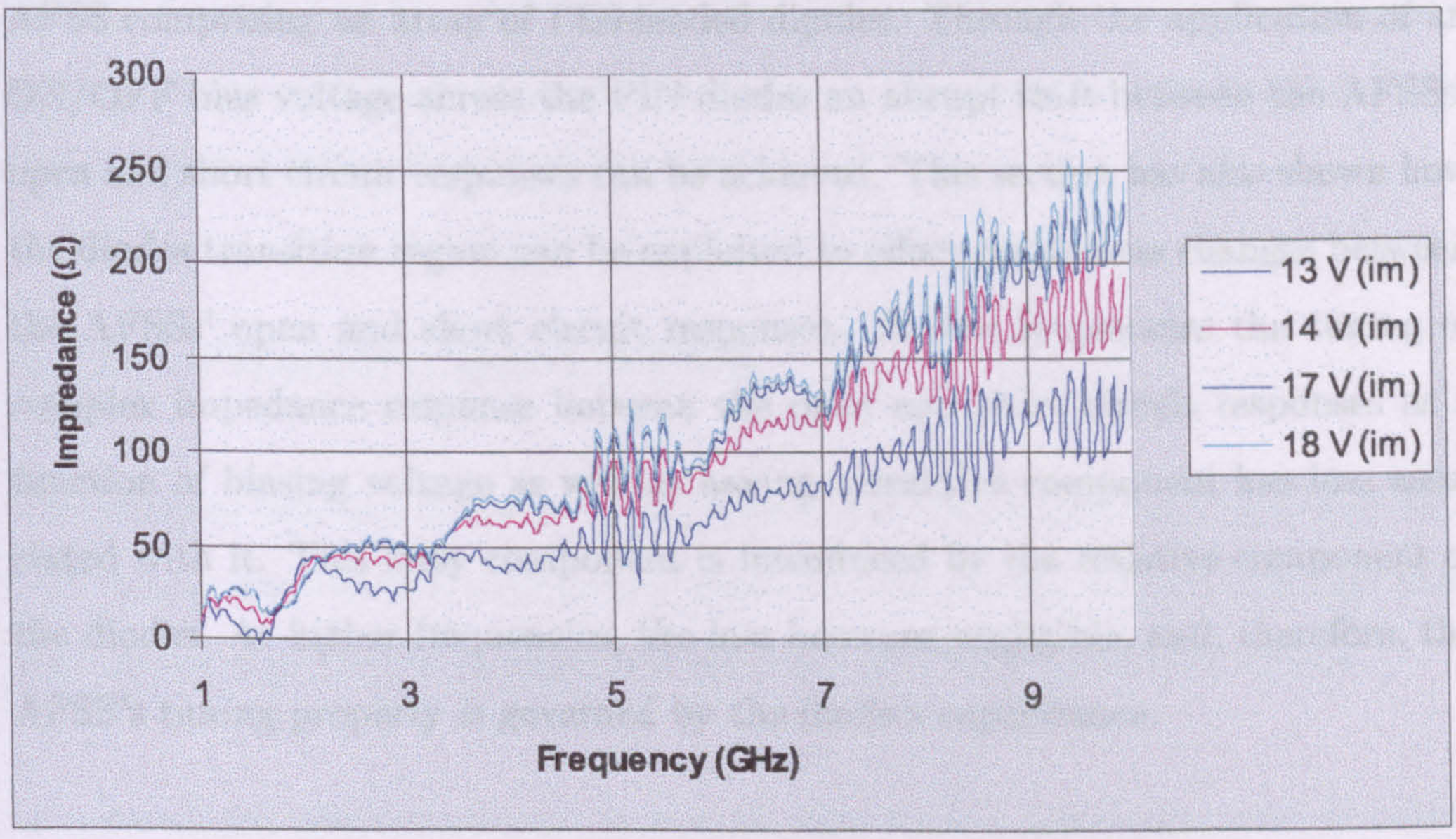

Figure 5.20: Measured dynamic imaginary part of the impedance response of DI-2 AFSS as a function of a biasing voltage between 13V to 18V.

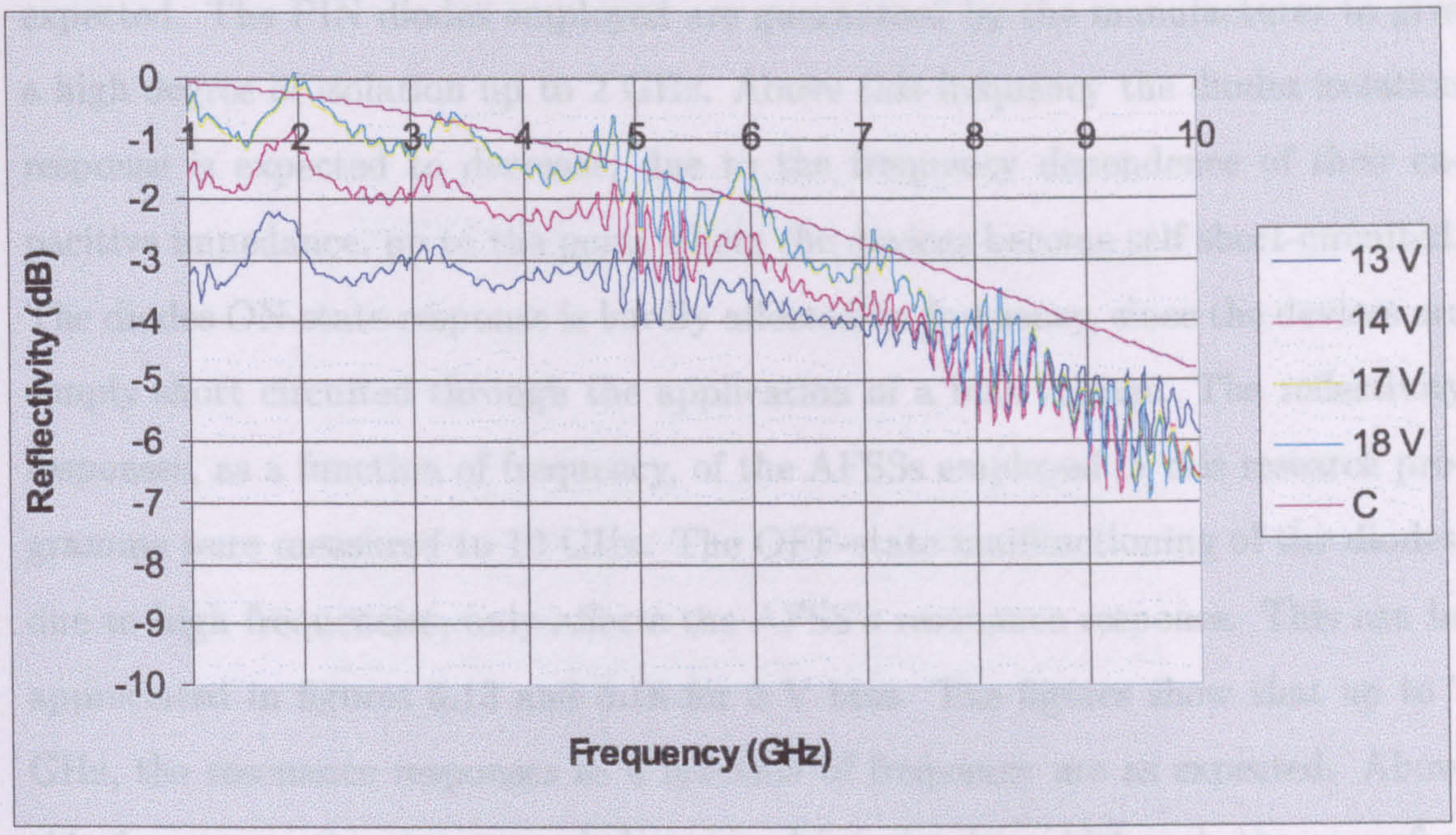

Figure 5.21: Measured dynamic reflectivity response of DI-2 AFSS as a function of a biasing voltage between 13V to 18V.

to introduced an open/short circuit response into the frequency properties of an AFSS comprising an array of PIN-loaded dipoles. Through the application of an ON/OFF bias voltage across the PIN diodes an abrupt shift between the AFSSs' open and short circuit responses can be achieved. This section has also shown how the diodes transition region can be exploited to effect continuous changes between the AFSSs' open and short circuit responses. At low frequencies the tuning of complex impedance response between the open and short circuit responses as a function of biasing voltage as well as having a reactive component has loss associated with it. This lossy component is introduced by the resistive component of the diodes. At higher frequencies, the loss becomes negligible, and, therefore, the AFSS's tuning property is governed by the diode's capacitance.

The technical specifications of the RF PIN diodes used in this investigation are outlined in table 5.3. As shown in the table their operating frequency range, recommended by the manufacturer, is from 1 MHz to 2 GHz. PIN diodes are used, in general, as ON/OFF switches. On their OFF state, a high degree of isolation is

expected. The PIN diodes employed are guaranteed by the manufacturer to give a high degree of isolation up to 2 GHz. Above this frequency the diodes isolation response is expected to decrease, due to the frequency dependence of their capacitive impedance, up to the point where the devices become self short-circuited. The diodes ON-state response is hardly affected by frequency, since the devices are simply short circuited through the application of a bias voltage. The reflectivity responses, as a function of frequency, of the AFSSs employed in this research programme were measured to 10 GHz. The OFF-state malfunctioning of the diodes, due to high frequencies, only affects the AFSS's resonance response. This can be appreciated in figures 5.13 and 5.18 for 0 V bias. The figures show that up to 7 GHz, the resonance responses as a function of frequency are as expected. Above this frequency, the structures behave as short circuits. Although the manufacturer recommends the diodes to be operated up to 2 GHz, figures 5.13 and 5.18 show that they are still useful up to 7 GHz. It is interesting to see that above 7 GHz, the diodes are harder on than when a bias voltage is dropped across them, see figure 5.9. Figures 5.5 and 5.6 show that the diodes ON-state is unaffected by high frequencies. The figures show that the measured responses closely follow the calculated ones, even at higher frequencies. This, thus, shows that the diodes ON-state are hardly affected by frequency.

5.4.2 Varactor-loaded AFSSs

The analysis outlined in the previous section has shown how loading a FSS with PIN diodes introduces low-frequency losses into the configuration's dynamic complex impedance when it is under the influence of a forward-biasing voltage.

In view of the aforementioned, it was thought that a practical course of action which may be taken to eliminate the effect of the diodes inherent loss was to load a dipole array with varactor diodes. Such configuration was chosen , rather than an array of inductive strips, for biasing purposes. A varactor diode is generically an

Technical Specifications.	
V_R (V)	50
I_F (mA)	50
I_R (nA) at 25°C	50
Operating Frequency Range	1MHz - 2GHz
Dimensions	
Length (mm)	2
Width (mm)	1

Table 5.3: Technical Specification and Dimensions of RF PIN Diode S0D 123 (SMT). V_R: Maximum Reverse Voltage, I_F: Forward Current, I_R: Reverse Current.

open-circuit device, and as such, a series connection of varactor diodes is infeasible.

Board	D_x mm	D_y mm	w mm	l mm	g mm	Sample size (cm^2)
DV-1	10	18	1	7	2	20x18

Table 5.4: Physical Parameters of Two AFSSs Composed of Varactor-loaded Dipoles.

Equivalent Circuit Analysis

Figure 5.22 shows a schematic diagram of an AFSS comprising an array of dipoles loaded with varactor diode together with its equivalent circuit. Consider the equivalent circuit. The AFSS's impedance Z_T is given by the series connection of the impedance due to the inductive strips Z_L and that due to capacitive effect of the

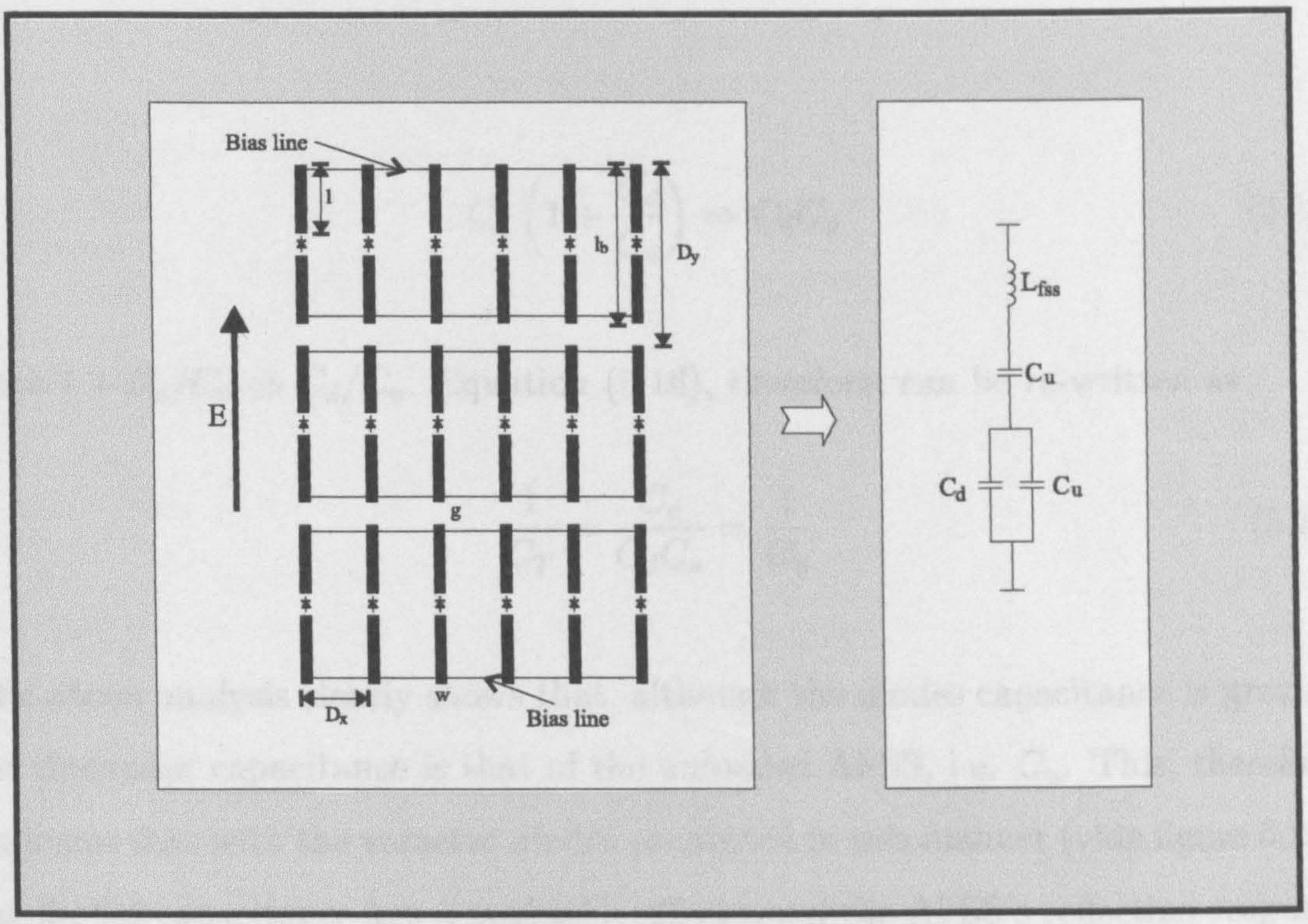

Figure 5.22: Schematic diagram of an AFSS loaded with varactor diodes and its equivalent circuit. L_{fss} is AFSS's inductance, C_u is the FSS's unloaded capacitance and C_d is the varactor diode capacitance.

loaded and unloaded dipoles Z_C. Such that

$$Z_T = Z_L + Z_C = j\omega L_{fss} - j\frac{1}{\omega C_T} \tag{5.13}$$

where $1/C_T$ is given by

$$\frac{1}{C_T} = \frac{2C_u + C_d}{C_u^2(1 + C_d/C_u)} \tag{5.14}$$

In the above equation C_d represents the diode's capacitance and C_u the capacitance between the dipoles. Now if $C_u < C_d$ the numerator and denominator of the above equation, respectively, become

$$2C_u + C_d \Rightarrow C_d \tag{5.15}$$

$$C_u^2\left(1+\frac{C_d}{C_u}\right) \Rightarrow C_d C_u \tag{5.16}$$

since $1 + C_d/C_u \Rightarrow C_d/C_u$. Equation (5.16), therefore, can be re-written as

$$\frac{1}{C_T} = \frac{C_d}{C_d C_u} = \frac{1}{C_u} \tag{5.17}$$

The above analysis clearly shows that, although the diodes capacitance is greater, the dominant capacitance is that of the unloaded AFSS, i.e. C_u. This, therefore, indicates that with the varactor diodes connected in this manner (vide figure 5.22), the diodes capacitance has a negligible effect upon the AFSS's reflection response when an increasing reverse-bias voltage is dropped across the diodes. This can be appreciated in figure 5.23. The figure depicts the dynamic reflection response of a varactor-loaded AFSS, namely DV-1. This AFSS was etched on a 200x180 mm^2 0.5 OZ Cu of thickness 0.611 mm and ϵ_r 2.20. The AFSSs' parameters are outlined in table 5.4. The figure clearly shows that a fully reverse bias voltage dropped across the varactor diodes has a very small effect in the reflection response of the the varactor-loaded AFSSs. Figure 5.24 the structure's complex impedance response as a function of frequency.

Although tuning of the complex impedance properties of this varactor-loaded AFSS is not possible, varactor loading does not introduce losses into the AFSS's complex impedance response. This is mainly because a varactor diode is operated in reverse mode where a reactive component is dominant. This is explained in chapter 3.

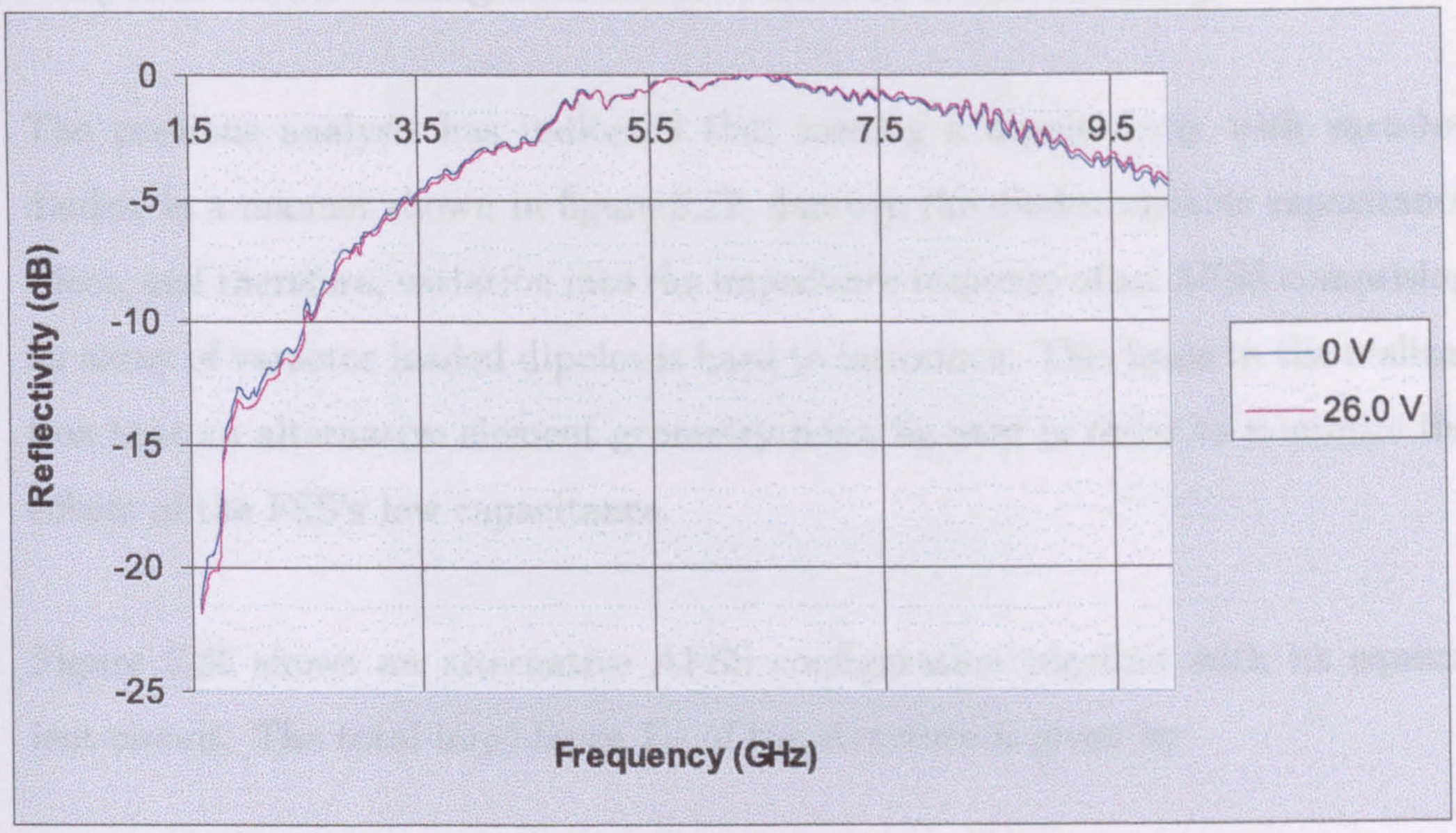

Figure 5.23: Measured dynamic reflectivity response of DV-1 AFSS as a function of 0V bias and -26V bias.

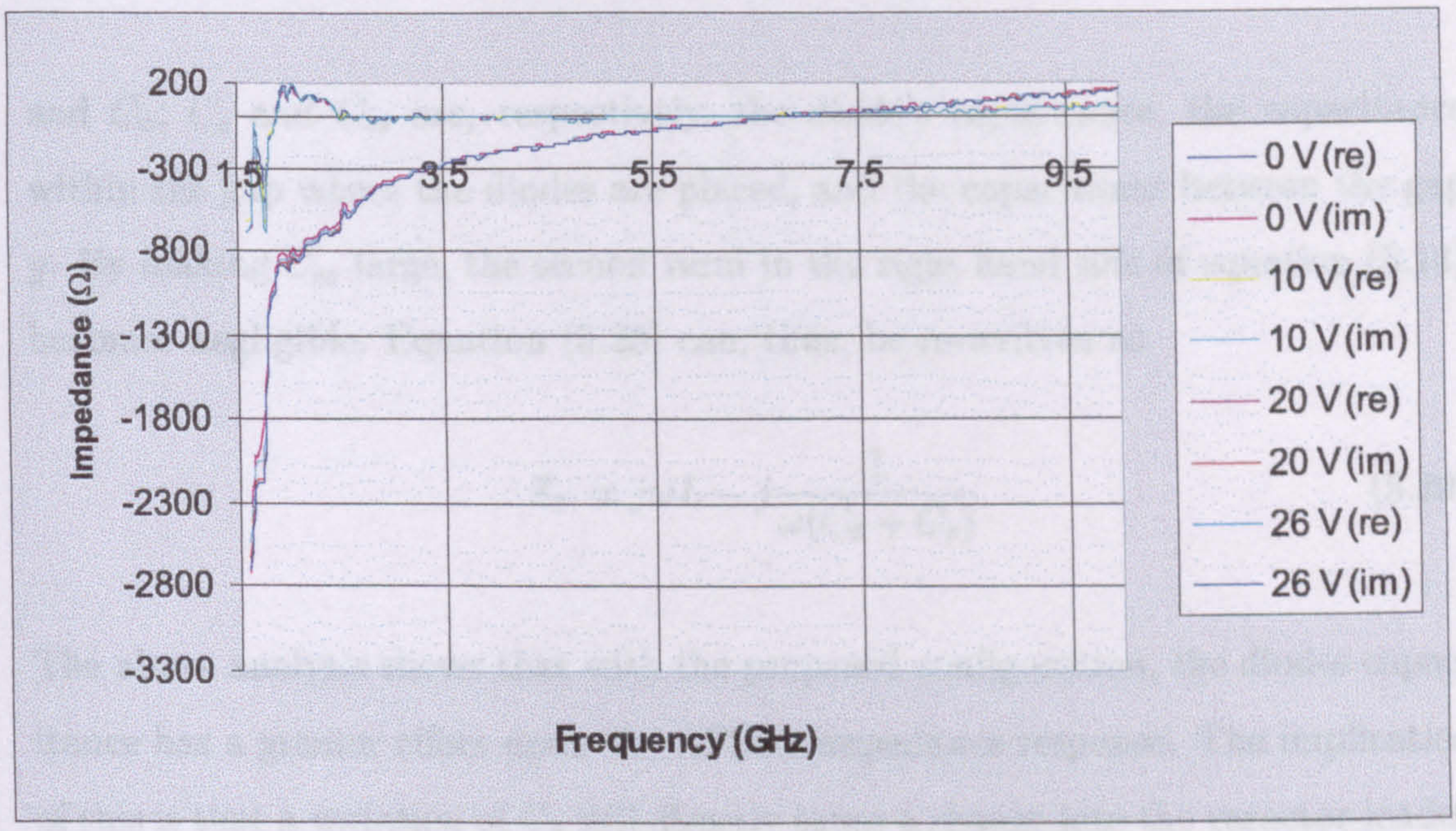

Figure 5.24: Measured dynamic complex impedance response of DV-1 AFSS as a function of a reverse biasing voltage between 0V and -26V.

Proposed AFSS Configuration for Varactor diode Loading

The previous analysis has indicated that loading a dipole array with varactor diodes, in a manner shown in figure 5.22, dampen the diodes variable capacitance effect, and therefore, variation into the impedance response of an AFSS comprising an array of varactor loaded dipoles is hard to introduce. This leads to the realization that an alternative element geometry must be used in order to minimize the effects of the FSS's low capacitance.

Figure 5.25 shows an alternative AFSS configuration together with its equivalent circuit. The total impedance Z_T of the structure is given by

$$Z_T = Z_l + Z_C = j\omega L + \frac{1}{j\omega C_T} \tag{5.18}$$

where $1/C_T$ is given by

$$\frac{1}{C_T} = \frac{1}{C_d + C_s} + \frac{1}{C_{cs}} \tag{5.19}$$

and C_d, C_s and C_{cs} are, respectively, the diode's capacitance, the capacitance within the gap where the diodes are placed, and the capacitance between the gap g. By making C_{cs} large, the second term in the right hand side of equation (5.18) becomes negligible. Equation (5.23) can, thus, be re-written as

$$Z_T = j\omega L - j\frac{1}{\omega(C_d + C_s)} \tag{5.20}$$

The above analysis shows that with the proposed configuration, the diodes capacitance has a greater effect upon the AFSS's impedance response. The implication of this is that a variation of C_d will directly cause a change into the varactor-loaded AFSS's complex impedance response. Now, C_{cs} can be made very large through

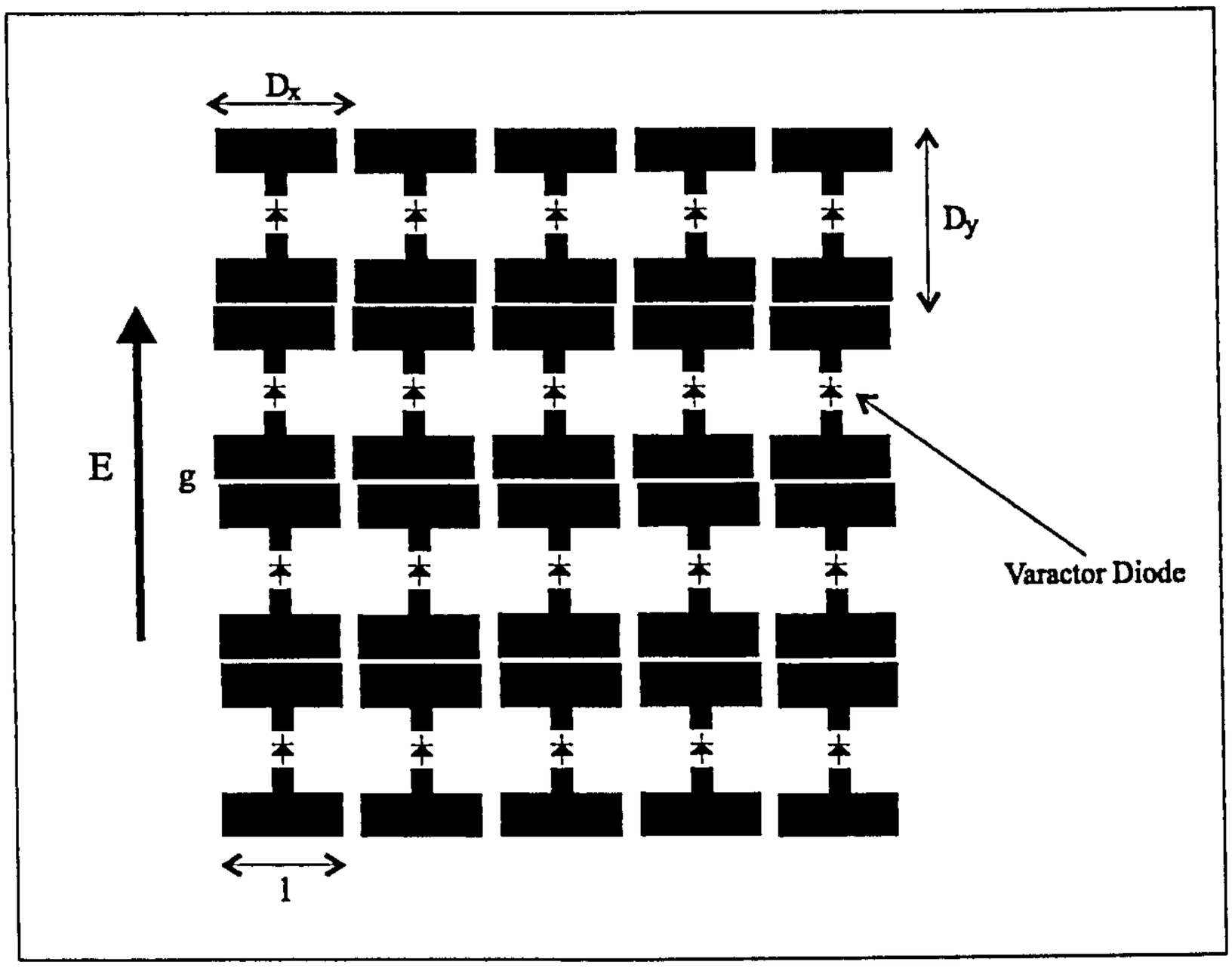

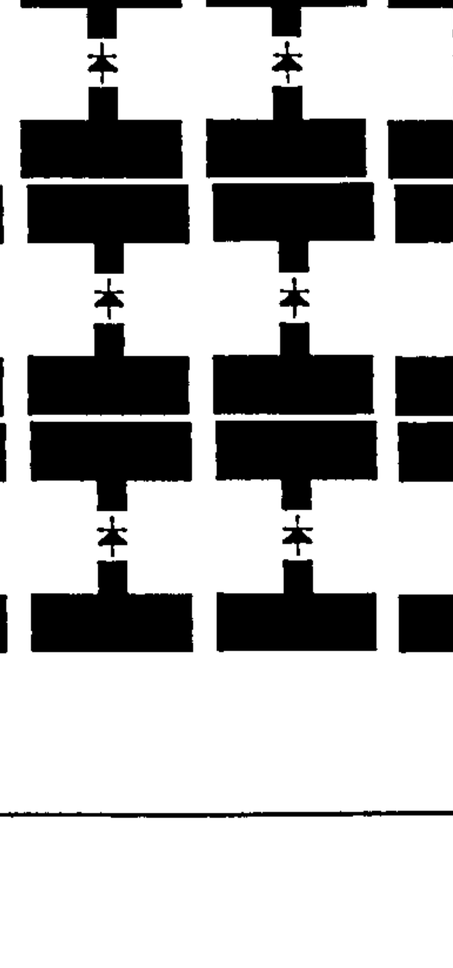

Figure 5.25: Schematic diagram of an alternative AFSS loaded with varactor diodes and its equivalent circuit. L_{fss} is AFSS's inductance, C_s is the FSS's unloaded capacitance and C_d is the varactor diode capacitance, C_{Cs} is the capacitance due to capacitive strips.

making the ratios l/D_x[5] and g/D_y[6] as close as possible to unity and as small as possible, respectively.

5.5 Summary

The adaptive complex impedance properties of Active Frequency Selective Surfaces loaded with semiconductor devices have been investigated. Two different AFSS configurations were studied. The first one was composed of an array of PIN-loaded dipoles, whose adaptive electrical properties are that of an open circuit and short circuit. The second one comprises an array of varactor-loaded dipoles whose frequency response is of a resonant type.

As well as the effect of applying OFF and ON bias voltages across the PIN-loaded AFSS, the effects of applying a forward biasing voltage between the diodes transition region was investigated and presented in this chapter. This was done to incur a continuous shift between the AFSS's open and short circuit responses. It was found that between the two extreme bias conditions, the complex impedance response is mainly reactive. In other words, there is little loss associated with such AFSS. However, within the transition region of the diodes the AFSS's dynamic frequency response not only depicts a reactive component, but also a lossy one. This loss, which is mainly present at low frequencies, has been found to be due to the PIN diodes series resistance.

In order to eliminate the the loss, an AFSS composed of an array of varactor-loaded dipoles was investigated. With this configuration, however, the inductive-resonant response is fundamentally infeasible to implement since varactor diodes are gener-

[5] l is the length of the capacitive metallic strips and D_x is the element's periodicity in the x direction (vide figure 5.23)

[6] g is the gap between the capacitive metallic strips and D_y is element's periodicity in the y direction (vide figure 5.23)

ically open-circuit devices, and, as such, cannot be operated when connected in series. Although the investigation into it showed that varactor loading introduces negligible loss into the frequency response of an AFSS, adaptive impedance properties could not be implemented. The reason for this is that with such configuration the low capacitance of the dipole array is more dominant than that of the varactor diodes, and, as such, dominates the AFSS's frequency response.

In view of the aforementioned, a alternative configuration was proposed. No measured data is presented. Nonetheless, the author believes that through varactor-loading the proposed configuration, the AFSS's complex impedance response can be varied through the application of a reverse-bias voltage.

Bibliography

[1] Brewitt-Taylor, C. R., *Fundamental Limit on the Performance of Radar Absorbing Materials*, Digest of IEEE Antennas and Propagation Symposium, Orlando, Florida, Vol 3, July 1999, pp. 1938-1941.

[2] Wong, P. T. C., Chambers, B., Anderson A. P., Wright, P. V., *large Area Conducting Polymer Composites and Their Use in Microwave Absorbing Material*, Electronics Letters, No. 28, pp. 1651-1653.

[3] Vardaxoglou, J. C., *Frequency Selective Surfaces - Analysis and Design*, John Wiley And Sons Ltd., 1997.

[4] Agrawal, V. D., Imbriale, W. A., *Design of a Dichroic Casegrain Subreflector*, IEEE Transaction on Antennas and Propgation, Vol. AP-27, No. 4, 1979, pp. 466-473.

[5] Torres, Al, *RF/IR Dichroic Beam Combiner*, Antenna Measurement Techniques Association: 20th Annual Meeting and Symposium, Montreal, Canada, October 1998, pp. 352-356.

[6] Antonopoulos, C., Cahill, R., Parker, E. A., Sturland, I. M., *Multilayer Frequency-Selective Surfaces for Millimetre and Submillimetre Wave Applications*, IEE Proceedings Microwave Antennas and Propagation, Vol. 144, No. 6, 1997, pp. 415-420.

[7] Wang, Z. L., Hashimoto, K., Shinohara, N., Matsumoto, H., *Frequency Selective Surface for Microwave Power Transmission*, IEEE Transactions on Microwave Theory and Techniques, Vol. 47, No. 10, 1999, pp. 2039-2042.

[8] Chekroun, C., Herrick, D., Michel, Y., Pauchard, R., Vidal, P., *Radant: New Method of Electronic Scanning*, Microwave Journal, 1981, pp. 45-53.

[9] Dittrich, K.W., *Multifunctional Skins*, Six European Electromagnetic Conference Proceedings, 1991, pp. 1-13.

[10] Philips, B., Parker, E.A., Langley, R.J., *Active FSS in an Experimental Horn Antenna Switchable between Two Beamwidths*, Electronics Letters, Vol. 31, No. 1, 1995, pp. 1-2.

[11] Lima, A.C de C., Parker, E.A., Langley, R.J., *Tunable Frequency Selective Surfaces using Liquid Substrates*, Electronics Letters, Vol. 30, No. 4, 1994, pp. 281-282.

[12] Vardaxoglou, J.C.,*Optical Switching of Frequency Selective Surface Bandpass Response*, Electronics Letters, Vol. 32, No. 25, 1996, pp. 2345-2346.

[13] Chang, T.K., Langley, R.J., Parker, E.A., *Frequency Selective Surfaces on Biased Ferrite Substrate*, Electronics Letters, Vol. 30, No. 15, 1994, pp. 1193-1194.

[14] Shuley, N.V., *Diode Loaded Frequency Selective Surfaces*, Proceedings of JINA 92 International Conference on Antennas, Nice, France, 1992, pp. 313-316.

[15] Chang, T.K., Langley, R.J., Parker, E.A., *An Active Square Loop Frequency Selective Surface*, IEEE Microwave and Guided Wave Letters, Vol. 3, No. 10, 1993, pp. 387-388.

[16] Chang, T.K., Langley, R.J., Parker, E.A., *Active Frequency Selective Surfaces* IEE Proceedings on Microwave and Antenna Propagation, Vol. 143, No. 1, 1996, pp. 62-66.

[17] Sigfrid Yngvesson, *Microwave Semiconductor Devices*, Kluwer Academic Publishers, 1991.

[18] Chang, K., *RF and Microwave Wireless Systems*, John Wiley and Sons, 2000.

[19] Callagham, P., Parker, E. A., Langley, R. J., *Influence of Supporting Dielectric Layers on the Transmission Properties of Frequency Selective Surfaces*, IEE Proceedings-H, Vol. 138, No. 5, 1991, pp. 448-454.

[20] Parker, E. A., Vardaxoglou, J. C., Langley, R., *Influence of Single and Multilayer Dielectric Substrate on the Band Spacing Available from a Concentric Ring Frequency Selective Surface*, International Journal in Electronics, Vol. 61, No. 3. 1985, pp. 291-297.

[21] Munk, B. A., Cornbau, T. W., *On the Stabilisation of the Bandwidth of a Dichroic Surface by Use of Dielectric Slab*, IEEE Transactions on Antennas and Propagation, Vol. AP-5, No. 4. 1985, pp. 349-373.

[22] Chandran, S., Vardaxoglou, J.C.,*Performance of Two-Single Layer Frequency Selective Surface as Spatial Filter*, Microwave and Optical Technology Letters, Vol. 6, 1993, pp. 339-342.

[23] Chen, Chao-Chun, *Scattering by a Two-Dimensional Periodic Array of Conducting Plates*, IEEE Transactions on Antennas and Propagation, 1970, pp. 660-665.

[24] Carroll, J. E., *Physical Model for Semiconductor Devices*, Edward Arnold, 1974.

Chapter 6

Dynamic RAM Optimization by Genetic Algorithm

6.1 Introduction

The domain solution in terms of wideband absorption of a Salisbury screen absorber embedded with a number of semiconductor-loaded AFSSs as well as being unknown is rather complex. The level of difficulty in finding the global broadband absorption solution of such a problem is not only determined by the AFSS's non-linear dynamic complex impedance properties, but also by the number of AFSSs embedded within the absorber. Due to this highly elaborated design problem, a genetic algorithm (GA) optimizer is employed in this research programme to find the nature of the space solution of the proposed absorber, which will ultimately lead to the much sought global solution.

Although this chapter starts with a short introduction to Genetic Algorithms, the aim of the chapter is, however, to present the fitness function which was employed in this research programme to find the global solution of the proposed absorber. The fitness function plays an important role in determining the optimum solution

of a multi-dimensional problem since it is the only physical link between the problem to be optimized and the optimizer.

The chapter also presents tests carried out on the GA software in order to validate it. Such tests were performed upon electromagnetic problem with well accepted solutions.

6.2 GA Algorithms

Genetic Algorithms (GAs), a type of Evolutionary Computing, is a powerful computational technique used in the search of optimum solution(s) of multi-dimensional problems. GAs mirror natural selection for propagation of successful genes, a concept which is based on Darwin's theory of evolution. His theory proposes that life on this planet, in all its diverse and well-adapted forms, has been created by Natural Selection. Natural Selection or Survival of the Fittest is the preservation of favorable individual differences and variations, and the destruction of those who are injurious [1]. In this way, individuals having any advantage, however slight, over others would have the best chances of survival and the procreation of their kind. GAs search algorithm is based on Nature's powerful search method, which is living proof that it works. It generates far better creatures which are well adapted to the most complex conditions of life. GAs work by first choosing a set of trial solutions or individuals which are evolved towards an optimal solution measured by the selective requirements of a fitness function. The theory behind genetic algorithms can be explained by the Schema Theorem[2].

As optimisers, Genetic Algorithms are classified as global methods in that their search technique is highly independent of the initial conditions. Some of the advantages of GAs over local techniques, such as the Conjugate Gradient, lie in that they are not dependent on the existence of a derivative in the form of a gradient. They are much better at dealing with solution spaces having discontinuities; and

they can deal better with a large number of dimensions with many potential local maxima [3]. Their downside is that their convergence rate is slower than the gradient techniques. However, in electromagnetic design problems convergence rate is sometimes not as important as getting a global solution, in particular for new problems in which the nature of the solution space is relatively unknown.

Although a fairly new search concept, GAs have successfully been implemented and used in different areas of electromagnetics. In the antenna sector, GAs have found applications in the optimum design of printed antenna [3], broadband antennas [4], integrated antennas [5], wire antennas [6], and antenna array thinning [7]. Another area where GA has been used is in the design of electromagnetic filtering structures such as multi-layer filters [8] and FSSs [9]. GAs have also been used in the absorber area to find optimum designs of Jaumann absorbers [10] and multi-layer microwave absorbers [11].

The Simple Genetic Algorithm

A flow chart of the simple GA optimizer, described by Golberg [12], is shown in figure 6.1. In general , a simple GA consisits of three phases. These are (i) initiation, (ii) reproduction and (iii) generation replacement. With reference to figure 6.1, initiation consists of filling an initial population with a predetermined number of chromosomes or *individuals*. This set of individuals is called the current population. The fitness of each individual is then evaluated through a performance or fitness function F. Each individual in the population is thus assigned a fitness value. The reproduction phase creates a new population from the current generation. This is done through accomplishing selection, crossover or asexual reproduction[1], and mutuation[2]. In selection a pair of individual or parents are chosen

[1]The act of genetic material crossing over from one chromosome to another. In GA, this is performed through a crossover probability operator (pcross).

[2]The act of introducing genetic material which is not present in the current population. In GA, this is performed through a mutation probability operator (pmut).

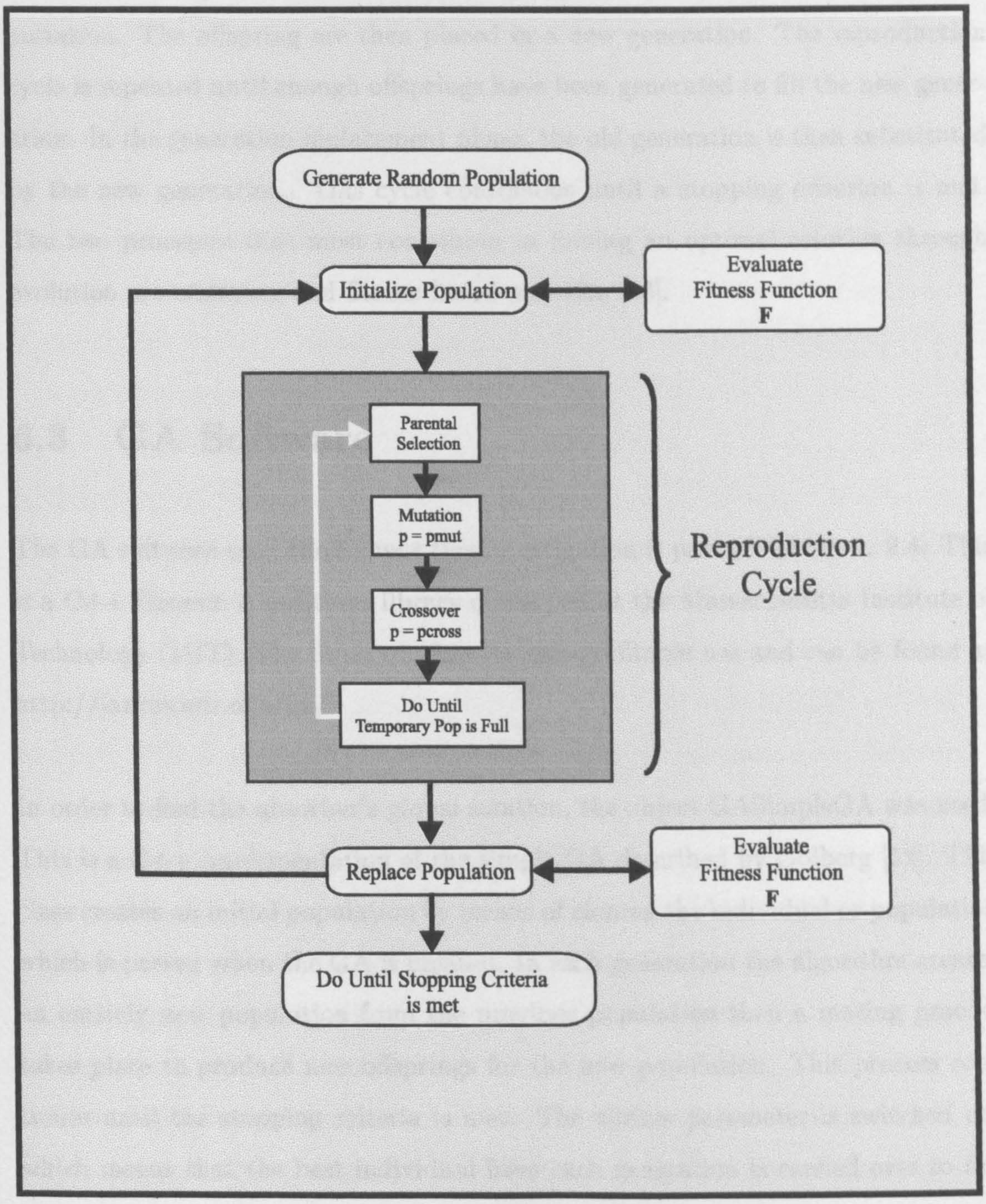

Figure 6.1: Simple GA flow chart.

to create a new pair of individuals or offspring through undergoing crossover and mutation. The offspring are then placed in a new generation. The reproduction cycle is repeated until enough offsprings have been generated to fill the new generation. In the generation replacement phase, the old generation is then substituted by the new generation. This cycle continuous until a stopping criterion is met. The two processes that most contribute to finding an optimal solution through evolution are crossover and fitness based selection [13].

6.3 GA Software

The GA software used throughout this investigation is part of GALib v. 2.4. This is a C+++ Genetic Algorithms library developed at the Massachusetts Institute of Technology (MIT). The library is free for non-profitable use and can be found at http://lancet.mit.edu/ga/.

In order to find the absorber's global solution, the object GASimpleGA was used. This is a C++ implementation of the simple GA described by Golberg [12]. This class creates an initial population by means of cloning the individual or population which is passed when the GA is created. In each generation the algorithm creates an entirely new population from the previous population then a mating process takes place to produce new offsprings for the new population. This process continues until the stopping criteria is met. The elitism parameter is switched on, which means that the best individual from each generation is carried over to the next generation. The simple GASimpleGA uses non-overlapping populations.

Before the aforementioned GA C++ library was employed to find the global solution, in terms of wide absorption bandwidth, of the proposed absorber methodology, it was first tested in electromagnetic problems with known solutions. Convergence of the solutions given by the library to the electromagnetic problems known solutions is a clear indicator of the proper functionality of the algorithm. Please

refer to appendix C.

6.4 Fitness Function

In an optimization procedure the fitness function is the only physical link between the problem being optimized and the optimizer. This means that proper choice of fitness function is of paramount importance in the search of a problem global, rather than a local, solution.

As described in chapter 4, the methodology proposed in this research programme to minimize the trade-off between absorber thickness and absorption bandwidth, without the need to rely on materials parameters, consists in generating a number of reflection nulls within a broad frequency band. This can be achieved by multiple partitioning a Salisbury absorber's total thickness through embedding within it PIN-loaded AFSSs with bi-state electrical properties, in the form of an open and short circuit characteristics, as well as with linear and continuous complex impedance tuning between the open and short circuit responses. The reflection nulls thus generated can be coarsely tuned as well as narrowly tuned over a broad and narrow frequency bands, respectively. Coarse tuning is implemented by exploiting the AFSS's short/open circuit response, while narrowband tuning through the linear and continuous shift between the AFSS's open and short circuit frequency response. As also explained in chapter 4, the realistic number of such AFSSs that can be used for this aim is two, since employing more will only result in the generation of reflection null redundancy. Now, in order to achieve the broadest possible absorption bandwidth the optimum placement of the AFSSs within a Salisbury screen absorber must be realized. The aim of the fitness function is, thus, to find the optimum placement of two AFSS within a Salisbury screen absorber, which yields the widest coarsely tuned absorption band solution while minimizing the absorber thickness.

The maximum absorption bandwidth occurs when both AFSSs (A1 and A2) placed within a Salisbury Screen absorber are operated in open circuit mode (state 1), and the AFSS closest to the 377-resistive film (A1) is operated in short circuit mode (state 4). The former sets the lowest absorption frequency ($f_{1.1}$), while the latter the maximum absorption frequency ($f_{4.1}$). The other two remaining states, namely 2 and 3, place two reflection nulls within $f_{1.1}$ and $f_{4.1}$. This solution, thus, places a number of reflection nulls at discrete frequencies over a wide frequency band. To completely cover the entire working band, narrow band tuning is applied between any two adjacent and coarsely tuned reflection nulls. It is, however, not required from the optimizer to find an optimum narrowband tuning solution. This is the case since the AFSS's frequency response can be linearly and continuously shifted between its open and short circuit responses, as shown in chapter 5. As explained in chapter 4, such characteristic, effectively, moves forward the short circuit structure placed behind the currently tuned AFSS, thus, achieving narrow band tuning.

In order to find the global solution of the proposed radar absorbing material design, two different fitness functions were developed and tested. Resemblance of their solutions is a indicator that a global solution has indeed been found. The fitness functions employed are shown in tables 6.5 and 6.6, namely FF1 and FF2, respectively, and are graphically depicted in figures 6.3 and 6.4, respectively.

FF1 is a function that maximizes the largest difference of the magnitude of the reflection coefficient Γ between any two states. The second fitness function FF2 maximizes twice the difference of reflection null frequency of state 4 (table 4.3), namely $f_{4.1}$, and that of state one, $f_{1.1}$. FF2 also looks for the reflection null frequencies of the intermediate states 2 and 3, i.e. $f_{2.1}$ and $f_{3.1}$. This fitness function, as well as the latter, equally spreads the reflection nulls over the frequency band. Both fitness equations are functions of the three permissible subthicknesses, namely d_1, d_2 and d_3, generated by the placement of two AFSSs within a Salisbury screen absorber.

Fitness Function: FF1
$F(d_1, d_3, d_5) = \Gamma_{s_{MAX}} - \Gamma_{s_{MIN}}$
where
$\Gamma_{s_{MAX}}(d_1, d_3, d_5)$
$\Gamma_{s_{MIN}}(d_1, d_3, d_5)$

Table 6.1: Fitness Function FF1. $\Gamma_{s_{MAX}}$ and $\Gamma_{s_{MIN}}$ are the maximum and minimum reflection coefficients for two different states or solutions.

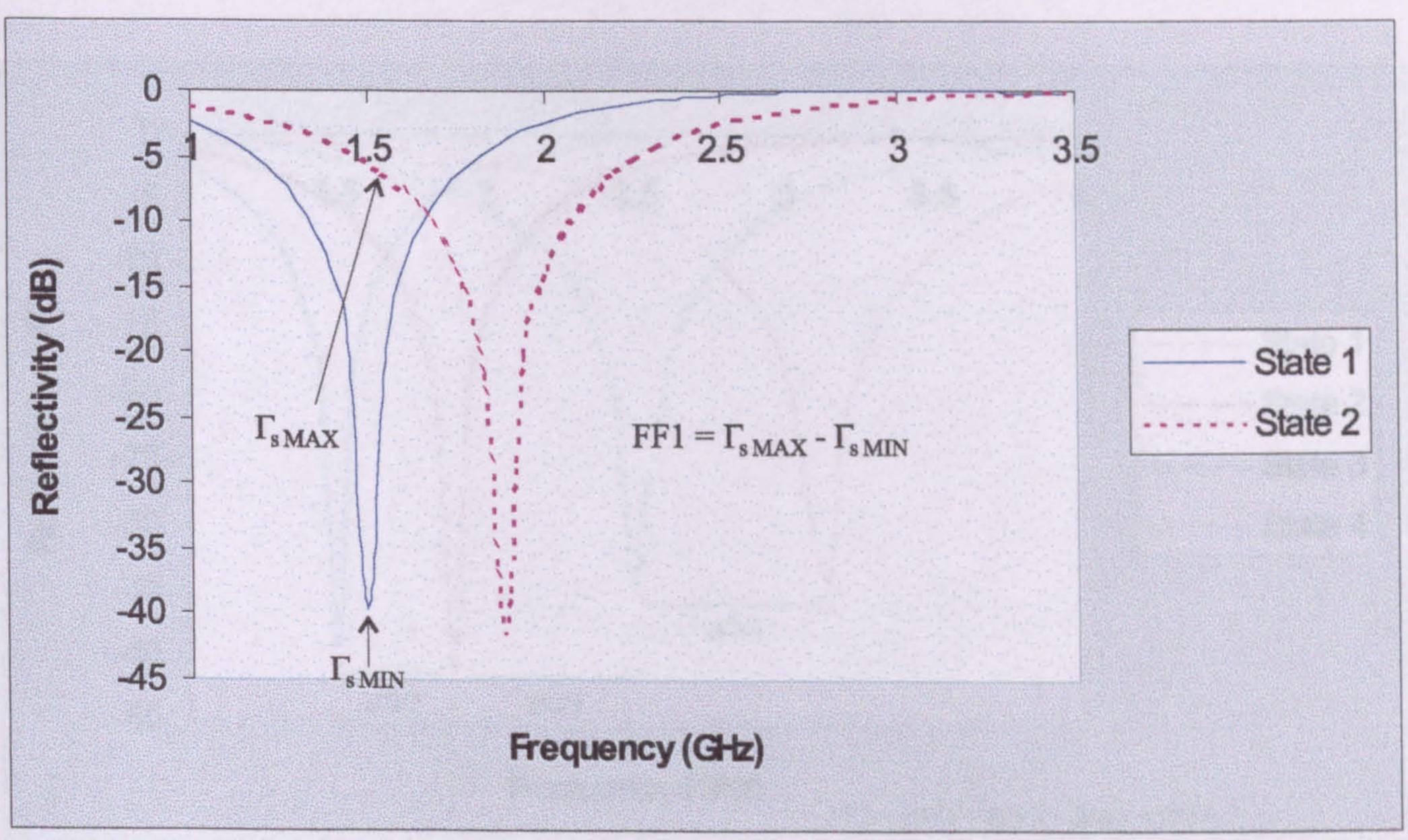

Figure 6.2: Graphical representation of FF1 fitness function.

Fitness Function FF2
$F(d_1, d_3, d_5) = BW1 + BW2 + BW3 + BW4$
where
$BW1(d_1, d_3, d_5) = f_{4.1} - f_{1.1}$
$BW2(d_1, d_3, d_5) = f_{3.1} - f_{1.1}$
$BW3(d_1, d_3, d_5) = f_{2.1} - f_{3.1}$
$BW4(d_1, d_3, d_5) = f_{4.1} - f_{2.1}$

Table 6.2: Fitness Function FF2. Key $f_{s.x}$, where f is the frequency of resonance, s is the state and x is the null number

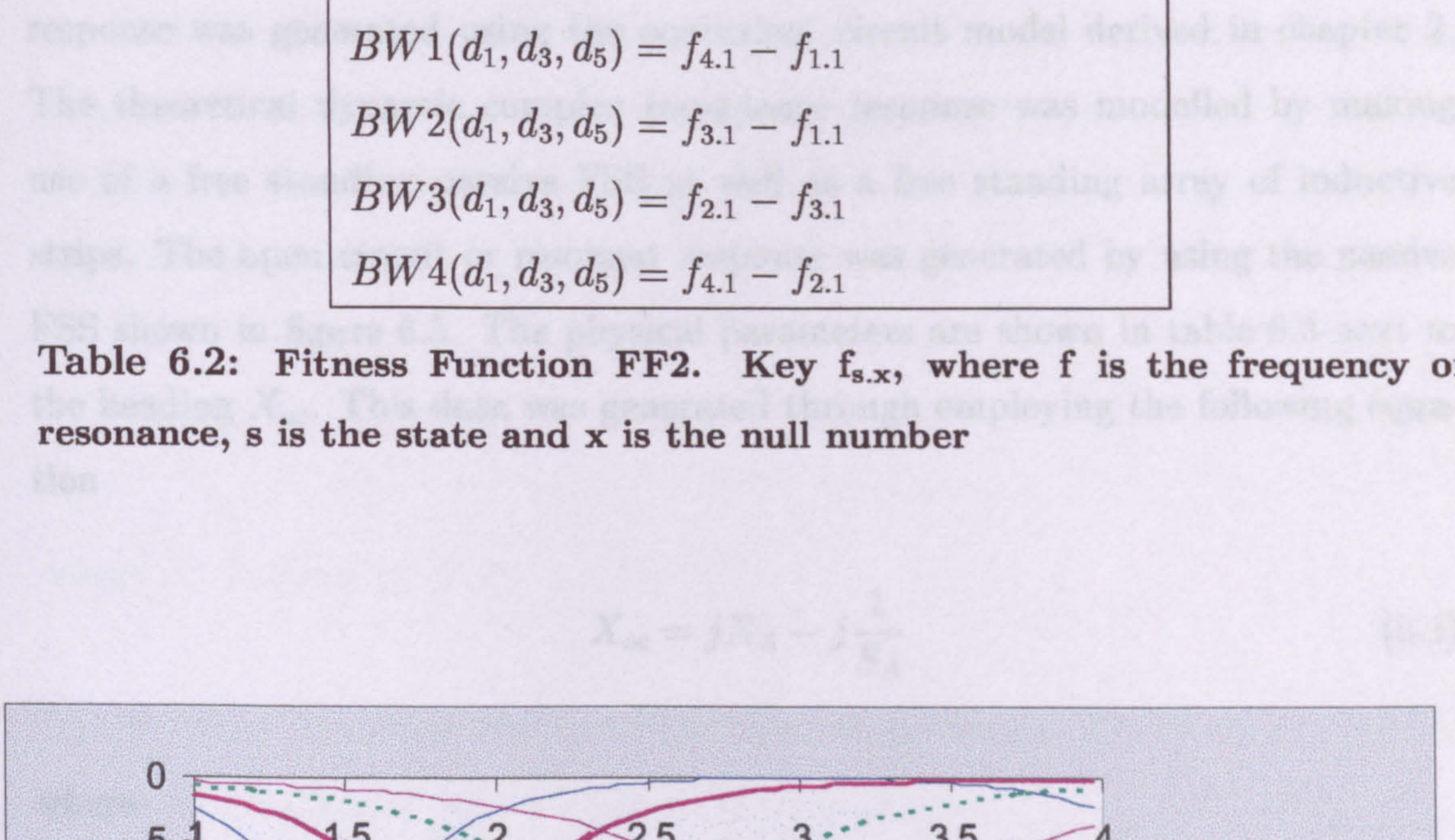

Figure 6.3: Graphical representation of FF2 fitness function.

6.4.1 Evaluation of Fitness Functions

The fitness functions were assessed with theoretically generated dynamic complex impedance data. The dynamic complex impedance data employed is graphically shown in figure 6.4 and was chosen to resemble the dynamic complex impedance behaviour of an AFSS comprising an array of PIN-loaded dipoles under the diodes extreme bias conditions, namely OFF and ON. The dynamic complex impedance response was generated using the equivalent circuit model derived in chapter 2. The theoretical dynamic complex impedance response was modelled by making use of a free standing passive FSS as well as a free standing array of inductive strips. The open circuit or resonant response was generated by using the passive FSS shown in figure 6.5. The physical parameters are shown in table 6.3 next to the heading X_{oc}. This data was generated through employing the following equation

$$X_{oc} = jX_A - j\frac{1}{S_A} \tag{6.1}$$

where

$$X_A = \frac{D_x Z_o}{\lambda}\cos\theta\left[\ln\csc\left(\frac{\pi w}{2D_x}\right)\right] + CF \tag{6.2}$$

and

$$S_A = \frac{4D_y Y_o}{\lambda}\cos\theta\left[\ln\csc\left(\frac{\pi g}{2D_y}\right)\right] + CF \tag{6.3}$$

Now, as soon as the dipoles on the AFSS are loaded with diodes, the diodes capacitance dominates, rather than that of the unloaded dipoles, the AFSS's frequency response. The loading effect results in an increase of capacitance, which, as demonstrated in chapter 4, virtually increases the dipole length. This, in turn,

shifts the resonant frequency down. In order to simulate the diodes loading effect, the structure depicted in figure 6.5 was used. By adding horizontal metallic strips at the dipole extremities, an increase of capacitance can be achieved.

The short circuit response, on the other hand, was generated by employing an array of free-standing inductive strips. Their physical parameters, namely strip width and periodical placement, are the same as those belonging to dipoles on the AFSSs employed in this research programme. The schematic diagram of this structure is shown in figure 6.6. The arrays' physical parameters are also shown in table 6.3, next to the heading X_{oc}. The data was theoretically generated using the following equation

$$X_{oc} = jX_A \tag{6.4}$$

where X_A is given by (6.2).

In the above equations $\cos\theta = 1$ for normal incidence. The equation for CF, the correction factor, can be found in Marcuvitz [14].

The theoretically generated dynamic complex impedance data was employed in the GA optimizer using FF1 and then FF2. The data was used in conjunction with the Salisbury screen absorber depicted in figure 6.8 with n = 2. The material used in the simulation was a lossless dielectric material with $\mu_r = 1$. The permittivity chosen was $\epsilon_r = 25.0$. In order to closely resemble the physical characteristics of the AFSSs, supporting dielectric layers of permittivity $\epsilon_r = 2.2$ were added to the reactive planar structures. These are displayed as d_2 and d_4.

Figures 6.8 and 6.9 depict the absorbers' solutions given by FF1 and FF2, respectively, with parameters as shown in table 6.4. When comparing these figures, it can clearly be seen that there is a strong similarity between both solutions. This clearly indicates that a global solution has been found, being of a multi-resonant

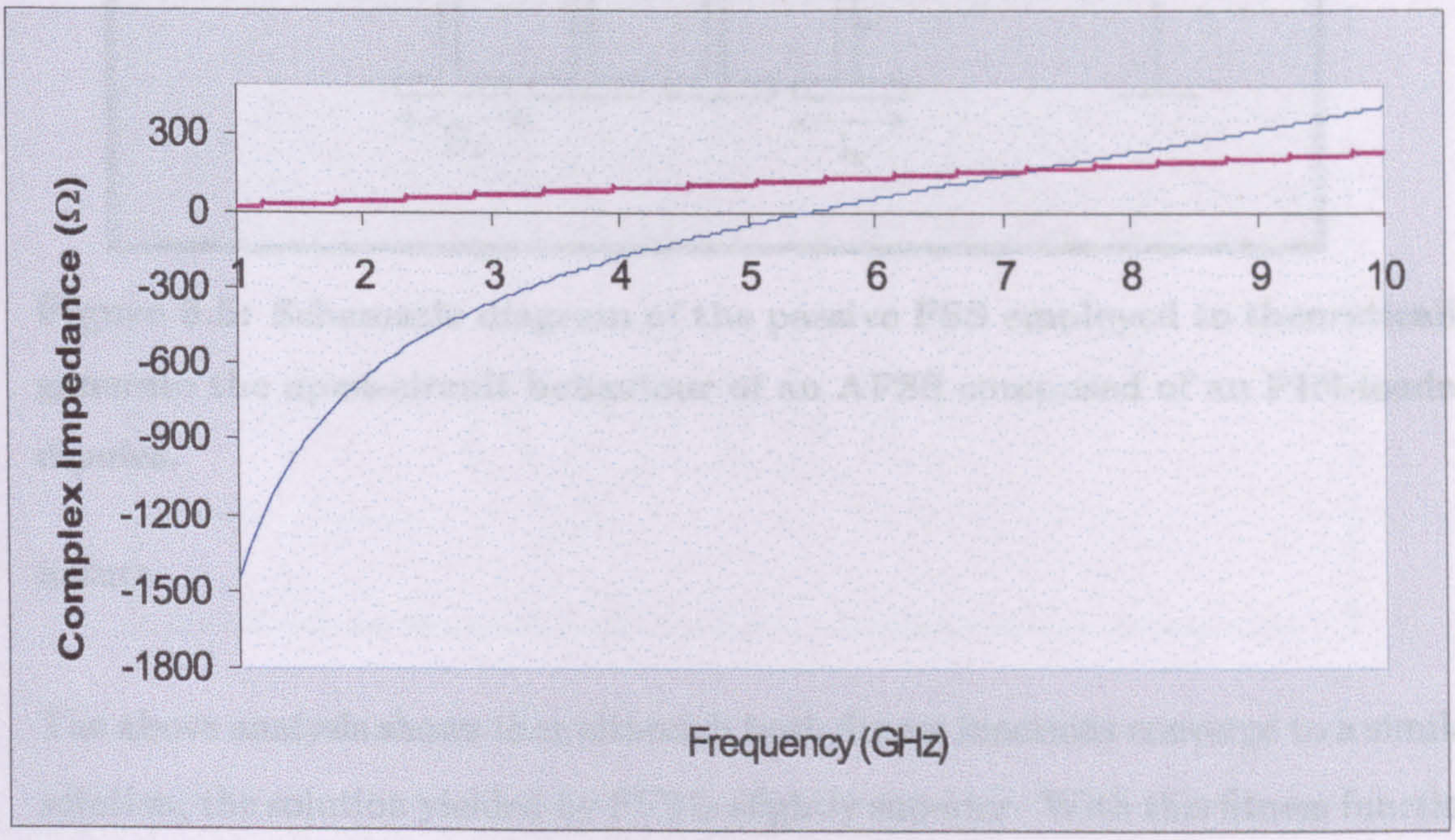

Figure 6.4: Complex impedance profiles of the two passive FSSs shown in figures 6.5 and 6.6. The blue line represents the complex impedance response given by the FSS of figure 6.5 (open circuit). The pink line shows the complex impedance response of the FSS shown in figure 6.6 (short circuit).

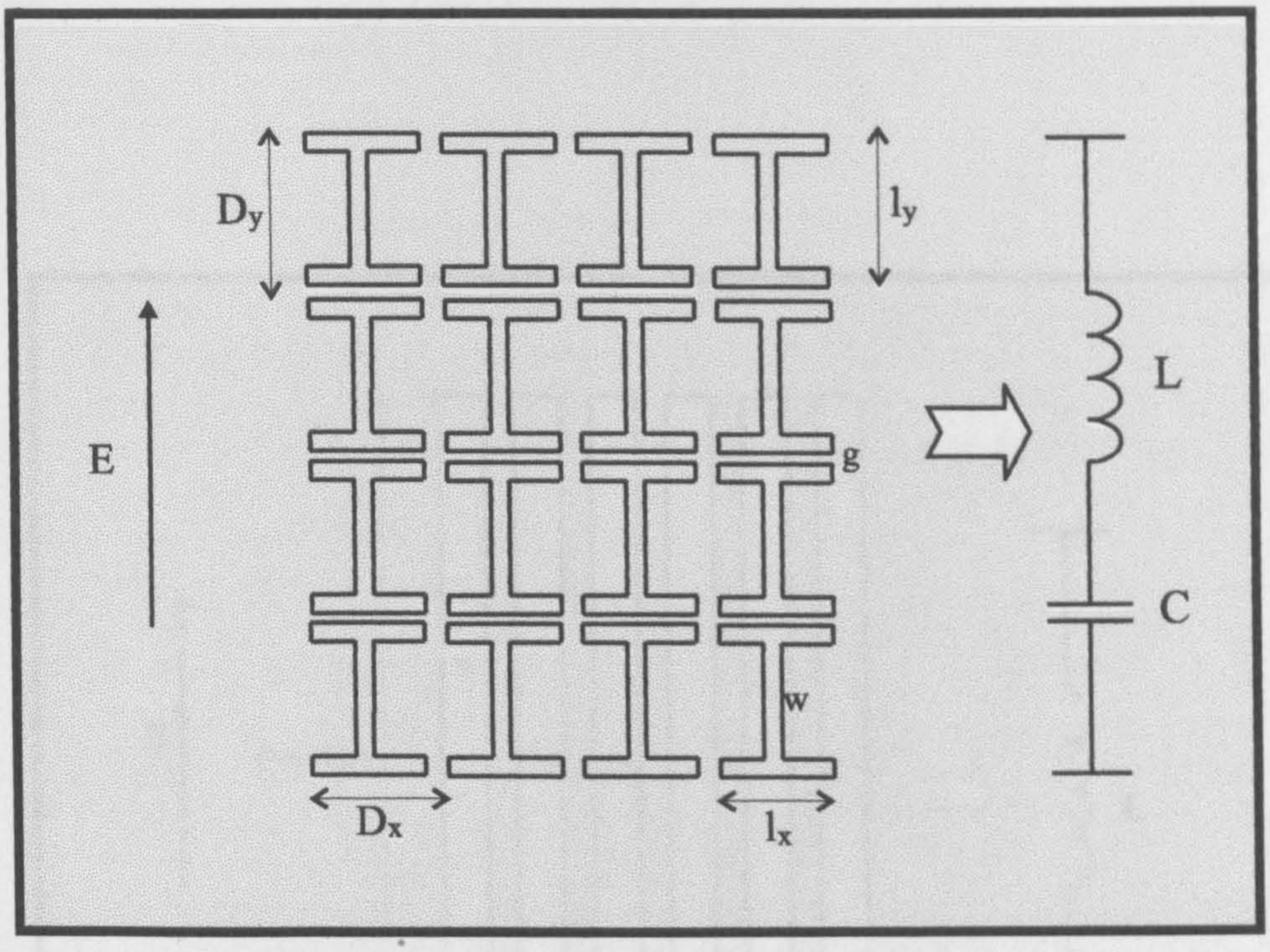

Figure 6.5: Schematic diagram of the passive FSS employed to theoretically generate the open-circuit behaviour of an AFSS composed of an PIN-loaded dipoles.

nature.

The above analysis shows that although both fitness functions converge to a similar solution, the solution yielded by FF2 is slightly superior. With this fitness function not only a better spread of reflection nulls is achieved across the working frequency band, but also null redundancy is minimized. This can be seen by comparing the results in figures 6.8 and 6.9. This suggests that FF2 is rather superior and was, therefore, employed to find the global wideband absorption solution of a Salisbury screen absorber loaded with AFSSs comprising an array of dipoles populated with PIN diodes.

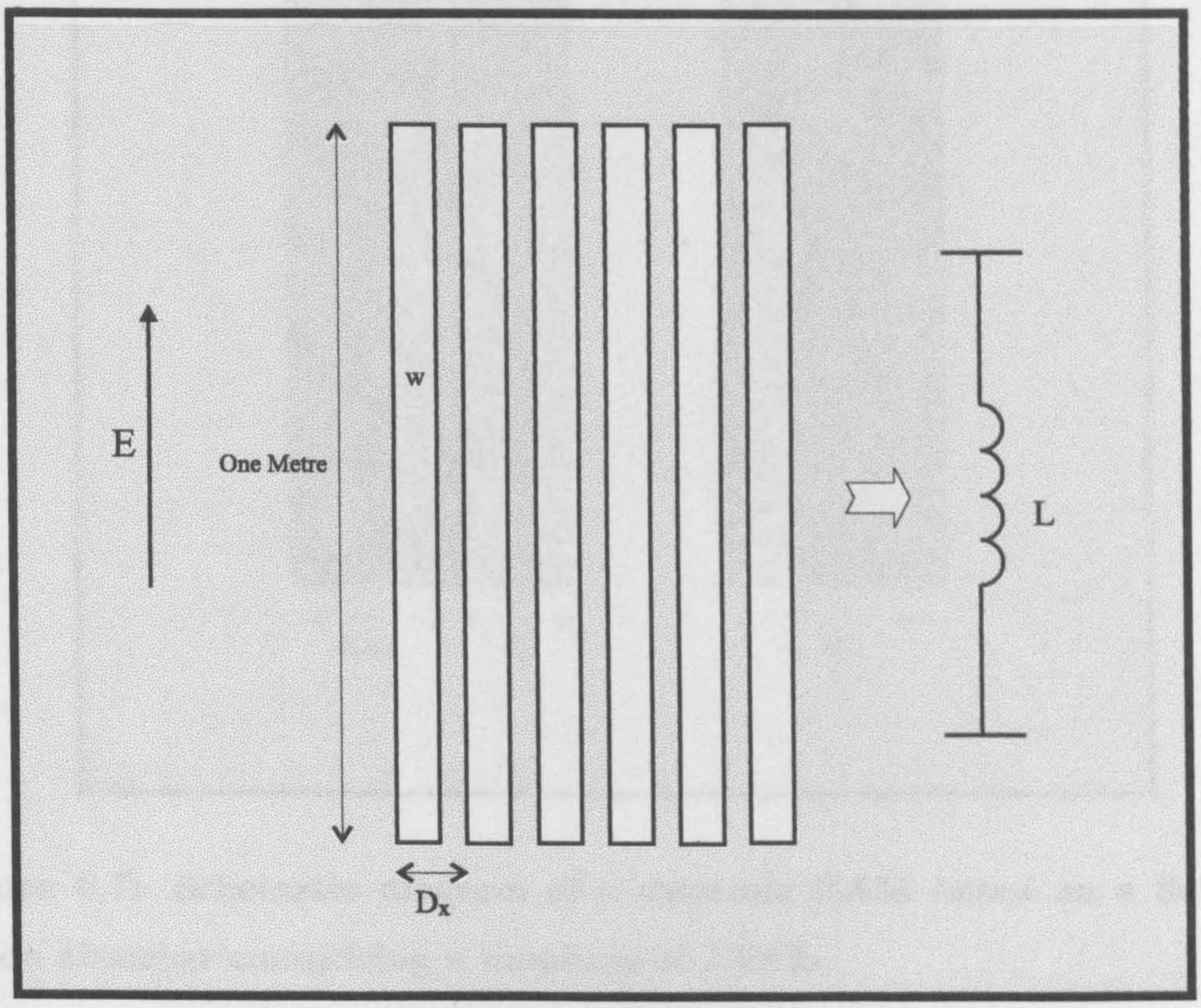

Figure 6.6: Schematic diagram of an array of metallic strips employed to theoretically generate the short circuit response of an AFSS composed of an array of PIN-loaded dipoles.

Response	D_x (mm)	D_y (mm)	l_x (mm)	l_y (mm)	g (mm)	w (mm)
X_{oc}	20	15	16	13	2	2
X_{sc}	-	10	-	-	-	1

Table 6.3: Element dimensions of the two reactive impedance structures whose schematic diagrams are shown in figures 6.6 (X_{oc}) and 6.7 (X_{sc}).

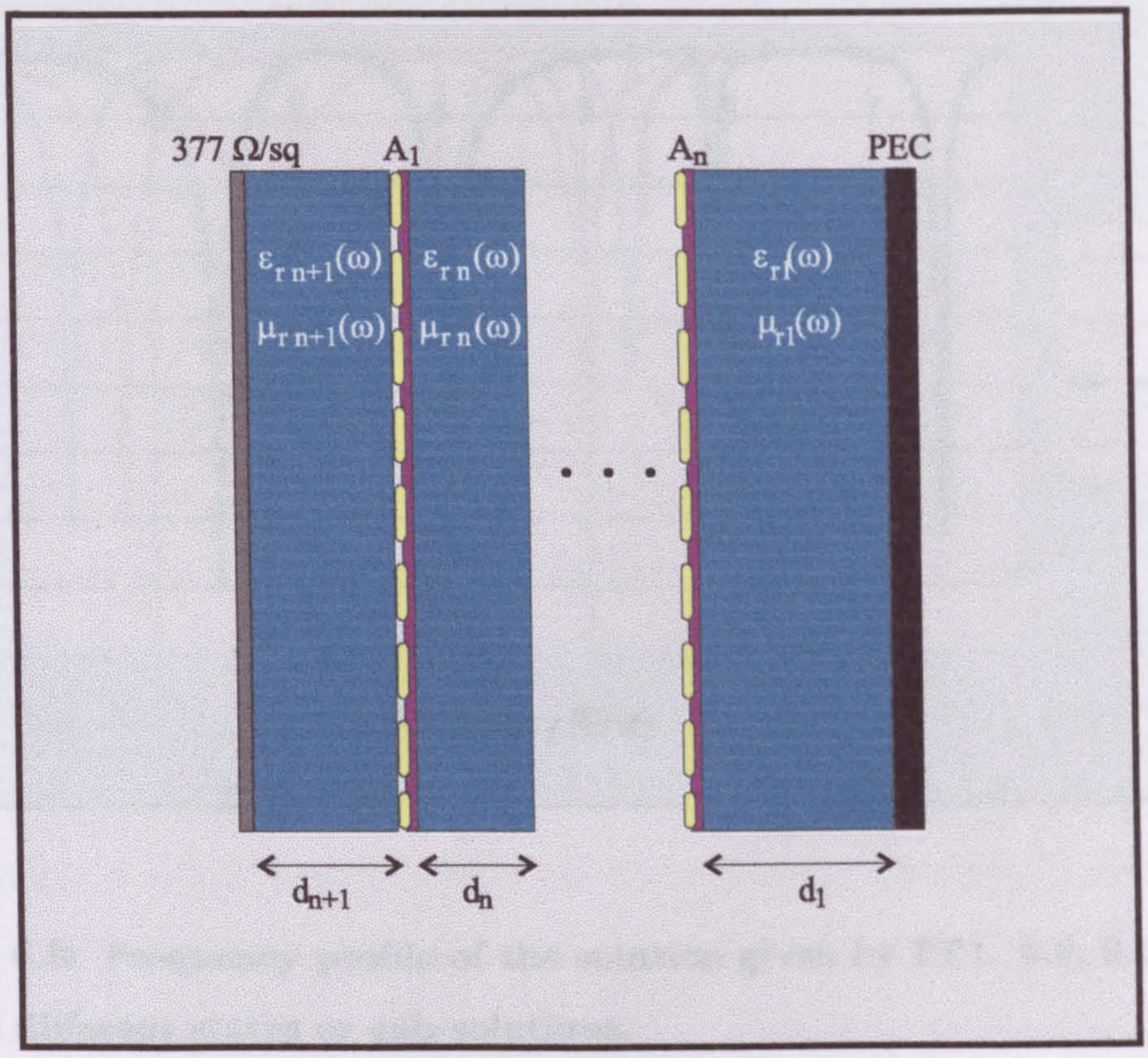

Figure 6.7: Schematic diagram of a dynamic RAM based on a Salisbury screen absorber comprising n numbers of AFSSs.

Fitness Function	FF1	FF2
d_1 (mm)	3.4	3.4
d_2 (mm)	0.611	0.611
d_3 (mm)	2.8	1.6
d_4 (mm)	0.611	0.611
d_5 (mm)	3.3	2.1
d_t (mm)	12.111	8.322

Table 6.4: Dynamic RAM parameters yielded by the two different fitness functions FF1 and FF2. $\epsilon_{r1,3,5} = 25.0$ and $\epsilon_{r2,4} = 2.20$.

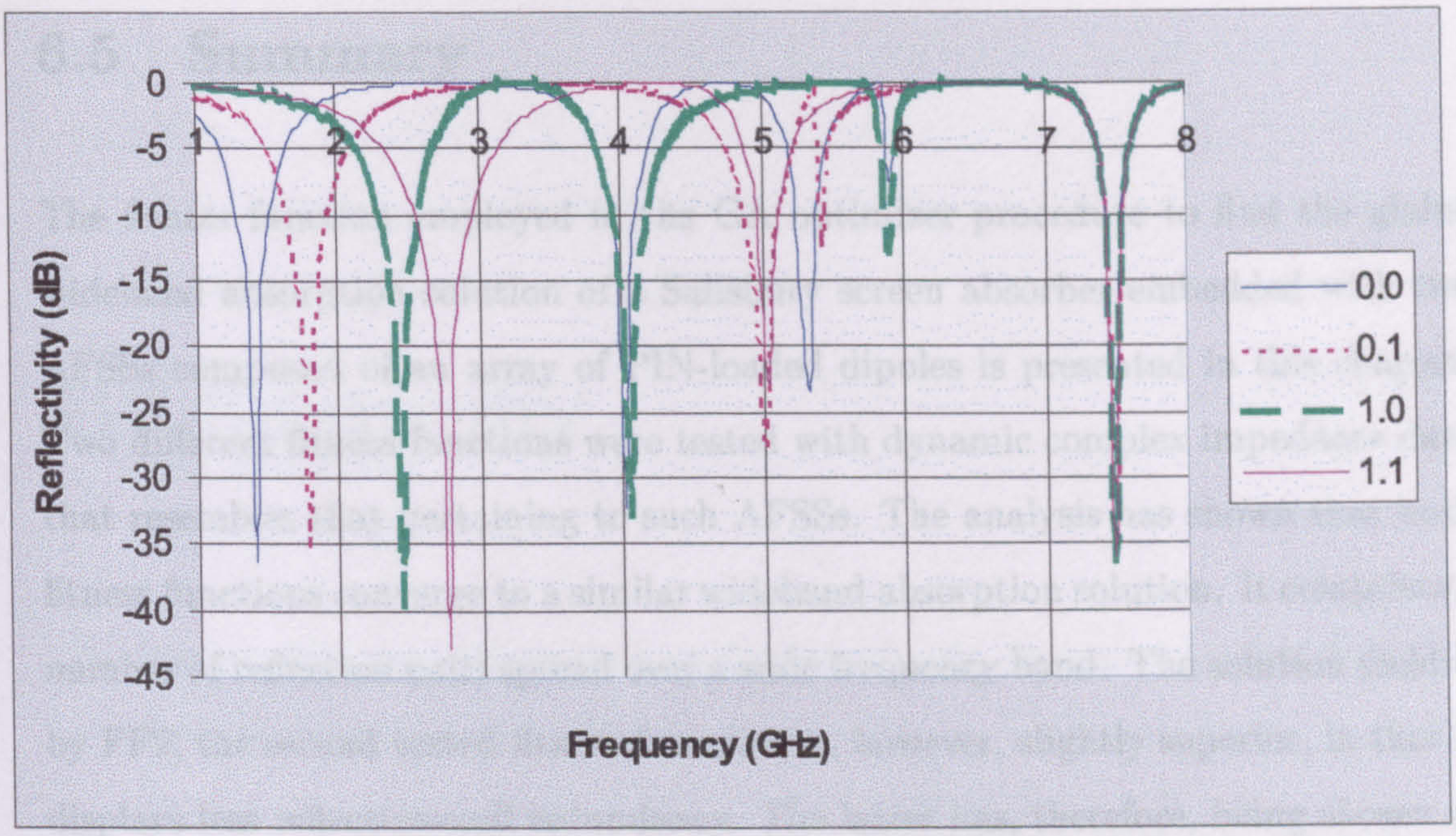

Figure 6.8: Frequency profile of the solution given by FF1. 0.0, 0.1, 0.1, 1.1 are the different states or sub-solutions.

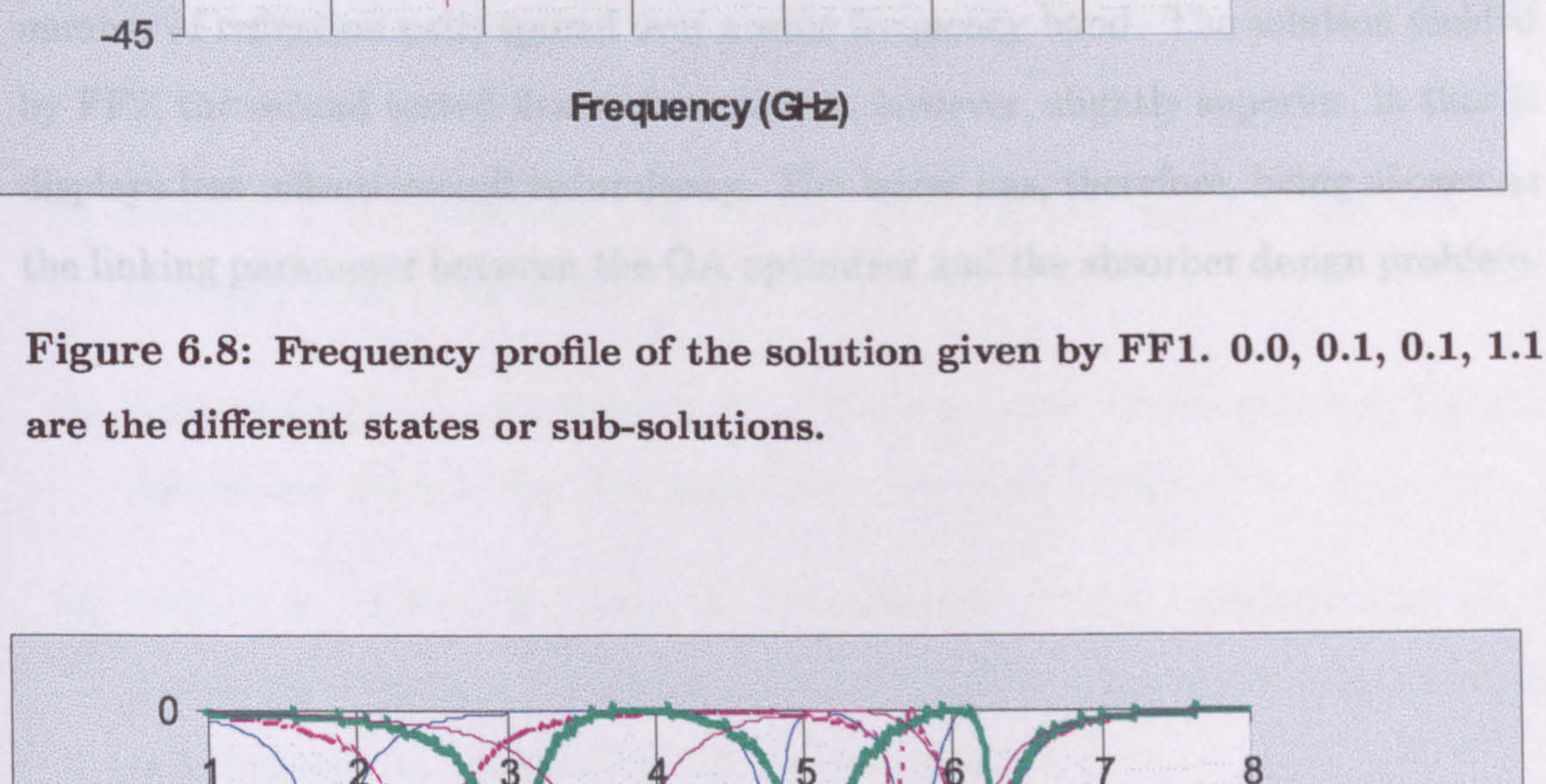

Figure 6.9: Frequency profile of the solution given by FF2. 0.0, 0.1, 0.1, 1.1 are the different states or sub-solutions.

6.5 Summary

The fitness function employed in the GA optimizer procedure to find the global wideband absorption solution of a Salisbury screen absorber embedded with two AFSSs composed of an array of PIN-loaded dipoles is presented in this chapter. Two different fitness functions were tested with dynamic complex impedance data that resembles that pertaining to such AFSSs. The analysis has shown that both fitness functions converge to a similar wideband absorption solution. It comprises a number of reflection nulls spread over a wide frequency band. The solution yielded by FF2, the second tested fitness function, is, however, slightly superior, in that it displays less reflection-null redundancy. The latter has, therefore, being chosen as the linking parameter between the GA optimizer and the absorber design problem.

Bibliography

[1] Darwin, Charles, *The Origin of the Species: By Means of Natural Selection*, John Murray, London, 1872.

[2] Holland, J. H., *Adaptation in Natural and Artificial Systems.* University of Michigan Press, Ann Arbor, 1975.

[3] Rahmat-Samii, Y., Michielssen, E., *Electromagnetic Optimization by Genetic Algorithms*, John Wiley And Sons Inc., New York, 1999.

[4] Altman, Z., Mittra, R., Boag, A., *New Design of Ultra Wideband Communication Antennas using a Genetic Algorithm*, IEEE Transactions on Antennas and Propagation, Vol 45. No. 10, pp. 1494-1501.

[5] Johnson, J. M., Rahmat-Samii, Y., *Genetic Algorithms and Method of Moments (GA/MOM) for the Design of Integrated Antennas*, IEEE Transactions on Antennas and Propagation, Vol 47. No. 10, pp. 1606-1614.

[6] Linden, D. S., *Automated Design and Optimazation of Wire Antennas using Genetic Algorithms*, Ph.D. Thesis, Massachussets Institute of Technology, Cambridge, MA, 1997.

[7] Haupt, R. L., *Thinned Arrays using Genetic Algorithm*, IEEE Transactions on Antennas and Propagations, Vol. 42, No. 7, pp. 993-999.

[8] Michielssen, E., Ranjithan, S., Mittra, R., *Optimal Multilayer Filter Design using Real Encoded Genetic Algorithms*, IEE Proceedings, 139-J(6), pp. 413-420.

[9] Michielssen, E., Weile, D. S., *The Use of Domain Decomposition Genetic Algorithms Exploiting Model Reduction for the Design of Frequency Selective Surfaces*, Computer Methods in Applied Mechanics and Engineering, Vol. 186, No. 2-4, pp. 439-458.

[10] Chambers B., Tennant A., *Optimised Design of Jaumann Radar Absorbing Materials*, IEE Proceedings on Radar, Sonar Navigation, Vol. 143, No. 1, 1996, pp. 23-29.

[11] Weile, D. S., Michielssen, E., Golberg, D. E., *Genetic Algorith Design of Pareto Optimal Broadband Microwave Absorber*, IEEE Transactions on Electromagnetic Compatability, Vol. 38, No. 3, 1996, pp. 518-525.

[12] Golberg, D. E., *Genetic Algorithms in Search, Optimization and Machine Learning*, Addison-Wesley, 1989.

[13] http://www.cs.cmu.edu/Groups/AI/html/faqs/ai/genetic/part2/faq-doc-2.html, *What's a Genetic Algorith GA?*, July 1999

[14] Marcuvitz, N., *Waveguide Handbook*, McGraw-Hill Book Company Inc., First Edition, 1951. .

[15] http://cs.felk.cvut.cz/ xobitko/ga/, *Introduction to Genetic Algorithm*, 1998.

Chapter 7

Results

7.1 Introduction

This chapter concentrates on validating the practical performance of the proposed absorber design philosophy presented in chapter four. Predicted and measured data for a number of dynamic absorbers are presented and discussed. The results shown here refer to all the theoretical aspects investigated and presented in this thesis.

7.2 Results

The dynamic frequency properties of the AFSSs as well as those of the absorbers built were established through free-field measurement techniques as explained in appendix A. The measurement set up was based on the Naval Research Laboratory (NRL) Arch Method. The sample under test (SUT), the absorber, was placed in the far field under an arch structure, which mounts a source and a detector. Although the system can be arranged to measure the effects of wide angle of incidence upon the SUT, measurements were carried out for normal incidence. The

NRL measurement system was set up for antenna measurements[1]. Both source and detector utilized to carry out frequency characterizations were wide-band horn antennas, operating between 1 to 10 GHz. These antennas were connected to a computer-control vector network analyzer (VNA), namely HP8510C. The use of a VNA together with broadband antennae permit rapid frequency measurements over a wide band.

Two types of AFSSs were investigated in this research programme in order to narrow the trade-off gap between the two equally important, but conflicting parameters in absorber design: broadband absorption bandwidth and small thickness. The first one comprised an array of PIN-loaded dipoles while the second was composed of an array of varactor-loaded dipoles. The dynamic range of the latter, in terms of adaptive complex impedance properties, was, however, found to be almost non-existent and, therefore, no absorber was either designed or built using this type of AFSS.

Two dielectric-backed AFSSs composed of arrays of PIN-loaded dipoles were designed and built. Their design methodology is fully explained in chapter 5. These structures, which were called DI-1 and DI-2 to differentiate one from the other, were then embedded within Salisbury screen absorbers. Although the rationale behind the design of DI-1 and DI-2 is the same (i.e. that of a short-open electrical characteristics), DI-2 was designed to be more transparent that DI-1. This was done to translate up in frequency its resonance frequency and, thus, create a AFSS with a larger adaptive complex impedance range.

Two different types of dynamic radar absorbing material, DRAM, based on the Salisbury screen absorber were designed and built. The design philosophy is thoroughly explained in chapter 4. The first type was built using a single dielectric-backed AFSS while the second one comprised two dielectric-backed AFSSs. As explained in chapter 4, the use of a single AFSS minimizes the complexity of the

[1]i.e. $R \geq 2D^2/\lambda$

problem. However, by making use of two AFSSs a superior design solution, in terms of the number of reflection nulls, can be achieved.

7.2.1 Absorbers built with a Single AFSS

The results presented in this section were obtained by using a single dielectric-backed AFSS of the type DI-1 in the DRAM design. As shown in chapter 4, the use of a single AFSS generates a solution comprising two switchable reflection nulls within any given band. The results shown in this section serve mainly to show the potential of using AFSSs to incur quasi-real time adaptive changes into the frequency properties of metal backplane type of absorbers.

Absorber with a Single AFSS

Figure 7.3 shows the measured dynamic frequency profile of an absorber whose schematic diagram is shown in figure 7.2, with $\mu_r = 1$, while its physical parameters are shown in table 7.2. The absorber is based on a Salisbury screen wherein the 377Ω/sq resistive sheet is replaced with a dielectric backed AFSS composed of an array of PIN-loaded dipoles, namely DI-1. The AFSS's schematic diagram is shown in figure 7.1, while its physical parameters are shown in table 7.1. The figure shows the frequency profile of the absorber under the influence of a range of bias voltages, starting at 0 V (No Bias) through to 11 V (Full Bias). In terms of adaptive properties, the absorber's measured frequency profile displays two main characteristics. First, tuning of a null is demonstrated at high frequencies. At these frequencies, the AFSS's adaptive complex impedance response is mainly reactive (vide figures 5.10, 5.16 and 5.17, chapter 5) and, therefore, null tuning is possible. Secondly, continuous variation of the depth of a null is illustrated at low frequencies. At these frequencies the AFSS's adaptive complex impedance properties not only exhibits a reactive component, but also a lossy part. Under this arrangement, the presence of a loss component dictates the AFSS's adaptive

Board	D_x mm	D_y mm	w mm	l mm	g mm
DI-1	10	15	1	13	2

Table 7.1: Physical parameters of DI-1 AFSS.

complex impedance properties and, in turn, those of the absorber. This, in turn, results in the ability to continuously change the depth of a reflection null.

Although the figure shows a resonating effect at low frequencies its depth level is not appropriate to absorb incoming energy. The reason for this is that the AFSS's lossy part is not adequate enough, distinctively 377 Ω, for a perfect impedance match, which will then cause a deep reflection null. This indicates that in order to increase the depth of the resonating effect more loss needs to be exhibited in the adaptive complex impedance properties of the AFSS.

A conventional Salisbury screen with a spacer thickness of 9.711 mm and permittivity $2.64 - j0.016$ will show in its frequency profile a reflection null at around 4.8 GHz. The reflection null of the proposed absorber, whose schematic diagram is shown in figure 7.2, occurs, however, at a frequency just below 3 GHz. This indicates that the presence of the AFSS has effectively increased the absorber's thickness. In other words, a dielectric-based absorber of smaller thickness is now capable of energy absorption at a lower frequency. This is an indication of how complex impedance structures can be used to circumvent material fundamental properties.

The frequency response of the absorber (figure 7.3) shows some rather peculiar positive reflectivity. This anomaly is down to the AFSS's loss slipping below 0 (negative loss) in the data inversion process (Appendix B). The latter arises from the associated one-port measurement errors (appendix A). Inspection of the Smith chart shows that when R is below zero, the magnitude of the reflection coefficient

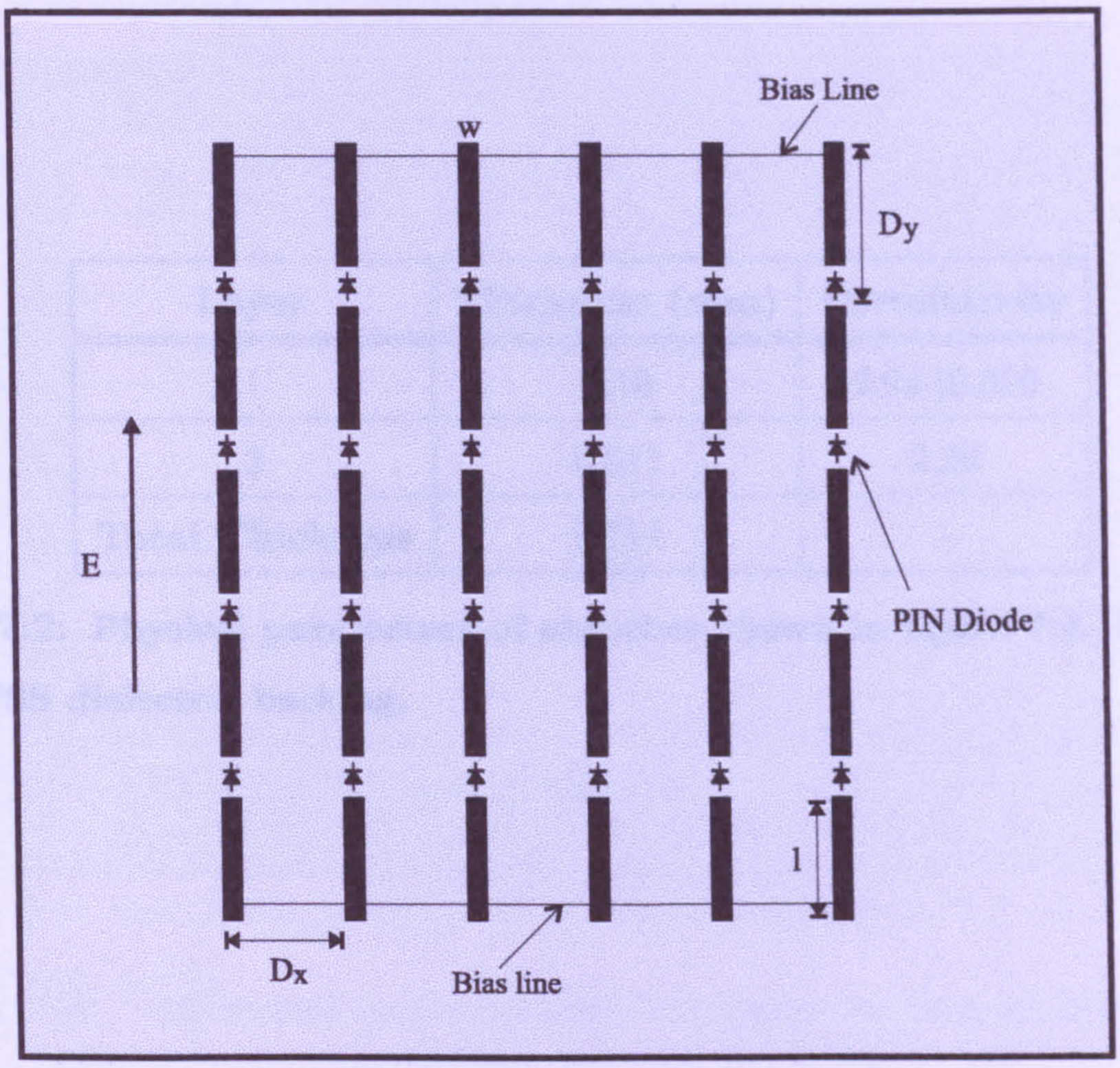

Figure 7.1: Schematic diagram of a PIN-loaded AFSS.

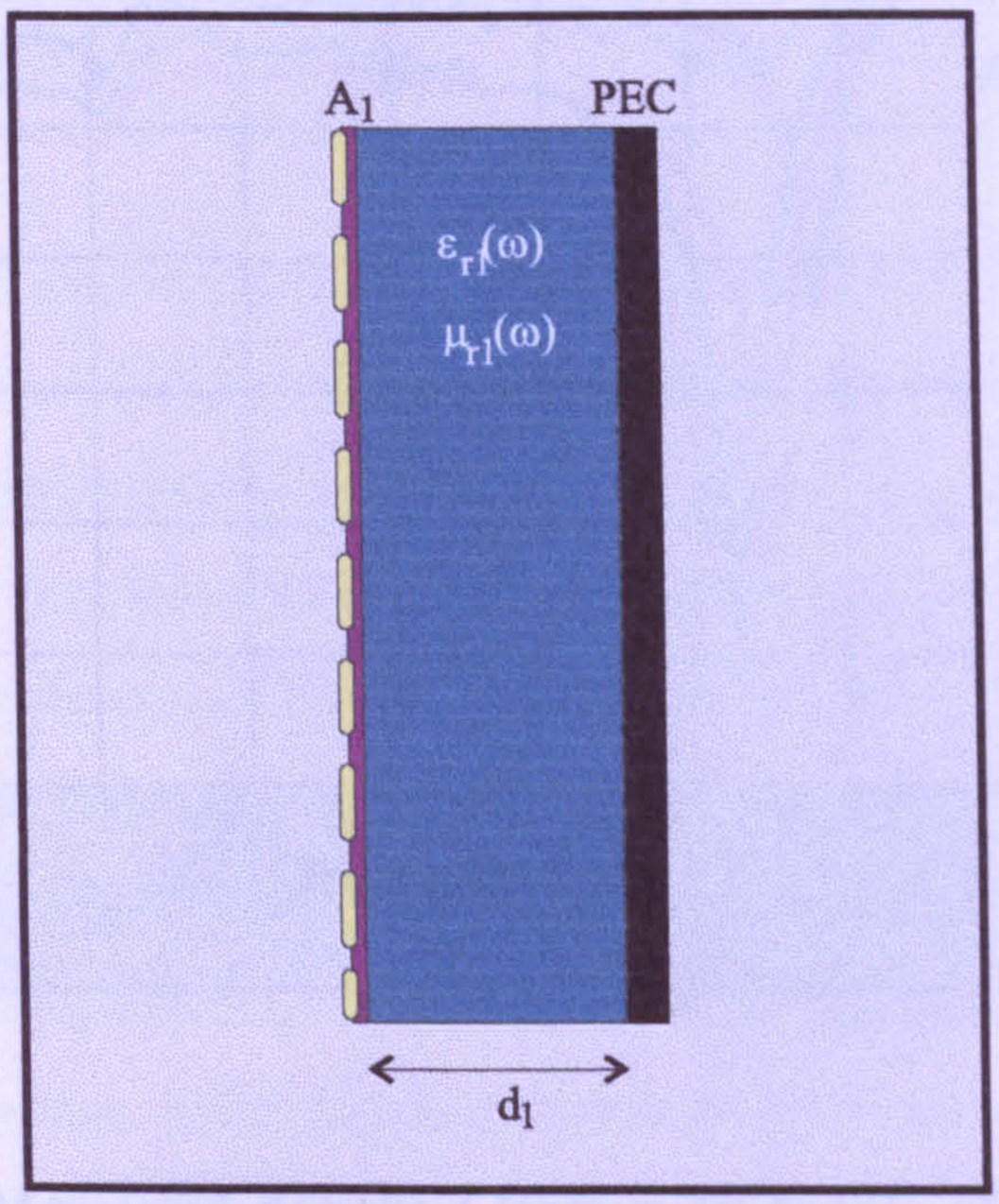

Figure 7.2: Schematic diagram of a typical dynamic absorber incorporating a Single dielectric-backed AFSS.

Layer	Thickness (mm)	Permittivity
1	9.10	2.64-j0.016
2	0.611	2.20
Total Thickness	9.711	-

Table 7.2: Physical parameters of absorber shown in figure 7.2. Layer 2 is the AFSS dielectric backing.

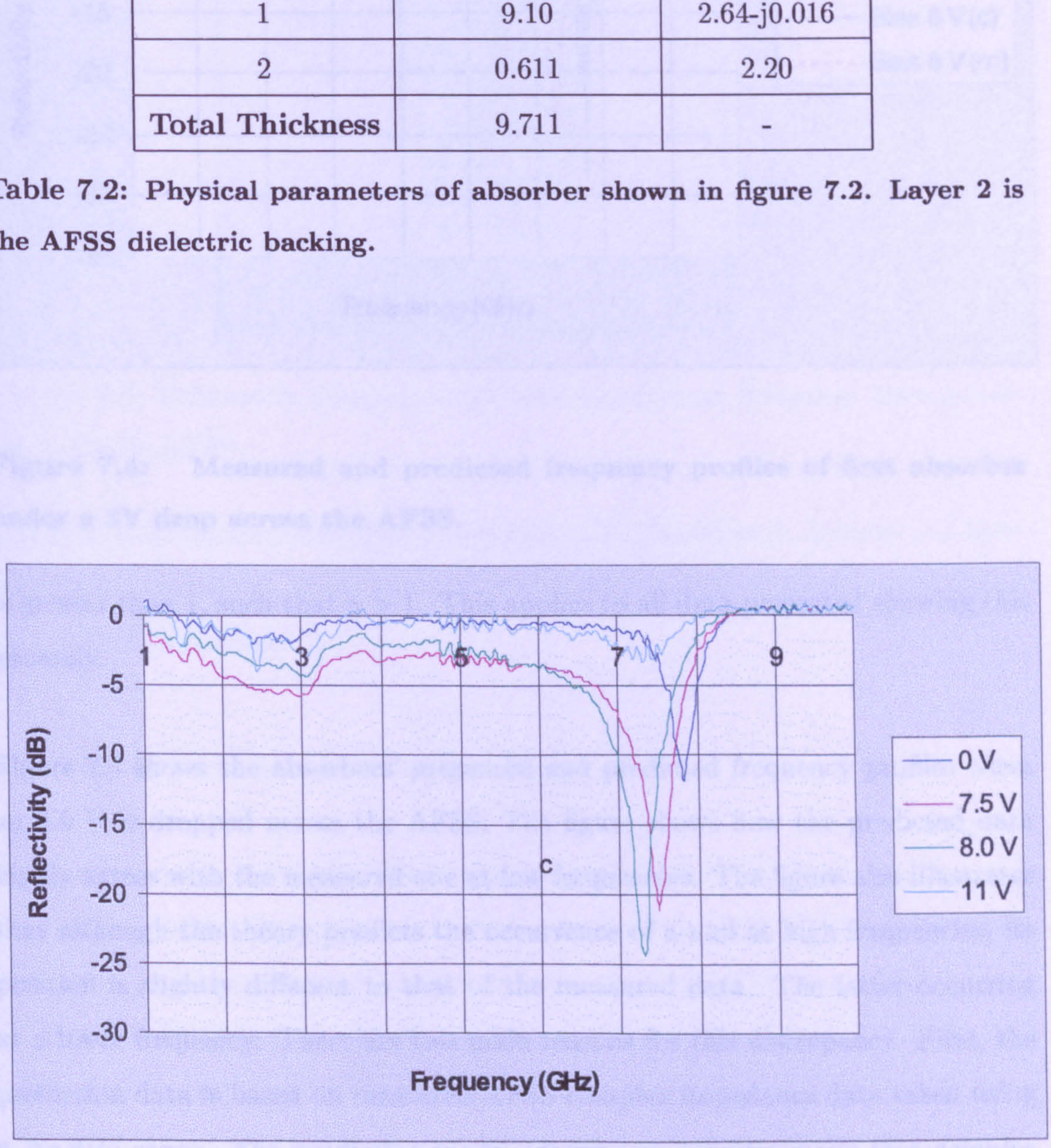

Figure 7.3: Measured dynamic frequency profile of first absorber.

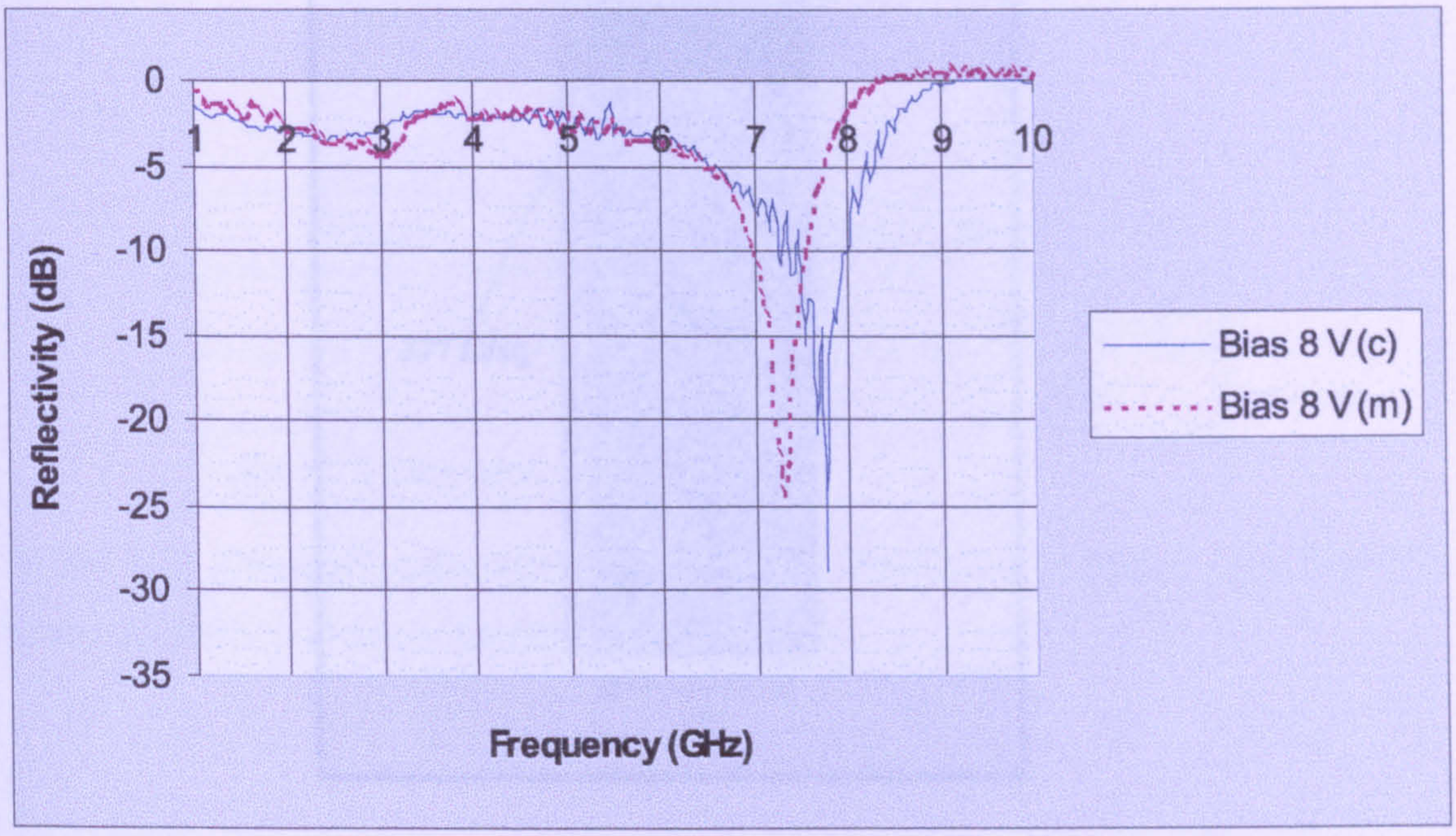

Figure 7.4: Measured and predicted frequency profiles of first absorber under a 8V drop across the AFSS.

is greater than 1, such that $\gamma > 1$. This applies to all data presented showing this anomaly.

Figure 7.4 shows the absorbers' measured and predicted frequency profiles when an 8.0 V is dropped across the AFSS. The figure shows how the predicted data highly agrees with the measured one at low frequencies. The figure also illustrates that although the theory predicts the occurrence of a null at high frequencies, its position is slightly different to that of the measured data. The latter occurring at a lower frequency. There are two main reasons for this discrepancy. First, the prediction data is based on measured AFSS complex impedance data taken using a far-field range. The prediction model assumes an infinitesimally thin complex impedance configuration. The AFSS is, however, of finite thickness due to the diodes finite dimensions. This, thus, introduces phase errors, whose detrimental effects are more evident at higher frequencies. Secondly, the model assumes

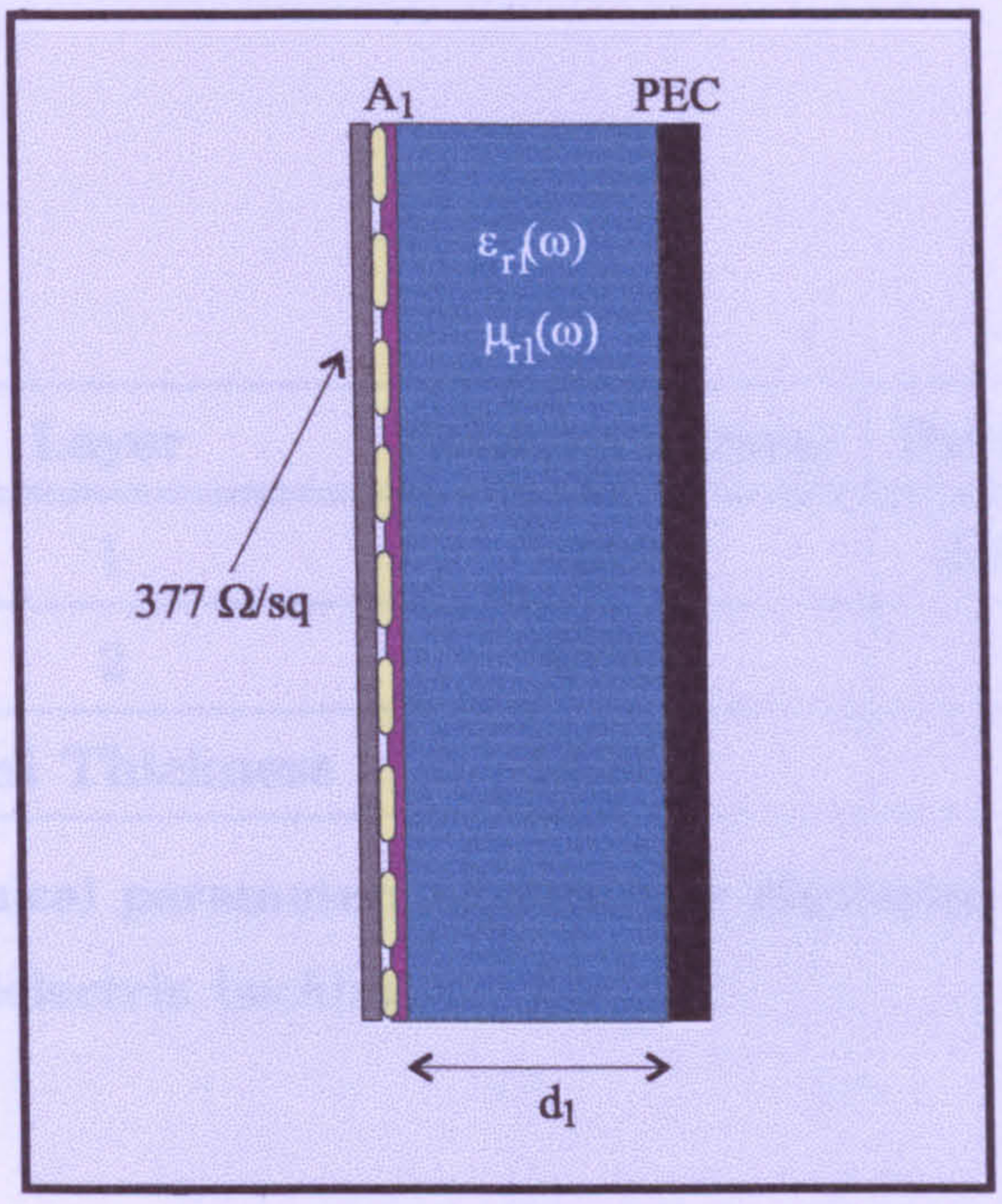

Figure 7.5: Schematic Diagram of a Salisbury Screen Absorber Incorporating a Single AFSS.

a structure of infinite transverse dimensions. The absorber is, however, of finite transverse dimensions. This, thus, results in the presence of unwanted scattered diffraction components.

Salisbury Screen Absorber with a Single AFSS

A second absorber was built. The schematic diagram of this absorber is shown in figure 7.5 while its physical parameters are outlined in table 7.3. The absorber is based on a Salisbury screen wherein a dielectric-backed AFSS comprising an array of PIN-loaded dipoles, namely DI-1, is placed within a 377 Ω/sq resistive film and a dielectric spacer. The AFSSs physical parameters are displayed in table 7.1. Figure 7.6 shows the absorber's measured dynamic frequency profile. A 0 indicates a no-bias condition while a 1 indicates a full bias condition. The figure shows two dynamic bands. The first one is located between 1 to 6 GHz, while the second one lies from 9 to 11 GHz. From the figure, it can be seen that the greatest change in

Layer	Thickness (mm)	Permittivity
1	13.9	2.64-j0.016
2	0.611	2.20
Total Thickness	14.5111	-

Table 7.3: Physical parameters of absorber displayed in figure 7.5. Layer 2 is the AFSS's dielectric backing.

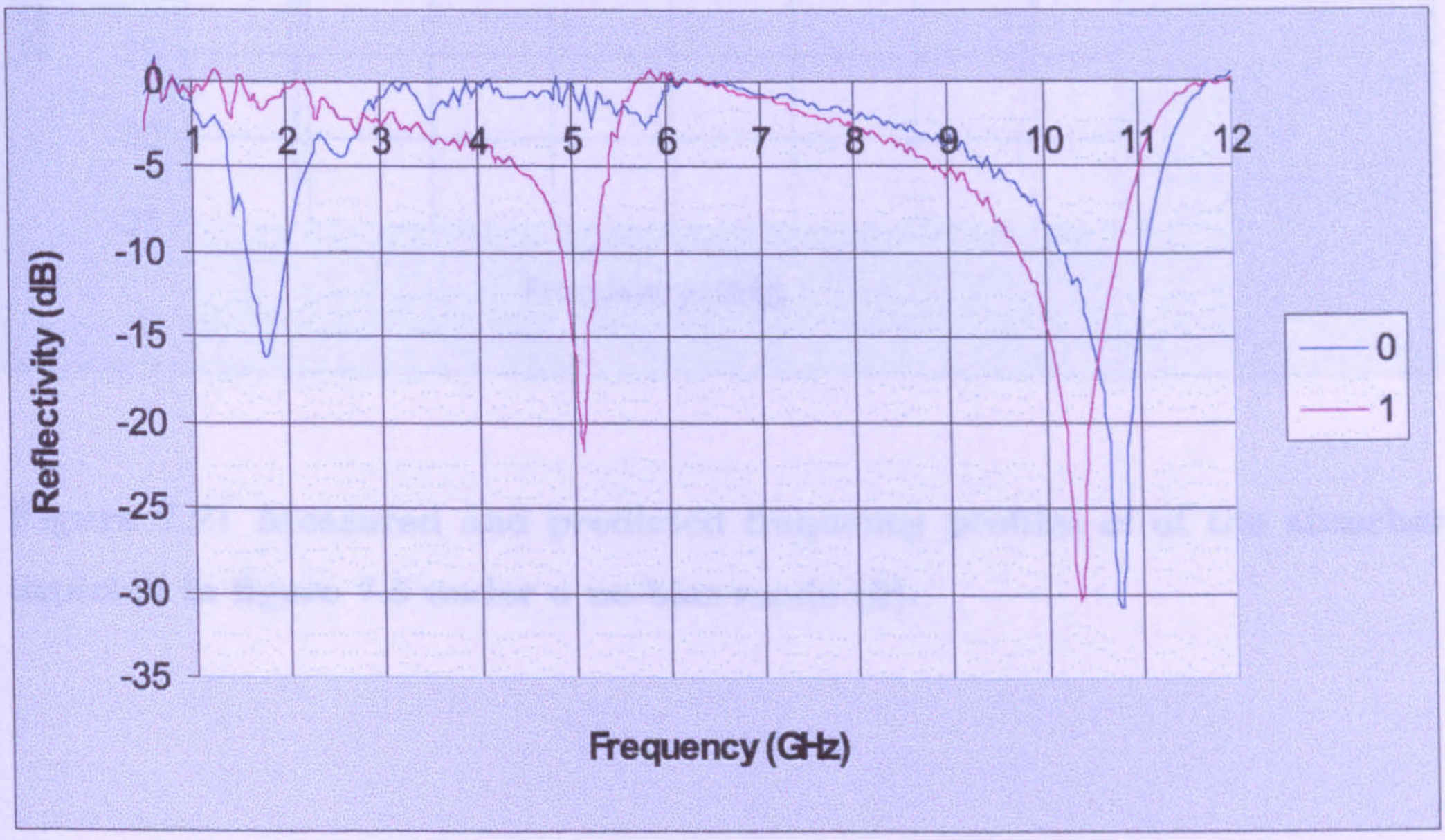

Figure 7.6: Measured dynamic frequency profile of absorber depicted in figure 7.5.

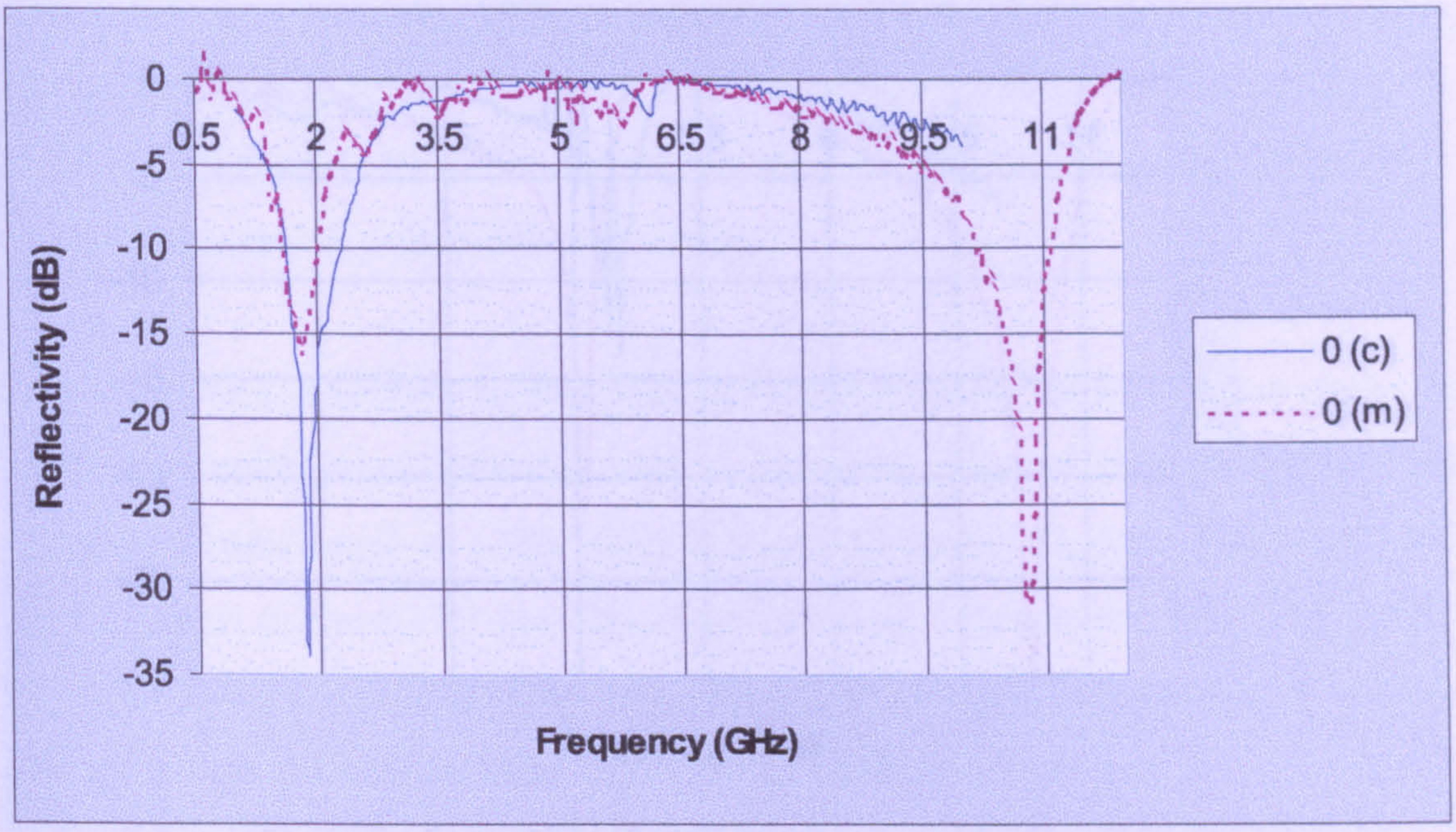

Figure 7.7: Measured and predicted frequency profiles of of the absorber depicted in figure 7.5 under a no-bias mode (0).

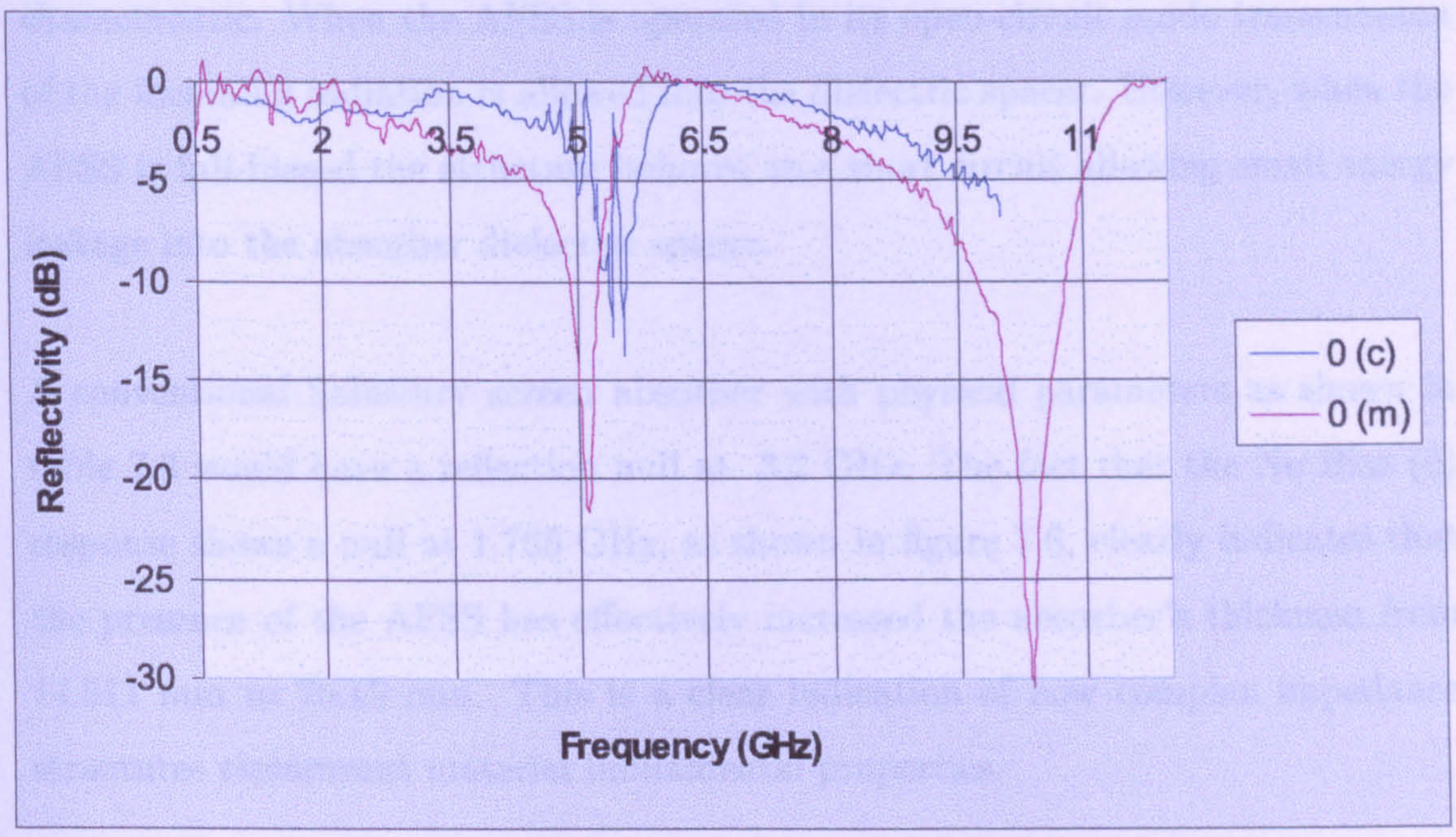

Figure 7.8: Measured and predicted frequency profiles of of the absorber depicted in figure 7.5 under a full bias mode (1).

reflection null position, incurred through voltage biasing the AFSS, occurs in the low frequency band. The null is shifted from 1.765 GHz to 5.1 GHz. Although the variation of a reflection null position is possible at higher frequencies, as exhibited in the figure, its displacement in frequency is relatively small. The reason for this lies in the AFSS's dynamic reflection response, which is shown in figure 5.7 of chapter five. The figure shows that at higher frequencies the AFSS's dynamic frequency response does not exhibit an open/short circuit behaviour. This results in the inability to shift a reflection null across a wide frequency band. At low frequencies, on the other hand, the structure exhibits an open and short circuit characteristic. When the AFSS is operated in its open-circuit mode transmission of the incoming radiation is allowed into the dielectric spacer. However, when the AFSS is full-biased the structure behaves as a short circuit allowing small energy leakage into the absorber dielectric spacer.

A conventional Salisbury screen absorber with physical parameters as shown in table 7.3 would have a reflection null at 3.2 GHz. The fact that the No Bias (0) response shows a null at 1.765 GHz, as shown in figure 7.6, clearly indicates that the presence of the AFSS has effectively increased the absorber's thickness from 14.511 mm to 26.15 mm. This is a clear indication of how complex impedance structures circumvent material fundamental properties.

Figures 7.7 and 7.8 display the absorbers' measured and predicted frequency responses for the two extreme bias conditions, namely No Bias (0) and Bias (1), respectively. Figure 7.7 shows good correlation between the measured and predicted data. Although the model predicts the occurrence of a high frequency reflection null located just above 5GHz, the measured response shows an offset in null position. This can be clearly appreciated in figure 7.8. As with the previous absorber's frequency profile, the reason for the divergence of null location can be attributed to measured phase errors introduced by the AFSS's finite thickness as well as the absorbers' transverse finite dimensions.

The results presented in this section show that as well as adaptive properties, seen as the translation of a reflection null in frequency, the presence of an AFSS within a Salisbury screen absorber with a small thickness is now capable of energy absorption at lower frequencies. The absorber thickness is, however, constant and, therefore, it can be argued that the real effect of the AFSS has been to incur changes into the dielectric properties, namely ϵ_r, of the material employed as the absorber spacer. In order to induce changes into an absorber thickness, it has to be physically altered. The presence of AFSSs has effectively implemented a $1/\omega^2$ variation, which, as shown by equation (4.7) of chapter 4, is necessary in order to shift a reflection null while keeping the absorber thickness constant. This, however, has to be the case over a wide frequency band in order to achieve a broadband absorption solution.

7.2.2 Absorbers Built with Two AFSSs

The results presented in the previous section have served as an insight into the attributes that can be achieved through embedding AFSSs, composed of PIN-loaded dipole arrays, within a Salisbury screen absorber. The direct implication of these findings is that the trade-off between absorber thickness and absorption bandwidth can be narrowed through the use of adaptive complex impedance structures, such as AFSSs. How?. The results have shown that the use of a single AFSS introduces dynamic frequency properties into a conventional Salisbury screen absorber. This, effectively, increases its absorption bandwidth through the translation of a reflection null in frequency. As well as the latter finding, the results exhibited in the previous section have shown how the use of AFSSs effectively increases the permittivity ϵ_r of the dielectric material employed to build the absorber.

The use of a single PIN-loaded AFSS does, however, highly inhibit more sophisticated solutions in terms of the number of reflection nulls that can be generated. Thus, in order to improve upon the trade-off of an absorbers two conflicting goals, namely wideband absorption and small thickness, it was thought appropriate to make use of two, rather than one, AFSSs. This, as explained in chapter 4, will yield a solution comprising more reflection nulls, which can be discretely spread over a wider frequency band.

Salisbury Screen Absorber Embedded with Two DI-1 Type AFSSs

The predicted dynamic frequency profile of one of the proposed absorber, named DI-1/1, is shown in figure 7.11. The absorber, whose schematic diagram is shown in figure 7.9 (with $n = 2$), while its physical parameters are shown in table 7.5, was realized with two dielectric-backed AFSSs of the type DI-1, having a measured dynamic complex impedance response as shown in figure 7.10.

The absorber's volumetric solution, as a function of spacers' thicknesses (d_1, d_3,

d_5), was found through the application of a GA with constrained range of input parameters as shown in table 7.4. From figure 7.11, it can be seen that the absorber's dynamic frequency response exhibits a number of reflection nulls spread over frequency band that extends between 1 to 5 GHz. The figure also shows that the absorber's dynamic range, in terms of reflectivity levels, covers a broad frequency bandwidth between 1 - 5 GHz.

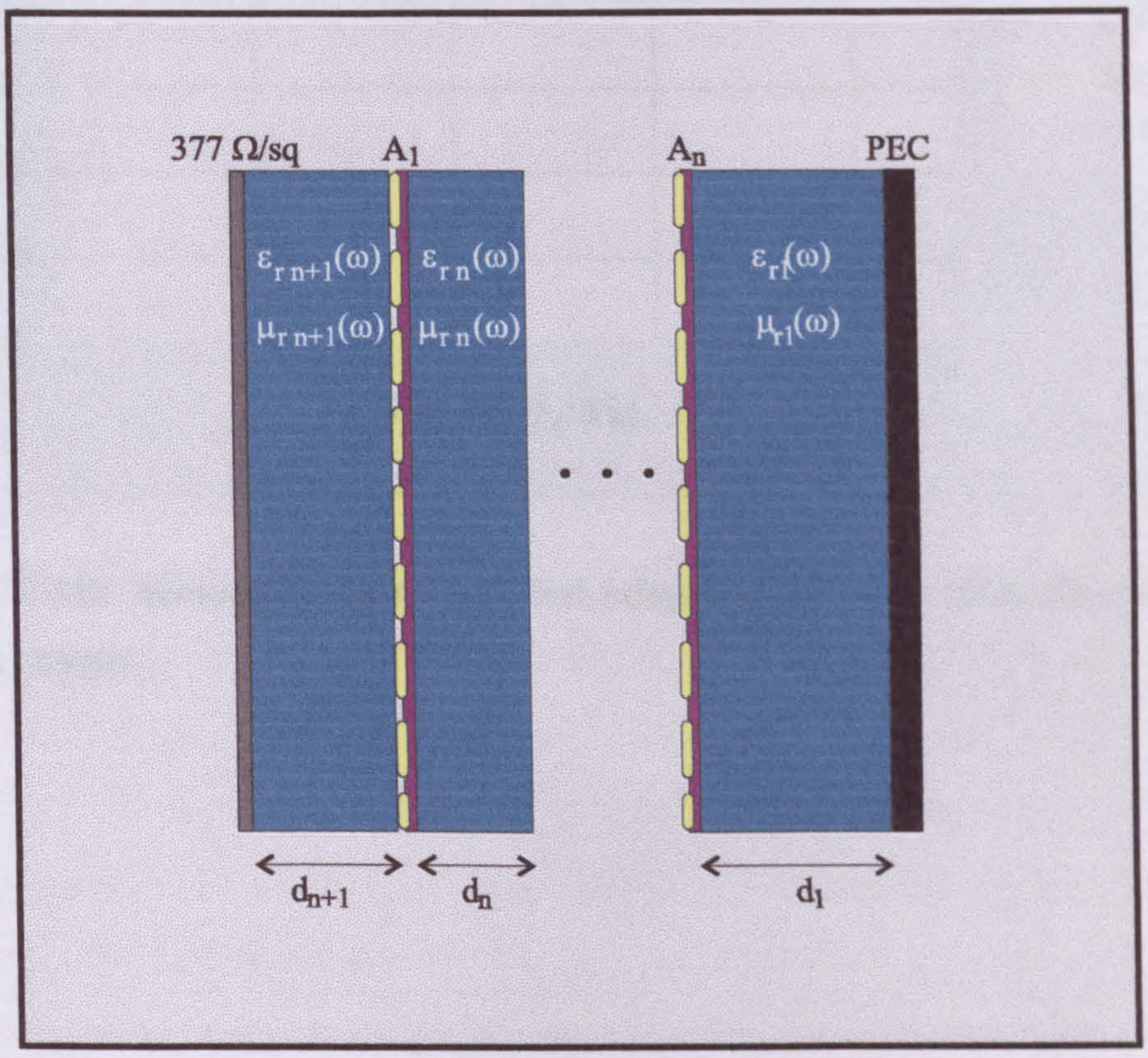

Figure 7.9: Schematic diagram of a Salisbury screen absorber incorporating a multiple number n of AFSSs.

Figures 7.12 through 7.15 display the absorbers' predicted and measured frequency responses for the four different states or sub-solutions allowed by the inclusion of two AFSSs, namely 0.0, 0.1, 1.0, 1.1. A 0 indicates a No-Bias condition, while a 1 a Bias condition. These figure show good correlation between measured and predicted data. In order to account for the finite thickness of the AFSSs intro-

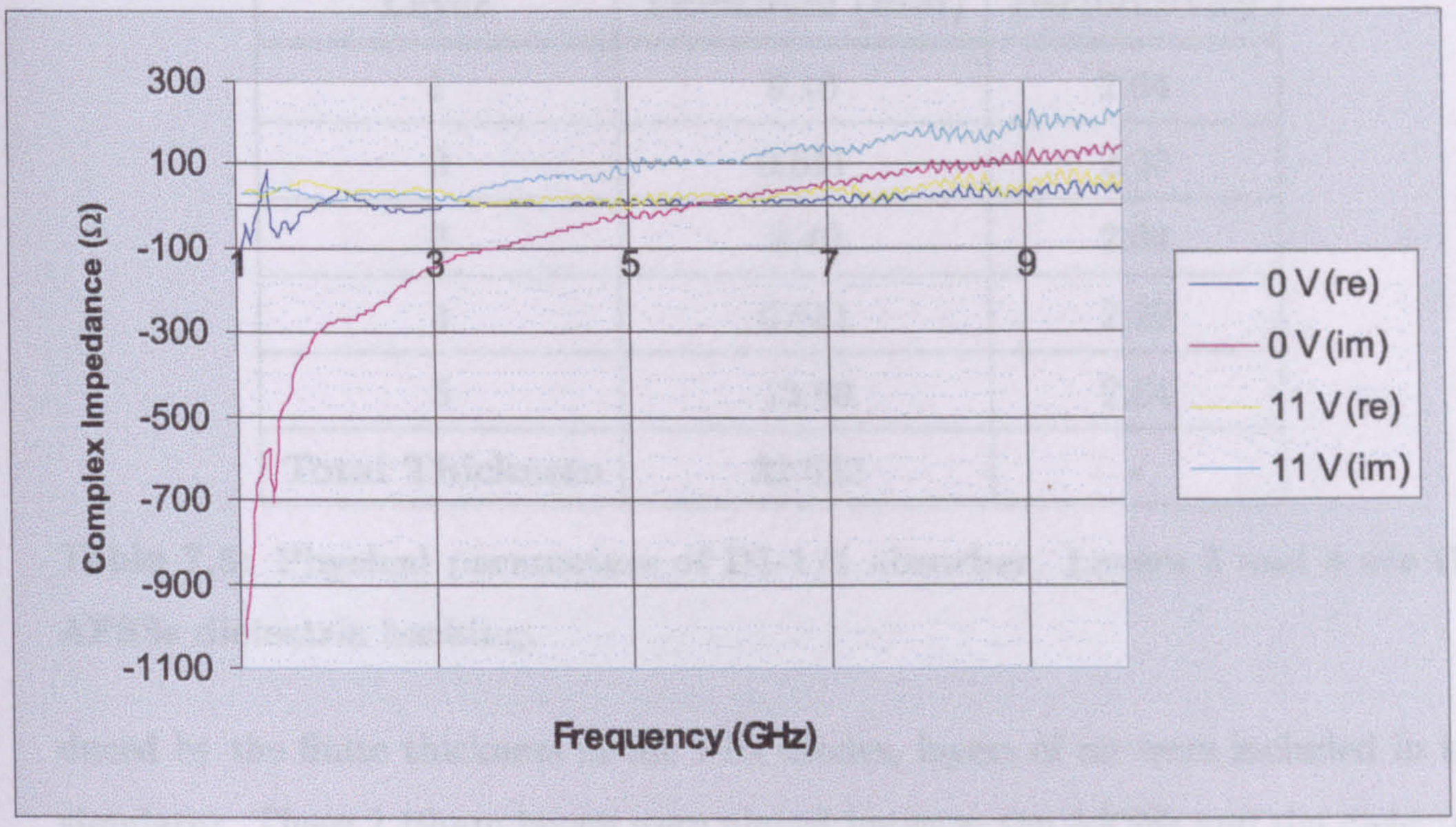

Figure 7.10: Measured de-embedded adaptive complex impedance response of DI-1 AFSS.

Search Bandwidth (GHz)	1.0 - 4.3
Layer Permitivitty Range	N/A
Layer Thickness Range (mm)	$d_{1,3,5} \in \{1.0, 20.0\}$

Table 7.4: GAs' parameters used to realised DI-1/1 Absorber.

Layer	Thickness (mm)	Permittivity
1	9.10	2.64
2	0.611	2.20
3	8.40	2.64
4	0.611	2.20
5	13.90	2.64
Total Thickness	32.622	-

Table 7.5: Physical parameters of DI-1/1 absorber. Layers 2 and 4 are the AFSSs dielectric backing.

duced by the finite thickness of the PIN diodes, layers of air were included in the simulator. These 2.19mm layers were placed between the AFSSs and the dielectric slabs located in front of each AFSS. It was found that the inclusion of these layers approximates better the measured and predicted results at higher frequencies.

Figure 7.16 shows the predicted dynamic frequency performance of a second absorber example, named DI-1/2. This absorber, which incorporates two dielectric-backed AFSSs, was realized with the physical parameters shown in table 7.7. The absorption solution of this absorber, as a function of spacers' thicknesses (d_1, d_3, d_5) and permittivities (ϵ_{r1}, ϵ_{r3}, ϵ_{r5}), was carried out through means of a GA with constrained input parameters as shown in table 7.6. From figure 7.16 it can be seen that the absorber's frequency response is of a switching-null nature with four different permissible states or sub-solutions. The absorber's switching behaviour prolongs over a bandwidth between 1 to 4 GHz, the equivalent of 2 octaves. Furthermore, the absorber's dynamic-range performance, in terms of reflectivity levels, extends between 1 to just over 5 GHz.

When comparing tables 7.5 and 7.7, it can be seen that the total thickness of

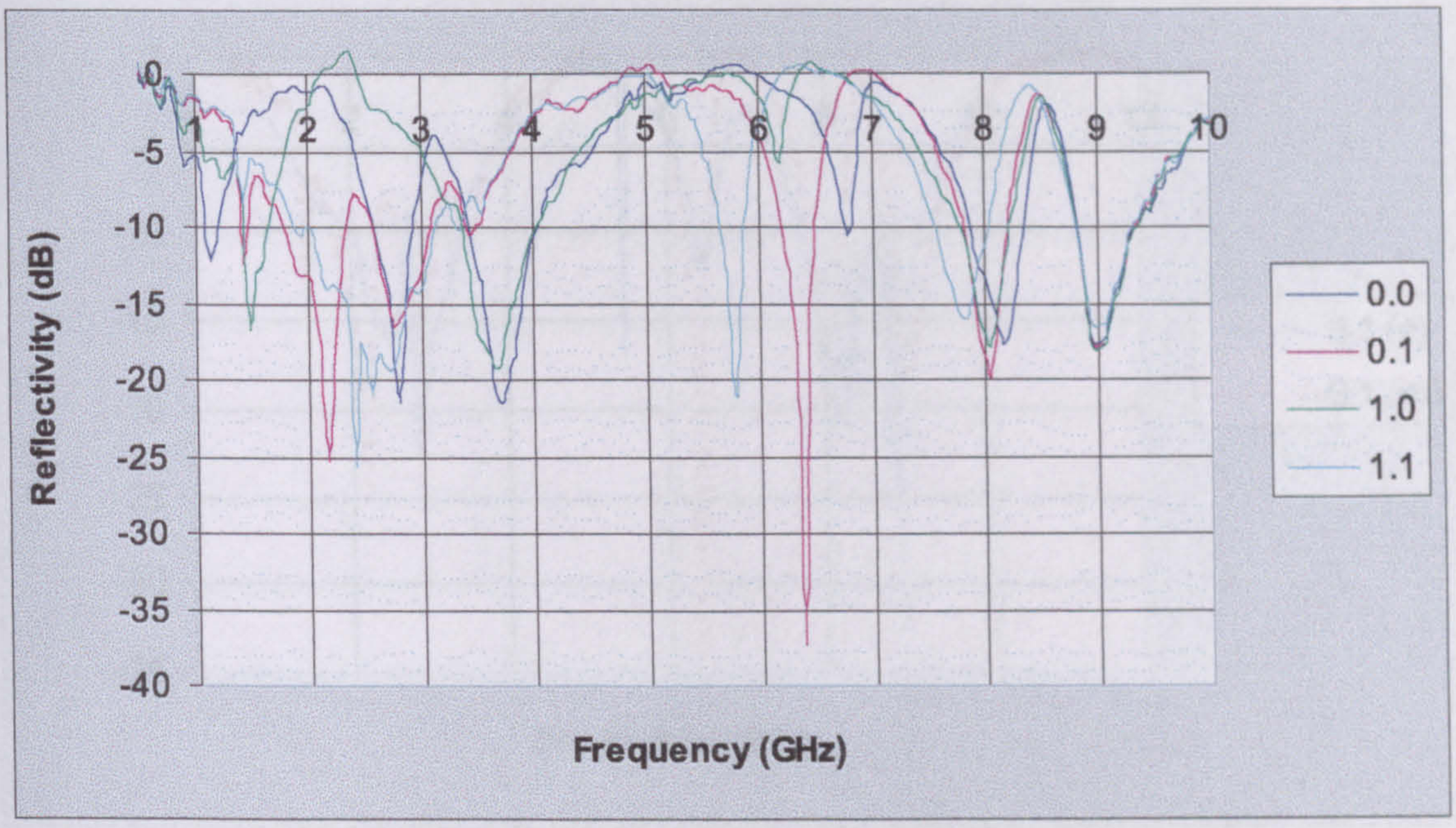

Figure 7.11: Measured dynamic frequency profile of absorber DI-1/1.

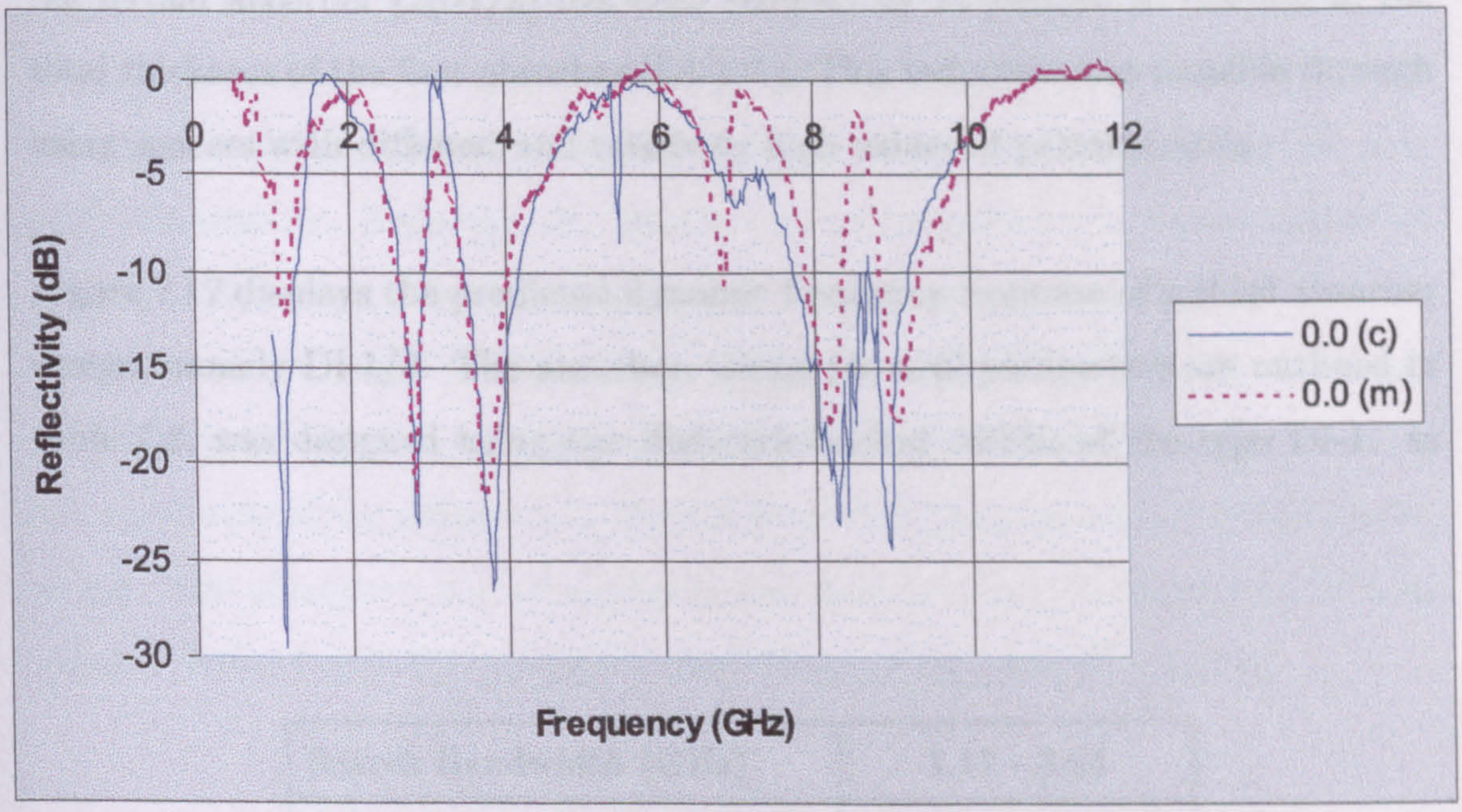

Figure 7.12: Predicted and measured frequency profiles of absorber DI-1/1: State 0.0

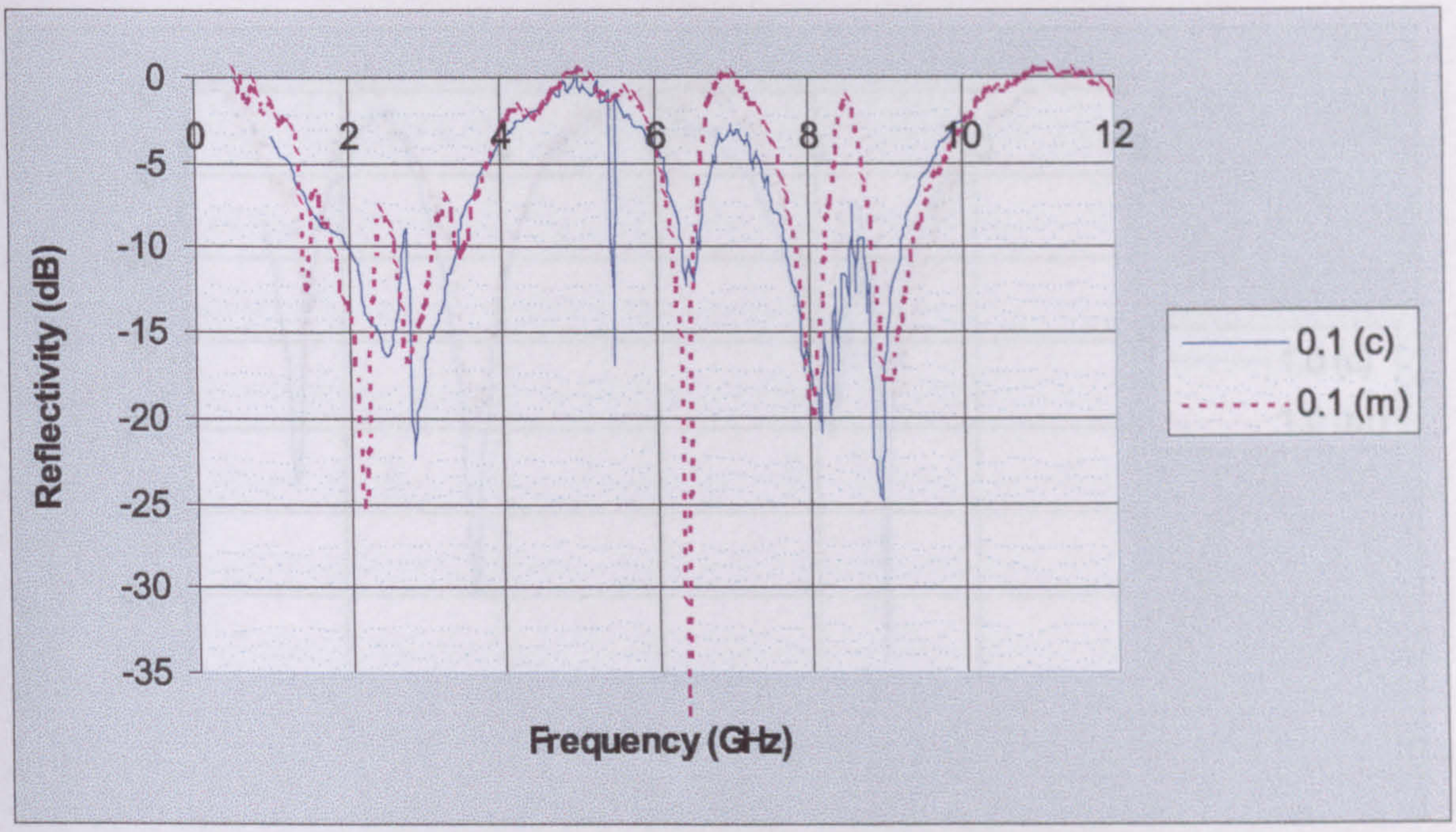

Figure 7.13: Predicted and measured frequency profiles of absorber DI-1/1: State 0.1

the second absorber (DI-1/2) has been reduced by 22 percent in relation to the total thickness of the first absorber (DI-1/1). This reduction was possible through using spacers with different and relatively high values of permittivities.

Figure 7.17 displays the predicted dynamic frequency response of a third absorber design, namely DI-1/3. The absorber, whose physical parameters are outlined in table 7.8, was designed using two dielectric-backed AFSSs of the type DI-1. as

Search Bandwidth (GHz)	1.11 - 3.64
Layer Permittivity Range	$\epsilon_{r_{1,3,5}} \in \{1.0, 32.0\}$
Layer Thickness Range (mm)	$d_{1,3,5} \in \{1.0, 12.0\}$

Table 7.6: GAs' parameters used to realized DI-1/2 Absorber.

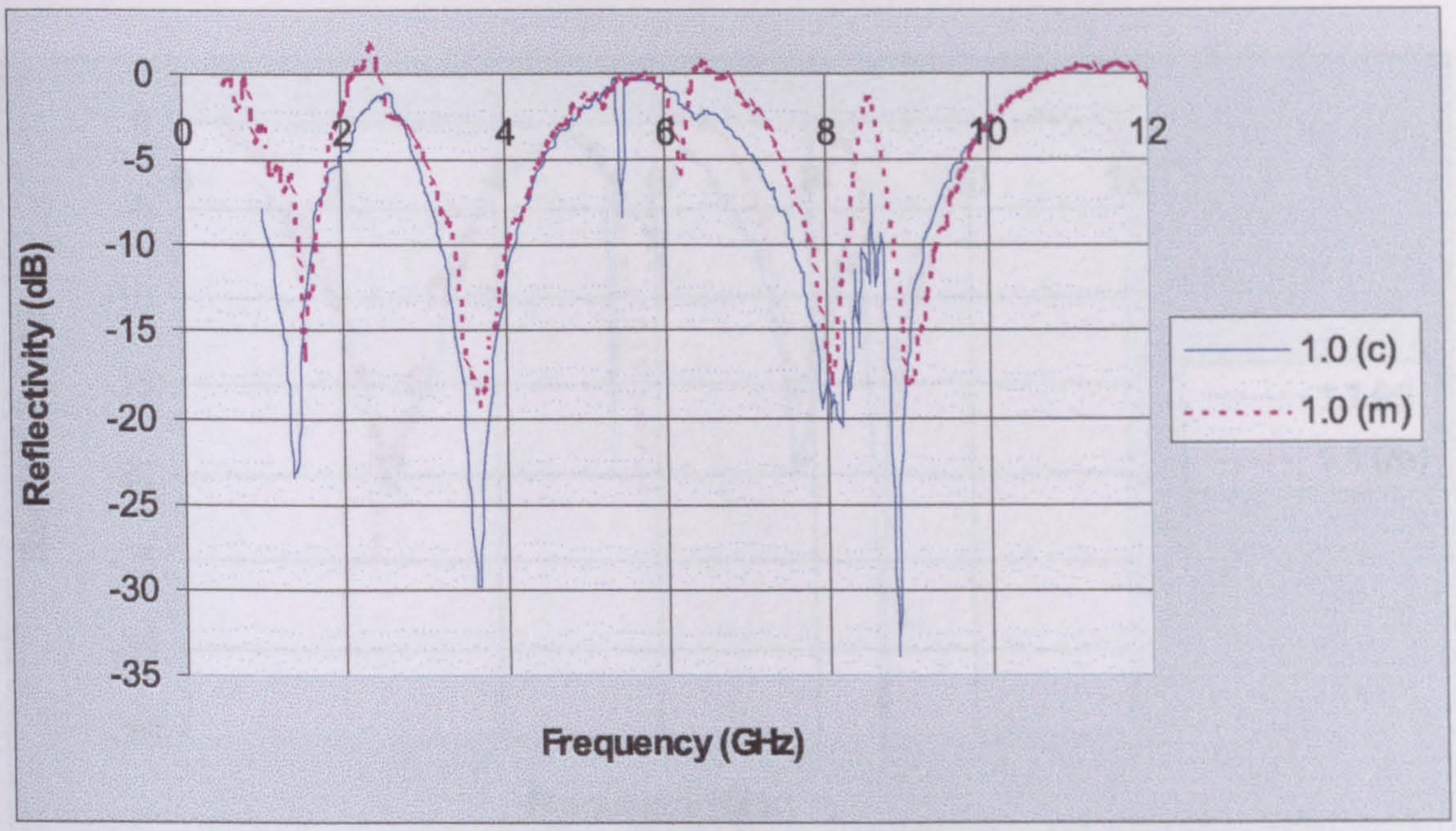

Figure 7.14: Predicted and measured frequency profiles of absorber DI-1/1: State 1.0

shown by table 7.8, the dielectric spacers employed are high permittivity ones. The previous absorber result, viz. that pertaining to DI-1/2, show that the thickness of the absorber can be reduced through employing dielectric spacers with high permittivity. Although the absorber shows a number of dynamic reflection nulls spread over a 2 octaves bandwidth, the null depths of states 1.0 and 0.1, located at 2 GHz and 3 GHz, respectively, are above the minimum null depth threshold level, viz. -15 dB. This solution was, however, found through increasing the amplitude of the reflection coefficient from 0.18 (previous absorbers examples) to 0.5. The absorber's overall thickness has, however, been substantially reduced when compared with that of DI-1/1 and DI-1/2, vide tables 7.5 and 7.8.

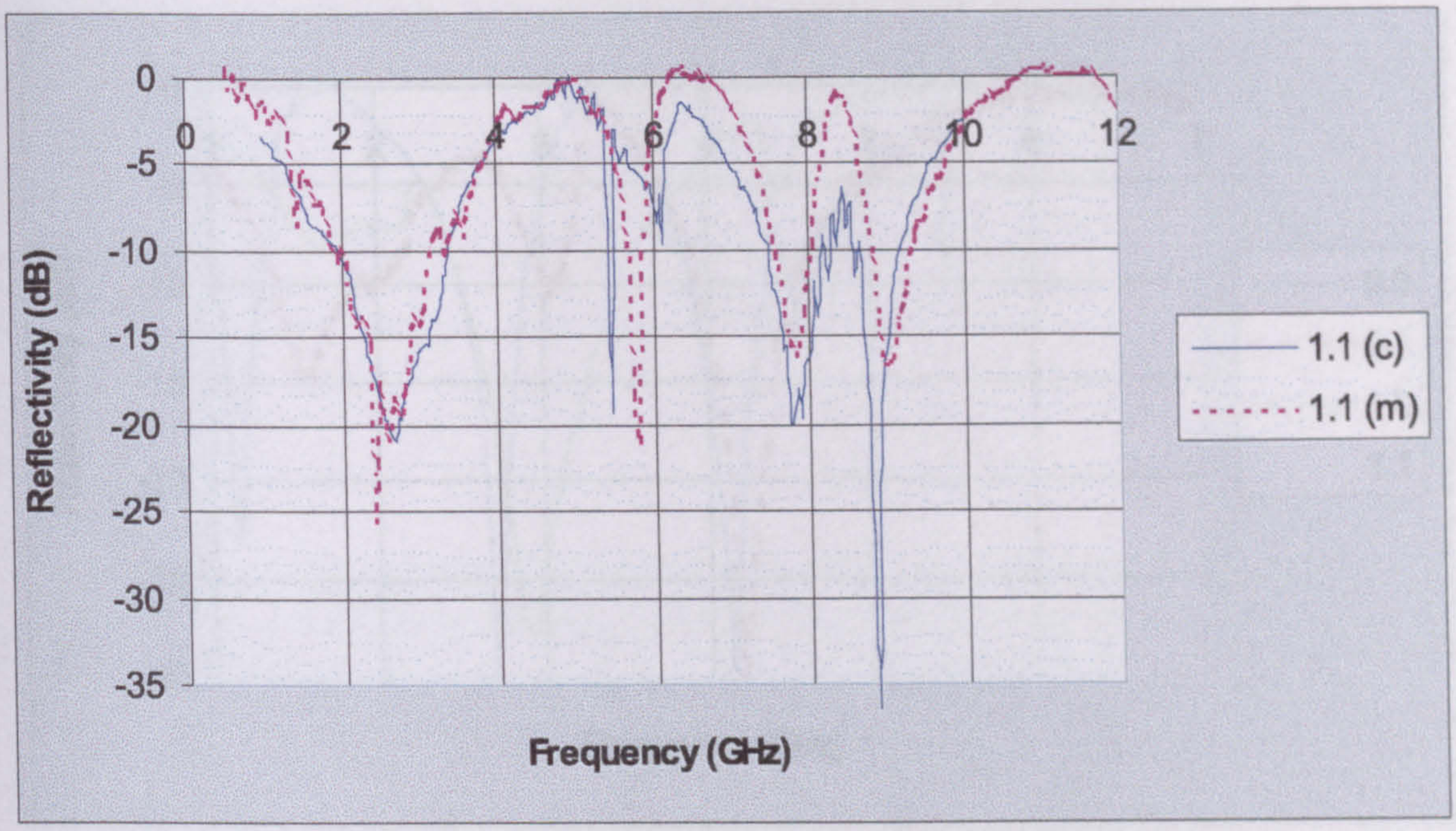

Figure 7.15: Predicted and measured frequency profiles of absorber DI-1/1: State 1.1

Layer	Thickness (mm)	Permittivity
1	8.90	20.0
2	0.611	2.20
3	3.90	2.07
4	0.611	2.20
5	11.4	4.0
Total Thickness	25.422	-

Table 7.7: Physical parameters of DI-1/2 absorber. Layers 2 and 4 are the AFSSs dielectric backing.

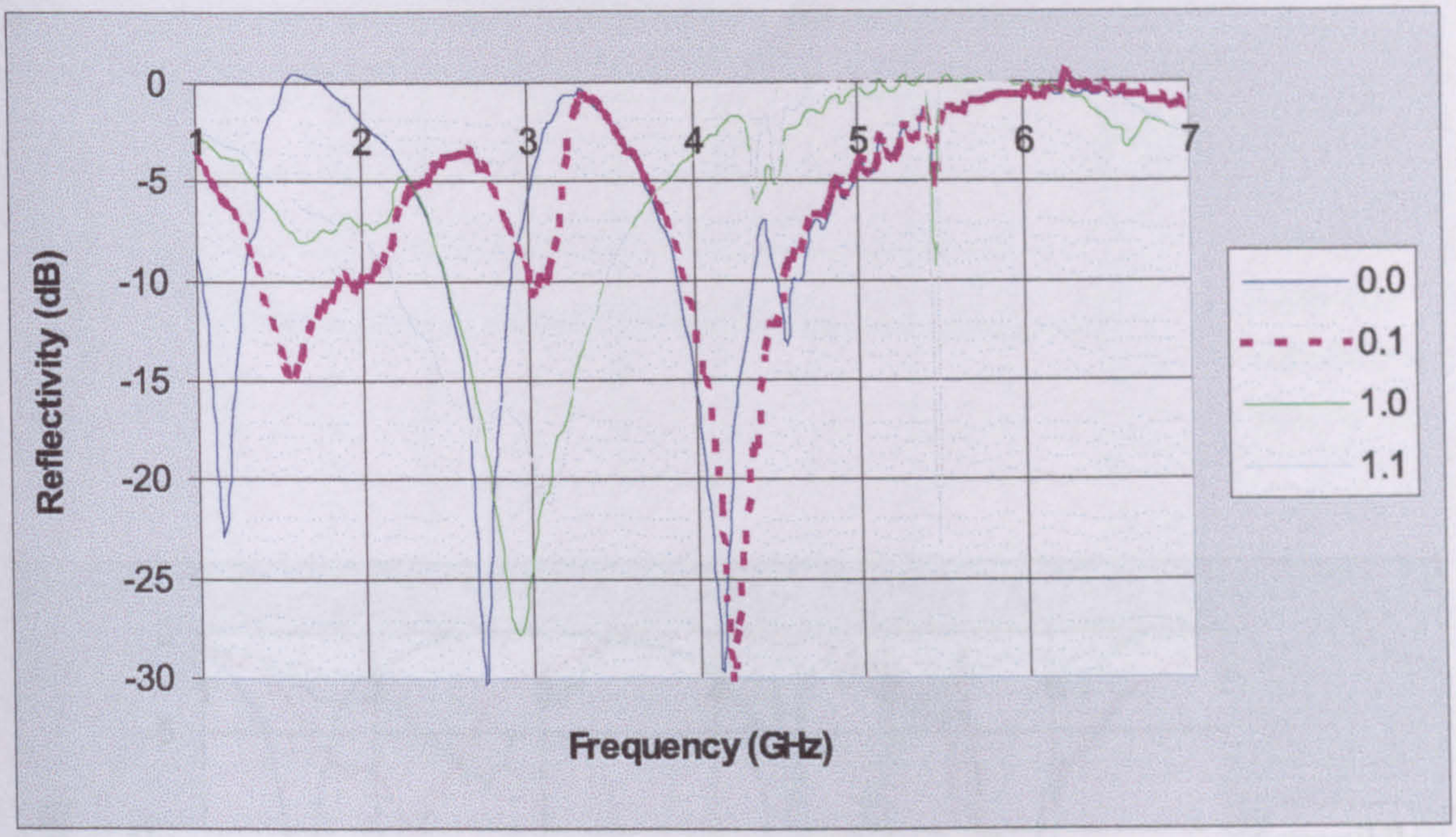

Figure 7.16: Predicted dynamic frequency profile of DI-1/2 absorber.

Layer	Thickness (mm)	Permittivity
1	3.90	25.0
2	0.611	2.20
3	1.20	25.0
4	0.611	2.20
5	2.5	25.0
Total Thickness	8.822	-

Table 7.8: Physical Parameters of DI-1/3 Absorber. layers 2 and 4 are the AFSSs dielectric backing.

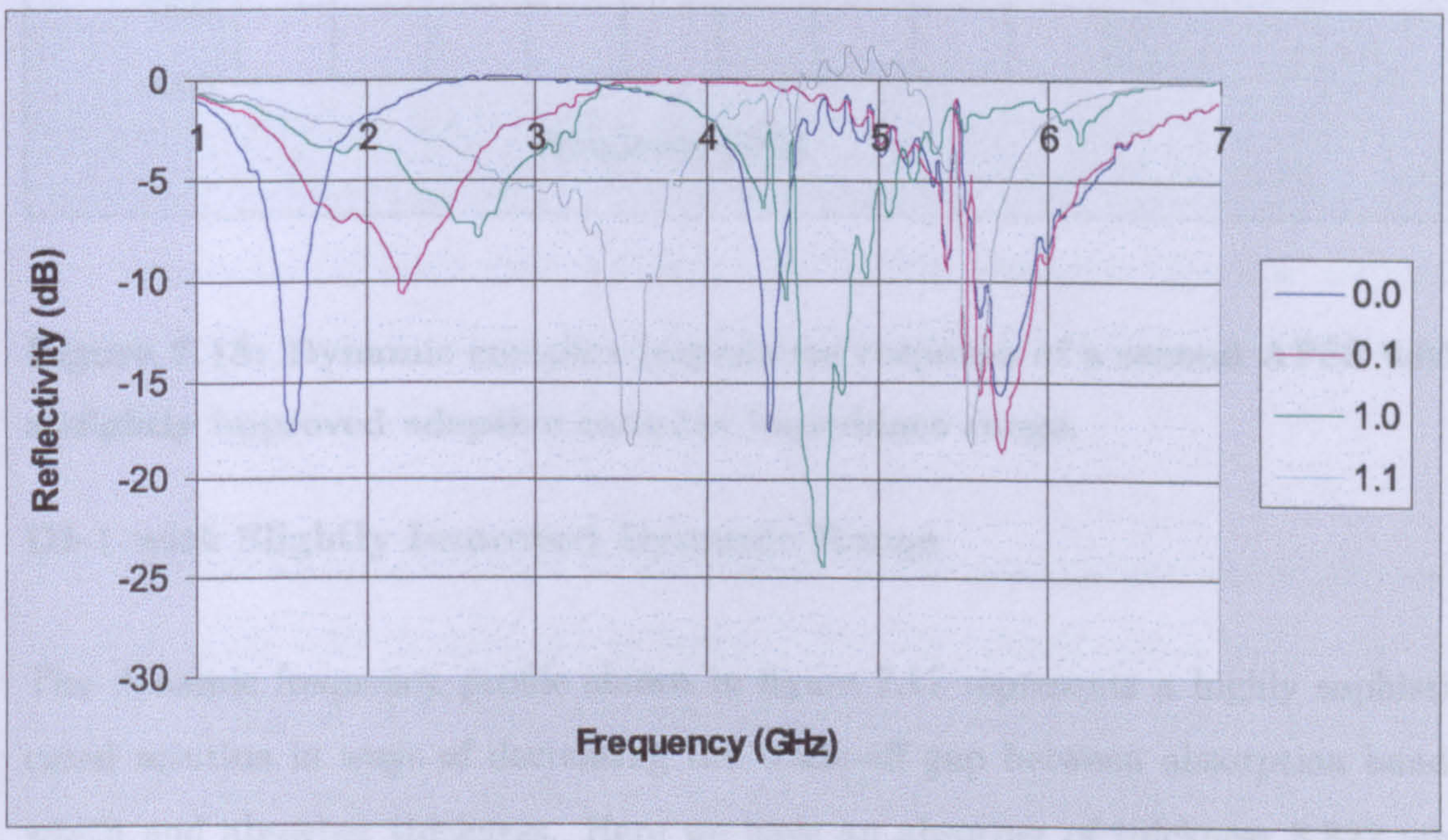

Figure 7.17: Predicted Dynamic Frequency Profile of DI-1/3 Absorber.

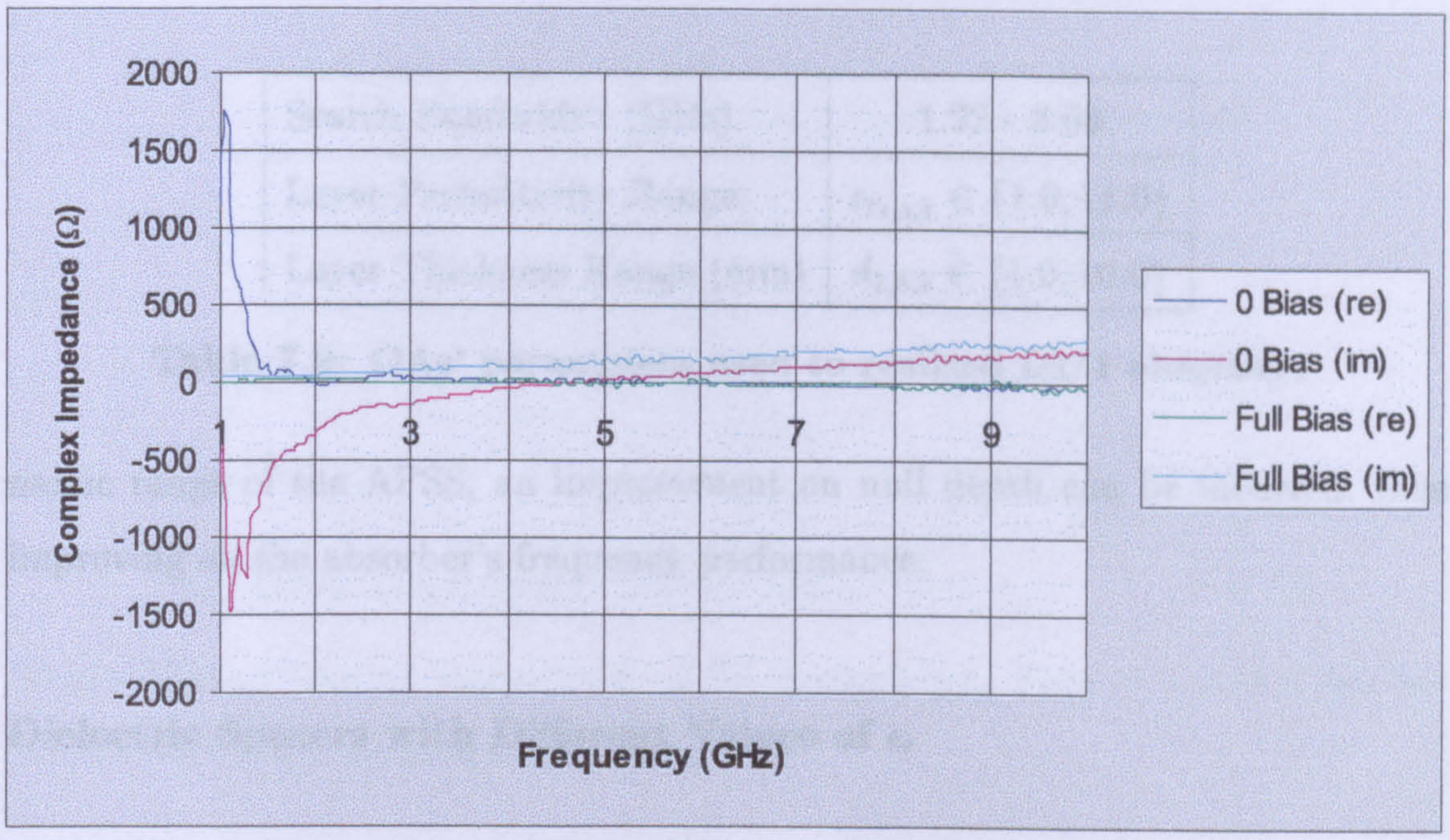

Figure 7.18: Dynamic complex impedance response of a second AFSS with a slightly improved adaptive complex impedance range.

DI-1 with Slightly Improved Dynamic Range

The dynamic frequency profile shown in figure 7.17 represents a highly sophisticated solution in ways of decreasing the trade-off gap between absorption bandwidth and absorber thickness. Here we have an absorber of thickness 8.822 mm whose discrete absorption bandwidth potentially covers a frequency range between ~1.5 to 6 GHz. However, the reflection depths of the absorbers' nulls between 2 GHz and just above 3 GHz, i.e. those belonging to states 0.1 and 1.0, are not satisfactory. The minimum allowable threshold level is -15 dB. At this point, it was anticipated that by ways of increasing the AFSS's dynamic range, i.e through making the boards more transparent, an improvement of null depth can be incurred.

The simulated results that follow will show how by slightly increasing the dy-

Search Bandwidth (GHz)	1.22 - 3.68
Layer Permittivity Range	$\epsilon_{r_{1,3,5}} \in \{1.0, 11.0\}$
Layer Thickness Range (mm)	$d_{1,3,5} \in \{1.0, 10.0\}$

Table 7.9: GAs' parameters used to realised DI/1 absorber.

namic range of the AFSS, an improvement on null depth can be incurred, thus improving on the absorber's frequency performance.

Dielectric Spacers with Different Values of ϵ_r

The results that follow were realized with AFSSs having a dynamic complex impedance response as shown in figure 7.18. The absorber's schematic diagram is shown in figure 7.9 with $n = 2$.

The dynamic frequency profile of an absorber, whose physical parameters are outlined in table 7.10, is depicted in figure 7.19. For identification purposes, the absorber is named DI/1. The absorber's absorption solution, as a function of both spacers' thicknesses (d_1, d_3, d_5) and permittivities (ϵ_{r1}, ϵ_{r3}, ϵ_{r5}), was found by a GA with constrained range of input parameters as depicted in table 7.9. From figure 7.19, it can be seen that the absorber's dynamic frequency profile depicts a series of reflection nulls, of acceptable depth, discreetly spread over a frequency bandwidth that prolongs between ~1.5 GHz and ~5.4 GHz. The figure also shows that the absorber's dynamic range, in terms of reflectivity levels, extends up to ~6 GHz. The fact that the absorption depth of all reflection nulls are on or below the minimum threshold level (-15 dB), clearly suggests that by increasing the AFSS's dynamic range, the absorber performance, in terms of null depth, can be greatly improved.

Layer	Thickness (mm)	Permittivity
1	8.30	2.0
2	0.611	2.20
3	3.20	4.0
4	0.611	2.20
5	4.40	10.0
Total Thickness	17.122	-

Table 7.10: Physical parameters of DI/1 absorber. Layers 2 and 4 are the AFSSs dielectric backing.

Figure 7.20 shows the computed dynamic frequency performance of a second example absorber, called DI/2. The absorber's physical parameters are summarized in table 7.12. The dynamic frequency profile of this absorber is very similar to that shown in figure 7.19, in that it has a number of reflection nulls discreetly placed over a wide frequency bandwidth. By comparing figures 7.19 and 7.20 it can seen that the new spacers parameters have incurred a small improvement on the absorber's dynamic bandwidth. However, it is table 7.12 which depicts the most significant enhancement incurred into this absorber's design. With the new spacers' permittivities the absorber's total thickness has been decreased from 17.122 mm to 10.522 mm. This represents a thickness reduction of 38 percent over that of the previous absorber design. This improvement has been achieved through increasing the value of the spacers permittivities.

Dielectric Spacers with Equal ϵ_r

The previous results as well as showing improvement upon null depth indicate that the use of dielectric materials with higher values of permittivity reduces the overall absorber thickness while keeping the absorber's dynamic frequency response

Search Bandwidth (GHz)	1.22 - 7.2
Layer Permittivity Range	$\epsilon_{r_{1,3,5}} \in \{1.0, 31.0\}$
Layer Thickness Range (mm)	$d_{1,3,5} \in \{1.0, 10.0\}$

Table 7.11: GAs' parameters used to realised DI/2 absorber.

Layer	Thickness (mm)	Permittivity
1	5.20	7.0
2	0.611	2.20
3	1.90	4.0
4	0.611	2.20
5	2.20	20.0
Total Thickness	10.522	-

Table 7.12: Physical parameters of DI/2 absorber. Layers 2 and 4 are the AFSSs dielectric backing.

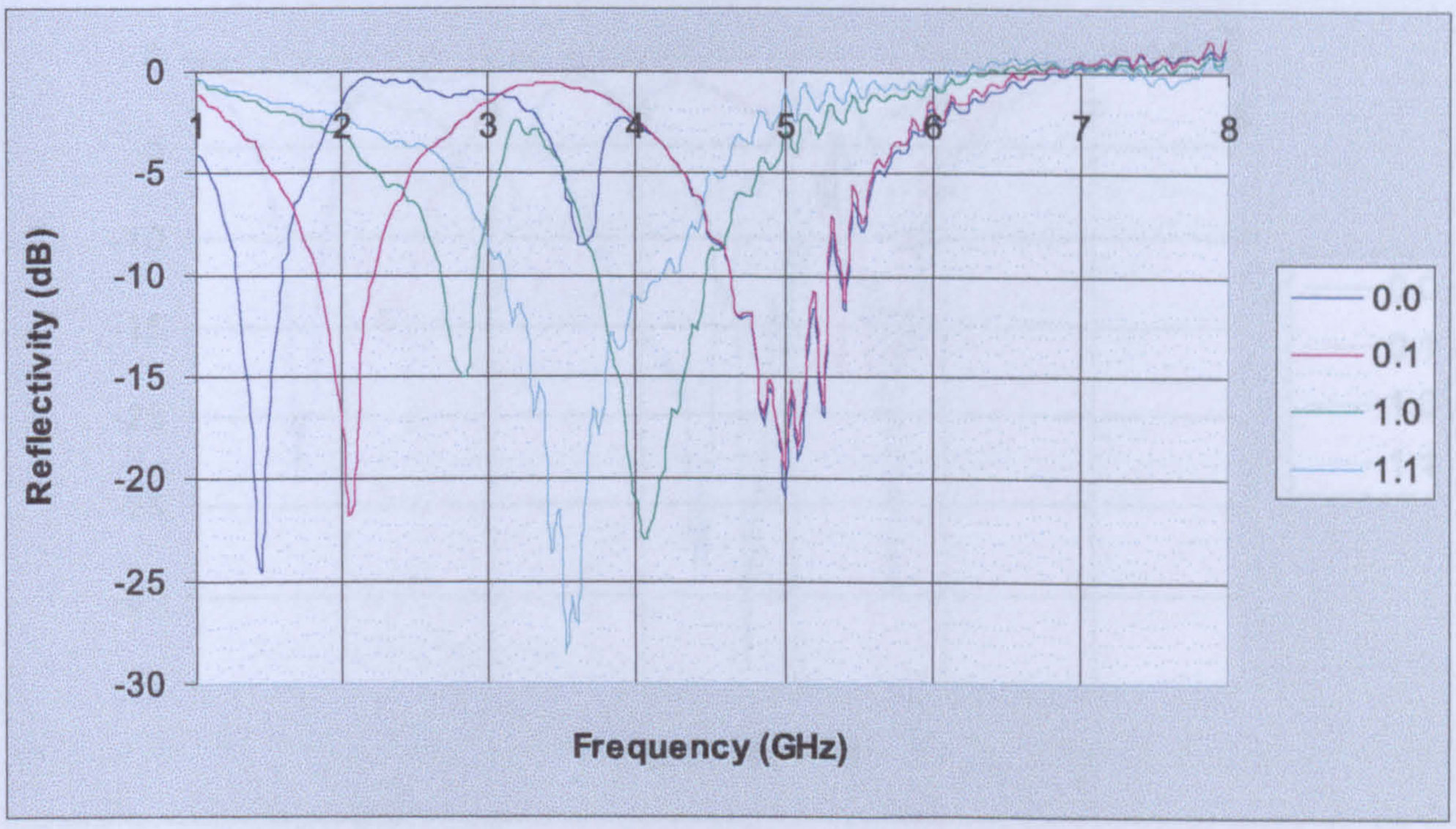

Figure 7.19: Predicted dynamic frequency profile of DI/1 absorber.

unchanged. In view of this fact and in an attempt to reduce further the absorbers overall thickness, it was decided to increase the permittivity of the dielectric spacer and keep it constant throughout the absorber. The absorber design problem thus became a volumetric one whose absorption solution is a function of the spacers thicknesses (d_1, d_3, d_5).

Figures 7.21, 7.22, and 7.23 show the computed dynamic frequency responses of three different absorber designs, namely DI/3, DI/4 and DI/5, whose parameters are outlined in tables 7.13, 7.14 and 7.15, respectively. When comparing these figures, it can see that the overall dynamic frequency responses of these absorbers are highly similar, all of them showing a number of discrete nulls spread over a wide frequency bandwidth that extends between ~1.5 GHz to ~6 GHz. When comparing tables 7.13, 7.14 and 7.15, it can be seen that DI/5, i.e. the absorber designed with the highest value of permittivity ($\epsilon_r = 30$), represents the absorber with the smallest thickness, being 8.222 mm.

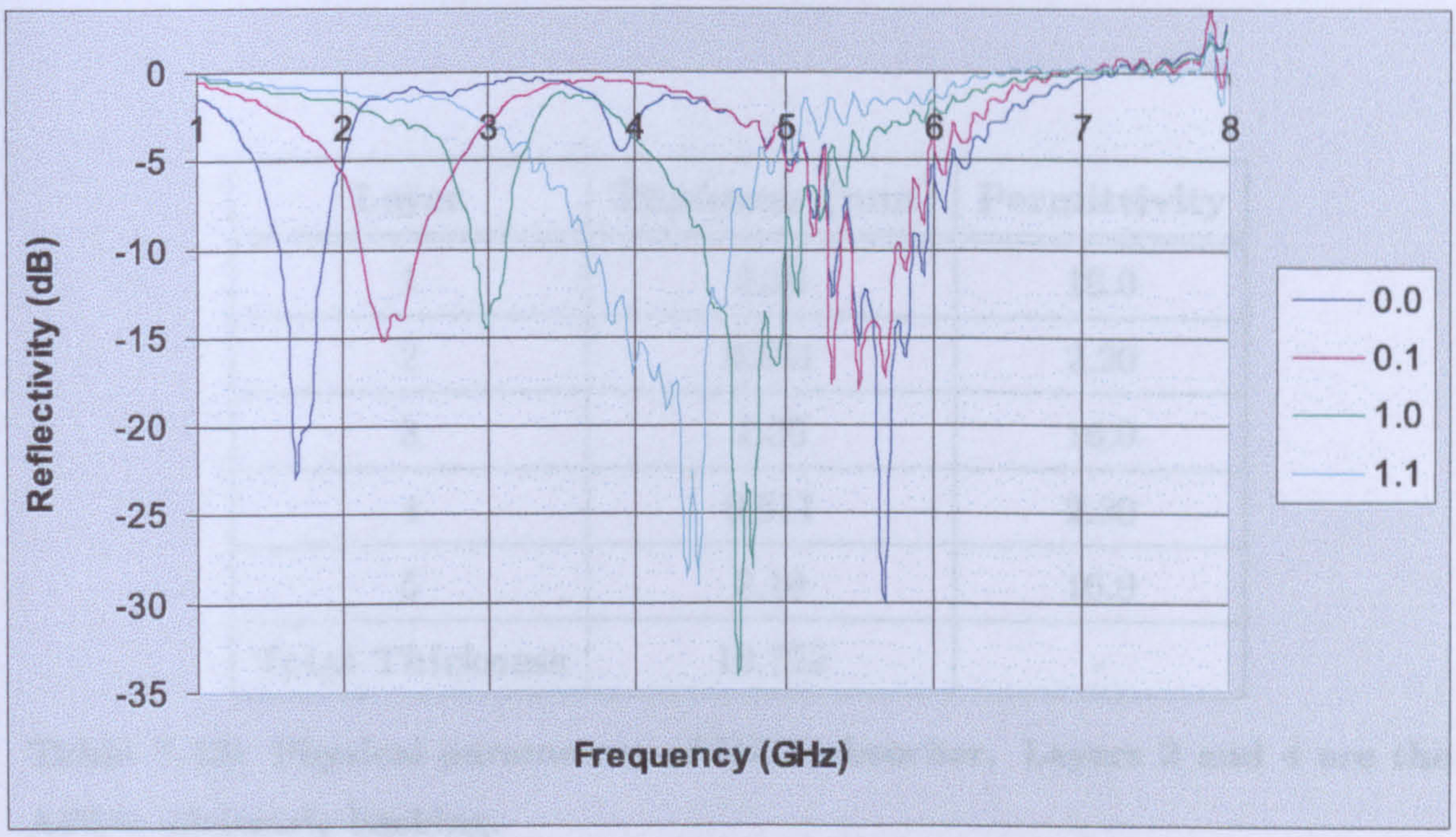

Figure 7.20: Predicted dynamic frequency profile of DI/2 absorber.

These results clearly demonstrate that the absorber's overall thickness can be reduced by means of employing materials with high ϵ_r. This improvement is performed while maintaining the absorber's frequency response almost unchanged. There is, however, a slight drawback with this approach. Whilst the absorber's absorption bandwidth is almost unchanged, the depth of the reflection nulls is reduced with increase spacer permittivity.

The simulated results shown in this section clearly demonstrate that the absorption bandwidth of a Salisbury screen absorber can greatly be increased through employing AFSSs with an open/short circuit characteristics. The absorption bandwidth is increased through the generation of a number of reflection nulls discretely placed over a wide frequency band. The results shown in this section have also shown that the absorber thickness is reduced through employing dielectric spacers with high permittivity. The use of high permittivity materials, however, slightly

Layer	Thickness (mm)	Permittivity
1	5.10	16.0
2	0.611	2.20
3	1.30	16.0
4	0.611	2.20
5	3.10	16.0
Total Thickness	10.722	-

Table 7.13: Physical parameters of DI/3 absorber. Layers 2 and 4 are the AFSSs dielectric backing.

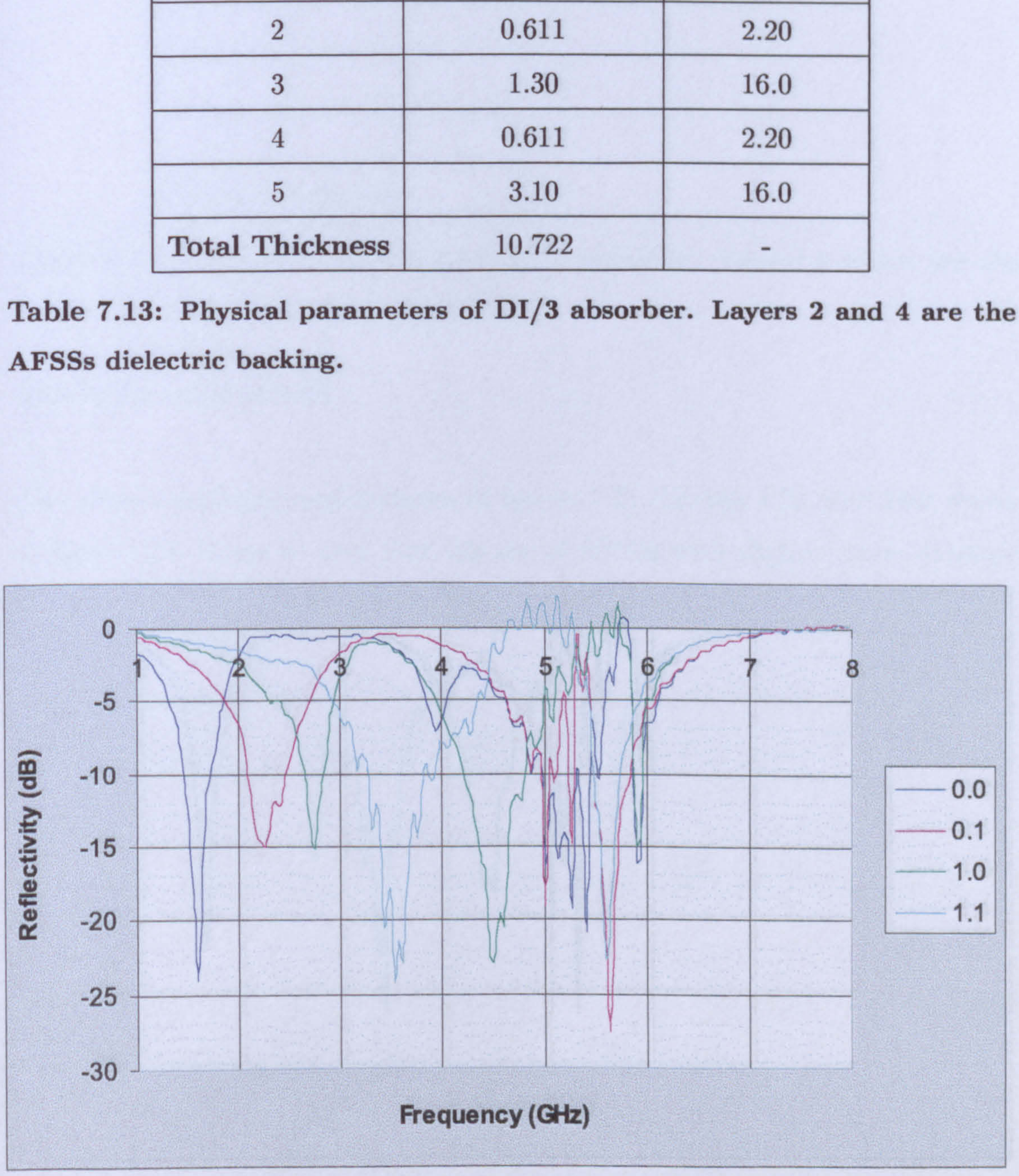

Figure 7.21: Predicted dynamic frequency profile of DI/3 absorber.

Layer	Thickness (mm)	Permittivity
1	3.90	25.0
2	0.611	2.20
3	1.20	25.0
4	0.611	2.20
5	2.50	25.0
Total Thickness	8.822	-

Table 7.14: Physical parameters of DI/4 absorber. Layers 2 and 4 are the AFSSs dielectric backing.

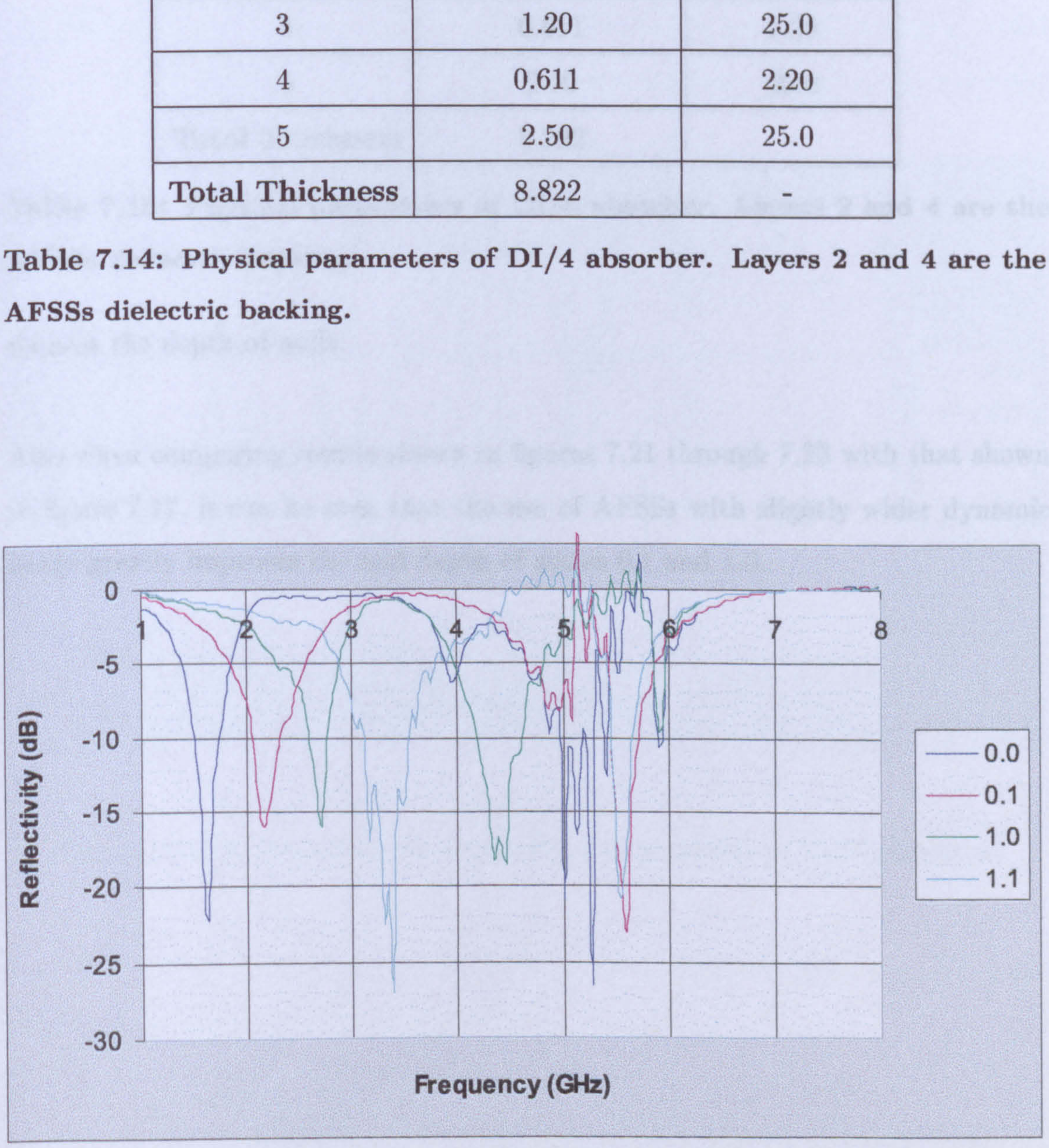

Figure 7.22: Predicted dynamic frequency profile of DI/4 absorber.

Layer	Thickness (mm)	Permittivity
1	3.00	30.0
2	0.611	2.20
3	1.80	30.0
4	0.611	2.20
5	2.20	30.0
Total Thickness	8.222	-

Table 7.15: Physical parameters of DI/5 absorber. Layers 2 and 4 are the AFSSs dielectric backing.

reduces the depth of nulls.

Also when comparing results shown in figures 7.21 through 7.23 with that shown in figure 7.17, it can be seen that the use of AFSSs with slightly wider dynamic range greatly improves the null depth of states 0.1 and 1.0.

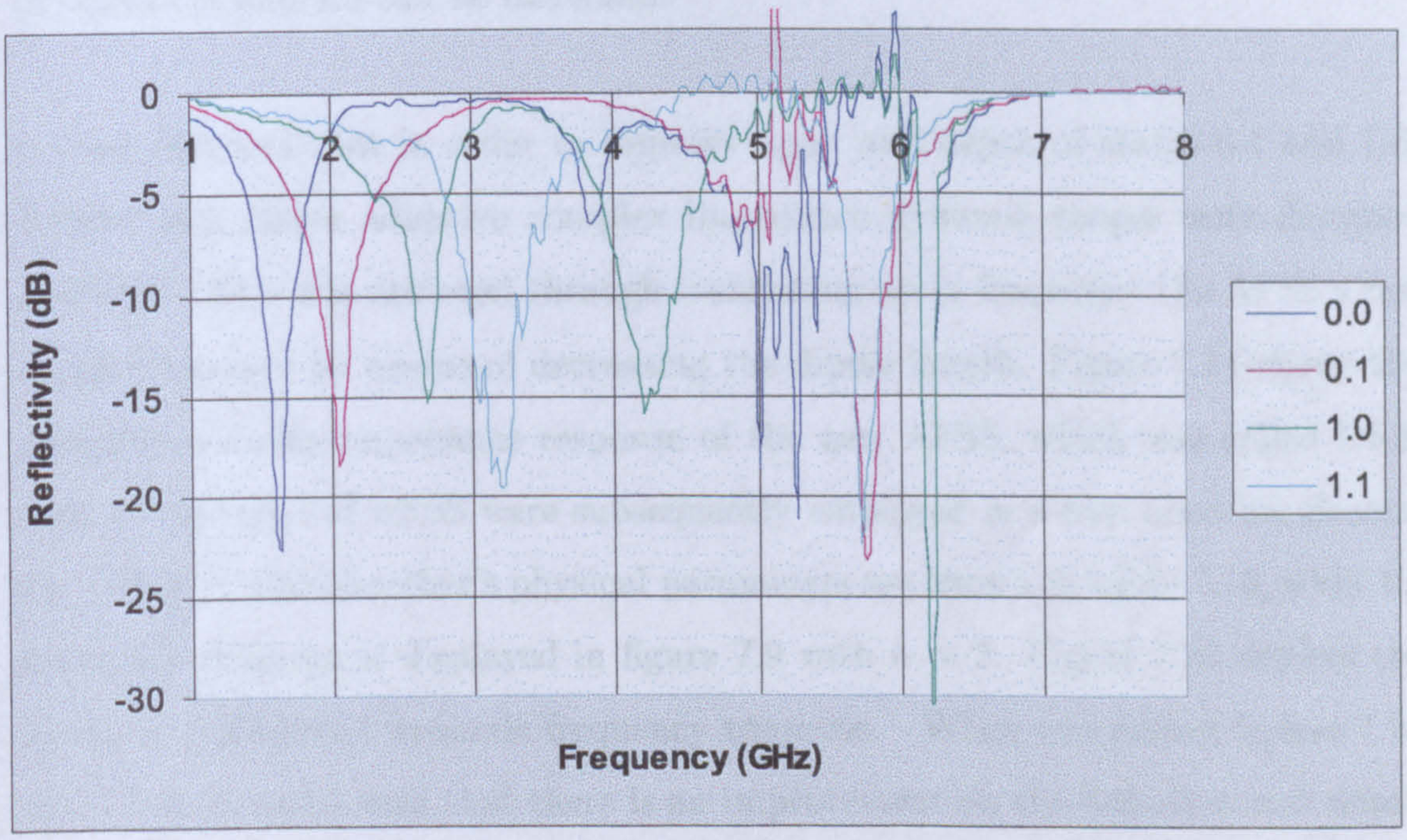

Figure 7.23: Predicted dynamic frequency profile of DI/5 absorber.

Salisbury Screen Absorbers Embedded with Two DI-2 Type AFSSs

The predicted results shown in figure 7.17 show that through placing AFSSs with bi-state electrical characteristics within a Salisbury screen absorber having high permittivity dielectric spacers, its absorption bandwidth can be substantially extended. The figure shows, however, that the reflection nulls pertaining to states 0.1 and 1.0 are above the minimum threshold reflection level of -15 dB. The data depicted in figures 7.21 through 7.23, nonetheless, demonstrate that through utilizing AFSSs with slightly larger adaptive complex impedance ranges, the null depth of states 0.1 and 1.0 can be increased.

It then followed that in order to improve upon null depth of states 0.1 and 1.0, AFSSs with larger adaptive complex impedance dynamic ranges were designed and built. This was achieved through translating up in frequency the AFSS's resonant frequency by means of decreasing the dipole length. Figure 7.24 shows the adaptive complex impedance response of the new AFSS, which was called DI-2. Two of this type of AFSS were subsequently employed in a new absorber design, viz. DI-2/1. The absorber's physical parameters are shown in table 7.16, while its schematic diagram is displayed in figure 7.9 with $n = 2$. Figure 7.25 depicts the absorber's predicted dynamic frequency response. When comparing figures 7.26 and 7.18, it can be seen that there is an improvement on the reflection null depth of states 0.1 and 1.0. This, however, has happened at cost. As shown in figure 7.26, there is a dead region within the 4 GHz band.

Salisbury Screen Absorbers Built with Two AFSSs of the type DI-1 and DI-2

In order to fill in the dead region seen in figure 7.25 another absorber design was created. This time, however, the absorber was constructed with two AFSSs having similar frequency properties, but with different dynamic ranges. The absorbers' physical parameters are outlined in table 7.17, while its schematic diagram is shown

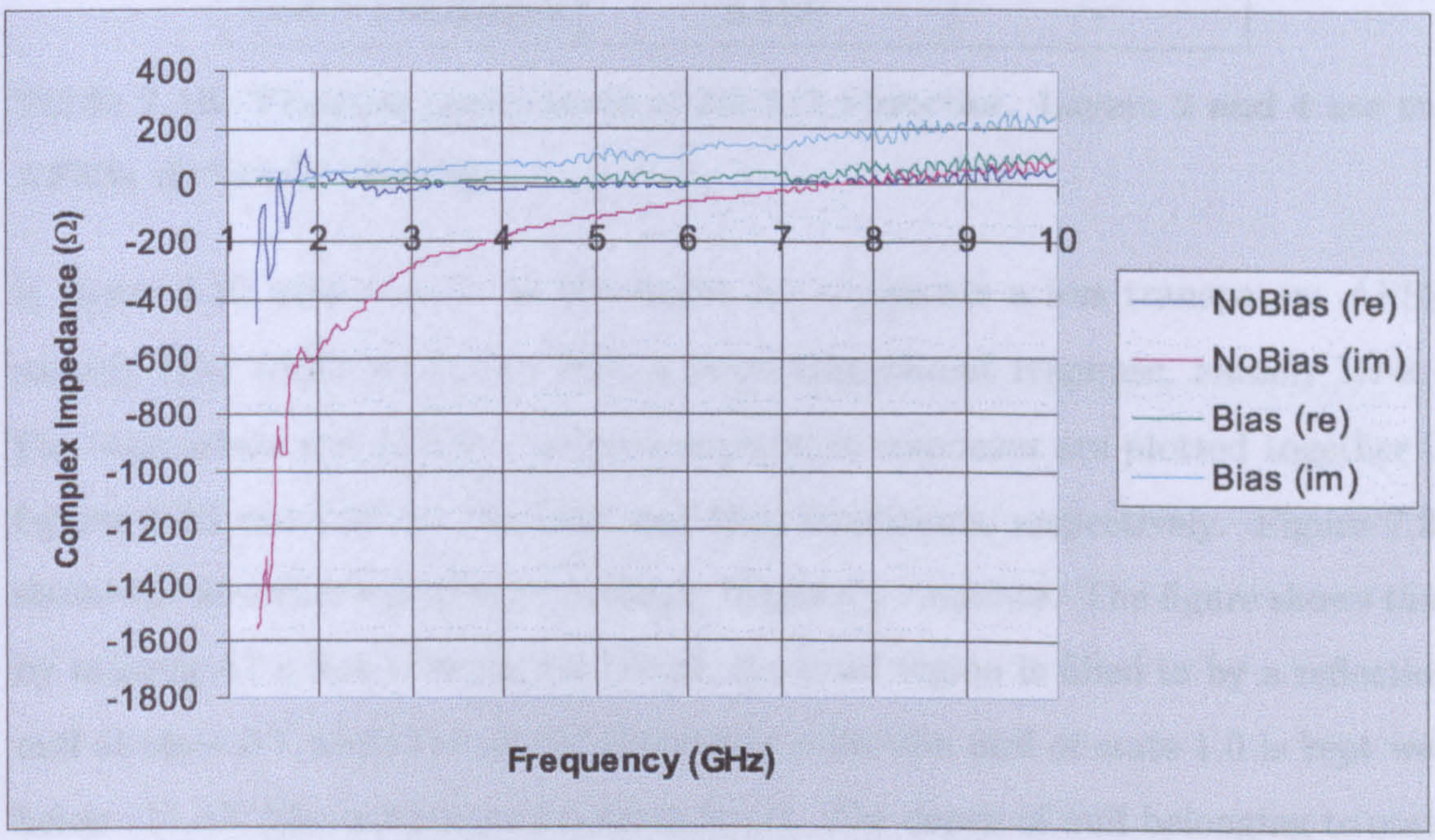

Figure 7.24: Measured de-embedded dynamic complex impedance response of DI-2 AFSS.

Layer	Thickness (mm)	Permittivity
1	3.10	25.0
2	0.508	2.20
3	1.4	25.0
4	0.611	2.20
5	2.50	25.0
Total Thickness	8.119	-

Table 7.16: Physical parameters of DI-2/1 absorber. Layers 2 and 4 are the AFSSs dielectric backing.

in figure 7.10 with $n = 2$. In the figure A1 represents a less transparent AFSS, namely DI-1 while A2 is one with a more transparent response, namely DI-2. For comparison the AFSSs' complex impedance responses are plotted together in figures 7.26 and 7.27 for No Bias and Bias conditions, respectively. Figure 7.28 shows the absorber's predicted dynamic frequency response. The figure shows that by making A1 a less transparent board, the dead region is filled in by a reflection null at state 0.1 while the depth of the first reflection null of state 1.0 is kept well below -15 dB (the minimum threshold level). The depth of null belonging to state 0.1 is, however, above the minimum threshold level.

Inclusion of Air Gap Layers

To validate the absorber dynamic frequency predictions shown in figure 7.25, DI-2/2 was built and its dynamic frequency properties were, subsequently, measured. Figure 7.30 shows the absorbers measured dynamic frequency response. When comparing figure 7.25 and 7.30 it can be seen that there are discrepancies between the measured and predicted data. The calculated dynamic frequency response of DI-2/2 absorber was generated by assuming the AFSSs to be infinitely thin pla-

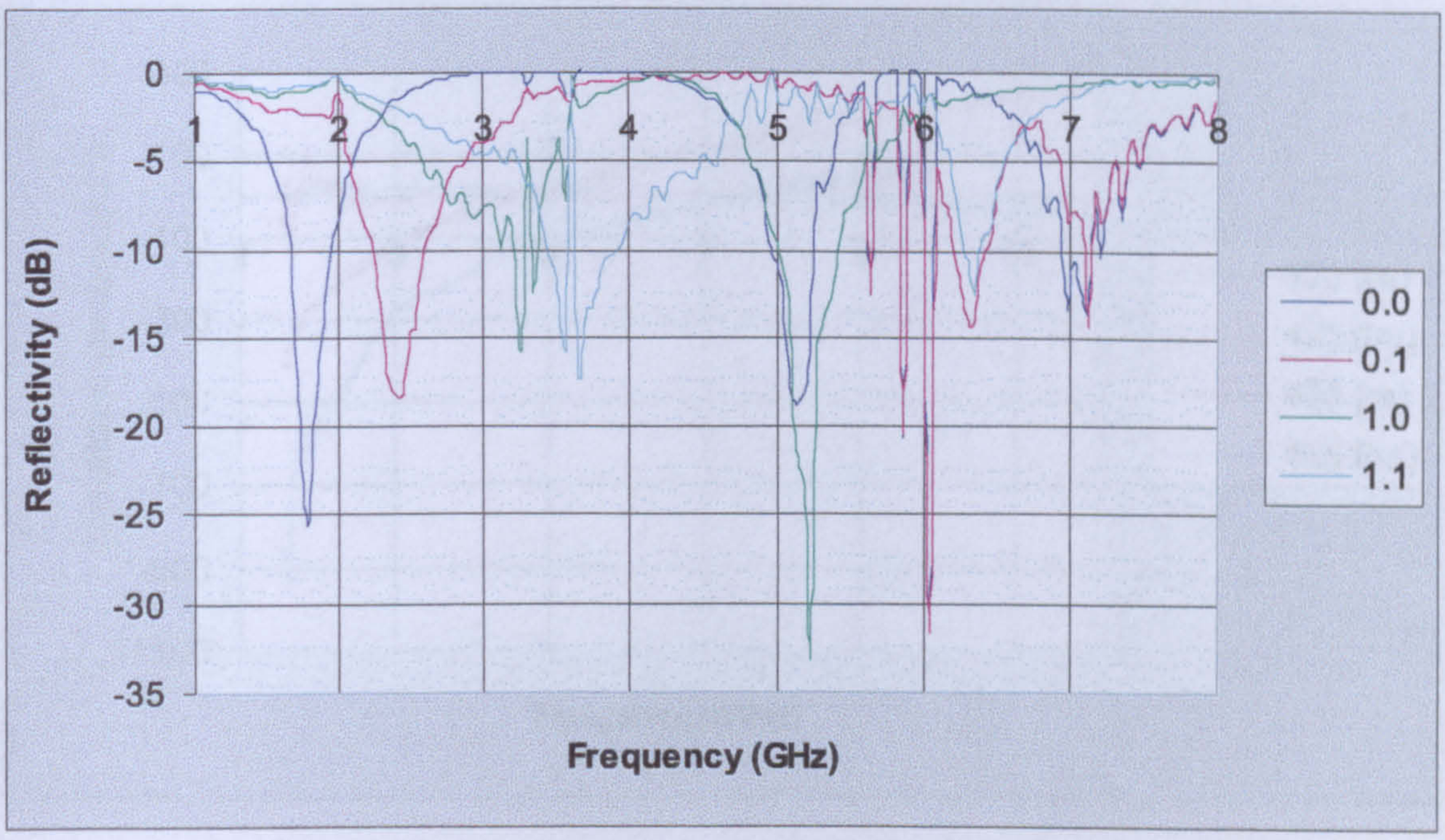

Figure 7.25: Predicted dynamic frequency profile of DI-2/1 absorber.

nar structures. In practice, however, the AFSSs are of finite thickness due to the finite dimensions of the PIN diodes. This, thus, introduces within the absorber two hybrid layers composed of mainly air and diode material. In view of the discrepancy, the dynamic frequency response of the absorber was re-simulated. This time, however, two additional air-gap layers of thickness 2.19mm were included in the simulation. The schematic diagram of the absorber incorporating the two additional air-gap layers is shown in figure 7.29. Figure 7.31 shows the new predicted dynamic frequency response of the absorber. Figures 7.32 through 7.35 show the measured and predicted frequency responses for each state. The figures show that the inclusion of air gap layers have brought closer the predicted and measured dynamic frequency responses of the absorber. Although the model predicts the occurrences of resonances at higher frequencies, their positions in frequency differ from the measured ones, with the latter occurring at lower frequencies. This is the consequence of phase error measurements when determining the frequency response of the AFSS together with error introduce by the finite thickness of the

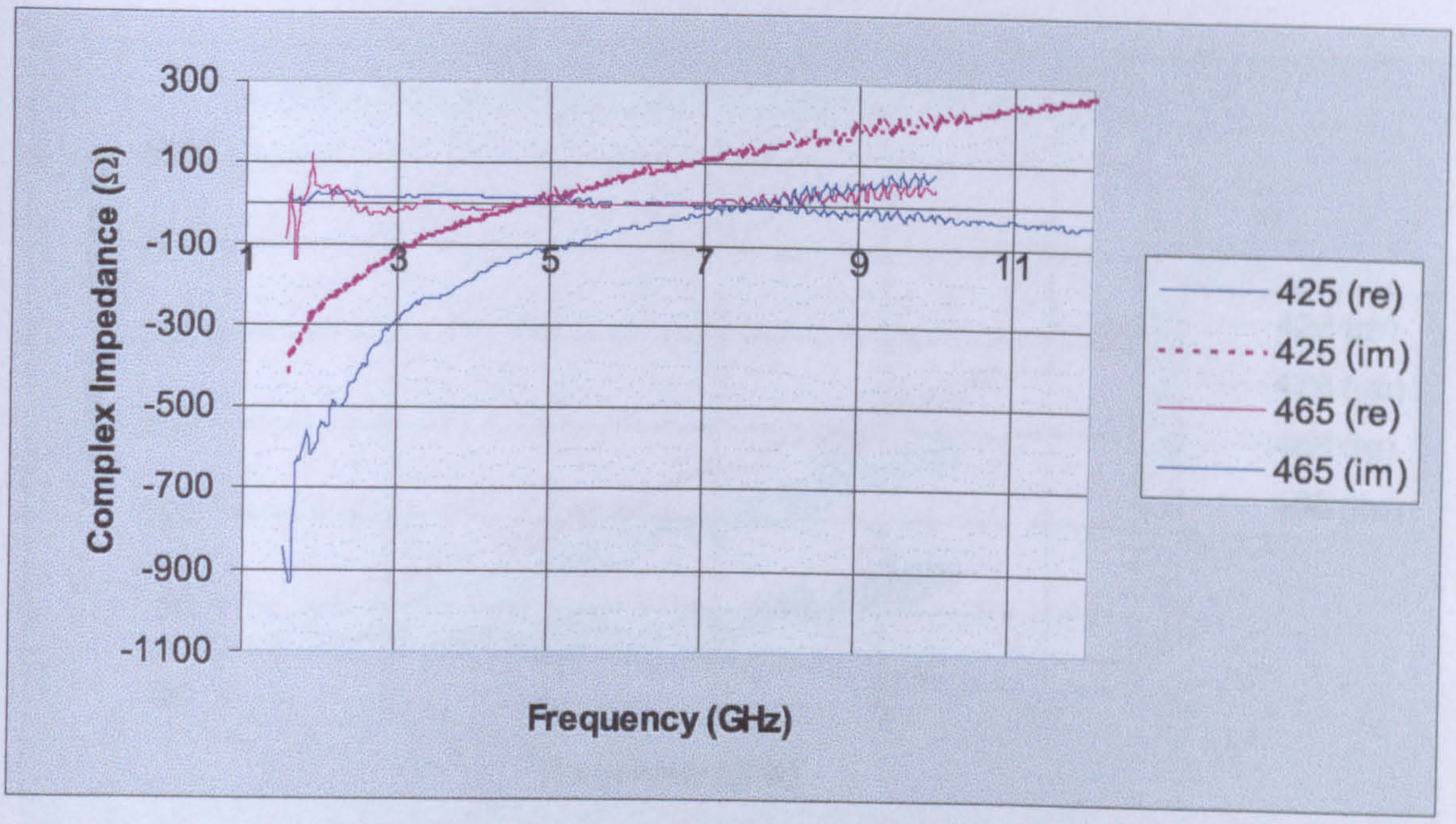

Figure 7.26: Dynamic de-embedded complex impedance responses of two AFSSs. These responses correspond to a No-Bias Condition. 425 represents data for A1 (DI-1) board while 465 is that of A2 (DI-2).

absorber sample.

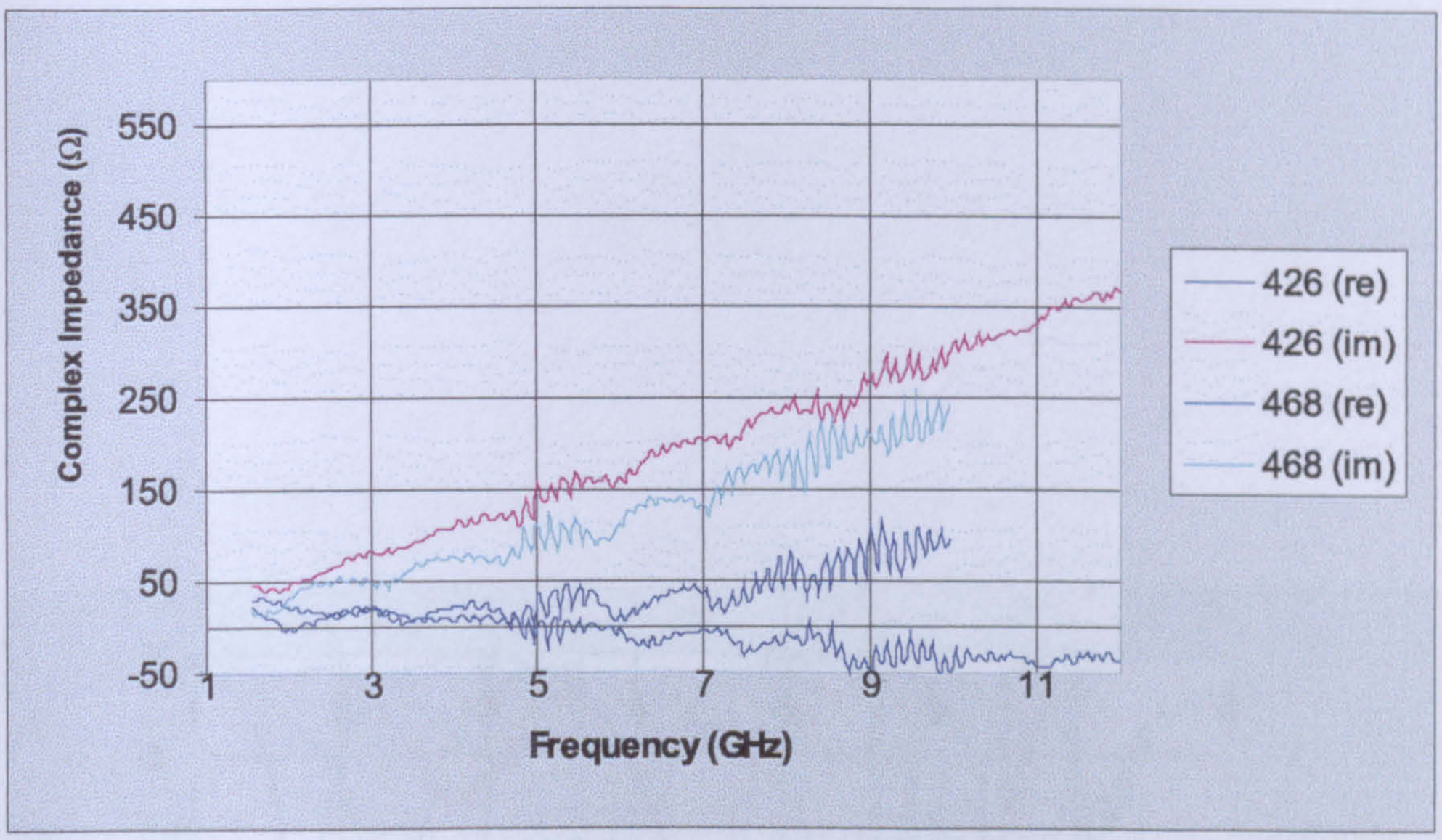

Figure 7.27: Dynamic de-embedded complex impedance responses of two AFSSs. These responses correspond to a Bias Condition. 426 represents Data for A1 (DI-1) board while 468 is that of A2 (DI-2).

Layer	Thickness (mm)	Permittivity
1	3.10	25.0
2	0.611	2.20
3	1.4	25.0
4	0.611	2.20
5	2.50	25.0
Total Thickness	8.222	-

Table 7.17: Physical parameters of DI-2/2 absorber. Layers 2 and 4 are the AFSSs dielectric backing.

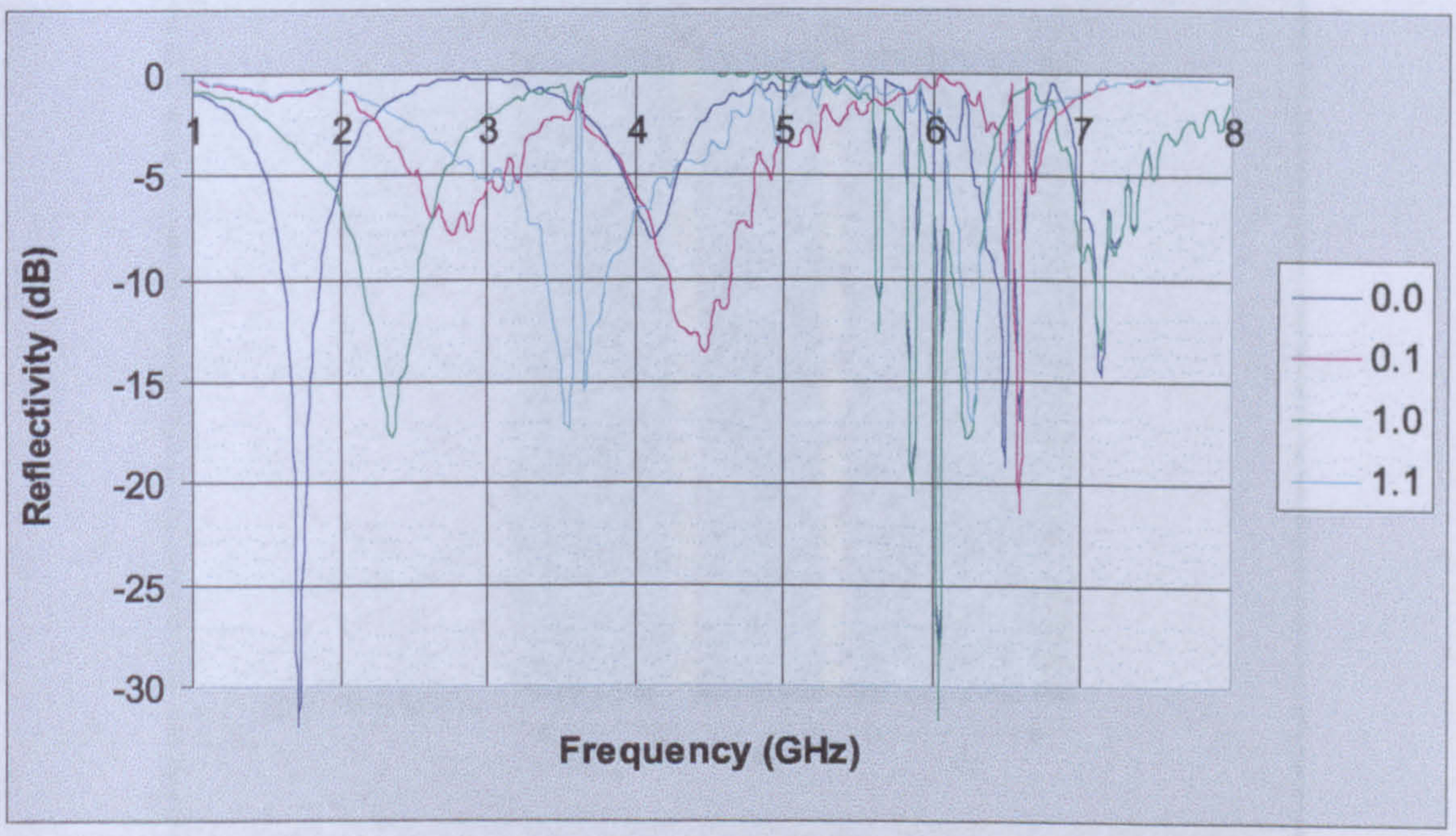

Figure 7.28: Predicted dynamic frequency profile of DI-2/2 absorber.

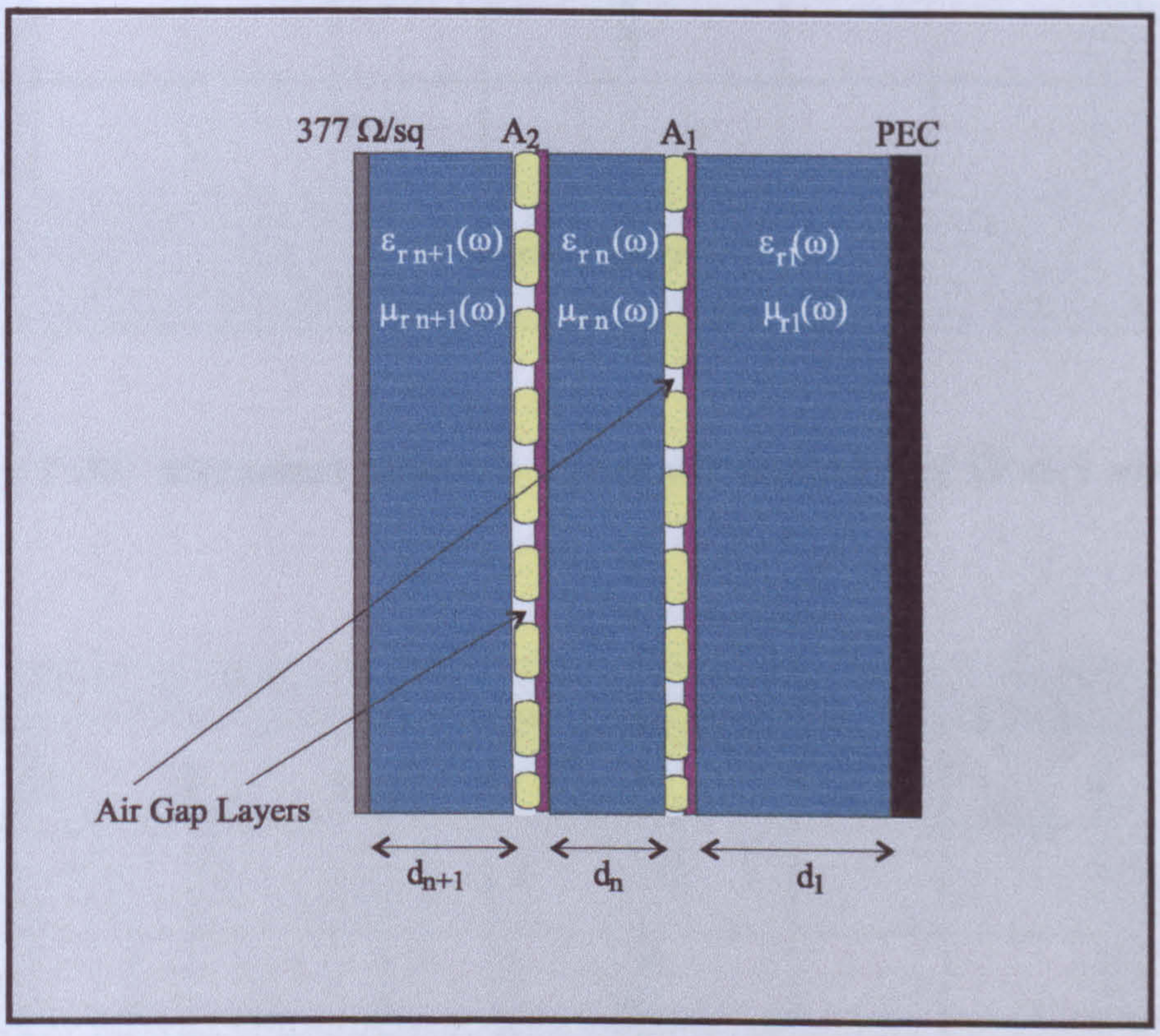

Figure 7.29: Schematic diagram of an active absorber showing air-gap layers.

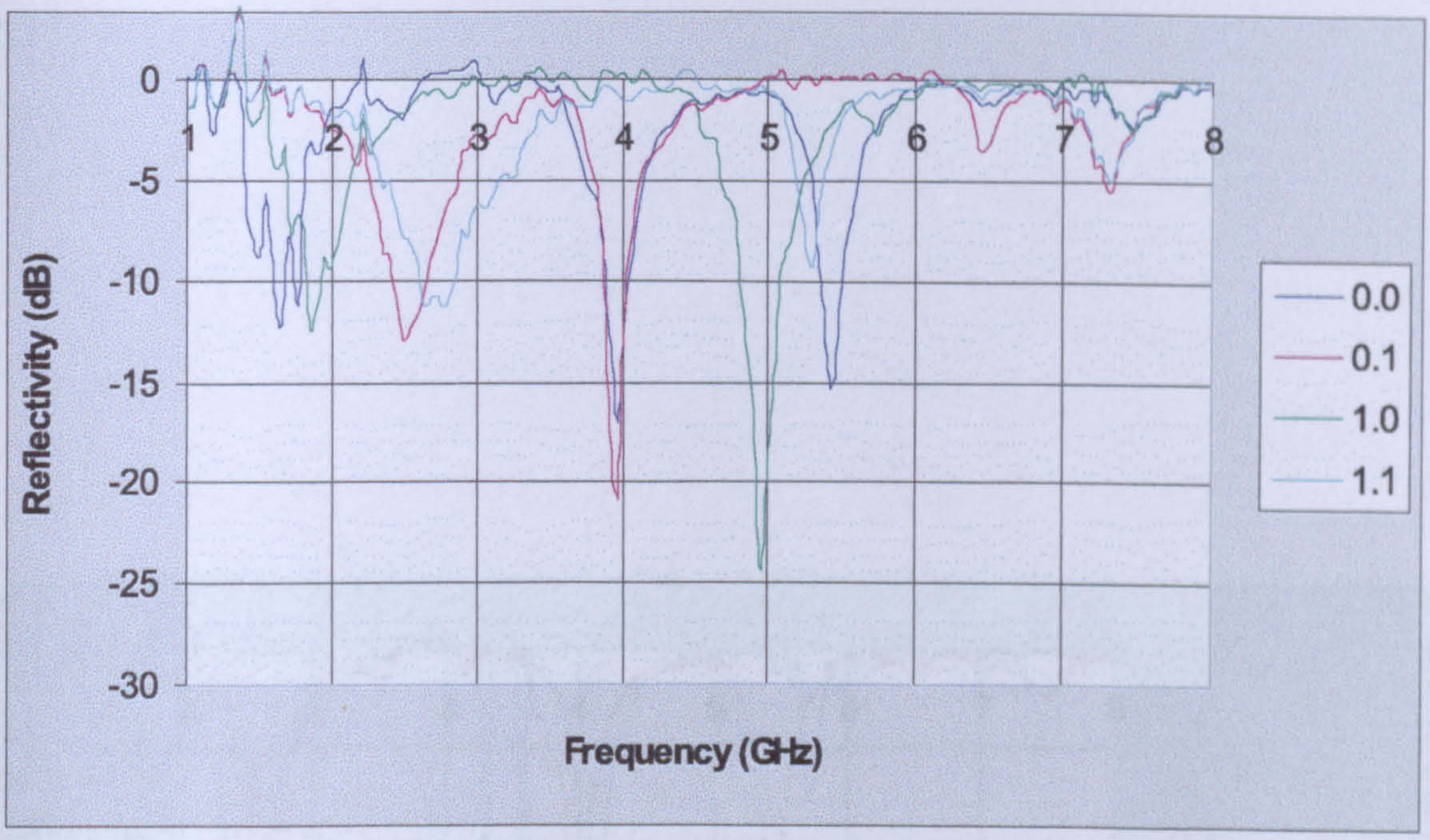

Figure 7.30: Measured dynamic frequency response of DI-2/1 absorber.

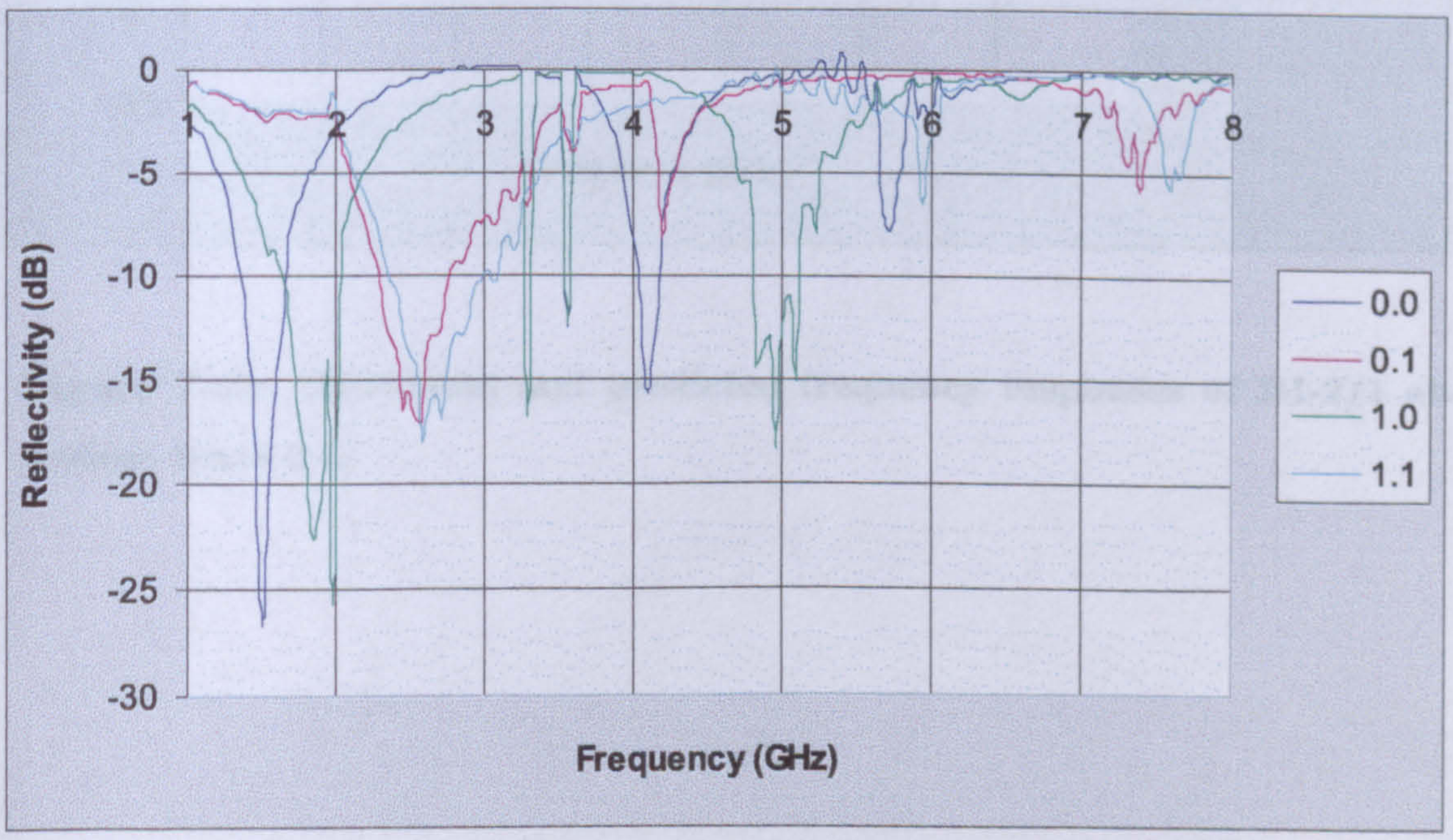

Figure 7.31: Calculated frequency response of DI-2/1 absorber. The prediction takes into account 2.19 mm air-gap layers.

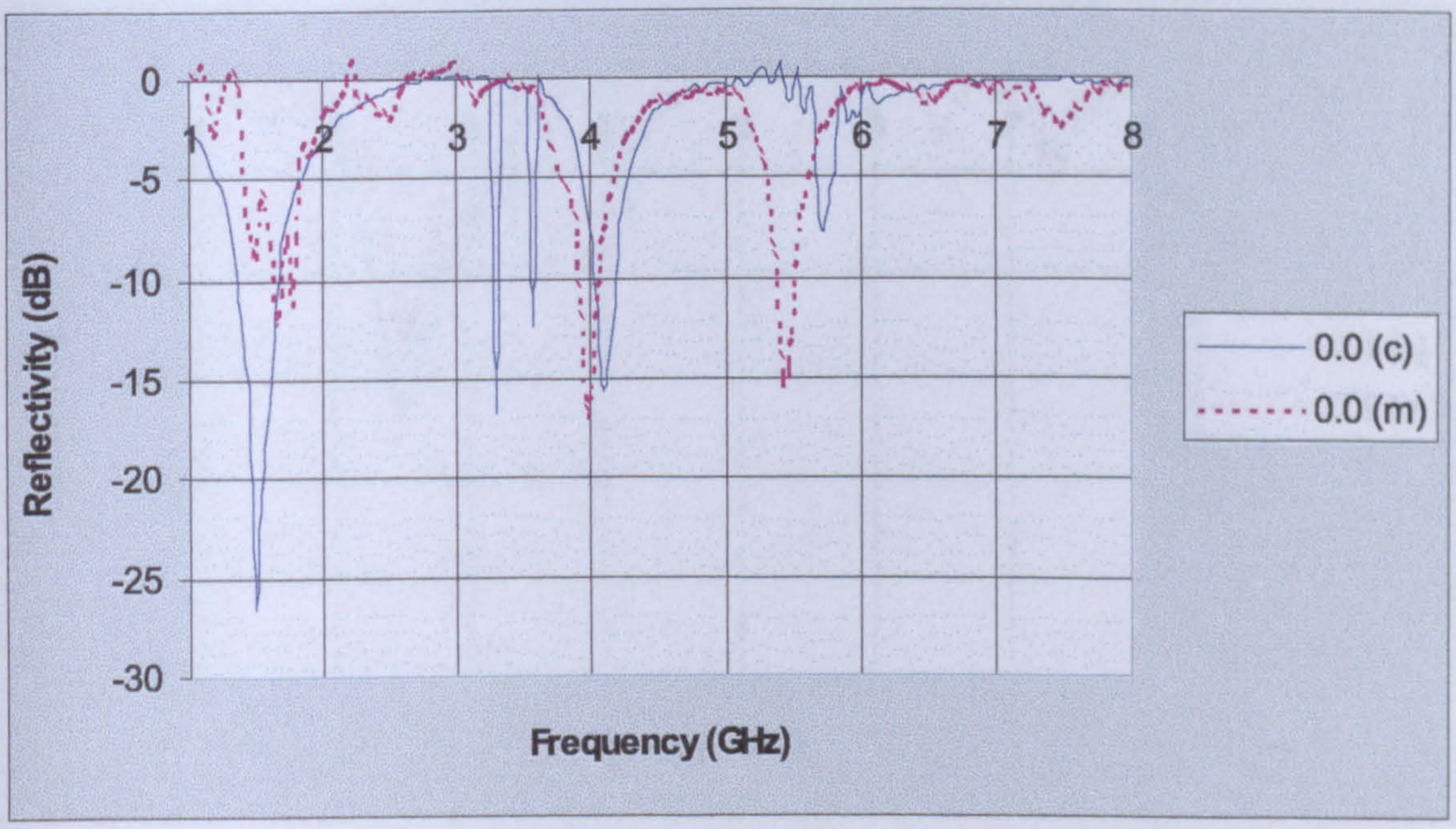

Figure 7.32: Calculated and predicted frequency responses of DI-2/1 absorber: State 0.0.

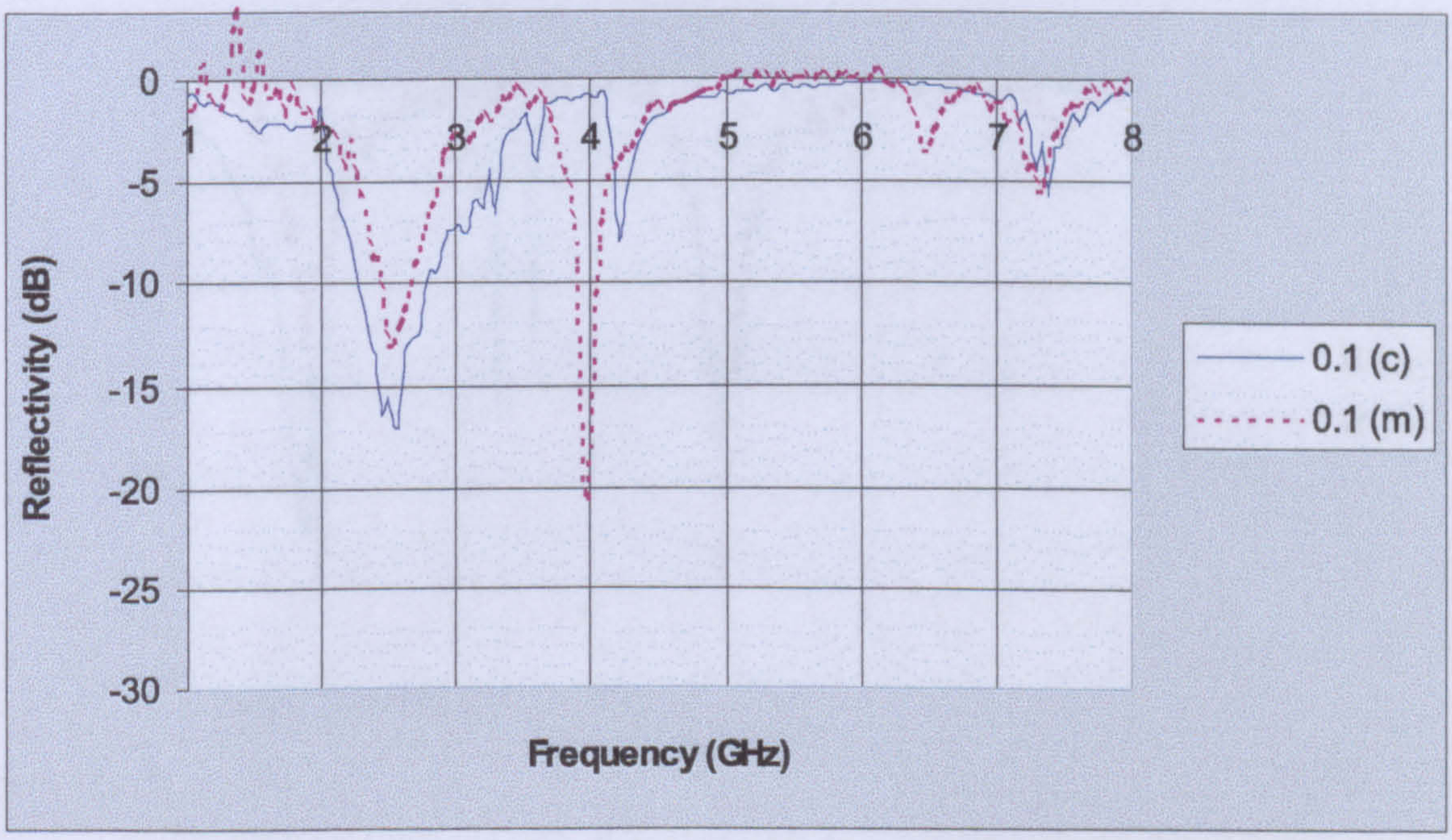

Figure 7.33: Calculated and predicted frequency responses of DI-2/1 absorber: State 0.1.

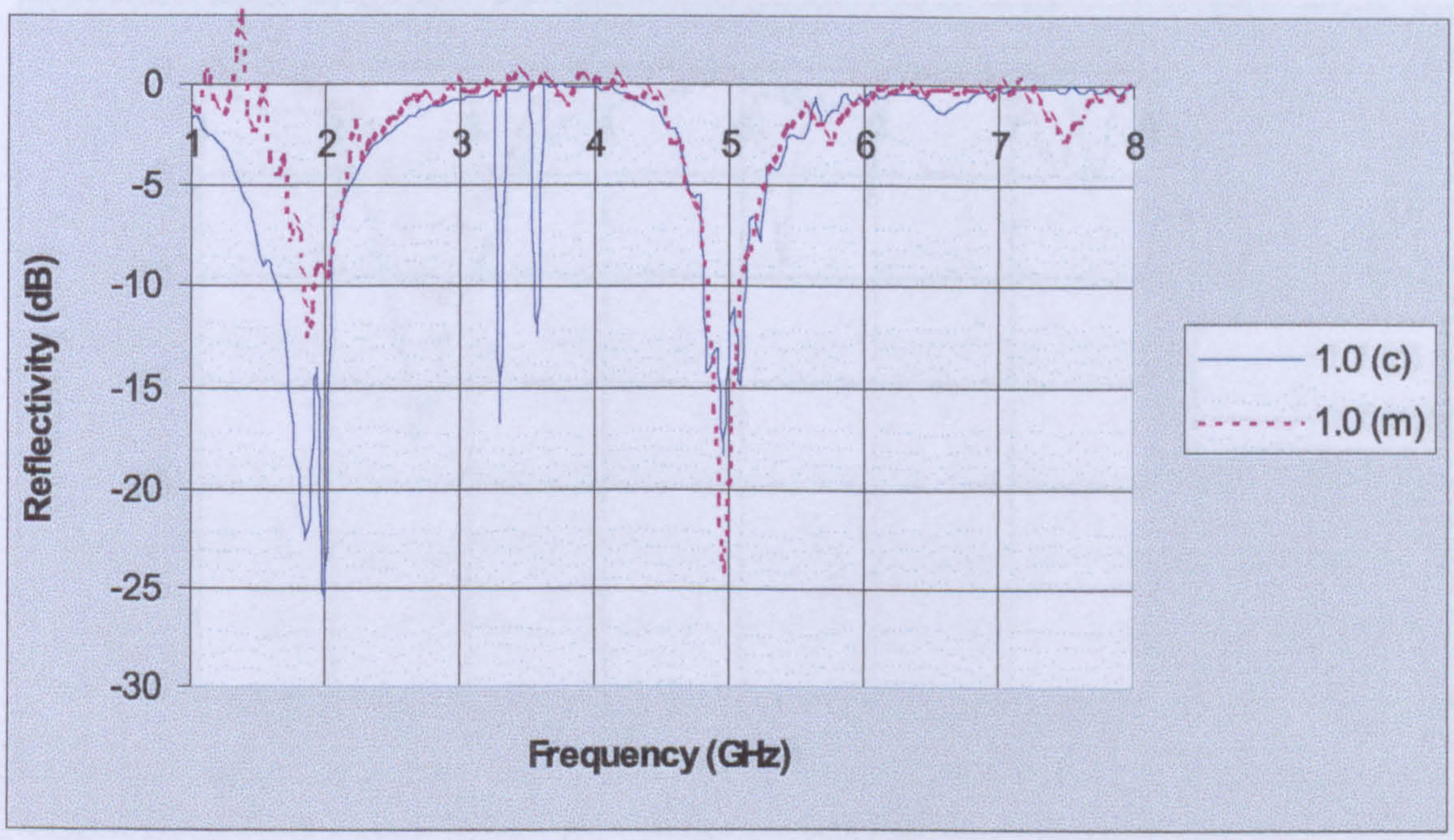

Figure 7.34: Calculated and predicted frequency responses of DI-2/1 absorber: State 1.0

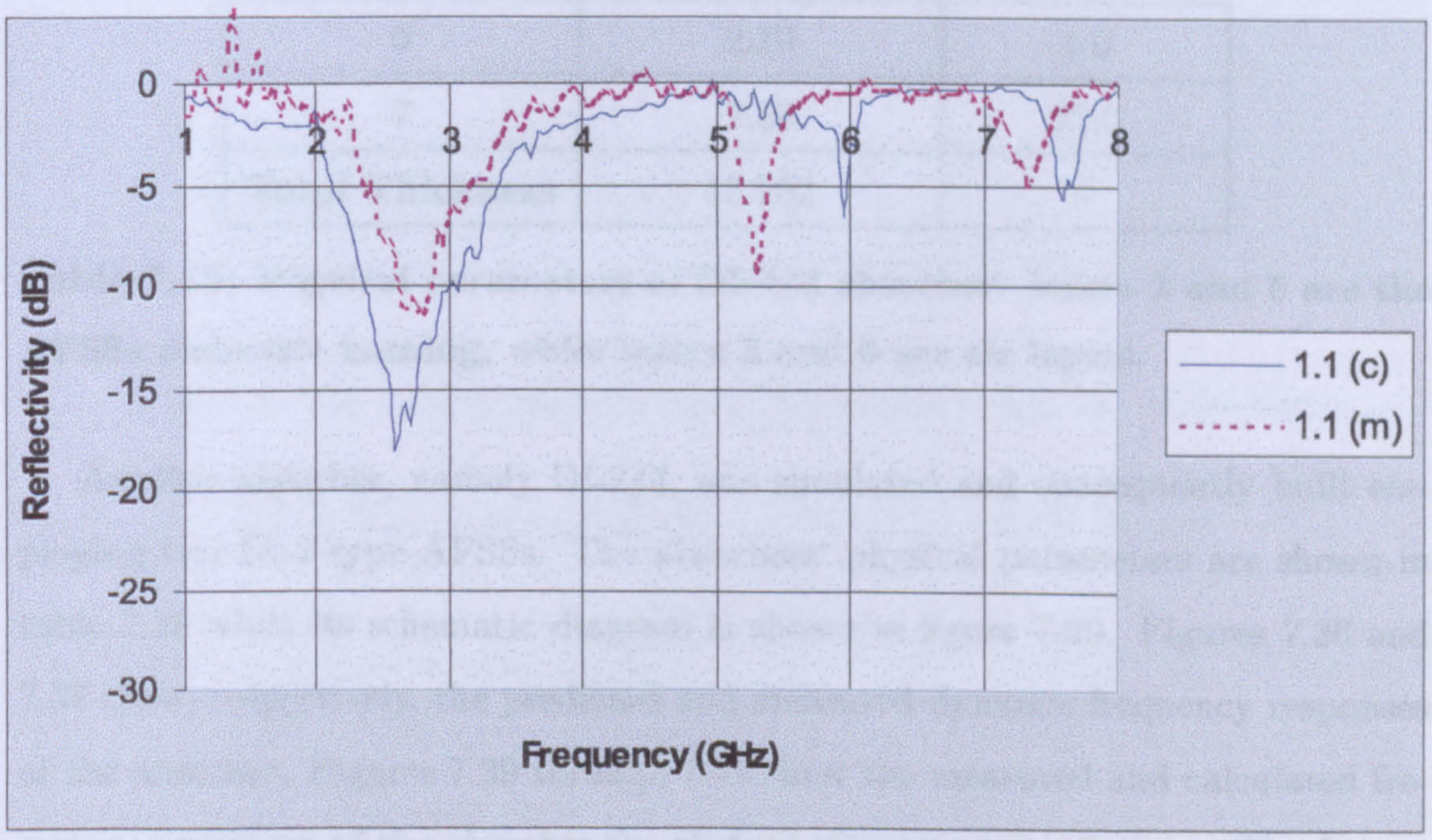

Figure 7.35: Calculated and predicted frequency responses of DI-2/1 absorber: State 1.1.

Layer	Thickness (mm)	Permittivity
1	3.10	25.0
2	0.611	2.20
3	2.19	1.0
4	3.9	25.0
5	0.611	2.20
6	2.19	1.0
7	2.50	25.0
Total Thickness	15.102	-

Table 7.18: Physical parameters of DI-2/3 absorber. layers 2 and 5 are the AFSSs dielectric backing, while layers 3 and 6 are air layers.

Another absorber, namely DI-2/3, was simulated and consequently built employing two DI-2 type AFSSs. The absorbers' physical parameters are shown in table 7.18 while its schematic diagram is shown in figure 7.29. Figures 7.36 and 7.37 show, respectively, the predicted and measured dynamic frequency responses of the absorber. Figures 7.39 through 7.42 show the measured and calculated frequency responses of the absorber for all four states or sub-solutions. The figures show a very close agreement between predicted and measured data. At higher frequencies, however, the model fails to predict the position of small resonances. This, however, should not be taken to be of extreme importance since at that frequency band the versatility of the absorber is non-existence. What is important is the absorber's dynamic frequency response that extends from 1.5 GHz to 6 GHz. Within this 2 octave frequency band, the absorber exhibits in its dynamic frequency response a number of switchable discretely placed reflection nulls.

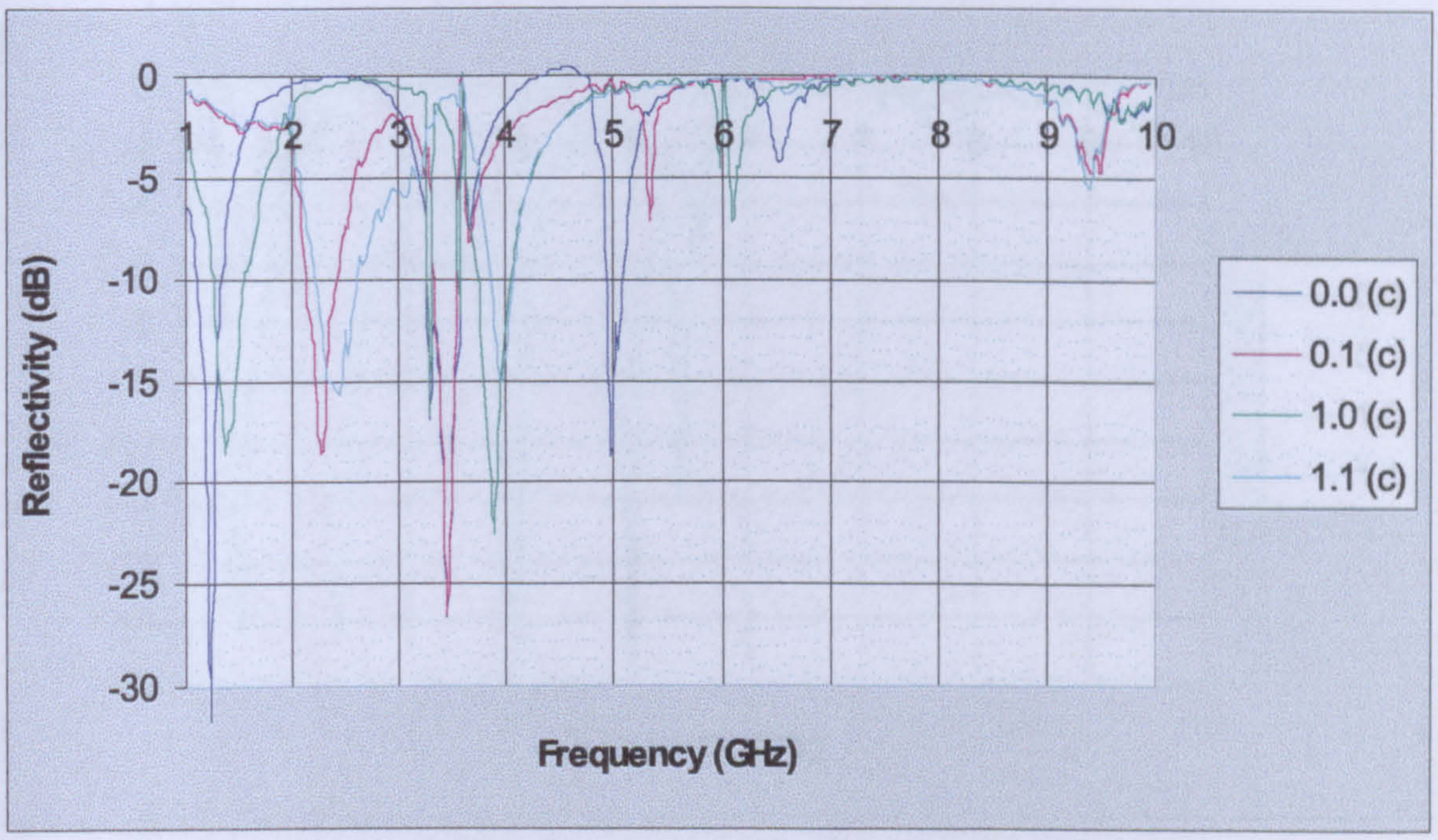

Figure 7.36: Calculated dynamic frequency response of DI-2/3.

Reflection Null Translation Between ON/OFF AFSS States

The results presented so far has shown that the inclusion of two AFSSs with bi-state electrical characteristics, namely open/short circuit response, within a Salisbury screen absorber substantially extend its absorption bandwidth by generating a number of switchable reflection nulls spread over a multi-octave frequency band. In chapter 5 it has been shown that through the application of a linear bias voltage the frequency characteristics of such AFSS can be linearly transposed from its open to its short circuit electrical characteristics. In view of this, an attempt was made to linearly and continuously translate in frequency a reflection null between any given states, namely 0.0, 0.1, 1.0, 1.1, through the application of a linear and continuous bias voltage across the AFSSs. However, it was found that in place of reflection null frequency translation, the null depth decreases with bias voltage variations up to a point where it disappears and then re-appears again at a different frequency location. In an effort to enforce frequency translation of a

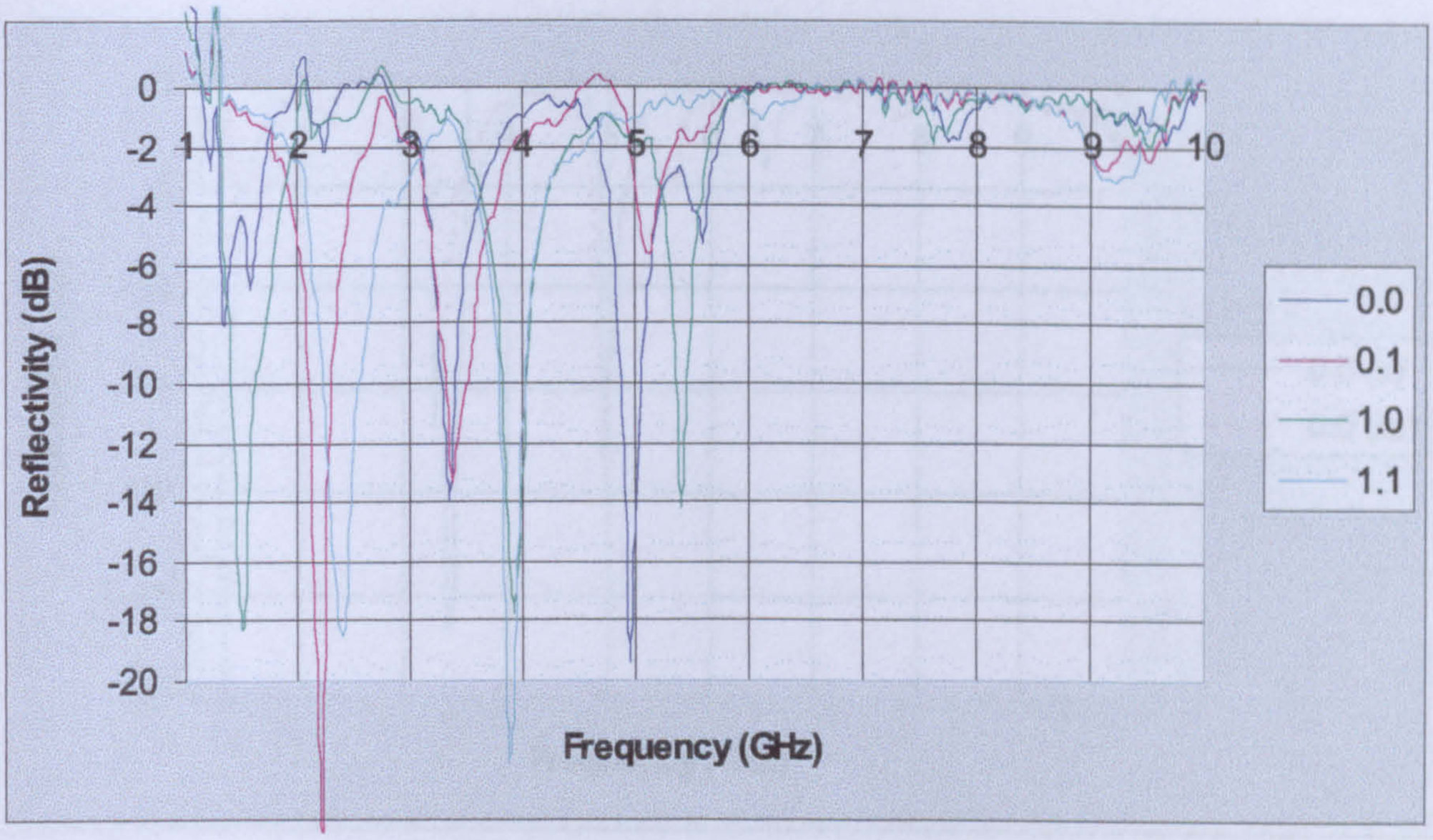

Figure 7.37: Measured dynamic frequency response of DI-2/3 absorber.

reflection null, the lossy part of the AFSSs adaptive complex impedance response was removed. It was found that without the lossy part, reflection null frequency translation is indeed an adaptive frequency characteristic of a Salisbury screen absorber embedded with two lossless AFSSs having bi-state electrical properties. However, as shown in chapter 5, loss is a fundamental low frequency property of AFSSs comprising an arrays of PIN-loaded dipoles. Therefore, its lossy part cannot be simply removed.

7.2.3 Analysis of Results

The results presented in this chapter provide strong evidence that a wideband absorption solution can, indeed, be implemented into the frequency properties of a small thickness Salisbury screen absorber without the need to exclusively rely upon material properties. As shown throughout the chapter, the latter is achieved through embedding within such an absorber a number of active frequency selec-

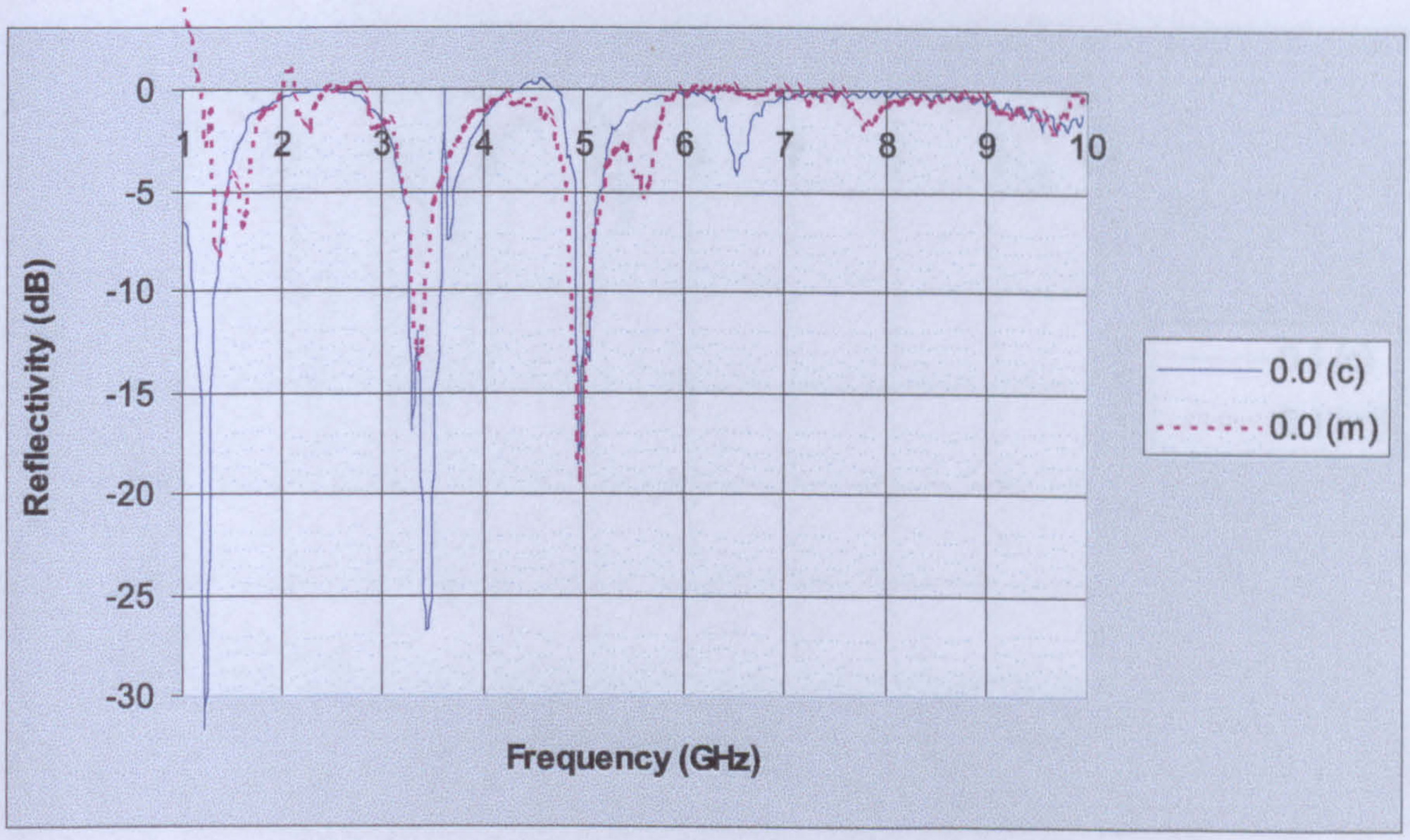

Figure 7.38: Calculated and predicted frequency responses of DI-2/3 absorber: State 0.0.

tive surfaces with bi-state electrical properties, namely open/short circuit response. The incorporation of this type of AFSSs permits the partitioning of the absorber thickness, which, in turn, results in the generation of a series of switchable reflection nulls spread over a wide frequency band. This design methodology, which represents a substantial improvement upon the absorption properties of a conventional Salisbury absorber, thus, circumvents the use of material properties to achieve a broadband absorption solution.

In order to implement an absorption solution over the entire frequency band, narrow band tunability of adjacent but widely placed reflection nulls must be shown in the frequency properties of the proposed absorber. Although some reflection null tuning properties were shown at high frequencies, at low frequencies this was not the case. The reason of why the latter could not be implemented into the absorber's frequency characteristics is down to the lossy component present in the

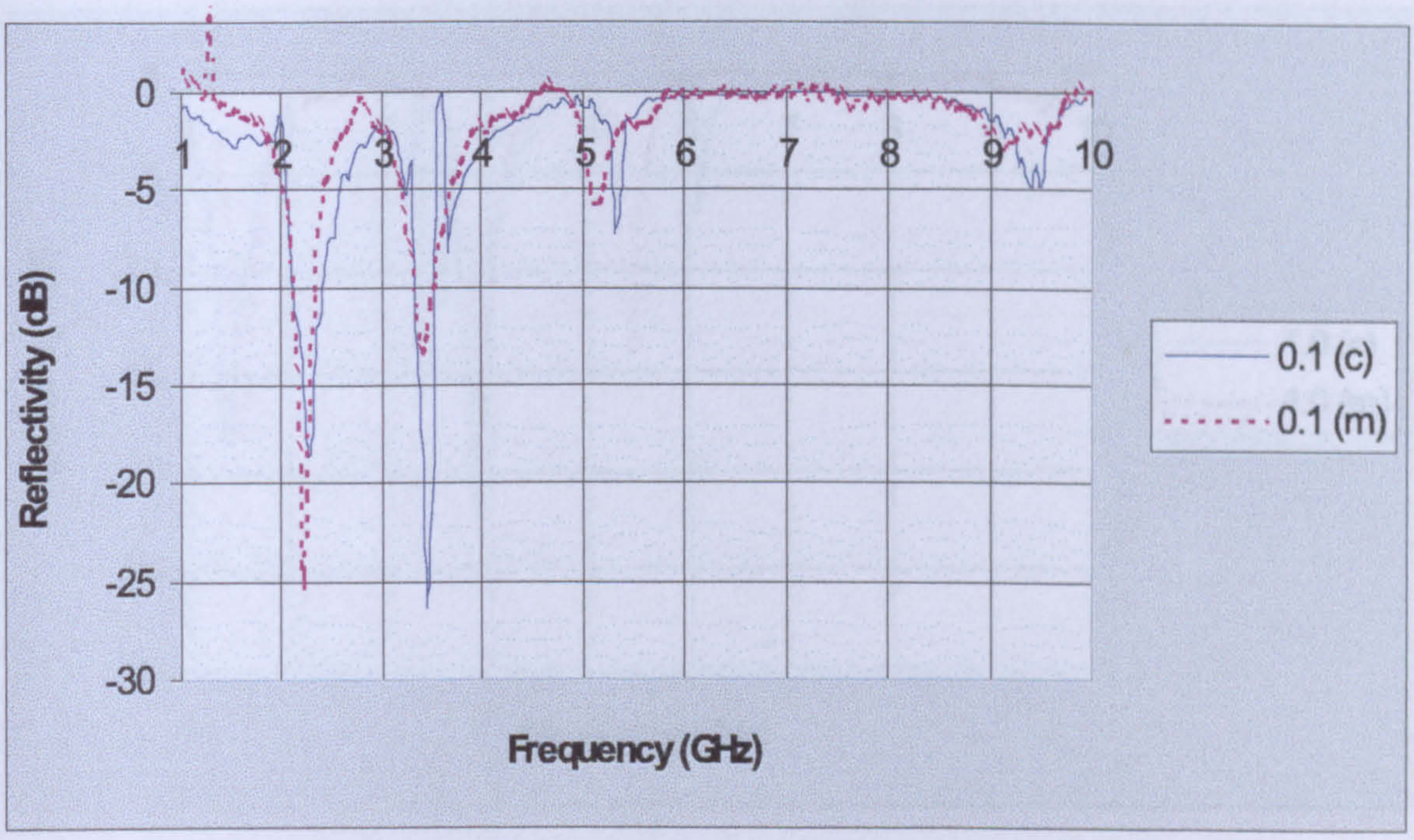

Figure 7.39: Calculated and predicted frequency responses of DI-2/3 absorber: State 0.1.

frequency properties of the PIN-loaded AFSSs, as shown in chapter 5. As the biasing voltage is increased from 0 V upwards, there is a lossy component present in the AFSSs frequency characteristics. This loss, which is due to the the diodes series resistance, is inversely proportional to three components, namely R_d (the AFSS's loss component), C_{fss}^2 (the AFSS's static capacitance) and f^2 (frequency), when the structure is operated in its open circuit mode. On the other hand, the loss is directly proportional to R_d when operated in its short circuit mode. In order to tune a reflection null over frequency the AFSSs adaptive electrical characteristics as a function of frequency must be purely reactive with no loss present, as shown by the analysis in chapter 4, specifically Margarita's equation.

Results presented in this thesis have also shown that the inclusion of AFSSs within a Salisbury screen absorber allows energy absorption at a lower frequency. That is to say, an absorber of thickness $d_T = \lambda_o/4\sqrt{\epsilon_r}$ is now capable of absorbing energy

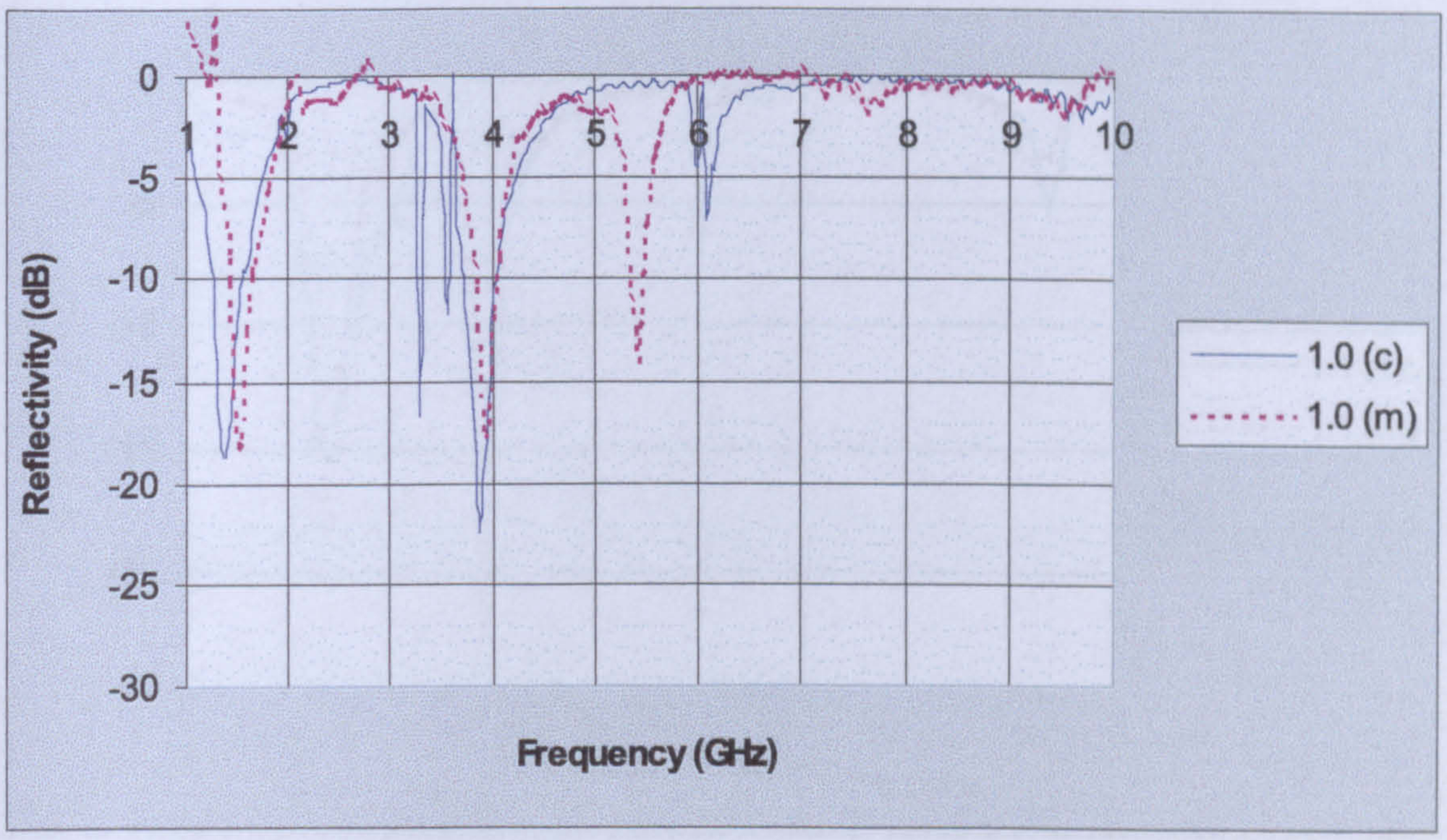

Figure 7.40: Calculated and predicted frequency responses of DI-2/3 absorber: State 1.0.

at λ_1, where $\lambda_1 > \lambda_o$. This observation is a clear indication that the presence of AFSSs does, indeed, effectively increases the the permittivity of the absorber spacer as, theoretically, shown by equation (4.37). The fact that energy absorption occurs at a lower frequency indicates that the reactive properties of the AFSSs is capacitive (negative reactance), which, is, indeed, the case.

The fact that PIN diodes are used on AFSSs permits fast control of its adaptive bi-state electrical properties. This, in turn, also allows fast control of the dynamic frequency properties of a Salisbury screen embedded with such structures.

And finally, the design methodology presented in this thesis to implement a broadband absorption solution is a step forward to circumventing the stringent limitations imposed on a wideband absorption solution by the constitutive parameters of materials. The design methodology introduced thus, indeed, narrows the trade-off

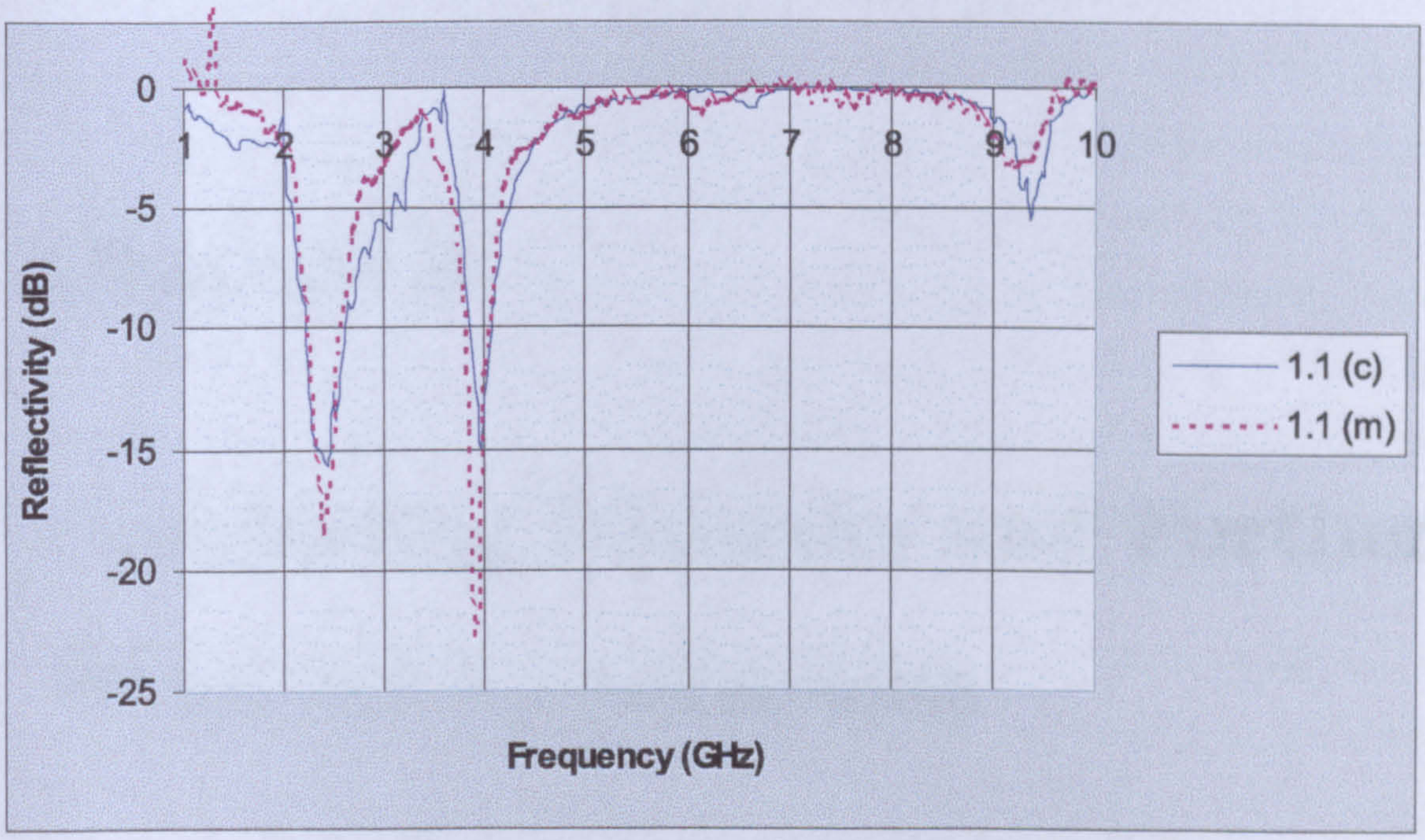

Figure 7.41: Calculated and predicted frequency responses of DI-2/3 absorber: State 1.1.

gap between absorption bandwidth and absorber thickness, the two conflicting but equally important parameters in broadband absorber design.

Chapter 8

Concluding Remarks and Further Work for Investigation

This chapter presents the conclusions of the research programme and recommendations for future work.

8.1 Conclusions

The work documented in this thesis has shown how the use of AFSSs composed of arrays of PIN-loaded dipoles significantly reduces the trade-off gap between the conflicting, though equally important, goals of absorber design, viz small thickness and wide absorption bandwidth. A conventional Salisbury absorber has an inherently narrow absorption bandwidth, which is mainly due to the limitations imposed by the non-dispersive characteristics of dielectric materials. For a wide-band absorption the dielectric materials used as spacers must be dispersive in a $1/\omega$ fashion.

In order to couteract fundamental material properties a new absorber design is proposed. A wide bandwidth absorption solution, while maintaining an absorber

with a small thickness, can be implemented through the partitioning of an absorber's spacer. This generates in the absorber frequency response a number of discretely placed reflection nulls spread over a wide frequency band. This design methodology is implemented through embedding a number AFSSs within small thickness Salisbury screen absorbers built with spacers of high permittivities. The AFSSs employed are composed of arrays of PIN-loaded dipoles and have bi-state electrical properties in the form of open and short circuit. Through switching between these two responses an absorber's thickness can be partitioned in quasi-real time, generating a number of reflection nulls spread over a wide frequency band.

In order to implement a bi-state electrical open and short circuit behaviour,the AFSSs used were composed of arrays of PIN-loaded dipoles. The short circuit response, activated when a full bias voltage is dropped across the AFSSs, is of an inductive nature and has a small reflection loss, thus closely mimicking a metallic surface. Under a no-bias voltage mode, the AFSS behaves as an array of dipoles and, as such, its frequency characteristic is that of a resonant structure. At low enough frequencies the AFSS's frequency response is opaque (high impedance), thus behaving as an open circuit. It then follows that by a matter of applying an OFF-ON voltage, the AFSS's dynamic response can be switched between its two main electrical characteristics. This, in turn, makes possible the ON/OFF switching of reflection nulls.

The effect of applying a linear and continuous forward voltage between the diodes' extreme bias conditions was also studied. The rationale behind this investigation was to introduce into the absorber frequency characteristics reflection null tuning properties between any two adjacent but widely apart reflection nulls so as to cover the entire frequency band. Although the tuning of a reflection null was shown at high frequencies, at low frequencies this was not the case. Why? At high frequencies the AFSS's dynamic complex impedance response is mainly reactive, having very little loss. Consequently, null tuning is possible through incurring small, linear and continuous changes into the phase of the electric field. On the other hand,

the AFSS's dynamic complex impedance response at low frequencies shows in its electrical characteristics as a function of frequency both loss and a reactive part. The lossy part being inversely proportional to three components, namely R_d (the AFSS's loss component), C_{fss}^2 (the AFSSs static capacitance), and f^2 (frequency), when the structure is operated in its open-circuit mode and directly proportional to R_d, when operated in its inductive or short-circuit mode. The loss, which is introduced by the diodes series resistance, increases with increasing bias voltage. However, as soon as the structure becomes inductive, the loss starts to decrease with increasing bias voltage. The loss, thus, dominates the adaptive properties of the absorber at low frequencies and, consequently, instead of reflection null tuning over frequency, null depth variation is achieved by ways of incurring changes into the amplitude of the electric field. In order to tune an absorber's reflection null, the dynamic electrical response of the structure must be highly reactive with no loss present. The latter is shown by Margarita's equation. This equation, theoretically, demonstrates how an adaptive complex impedance structure, with no loss, embedded within a Salisbury screen absorber can be used to tune a reflection null over a frequency range. The latter is possible through effectively varying the dielectric properties of the absorber by a factor of $4X^2$ (X being the reactance, which can be inductive or capacitive), as shown by equation (4.37). This equation clearly demonstrates that the constitutive parameters of materials can, indeed, be effectively altered through employing structures with purely reactive properties. The presence of a purely inductive reactance structure within the absorber effectively decreases the absorber thickness, while that of a purely capacitive structure effectively increases the absorber thickness. In other words, the use of a purely variable inductive structure will tune a reflection null up in frequency, while a purely variable capacitive structure will tune a reflection null down in frequency.

Due to the unknown and complex nature of the problem, a simple linear GA was employed to find the nature of the problem's solution. The level of difficulty in finding the absorber's global solution was not only determined by the AFSS's non-linear dynamic complex impedance properties, but also by the number of

structures embedded within the Salisbury screen absorber.

8.2 Further Research

There are a number of studies which can be undertaken in order to enhance the work documented in this thesis. First, it is recommended that further work should be carried out in order to increment the depth of the reflection nulls. Secondly, a numerical characterization of semiconductor-loaded AFSSs would be advantageous. For this to be possible the frequency properties of PIN diodes, or any semiconductor used, must, however, be well known over a wide frequency range. In this case of this research programme, between 1 to 10 GHz. Thirdly, it is advisable to investigate into the use of semiconductor-loaded AFSS composed of different geometries, such as the one shown in in figure 4.25 (vide chapter 5). Fourthly, studies into the use of different semiconductor devices, such as FETs or diodes will less loss, would be interesting to pursue. This will facilitate tuning of reflection nulls at low frequencies. Fifthly, optimization of the AFSSs' physical parameters would be advantageous in order to get the required dynamic response. And finally, a study into the use of magnetic materials as spacers will substantially enhance the work reported in this thesis. That is to say, embedding semiconductor-loaded AFSSs within magnetic absorbers. Absorbers constructed from magnetic materials are thinner than those constructed with dielectric materials.

Although the aforementioned further-work recommendations will greatly enhance the work reported in this thesis, there is one which I feel is of great importance. As reported in chapter 6, the absorber's global solution was found through a simple GA by means of a linear optimization procedure. Although the absorber problem is a two-dimensional one, the optimization performed was of a linear nature, in that a single goal was sought. The objective goal was achieved through limiting one of the problem goals, viz the maximum absorber thickness allowed. Through this course of action, the optimizer was somehow dampened to find the optimum array

solution in terms of the absorbers' two contradicting goals. Because of the fact that absorber design is a multi-goal problem, a multi-objective optimization must be performed. Once this is done, a truly and coherent comparison of absorbers properties can then be made between conventional absorbers and the dynamic ones. It is, therefore, of great importance, to implement a Pareto GA to determine the physical limitations of the proposed absorber.

8.2.1 Pareto Optimal

The members of the population of conventional GAs converge to a single design solution. A single point in space or solution, however, does not convey enough information to define the fundamental boundary between the feasible and physically unrealisable regions of a multi-goal system or problem. In the case of a dual goal problem, a linear criteria or boundary is needed to set the two regions apart.

Absorber design is a dual-goal problem in that small thickness and wide absorption bandwidth are equally important. As a dual-goal problem, an absorber's solution exists in a surface domain. In other words, there is not a single optimal solution, but an array of optimal solutions. In a 2-D objective optimization, the aim is to converge the optimal-solution array towards a boundary which serves as a defining line between the problems' feasible solutions and the physically impossible solutions. The dual-goal characteristic of absorbers can, therefore, be exploited to find the physically realisable boundary of any absorber design.

A Pareto GA (PGA) is an optimization procedure which has been successfully used to solve dual-goal problems. In the area of electromagnetics, PGAs have been used to find a set of optimal designs of microwave abosorbers [1]. In the antenna area, PGAs have been employed to design thinned antenna arrays with low beamwidth and sidelobe levels [2].

Unlike conventional GAs, a pareto GA forces the population to converge to a number of optimal designs spread along a boundary line called the Pareto front, as displayed in figure 8.1(i). The Pareto front thus defines the boundary between the feasible and infeasible region of a bi-goal problem. The difference between a conventional GA and a Pareto GA can be appreciated in figures 8.1(ii) and 8.1(iii). Figure 8.1(ii) shows that in a single objective GA, all population members converge to a single point on the Pareto front whereas in a PGA the population members converge to the pareto front (figure 8.1(iii)).

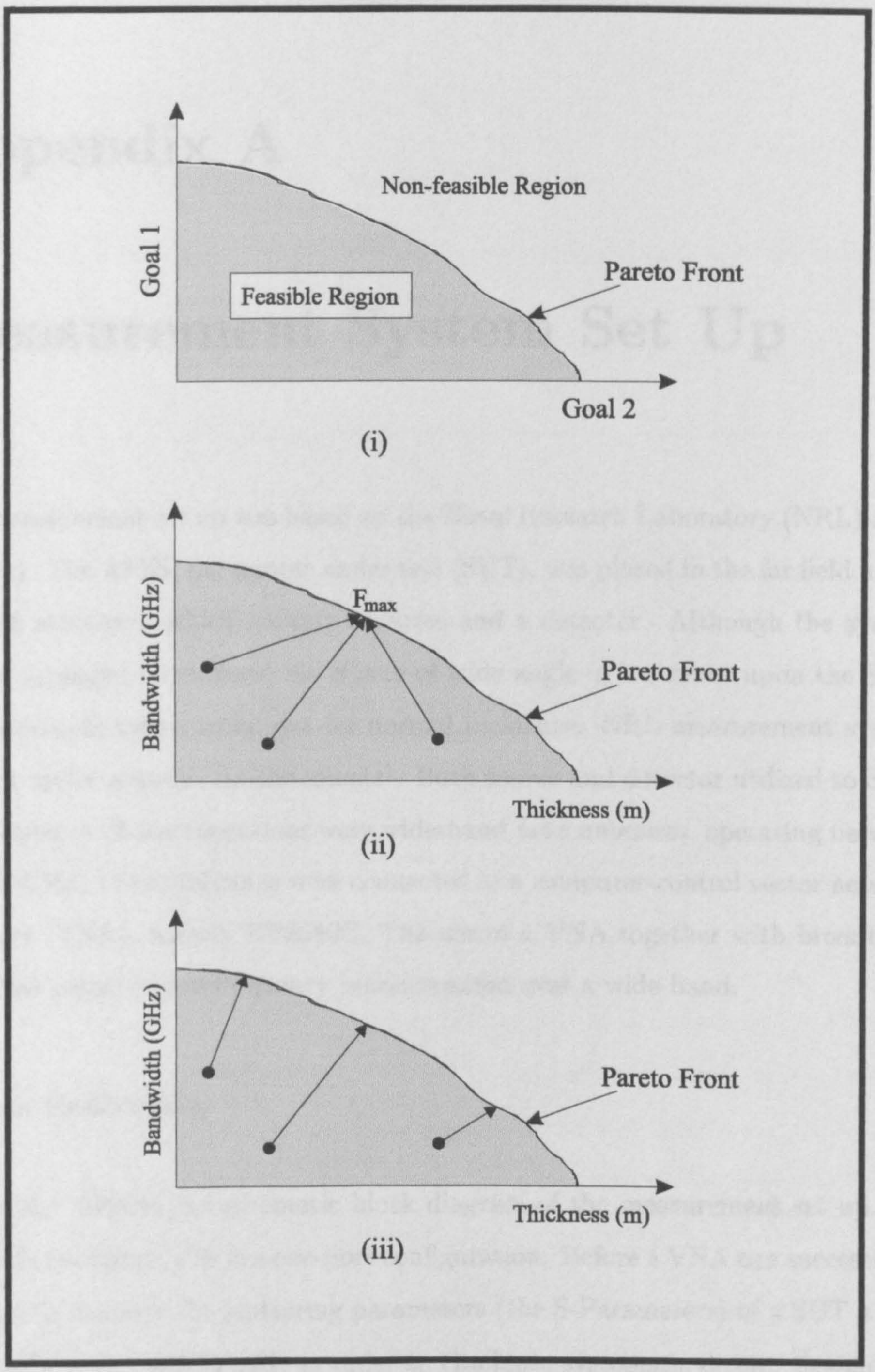

Figure 8.1: (i) A typical Pareto front. Designs in the dark region are mediocre designs, designs in the white region are physically impossible. (ii) Standard GA convergence. (iii) Pareto GA convergence.

Appendix A

Measurement System Set Up

The measurement set up was based on the Naval Research Laboratory (NRL) Arch Method. The AFSS, the sample under test (SUT), was placed in the far field under an arch structure, which mounts a source and a detector. Although the system can be arranged to measure the effects of wide angle of incidence upon the SUT, measurements were carried out for normal incidence. NRL measurement system was set up for antenna measurements[1]. Both source and detector utilized to carry out frequency characterizations were wide-band horn antennas, operating between 1 to 10 GHz. These antennas were connected to a computer-control vector network analyzer (VNA), namely HP8510C. The use of a VNA together with broadband antennae permit rapid frequency measurements over a wide band.

System Calibration

Figure A.1 depicts the schematic block diagram of the measurement set up. As shown in the figure, this is a one-port configuration. Before a VNA can successfully be used to measure the scattering parameters (the S-Parameters) of a SUT a system calibration must precede in order to eliminate systematic errors. Systematic

[1]i.e. $R \geq 2D^2/\lambda$, where R is the distance from the antenna to the sample to be measured and D is the sample diameter

errors may arise due to the following:

1. Non-infinite directivity in the antennae.

2. Imperfect matching at the insertion point.

3. Departures from perfect tracking in the transmitting and receiving antennae.

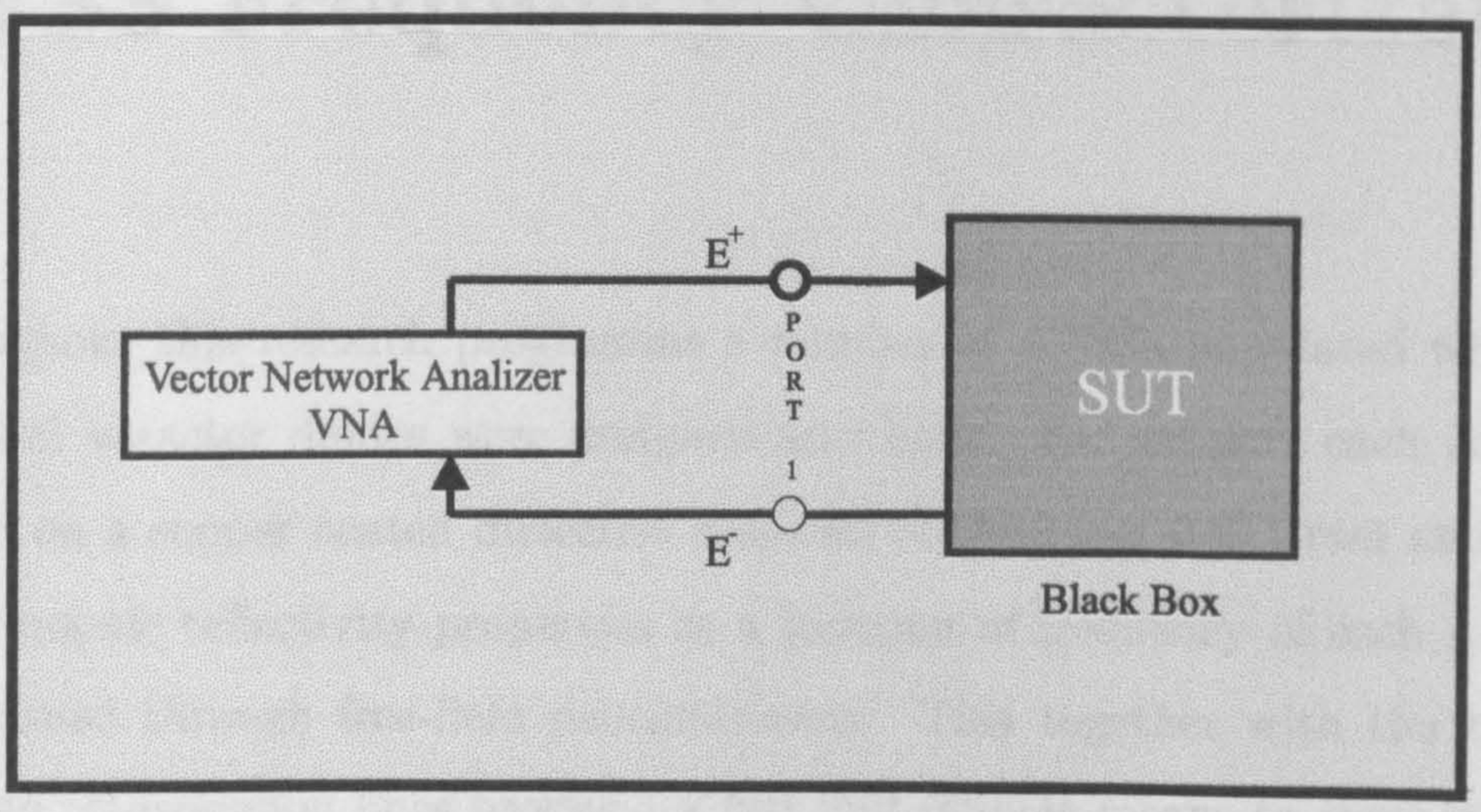

Figure A.1: One port system.

These systematic errors can be eliminated by way of a three-stage calibration procedure. In (1), the reflection coefficient is measured with a match termination. For the measurement performed, this was done using the sample platform which was built from polysterene. (2) is due to the finite size of the sample and can be theoretically eliminated through a reflection measurement with a direct open placed on the SUT terminal. In practice, however, an open circuit is not feasible. Nonetheless, the latter was achieved through a reflection measurement with $\lambda/4$ offset short. And finally (3) was eliminated through reflection measurement with a direct short placed on the SUT platform.

Appendix B

AFSS Frequency Characterization

Throughout this research programme a number of AFSSs populated with either PIN and varactor diodes were designed and built. For support each AFSS was etched on a copper coated dielectric material of thickness 0.611 mm and ϵ_r 2.20. The dynamic reflectivity properties as a function of frequency of each AFSS was determined through free-field measurements. This together with the theory of uniform transmission lines provided a fast and reliable means to characterize the dynamic complex impedance response of each AFSS. Although numerical methods, such as method of moment (MoM) or finite domain time domain (FTDT), could have been employed to characterize the reflectivity properties of the built AFSSs, this would have taken a long time. Furthermore, the success of it would have depended on accurate mathematical models of the semiconductor devices employed.

Once the reflectivity properties as a function of frequency for each AFSS was measured, the theory of uniform transmission lines was employed to extract or de-embed the AFSS's dynamic complex impedance response.

The following theory was used to extract the complex impedance response as a function of frequency of each AFSS employed in the research programme. The

reflection coefficient $\Gamma(\omega)$ is given by

$$\Gamma(\omega) = \frac{Z_{in}(\omega) - Z_o}{Z_{in}(\omega) + Z_o} \tag{B.1}$$

where $Z_{in}(\omega)$, as shown in figure B.1, is the input impedance seen by the incoming radiation when it strikes the AFSS and Z_o is the impedance of air. By re-arranging the above equation $Z_{in}(\omega)$ can be expressed as

$$Z_{in}(\omega) = Z_o \frac{\Gamma(\omega) + 1}{\Gamma(\omega) - 1} \tag{B.2}$$

Now the AFSS complex impedance $X_{afss}(\omega)$ is given by

$$X_{afss}(\omega) = \frac{Z_{in}(\omega)}{Z_{in_m}(\omega) - Z_{in}(\omega)} \tag{B.3}$$

where $Z_{in_m}(\omega)$ is the impedance of supporting substrate and is give by

$$Z_{in_m}(\omega) = Z_m \frac{Z_L + jZ_m \tan[\beta l]}{Z_m + j \tan[\beta l]} \tag{B.4}$$

In the above equation Z_m is the intrinsic impedance of the supporting dielectric; Z_L is the load impedance, which, as shown in figure B.1, is air; l is the substrate thickness and $\beta = 2\pi\sqrt{\epsilon_r}/\lambda$.

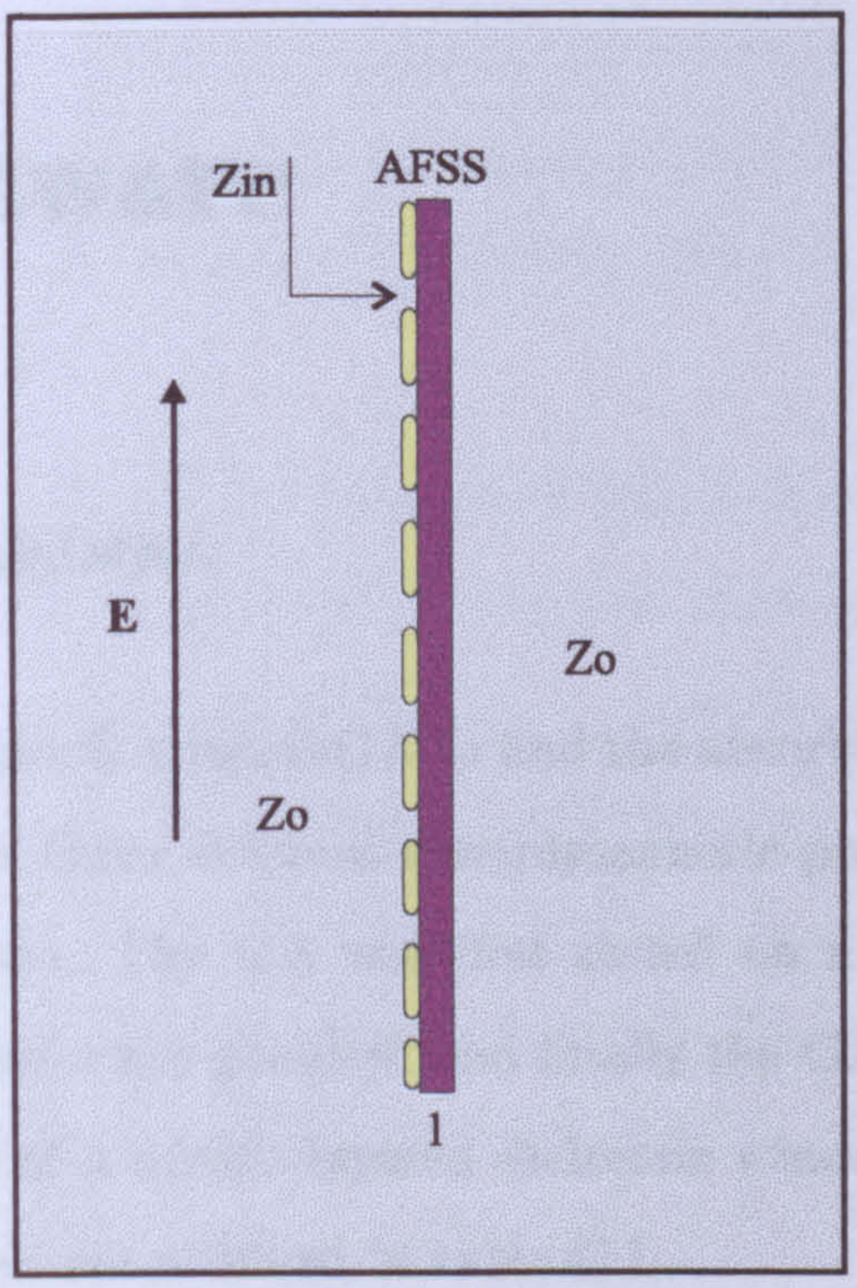

Figure B.1: AFSS with supporting dielectric substrate standing in air.

Appendix C

GA Software

GA Software Validation

Before using the class GASimpleGA to find the absorber's global solution the software was tested on three different electromagnetic problems which are known to have exact solutions. The GA was first tested on a Salisbury screen absorber, then on a $\lambda/4$ transformer problem and finally the GA was employed to seek the matching problem of a double-layered dielectric window suspended in free space. The GA parameters are outlined in table C.1.

Salisbury Screen Absorber: The problem given to the GA optimiser was to find the known solution of a fixed-thickness Salisbury screen absorber, through max-

Graph	GA Parameters			
	Population	Generations	PCross	PMut
1	30	100	0.6	0.01

Table C.1: GA Parameters.

	a	b	c
Fitness Function $F(R, \epsilon_r)$	-	$10\Gamma_o + 10BW$	$1/\Gamma_o + 500BW$
R (Ω/sq)	376.6	333.638	368.586
ϵ_r	1.0	1.01	1.01

Table C.2: GA output parameters. Where Γ_o is the reflection null and $BW = f_u - f_l$, f_u and f_l are the upper and lower frequencies, respectively, at -20 dB. a: Salisbury screen with known solution. b: GA first solutions. c: GA second solution.

imizing a fitness function F, in terms of values of resistive film, R and spacer's permittivity ϵ_r. The search was performed over the search area 1-4.05 GHz, with constrained parameters of R and ϵ_r over the ranges $R \in \{5\Omega, 900\Omega\}$ and $\epsilon_r \in \{1.0, 4.0\}$, respectively. The GA software was run twice with two different fitness functions. These are displayed in table C.2. The GAs' solutions, whose parameters are also outlined in table C.2, are shown in figure C.1. For comparison, the absorber's known solution is plotted together with the GAs' solutions. The figure shows that both solutions converge to the Salisbury screen's known solution. However, a closer match is found with the second fitness function. This clearly indicates that proper choice of fitness function is important in order to find the closest convergence possible to a global solution.

The $\lambda/4$ Transformer: A $\lambda/4$ transformer is a narrow band device used as a connecting link for impedance matching of structures with different impedances. For this problem we sought to find the solution which would adequately match a 70Ω-load operating at 3GHz ($\lambda = 100$mm) to free space through maximizing a fitness function F. The solution is in terms of stub's spacer thickness, d, and its permittivity ϵ_r. The general solution of this problem is $n\lambda/4\sqrt{\epsilon_r}$ [1]. The search space

[1] where $n = 1, 3, 5, ...$

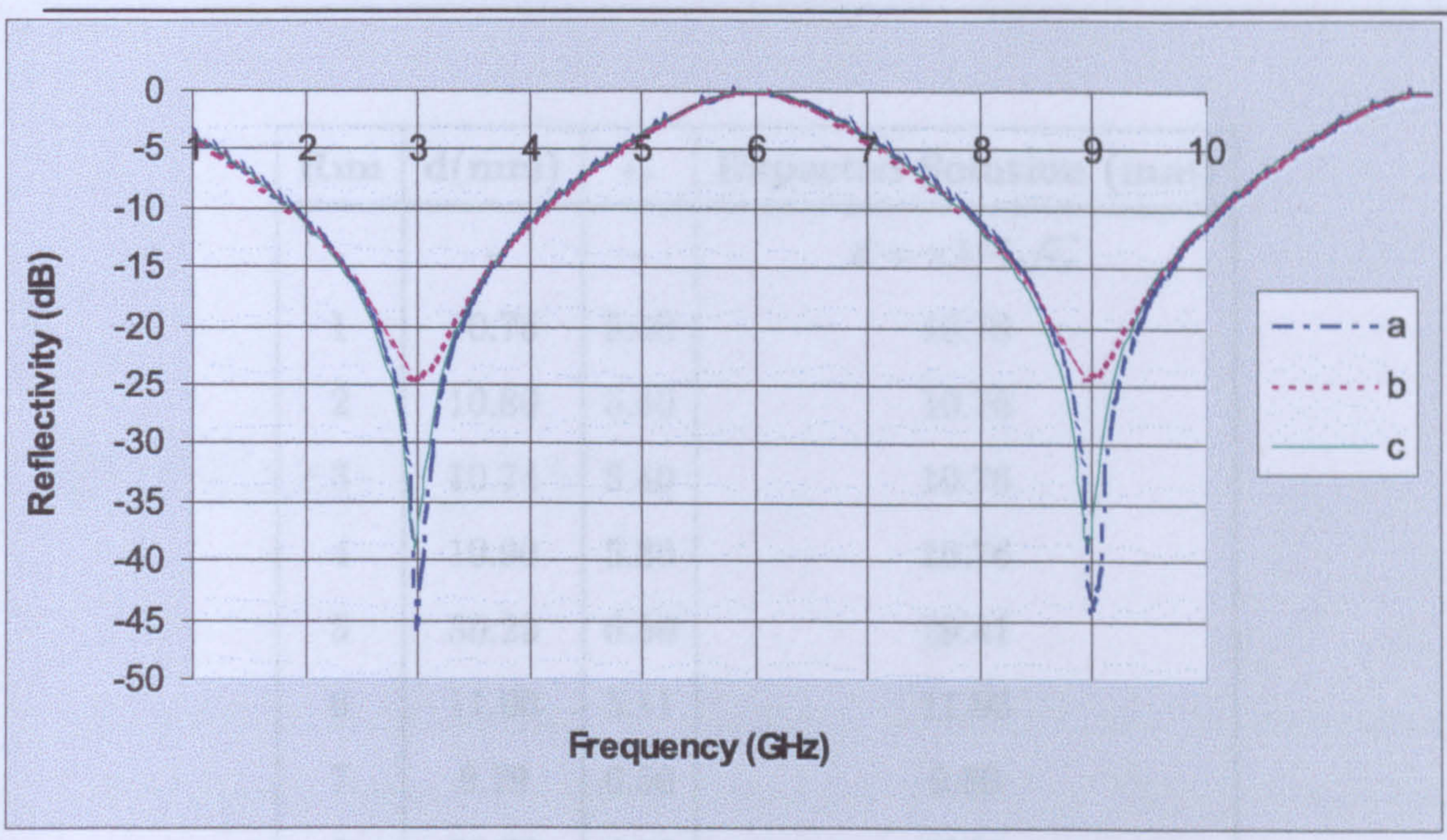

Figure C.1: a: Frequency profile of a Salisbury screen absorber. b: GA first solution. c: GA second solution.

was constrained to the parameters ranges given by $d \in \{0.001, 0.040\}$ in m and $\epsilon_r \in \{1.0, 12.0\}$. Table C.3 shows the result for 10 runs of the software. The results shown in columns 2 and 4 are closely matched to the known global solution. This suggests that the GA converges to the expected solution and therefore it performs.

Two-Layer Dielectric Window: The match-load solution of a 2-layer dielectric window suspended in air and which is operated at 3 GHz ($\lambda = 100$mm) requires that the total thickness d_T of the combined layers of equal permittivity (in this example $\epsilon_r = 4.0$) be such that $d_T = d_1 + d_2 = n\lambda/2\sqrt{\epsilon_r}$ [2]. In this optimization problem, the input parameters were constrained to the ranges $d_1 \in \{0.001, 0.030\}$ and $d_2 \in \{0.001, 0.030\}$, both in m. Table C.4 shows the GA solutions of 10 different runs of the software, the 0*-run being the expected solution. From this table it can be seen that that the GA's output trend closely follows the expected solution(s).

[2] where $n = 1, 2, 3, ...$

Run	d(mm)	ϵ_r	Expected Solution (mm)
-	-	-	$d = n\lambda/4\sqrt{\epsilon_r}$
1	10.75	5.40	10.76
2	10.80	5.40	10.76
3	10.74	5.40	10.76
4	10.90	5.30	10.76
5	30.25	6.50	29.41
6	11.00	5.11	11.06
7	9.79	6.50	9.80
8	33.70	4.95	33.71
9	32.50	5.33	32.49
10	11.10	5.10	11.07

Table C.3: $\lambda/4$ Transformer GA Results. The fitness function is $F(d, \epsilon_r) = 1/\Gamma_o$ (Γ_o is the reflection coefficient). $\lambda = 100$ mm.

Run	d_1(mm)	d_2(mm)	Expected Solution (mm)
0*	d_1	d_2	$d_T = d_1 + d_2 = n\lambda/2\epsilon_r$
1	28.20	21.80	50
2	1.82	23.2	25.02
3	13.54	11.5	25.04
4	6.89	18.11	25.00
5	12.1	12.9	25.00
6	26.50	22.35	48.85
7	24.76	25.24	50.20
8	26.57	23.43	50.00
9	17.88	7.12	25.00
10	14.99	10.00	24.99

Table C.4: Two-Layer Dielectric Window GA Results. The fitness function is $F(d_1, d_2) = 1/\Gamma_o$ (Γ_o is the reflection coefficient). $\lambda = 100$ mm and $\epsilon_r = 4.0$.

Bibliography

[1] Weile, D. S., Michielssen, E., Goldberg, D. E.,, *Genetic Algorithm Design of Pareto Optimal Broadband Microwave Absorbers*, IEEE transactions on Electromagnetic Compatibility, Vol 38, No. 3, August 1996, pp. 518-525.

[2] Weile, D. S., Michielssen, *Integer Coded Pareto Genetic Algorithm Design of Constrained Antenna Arrays*, Electronics letters, Vol 32, No. 19, September 1996, pp. 1744-1745.

[3] Bailey, A.E., *Microwave Measurements*, IEE Publication, Peter Peregrinus Ltd., 2nd Edition, 1989.